Royal Norwegian Council
for Scientific and Industrial Research
(NTNF)

NORSAR

(1)

NORSAR Scientific Report No. 2-90/91

Semiannual Technical Summary

1 October 1990 — 31 March 1991

Kjeller, May 1991

UNCLASSIFIED
SECURITY CLASSIFICATION OF THIS PAGE

REPORT DOCUMENTATION PAGE

1a. REPORT SECURITY CLASSIFICATION: UNCLASSIFIED	1b. RESTRICTIVE MARKINGS: NOT APPLICABLE
2a. SECURITY CLASSIFICATION AUTHORITY: NOT APPLICABLE	3. DISTRIBUTION/AVAILABILITY OF REPORT: APPROVED FOR PUBLIC RELEASE DISTRIBUTION UNLIMITED
2b. DECLASSIFICATION/DOWNGRADING SCHEDULE: NOT APPLICABLE	
4. PERFORMING ORGANIZATION REPORT NUMBER(S): Scientific Report 2-90/91	5. MONITORING ORGANIZATION REPORT NUMBER(S): Scientific Rep. 2-90/91
6a. NAME OF PERFORMING ORGANIZATION: NTNF/NORSAR; 6b. OFFICE SYMBOL (If applicable):	7a. NAME OF MONITORING ORGANIZATION: HQ/AFTAC/TTS
6c. ADDRESS (City, State, and ZIP Code): Post Box 51, N-2007 Kjeller, Norway	7b. ADDRESS (City, State, and ZIP Code): Patrick AFB, FL 32925-6001
8a. NAME OF FUNDING/SPONSORING ORGANIZATION: Defense Advanced Research Projects Agency; 8b. OFFICE SYMBOL (If applicable): NMRO	9. PROCUREMENT INSTRUMENT IDENTIFICATION NUMBER: Contract No. F08606-89-C-0005
8c. ADDRESS (City, State, and ZIP Code): 1400 Wilson Blvd, Arlington, VA 22209-2308	10. SOURCE OF FUNDING NUMBERS: PROGRAM ELEMENT NO. R&D; PROJECT NO. NORSAR Phase 3; TASK NO. SOW Task 5.0; WORK UNIT ACCESSION NO. Seq.no.003A2

11. TITLE (Include Security Classification)

SEMIANNUAL TECHNICAL SUMMARY, 1 OCTOBER 1990 - 31 MARCH 1991 (UNCLASSIFIED)

12. PERSONAL AUTHOR(S)

13a. TYPE OF REPORT	13b. TIME COVERED	14. DATE OF REPORT (Year, Month, Day)	15. PAGE COUNT
Scientific Summary	FROM 1 Oct 90 TO 31 Mar 91	May 1991	164

16. SUPPLEMENTARY NOTATION

NOT APPLICABLE

17. COSATI CODES			18. SUBJECT TERMS (Continue on reverse if necessary and identify by block number)
FIELD	GROUP	SUB-GROUP	NORSAR, NORWEGIAN SEISMIC ARRAY
8	11		

19. ABSTRACT (Continue on reverse if necessary and identify by block number)

(Please see reverse side)

20. DISTRIBUTION/AVAILABILITY OF ABSTRACT: ☐ UNCLASSIFIED/UNLIMITED ☐ SAME AS RPT ☐ DTIC USERS	21. ABSTRACT SECURITY CLASSIFICATION
22a. NAME OF RESPONSIBLE INDIVIDUAL: Mr. Lee Bridges	22b. TELEPHONE (Include Area Code): (407) 494-7765; 22c. OFFICE SYMBOL: AFTAC/TTS

DD FORM 1473, 84 MAR — 83 APR edition may be used until exhausted. All other editions are obsolete. — SECURITY CLASSIFICATION OF THIS PAGE

UNCLASSIFIED

Abstract

This Semiannual Technical Summary describes the operation, maintenance and research activities at the Norwegian Seismic Array (NORSAR), the Norwegian Regional Seismic Array (NORESS) and the Arctic Regional Seismic Array (ARCESS) for the period 1 October 1990 - 31 March 1991. Statistics are also presented for additional seismic stations, which through cooperative agreements with institutions in the host countries provide continuous data to the NORSAR Data Processing Center (NPDC). These stations comprise the Finnish Experimental Seismic Array (FINESA), the German Experimental Seismic Array (GERESS), and two 3-component stations in Poland: Ksiaz and Stary Folwark. This Semiannual Report also presents statistics from operation of the Intelligent Monitoring System (IMS). The IMS has been operated in an experimental mode using NORESS and ARCESS data, and the performance has been very satisfactory.

The NORSAR Detection Processing system has been operated throughout the period with an average uptime of 98.6% as compared to 98.0% for the previous reporting period. A total of 1837 seismic events have been reported in the NORSAR monthly seismic bulletin. The performance of the continuous alarm system and the automatic bulletin transfer by telex to AFTAC has been satisfactory. A system for direct retrieval of NORSAR waveform data through an X.25 connection has been implemented, and has been tested successfully for acquiring such data by AFTAC. Processing of requests for full NORSAR/NORESS data on magnetic tapes has progressed according to established schedules.

On-line detection processing and data recording at the NORSAR Data Processing Center (NDPC) of NORESS, ARCESS and FINESA data have been conducted throughout the period, with an average uptime of 99.2% for NORESS, 98.4% for ARCESS and 98.9% for FINESA. The Intelligent Monitoring System was installed at NORSAR in December 1989 and has been operated experimentally since 1 January 1990. Results of the IMS analysis for the reporting period are given.

There have been no modifications made to the NORSAR data acquisition system. The process of evaluating and testing technical options for refurbishment of the array is continuing.

The routine detection processing of NORESS, ARCESS and FINESA is running satisfactorily on each of the arrays' SUN-3/280 data acquisition systems. The routine processing of FINESA data at NORSAR is similar to what is done in Helsinki. GERESS data acquisition and detection processing has been conducted in an experimental mode during the period, in a way similar to what is done in Bochum.

Maintenance activities in the period comprise preventive/corrective maintenance in connection with all the NORSAR subarrays, NORESS and ARCESS. In addition, the maintenance center has been involved with occasional maintenance of equipment for FINESA and preparatory work in connection with the two stations in Poland. Other activities involved testing of the NORSAR communications systems.

We have continued our work aimed at evaluating the stability of RMS Lg for yield estimation purposes. We have carried out a detailed RMS Lg analysis of NORSAR recordings of Novaya Zemlya underground explosions, and in addition conducted similar analysis of Gräfenberg (GRF) array recordings (available after 1976). The results show a tight clustering in M(Lg) of 13 NORSAR-recorded explosions after 1976, and GRF data of the 27 Sep 78 explosion, for which no NORSAR data are available, indicate that this event is of similar size. The correspondence between M(Lg) for NORSAR vs GRF is excellent, with an orthogonal standard deviation of only 0.02–0.03 magnitude units. This correspondence fully matches the excellent results previously obtained for Semipalatinsk explosions, and confirms the promise of RMS Lg as a stable estimator of relative yields.

The concept of threshold monitoring, introduced by Ringdal and Kværna, is a method of monitoring the seismic amplitude levels for the purpose of using this information to assess the largest size of events that might go undetected by a given network. In an effort to demonstrate the capabilities of this threshold monitoring technique, we have conducted a simulation experiment, which has involved down-scaling the recorded signals of the 24 October 1990 Novaya Zemlya explosion ($m_b = 5.6$) by a factor of 1000 (i.e., 3 orders of magnitude). The resulting NORESS, ARCESS and FINESA traces of this "$m_b = 2.6$ event" were added at hourly intervals to the actual recordings for a full data day, and the threshold monitor was then applied. The results demonstrated that every one of these 24 "events" were clearly identifiable on the threshold trace. While this clearly gives a very simplified picture, it serves to document the excellent monitoring potential of these three arrays for the Novaya Zemlya test site.

A significant part of our research effort has been directed toward the further development of European high frequency arrays and high quality three-component stations. The aim has been to provide for continuous transmission of data (by satellite or land line) to NDPC and integration of this data stream into the input base for the Intelligent Monitoring System (IMS). These efforts have proceeded satisfactorily. During the reporting period, particular emphasis has been placed upon optimizing the GERESS beam deployment (in cooperation with Ruhr University scientists) and completing the integration into the network of the KSP and SFP stations in Poland. All of these network stations are scheduled for participation in the 1991 GSETT-2 experiment.

The multichannel statistical data processing algorithms described in previous NORSAR Semiannual Technical summaries have now been integrated into the Event Processor system currently in operation at NORSAR. A description of the program and some of the recent results are provided. At present, these algorithms are used only experimentally, in an offline fashion, but plans to start testing them in an operational environment have been made.

Results are presented from a two-dimensional finite difference approach to modeling seismic wave propagation in the crust. These results are based on a cooperative effort with scientists at the IBM Bergen Scientific Centre. In the generation of synthetic seismograms, a homogeneous crust of thickness 30 km and P_{vel} = 6.5 km/sec has been used as a basis, with options for perturbation comprising multilayering, piece-wise linear velocity gradients as well as large-scale discontinuities. Randomized scattering effects have so far not been considered. It appears that the synthetics generate all major phases, but with a relatively weak body-wave coda generation compared to real seismograms. The introduction of scatterers is expected to be of importance in remedying this problem, and will be the subject of future investigations.

An overview is presented of results related to determining the crustal thicknesses in Fennoscandia. A detailed contour map (2 km contour intervals) has been developed for the entire region. In view of the extrensive sediment deposits, a map of the crystalline crustal thicknesses is also presented for the SW part of the area. In general, the oldest parts of the Baltic Shield exhibit the greatest crustal thicknesses (in some areas exceeding 50 km). In the offshore Norway areas, the crystalline thicknesses are of the order of 15–20 km, while the sedimentary overburdens can exceed 10 km. An interesting observation is that the Moho depth variation appears to have a counterpart in the spatial distribution of earthquakes in the Fennoscandian region.

In the current IMS implementation of the threshold monitoring method, a limited number of specific target sites are monitored. These sites include several mines in Scandinavia and Western Russia, along with the Novaya Zemlya and Semipalatinsk nuclear test sites. We have now initiated a study to determine how this method could be applied to monitoring more extensive geographical regions. The key to achieving this is to develop "generic" relations for attenuation and magnitude correction factors for seismic phases of interest, and to deploy a sufficient number of beams to ensure adequate coverage. So far, we have developed preliminary relations and correction factors for the Pn and Lg phases. These "generic" relations are based upon systematic analysis of several hundred phase observations of regional events in various geographical areas. The results are applicable to Northern Europe and adjacent regions. Factors that remain to be assessed in detail include the effect of uncertainties in reference M_L magnitudes for the events in the data base and the effect of signal loss in the array beamforming.

Using the "generic" amplitude relations described above, we have generated a very extensive beam set for a short test interval using NORESS, ARCESS and FINESA data. The results of TM processing for this time period, which are presented in the form of regional threshold maps, are very encouraging, and indicate that this is indeed a potentially very useful extension of the concept. However, an "operational" implementation might require computer processing capacity of about an order of magnitude greater than is currently available on a Sun Workstation (type Sparc station 1).

AFTAC Project Authorization	:	T/9141/B/PKP
ARPA Order No.	:	4138 AMD # 16
Program Code No.	:	0F10
Name of Contractor	:	Royal Norwegian Council for Scientific and Industrial Research
Effective Date of Contract	:	1 Oct 1988
Contract Expiration Date	:	30 Sep 1991
Project Manager	:	Frode Ringdal (06) 81 71 21
Title of Work	:	The Norwegian Seismic Array (NORSAR) Phase 3
Amount of Contract	:	$ 6,401,883
Contract Period Covered by Report	:	1 Oct 1990 – 31 Mar 1991

This research was supported by the Advanced Research Projects Agency of the Department of Defense and was monitored by AFTAC, Patrick AFB, FL 32925, under contract no. F08606-89-C-0005.

NORSAR Contribution No. 444

Table of Contents

1 Summary

This Semiannual Technical Summary describes the operation, maintenance and research activities at the Norwegian Seismic Array (NORSAR), the Norwegian Regional Seismic Array (NORESS) and the Arctic Regional Seismic Array (ARCESS) for the period 1 October 1990 - 31 March 1991. Statistics are also presented for additional seismic stations, which through cooperative agreements with institutions in the host countries provide continuous data to the NORSAR Data Processing Center (NPDC). These stations comprise the Finnish Experimental Seismic Array (FINESA), the German Experimental Seismic Array (GERESS), and two 3-component stations in Poland: Ksiaz and Stary Folwark. This Semiannual Report also presents statistics from operation of the Intelligent Monitoring System (IMS). The IMS has been operated in an experimental mode using NORESS and ARCESS data, and the performance has been very satisfactory.

The NORSAR Detection Processing system has been operated throughout the period with an average uptime of 98.6% as compared to 98.0% for the previous reporting period. A total of 1837 seismic events have been reported in the NORSAR monthly seismic bulletin. The performance of the continuous alarm system and the automatic bulletin transfer by telex to AFTAC has been satisfactory. A system for direct retrieval of NORSAR waveform data through an X.25 connection has been implemented, and has been tested successfully for acquiring such data by AFTAC. Processing of requests for full NORSAR/NORESS data on magnetic tapes has progressed according to established schedules.

On-line detection processing and data recording at the NORSAR Data Processing Center (NDPC) of NORESS, ARCESS and FINESA data have been conducted throughout the period, with an average uptime of 99.2% for NORESS, 98.4% for ARCESS and 98.9% for FINESA. The Intelligent Monitoring System was installed at NORSAR in December 1989 and has been operated experimentally since 1 January 1990. Results of the IMS analysis for the reporting period are given.

There have been no modifications made to the NORSAR data acquisition system. The process of evaluating and testing technical options for refurbishment of the array is continuing.

The routine detection processing of NORESS, ARCESS and FINESA is running satisfactorily on each of the arrays' SUN-3/280 data acquisition systems. The routine processing of FINESA data at NORSAR is similar to what is done in Helsinki. GERESS data acquisition and detection processing has been conducted in an experimental mode during the period, in a way similar to what is done in Bochum.

Maintenance activities in the period comprise preventive/corrective maintenance in connection with all the NORSAR subarrays, NORESS and ARCESS. In addition, the maintenance center has been involved with occasional maintenance of equipment for FINESA and preparatory work in connection with the two stations in Poland. Other activities involved testing of the NORSAR communications systems.

We have continued our work aimed at evaluating the stability of RMS Lg for yield estimation purposes. We have carried out a detailed RMS Lg analysis of NORSAR recordings of Novaya Zemlya underground explosions, and in addition conducted similar analysis of Gräfenberg (GRF) array recordings (available after 1976). The results show a tight clustering in M(Lg) of 13 NORSAR-recorded explosions after 1976, and GRF data of the 27 Sep 78 explosion, for which no NORSAR data are available, indicate that this event is of similar size. The correspondence between M(Lg) for NORSAR vs GRF is excellent, with an orthogonal standard deviation of only 0.02–0.03 magnitude units. This correspondence fully matches the excellent results previously obtained for Semipalatinsk explosions, and confirms the promise of RMS Lg as a stable estimator of relative yields.

The concept of threshold monitoring, introduced by Ringdal and Kværna, is a method of monitoring the seismic amplitude levels for the purpose of using this information to assess the largest size of events that might go undetected by a given network. In an effort to demonstrate the capabilities of this threshold monitoring technique, we have conducted a simulation experiment, which has involved down-scaling the recorded signals of the 24 October 1990 Novaya Zemlya explosion (m_b = 5.6) by a factor of 1000 (i.e., 3 orders of magnitude). The resulting NORESS, ARCESS and FINESA traces of this "m_b = 2.6 event" were added at hourly intervals to the actual recordings for a full data day, and the threshold monitor was then applied. The results demonstrated that every one of these 24 "events" were clearly identifiable on the threshold trace. While this clearly gives a very simplified picture, it serves to document the excellent monitoring potential of these three arrays for the Novaya Zemlya test site.

A significant part of our research effort has been directed toward the further development of European high frequency arrays and high quality three-component stations. The aim has been to provide for continuous transmission of data (by satellite or land line) to NDPC and integration of this data stream into the input base for the Intelligent Monitoring System (IMS). These efforts have proceeded satisfactorily. During the reporting period, particular emphasis has been placed upon optimizing the GERESS beam deployment (in cooperation with Ruhr University scientists) and completing the integration into the network of the KSP and SFP stations in Poland. All of these network stations are scheduled for participation in the 1991 GSETT-2 experiment.

The multichannel statistical data processing algorithms described in previous NORSAR Semiannual Technical summaries have now been integrated into the Event Processor system currently in operation at NORSAR. A description of the program and some of the recent results are provided. At present, these algorithms are used only experimentally, in an offline fashion, but plans to start testing them in an operational environment have been made.

Results are presented from a two-dimensional finite difference approach to modeling seismic wave propagation in the crust. These results are based on a cooperative effort with scientists at the IBM Bergen Scientific Centre. In the generation of synthetic seismograms, a homogeneous crust of thickness 30 km and P_{vel} = 6.5 km/sec has been used as a basis, with options for perturbation comprising multilayering, piece-wise linear velocity gradients as well as large-scale discontinuities. Randomized scattering effects have so far not been considered. It appears that the synthetics generate all major phases, but with a relatively weak body-wave coda generation compared to real seismograms. The introduction of scatterers is expected to be of importance in remedying this problem, and will be the subject of future investigations.

An overview is presented of results related to determining the crustal thicknesses in Fennoscandia. A detailed contour map (2 km contour intervals) has been developed for the entire region. In view of the extrensive sediment deposits, a map of the crystalline crustal thicknesses is also presented for the SW part of the area. In general, the oldest parts of the Baltic Shield exhibit the greatest crustal thicknesses (in some areas exceeding 50 km). In the offshore Norway areas, the crystalline thicknesses are of the order of 15-20 km, while the sedimentary overburdens can exceed 10 km. An interesting observation is that the Moho depth variation appears to have a counterpart in the spatial distribution of earthquakes in the Fennoscandian region.

In the current IMS implementation of the threshold monitoring method, a limited number of specific target sites are monitored. These sites include several mines in Scandinavia and Western Russia, along with the Novaya Zemlya and Semipalatinsk nuclear test sites. We have now initiated a study to determine how this method could be applied to monitoring more extensive geographical regions. The key to achieving this is to develop "generic" relations for attenuation and magnitude correction factors for seismic phases of interest, and to deploy a sufficient number of beams to ensure adequate coverage. So far, we have developed preliminary relations and correction factors for the Pn and Lg phases. These "generic" relations are based upon systematic analysis of several hundred phase observations of regional events in various geographical areas. The results are applicable to Northern Europe and adjacent regions. Factors that remain to be assessed in detail include the effect of uncertainties in reference M_L magnitudes for the events in the data base and the effect of signal loss in the array beamforming.

Using the "generic" amplitude relations described above, we have generated a very extensive beam set for a short test interval using NORESS, ARCESS and FINESA data. The results of TM processing for this time period, which are presented in the form of regional threshold maps, are very encouraging, and indicate that this is indeed a potentially very useful extension of the concept. However, an "operational" implementation might require computer processing capacity of about an order of magnitude greater than is currently available on a Sun Workstation (type Sparc station 1).

2 NORSAR Operation

2.1 Detection Processor (DP) operation

There have been 48 breaks in the otherwise continuous operation of the NORSAR online system within the current 6-month reporting interval. The uptime percentage for the period is 98.6 as compared to 98.0 for the previous period.

Fig. 2.1.1 and the accompanying Table 2.1.1 both show the daily DP downtime for the days between 1 October 1990 and 31 March 1991. The monthly recording times and percentages are given in Table 2.1.2.

The breaks can be grouped as follows:

a)	Hardware failure	8
b)	Stops related to program work or error	2
c)	Hardware maintenance stops	6
d)	Power jumps and breaks	0
e)	TOD error correction	0
f)	Communication lines	32

The total downtime for the period was 86 hours and 3 minutes. The mean-time-between-failures (MTBF) was 4.1 days, as compared to 3.2 for the previous period.

J. Torstveit

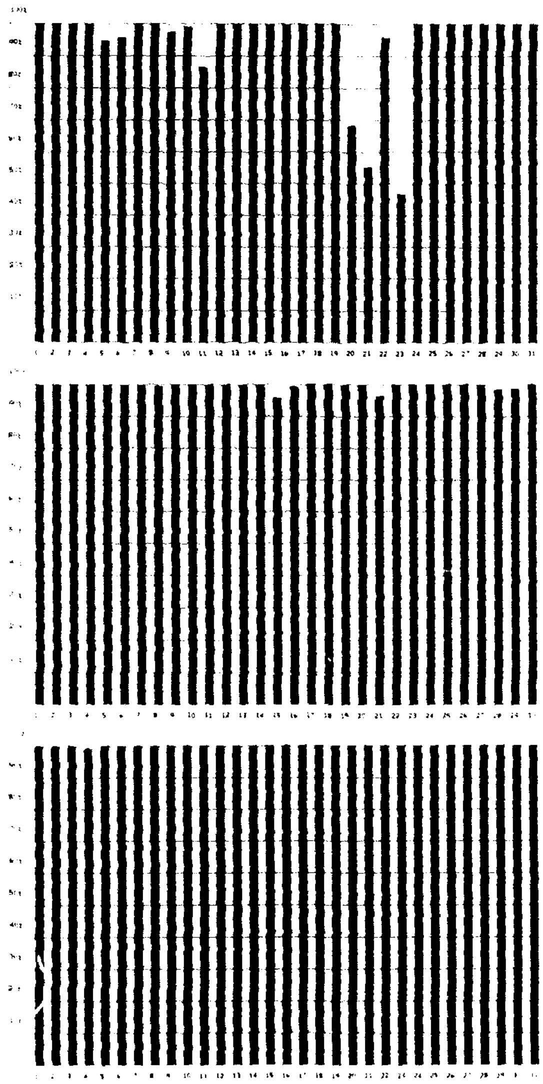

Fig. 2.1.1 Detection Processor downtime for October (top), November (middle) and December (bottom) 1990.

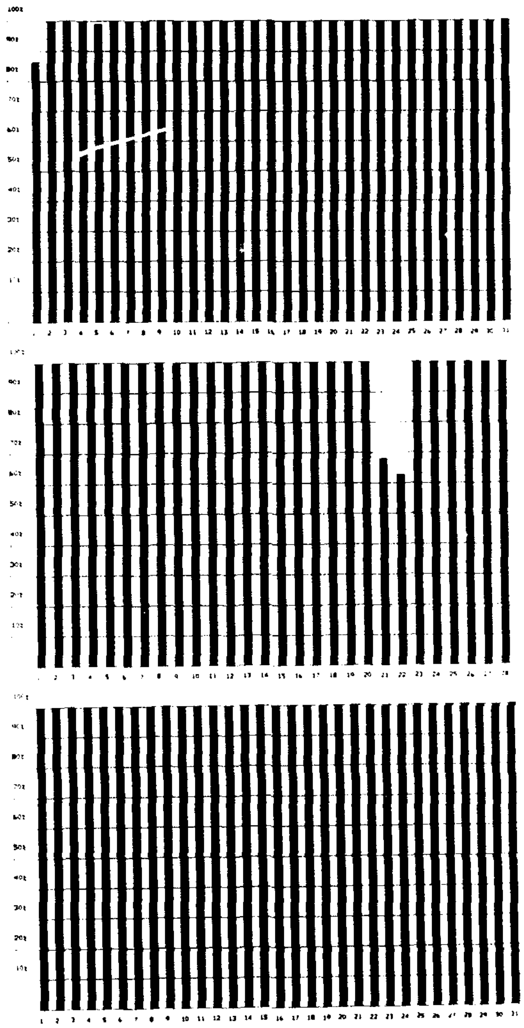

Fig. 2.1.1 Detection Processor downtime for January (top), February (middle) and March (bottom) 1991.

Date	Time	Cause
5 Oct	0032-0146	Hardware failure NDPC
6 Oct	1656-1758	Hardware failure NDPC
9 Oct	1216-1252	Hardware failure NDPC
10 Oct	1304-1314	Hardware failure NDPC
11 Oct	0042-0144	Hardware failure NDPC
11 Oct	0754-1006	Hardware maintenance NDPC
20 Oct	1624-	Hardware failure NDPC
21 Oct	-1043	Hardware failure NDPC
22 Oct	2300-	Hardware failure NDPC
23 Oct	-1245	Hardware failure NDPC
16 Nov	0855-0903	Hardware maintenance NDPC
21 Nov	1801-1850	Hardware failure NDPC
28 Nov	0120-0140	Operator error NDPC
29 Nov	1515-1534	Hardware failure NDPC
4 Dec	1212-1223	Hardware maintenance NDPC
1 Jan	1037-1351	Software work (new year)
3 Jan	1017-1023	Hardware maintenance NDPC
21 Feb	1620-	Hardware failure NDPC
22 Feb	-0855	Hardware failure NDPC

Table 2.1.1 The major downtimes in the period 1 October 1990 – 31 March 1991.

Month	DP Uptime Hours	DP Uptime %	No. of DP Breaks	No. of Days with Breaks	DP MTBF* (days)
OCT 90	705.52	94.83	12	10	2.3
NOV 90	717.58	99.61	11	8	2.5
DEC 90	743.55	99.96	4	4	6.2
JAN 91	740.33	99.51	7	7	3.9
FEB 91	655.08	97.48	11	7	2.3
MAR 91	719.88	99.98	3	3	7.5
		98.56	48	39	4.1

*Mean-time-between-failures = total uptime/no. of up intervals.

Table 2.1.2 Online system performance, 1 October 1990 - 31 March 1991.

2.2 Array communications

General

Table 2.2.1 reflects the performance of the communications system throughout the reporting period.

The most common events which have affected the NORSAR array have been: damaged communications cables, loss of subarray power, irregularities in the NTA transmission systems and incorrect line level.

Detailed summary

October (weeks 40-44), 1.10-4.11.90

01A was affected by a bad communications cable (week 44). 01B was affected by a communications cable damaged by excavation (weeks 40-41). Also the 02C communications cable was affected for the same reason (week 46). In addition we had sync problems (week 44) in connection with 02B, 02C and 06C.

November (weeks 45-48), 5.11-2.12.90

01A resumed operation 6 November. 01B was affected approximately 6 hours week 45, cause not stated. 02C resumed operation 20 November after communications cable repair by NTA/Hamar. 04C was affected 12, 21 and 28 November in connection with an irregularity between Hamar and Elverum, including a change to spare transmission equipment. 06C was affected weeks 45, 45 and 47, reason unknown.

December (weeks 49-52), 3-30.12.90

03C and 06C were affected during this period; 03C weeks 49 and 52, 06C weeks 51 and 52. In order to improve the 03C performance NTA/Lillestrøm raised the level towards Kjeller by 3.5 dBm. 06C resumed operation after a Modcomp restart 27 December.

January (weeks 1-5), 31.12.90-3.1.91

Week 1 three subarrays were affected: 02B 3 January in connection with a scheduled movement to another transmission group, 4-5 January due to power failure; 02C 4 January and 03C 4-5 January, probably caused by interruption related to NTA equipment. In Week 2 (8 January) 02C data disappeared. According to NTA/Lillestrom a cable was damaged in connection with road-work. On 10 January the cable was repaired. In Week 3 (18 January) power to 02B again failed. After repair and replacement of the main fuses, the SLEM was finally reset 23 January. The subarray then again delivered data. 03C lost synchronization 23 January. After a Modcomp restart, sync was again established.

February (weeks 6-9), 4.2-3.3.91

In this period 4 subarrays were affected: 02B, 02C week 9; 03C weeks 7 and 9; and finally 06C weeks 7, 8 and 9. There were short interruptions in NTA transmission equipment/lines, which again resulted in sync problems.

March (weeks 10-13), 4-31.3.91

The subarrays 02B, 02C and 06C were affected 1 March, and 03C on 3 March. All were resynchronized 4 March after a Modcomp restart. A communications cable damaged by an excavation 4 March resulted in loss of data from subarray 03C. 5 March the cable was repaired.

O.A. Hansen

Sub-arrays	Oct 90 (5) 1.10-4.11	Nov 90 (4) 5.11-2.12	Dec 90 (4) 3-30.12	Jan 91 (5) 31.12.90-3.2.91	Feb 91 (4) 4.2-3.3	Mar 91 (4) 4-31.3	Average 1/2 year
01A	1)*0.0019	4)*0.0030	0.0006	0.0006	0.0009	0.0007	0.004
01B	2)*0.0040	0.896	0.001	0.023	0.0008	17)*0.002	0.160
02B	*0.364	0.025	0.011	10)*0.004	13)*0.010	*0.458	0.145
02C	3)*0.0002	5)*0.0002	0.0009	11)*0.447	14)*0.003	*0.448	0.150
03C	0.008	0.004	8)*0.002	12)*0.002	15)*0.027	*0.448	0.081
04C	0.003	6)*1.197	0.001	0.001	0.002	0.001	0.200
06C	*0.011	7)*2.398	9)*0.0006	0.003	16)*0.0007	*0.343	0.459
AVER	0.063	0.646	0.002	0.068	0.006	0.243	0.171

*See Section 2.2 regarding figures preceded by an asterisk.
Figures representing error rate (in per cent) preceded by a number 1), 2), etc., are related to legend below.

1),11),12)	Average 4 weeks (40-43/90), (1-5/91)
2),4),7),13),14),17)	Average 3 weeks (42-44,46-48/90), (6-8,10-13/91)
3),6),8),9),10),15)	Average 2 weeks (41-42,45-47,49-51/90), (2,5,8/91)
5),16)	Average 1 week (48/90), (6/91)

Table 2.2.1 Communications performance. The numbers represent error rates in per cent based on total transmitted frames/week (1 October 1990 - 31 March 1991).

2.3 Event detection operation

In Table 2.3.1 some monthly statistics of the Detection and Event Processor operation are given. The table lists the total number of detections (DPX) triggered by the on-line detector, the total number of detections processed by the automatic event processor (EPX) and the total number of events accepted after analyst review (teleseismic phases, core phases and total).

	Total	Total	Accepted events			
	DPX	EPX	P-phases	Core phases	Sum	Daily
Oct 90	11300	1381	211	70	281	9.1
Nov 90	12225	1411	241	64	305	10.2
Dec 90	14158	1471	283	62	345	11.1
Jan 91	12849	1354	206	59	265	8.5
Feb 91	12025	1497	204	43	247	8.8
Mar 91	11200	1409	329	65	394	12.7
			1474	363	1837	10.1

Table 2.3.1. Detection and Event Processor statistics, 1 October 1990 - 31 March 1991.

B. Paulsen

3 Operation of Regional Arrays

3.1 Recording of NORESS data at NDPC, Kjeller

Table 3.1.1 lists the main outage times and reasons, and as can be seen the main reasons for the outages are hardware failure at the HUB and software failure al NDPC.

The average recording time was 99.2% as compared to 92.9% for the previous period.

Date	Time	Cause
12 Oct	0910-0914	Service at HUB
12 Oct	1025-1033	Service at HUB
18 Oct	0103-0145	Timing failure HUB
19 Oct	0058-0151	Timing failure HUB
22 Oct	1238-1259	Service at HUB
1 Nov	0850-0911	Line failure
14 Nov	0840-0845	Service at HUB
16 Nov	0037-0045	Line failure
21 Nov	2034-2104	Software failure
22 Nov	0600-0608	Software failure
23 Nov	2316-2352	Software failure
24 Nov	0921-0943	Software failure
26 Nov	2029-2216	Software failure
26 Nov	2300-	Software failure
27 Nov	-0621	Software failure
28 Nov	1159-1354	Power failure HUB
28 Nov	1430-1711	Power failure HUB
3 Dec	0810-0824	Hardware failure NDPC
8 Dec	2200-2205	Software failure
18 Dec	0855-1029	Line failure
24 Dec	0534-0549	Line failure
31 Dec	2035-2045	Line failure
9 Jan	1045-1112	Service at HUB
11 Jan	1225-1228	Service at HUB

20 Jan	2101-2105	Line failure
20 Jan	2112-2117	Line failure
20 Jan	2132-2135	Line failure
6 Feb	2238-2242	Line failure
2 Mar	0100-1325	Software failure

Table 3.1.1. Interruptions in recording of NORESS data at NDPC, 1 October 1990 - 31 March 1991.

Monthly uptimes for the NORESS on-line data recording task, taking into account all factors (field installations, transmissions line, data center operation) affecting this task were as follows:

October	:	99.8%
November	:	97.8%
December	:	99.6%
January	:	99.9%
February	:	100.0%
March	:	98.4%

Fig. 3.1.1 shows the uptime for the data recording task, or equivalently, the availability of NORESS data in our tape archive, on a day-by-day basis, for the reporting period.

J. Torstveit

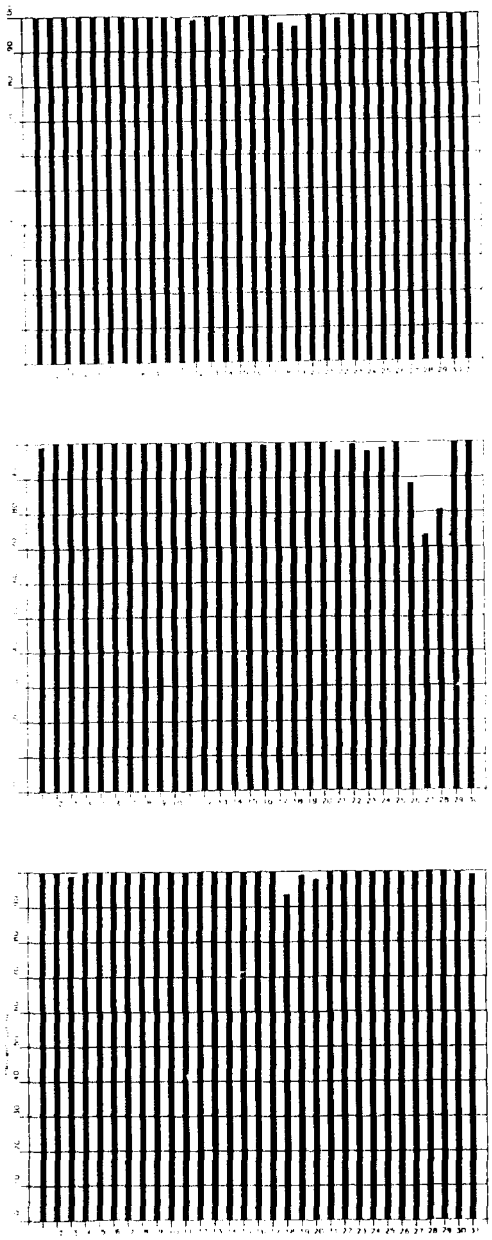

Fig. 3.1.1. NORESS data recording uptime for October (top), November (middle) and December (bottom) 1990.

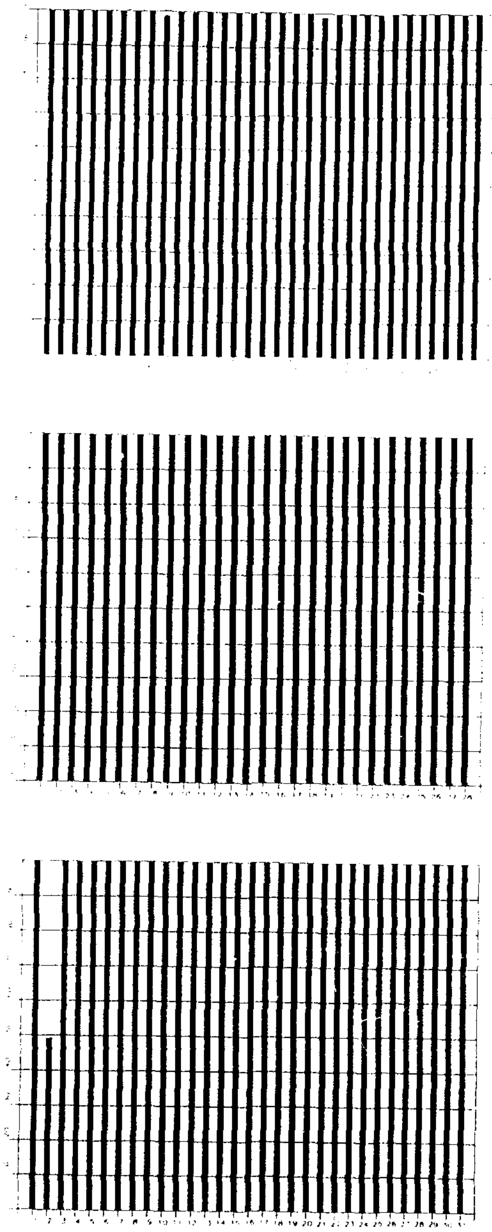

Fig. 3.1.1. (cont.) NORESS data recording uptime for January (top), February (middle) and March (bottom) 1991.

3.2 Recording of ARCESS data at NDPC, Kjeller

The main reasons causing most of the ARCESS outage in the period are: Hardware failure at NDPC and line failure. Outage intervals are listed in Table 3.2.1.

The average recording time was 98.4% as compared to 95.6% for the previous period.

Date	Time	Cause
5 Oct	0413-0438	Power break HUB
5 Oct	0456-0523	Power break HUB
5 Oct	0629-0723	Power break HUB
5 Oct	1321-1620	Instaling UPS at HUB
5 Oct	2038-2236	Instaling UPS at HUB
7 Oct	0743-0756	Software failure
10 Oct	0810-0911	Software failure
10 Oct	2138-2220	Software failure
13 Oct	1410-1511	Software failure
14 Oct	1120-1232	Software failure
15 Oct	1100-1133	Software failure
19 Oct	1603-1644	Software failure
22 Oct	1333-1534	Hardware failure
23 Oct	1355-1406	Software failure
25 Oct	0650-0834	Software failure
25 Oct	1555-1606	Software failure
9 Nov	0034-0107	Software failure
10 Nov	1900-1929	Software failure
13 Dec	0315-	Line failure
14 Dec	-1845	Line failure
31 Dec	2310-	Line failure
1 Jan	-0001	Line failure
7 Feb	0952-1025	Hardware failure
14 Feb	2141-2238	Hardware failure
16 Feb	0026-0130	Hardware failure
17 Feb	1144-1149	Hardware failure
17 Feb	1602-1657	Hardware failure

17 Feb	1708-1738	Hardware failure
18 Feb	1259-1311	Hardware maintenance
19 Feb	1031-1038	Hardware failure
19 Feb	1234-1238	Hardware failure
19 Feb	1451-1507	Hardware failure
19 Feb	1556-1759	Hardware failure
19 Feb	1839-1910	Hardware failure
21 Feb	1725-1741	Hardware failure
21 Feb	2300-	Hardware failure
22 Feb	-0721	Hardware failure
22 Feb	1008-1012	Hardware failure
22 Feb	1032-1058	Hardware failure
22 Feb	1113-1123	Hardware failure
22 Feb	1144-1155	Hardware failure
23 Feb	0825-0832	Hardware failure
26 Feb	0715-0736	Hardware maintenance
6 Mar	1142-1209	Software maintenance
6 Mar	1214-1245	Software maintenance

Table 3.2.1. The main interruptions in recording of ARCESS data at NDPC, 1 October 1990 - 31 March 1991.

Monthly uptimes for the ARCESS on-line data recording task, taking into account all factors (field installations, transmissions line, data center operation) affecting this task were as follows:

October	:	98.2%
November	:	99.9%
December	:	94.6%
January	:	100.0%
February	:	98.2%
March	:	99.9%

Fig. 3.2.1 shows the uptime for the data recording task, or equivalently, the availability of ARCESS data in our tape archive, on a day-by-day basis, for the reporting period.

J. Torstveit

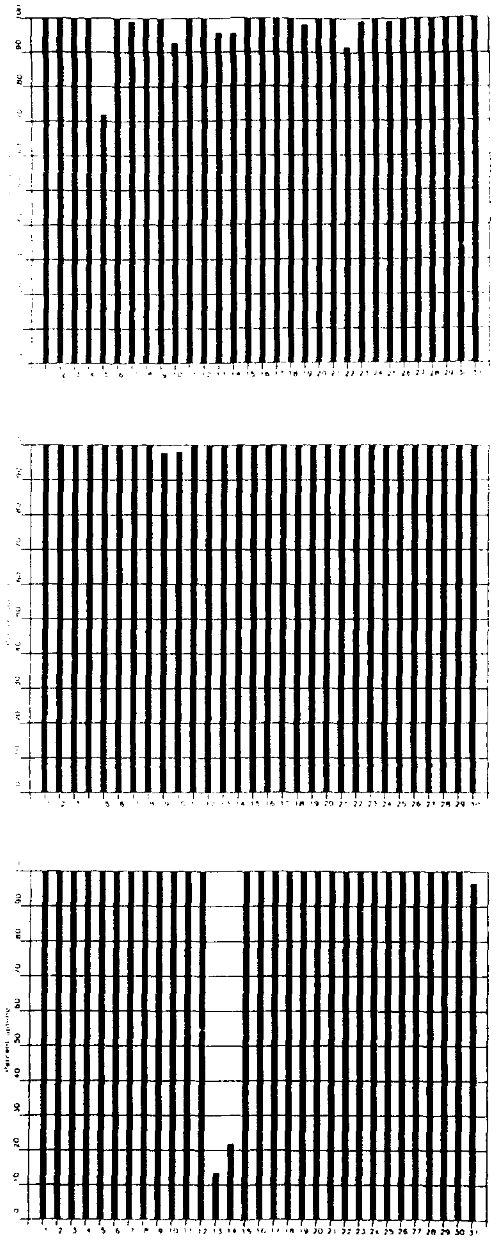

Fig. 3.2.1. ARCESS data recording uptime for October (top), November (middle) and December (bottom) 1990.

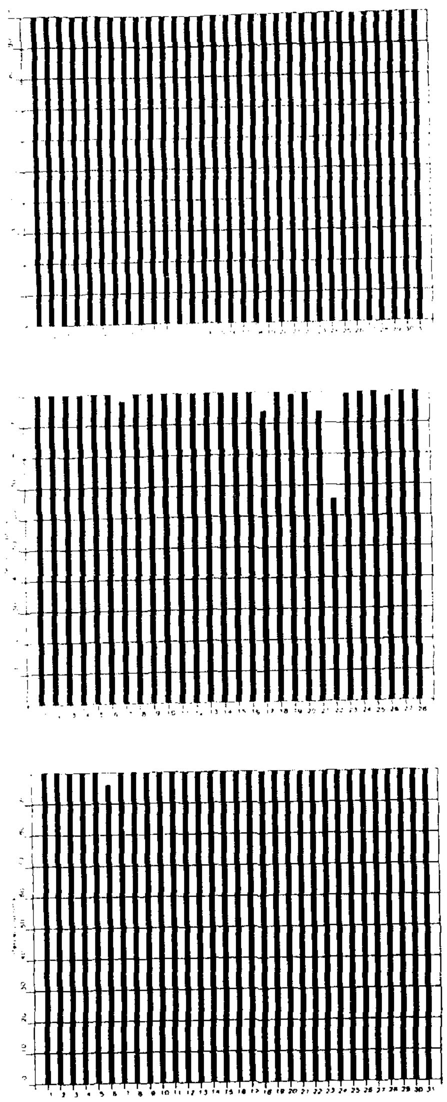

Fig. 3.2.1. (cont.) ARCESS data recording uptime for January (top), February (middle) and March (bottom) 1991.

3.3 Recording of FINESA data at NDPC, Kjeller

The main reason for downtime ot the FINESA array in the period are line failure, either between Norsar and Helsinki or between Helsinki and the field installation.

The average recording time was 98.9% as compared to 39.0% for the previous period.

Date	Time	Cause
3 Oct	0823-0844	Line failure
3 Oct	0902-0907	Line failure
3 Oct	0917-1034	Line failure
4 Oct	1115-	Line failure
5 Oct	-0627	Line failure
15 Oct	1604-1615	Line failure
27 Oct	0241-0340	Line failure
31 Oct	2322-	Line failure
1 Nov	-0530	Line failure
10 Nov	1750-1757	Line failure
12 Nov	1014-1104	Line failure
13 Nov	0753-0757	Line failure
19 Nov	2215-2230	Line failure
20 Nov	0029-0045	Line failure
19 Dec	2215-2230	Line failure
20 Dec	0029-0045	Line failure
11 Jan	0651-0705	Line failure
16 Jan	1233-1257	Line failure
19 Jan	0810-0817	Line failure
19 Jan	0846-0853	Line failure
20 Jan	2306-	Line failure
21 Jan	-0118	Line failure
24 Jan	0119-0744	Line failure
13 Feb	0832-0849	Line failure
25 Feb	1240-1245	Line failure
7 Mar	2010-2017	Line failure
12 Mar	2232-2238	Line failure
24 Mar	1006-1200	Hardware failure

26 Mar	0920-1739	Hardware failure
27 Mar	0624-0757	Hardware failure
27 Mar	1043-1349	Hardware maintenance

Table 3.3.1 The main interruptions in recording of FINESA data at NDPC, 1 October 1990 – 31 March 1991.

Monthly uptimes for the FINESA on-line data recording task, taking into account all factors (field installations, transmissions line, data center operation) affecting this task were as follows:

October	:	97.0%
November	:	99.8%
December	:	99.9%
January	:	98.7%
February	:	99.9%
March	:	97.8%

Fig. 3.3.1 shows the uptime for the data recording task, or equivalently, the availability of FINESA data in our tape archive, on a day-by-day basis, for the reporting period.

J. Torstveit

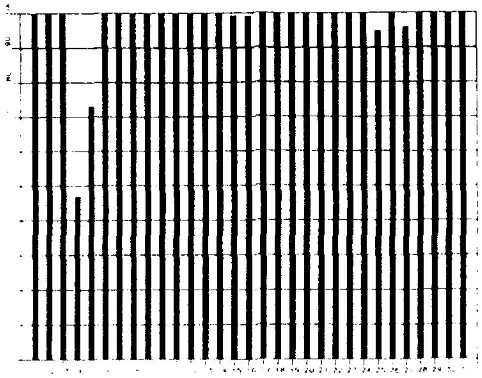

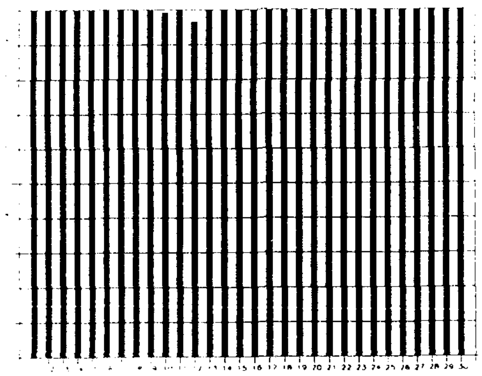

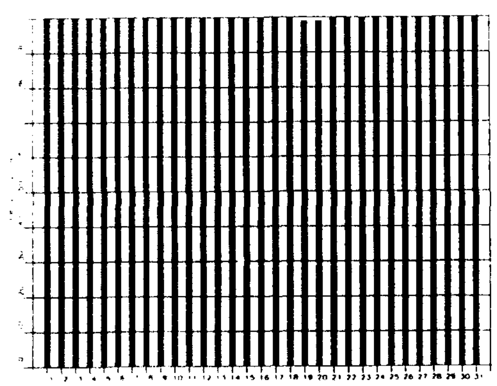

Fig. 3.3.1. FINESA data recording uptime for October (top), November (middle) and December (bottom) 1990.

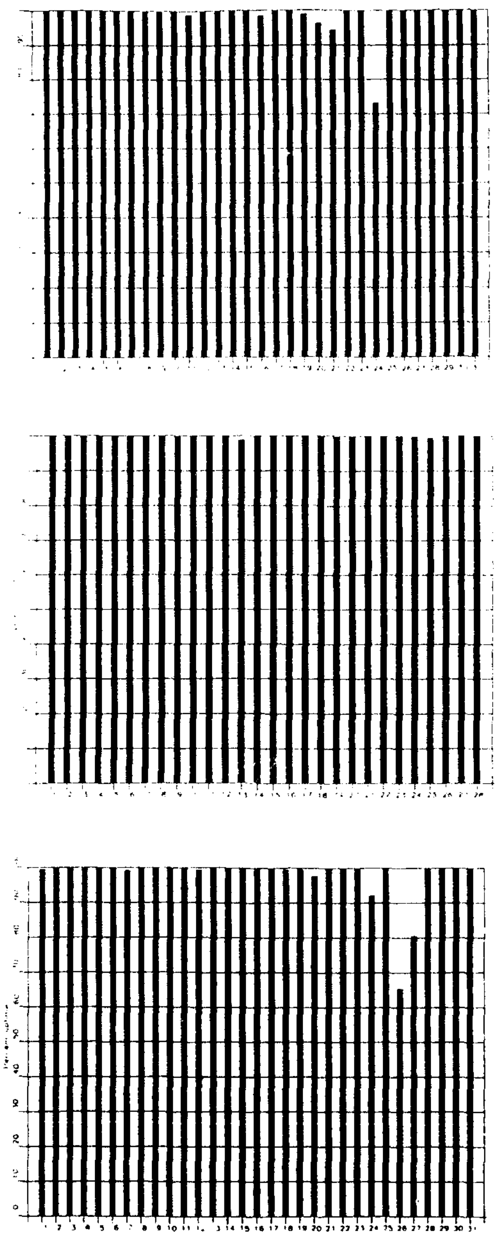

Fig. 3.3.1. (cont.) FINESA data recording uptime for January (top), February (middle) and March (bottom) 1991.

3.4 Event detection operation

This section reports on results from simple one-array automatic processing using signal processing recipes and the 'ronap' recipes for the ep program, as described in NORSAR Sci. Rep. No. 2-88/89.

IMS results are reported in Section 3.5.

NORESS detections

The number of detections (phases) reported during day 274, 1990, through day 090, 1991, was 39990, giving an average of 220 detections per processed day (182 days processed).

Table 3.4.1 shows daily and hourly distribution of detections for NORESS.

Events automatically located by NORESS

During days 274, 1990, through 090, 1991, 2298 local and regional events were located by NORESS, based on automatic association of P- and S-type arrivals. This gives an average of 12.6 events per processed day (182 days processed). 58 % of these events are within 300 km, and 87 % of these events are within 1000 km.

ARCESS detections

The number of detections (phases) reported during day 274, 1990, through day 090, 1991, was 64359, giving an average of 354 detections per processed day (182 days processed).

Table 3.4.2 shows daily and hourly distribution of detections for ARCESS.

Events automatically located by ARCESS

During days 274, 1991, through 090, 1991, 3446 local and regional events were located by ARCESS, based on automatic association of P- and S-type arrivals. This gives an average of 18.9 events per processed day (182 days processed). 53 % of these events are within 300 km, and 86 % of these events are within 1000 km.

FINESA detections

The number of detections (phases) reported during day 274, 1990, through day 090, 1991, was 60547, giving an average of 333 detections per processed day (182 days processed).

Table 3.4.3 shows daily and hourly distribution of detections for FINESA.

Events automatically located by FINESA

During days 274, 1990, through 090, 1991, 3838 local and regional events were located by FINESA, based on automatic association of P and S type arrivals. This gives an average of 21.1 events per processed day (182 days processed). 72 % of these events are within 300 km, and 88 % of these events are within 1000 km.

GERESS detections

The number of detections (phases) reported during day 274, 1990, through day 090, 1991, was 21480, giving an average of 185 detections per processed day (116 days processed).

Table 3.4.4 shows daily and hourly distribution of detections for GERESS.

Events automatically located by GERESS

During days 292, 1990, through 090, 1991, 1181 local and regional events were located by GERESS, based on automatic association of P and S type arrivals. This gives an average of 10.7 events per processed day (110 days processed). 68 % of these events are within 300 km, and 83 % of these events are within 1000 km.

J. Fyen

NRS .FKX Hourly distribution of detections

Day	00	01	02	03	04	05	06	07	08	09	10	11	12	13	14	15	16	17	18	19	20	21	22	23	Sum	Date
274	21	3	7	6	4	7	4	3	12	5	10	7	8	17	9	13	11	12	10	3	1	12	3	2	190	Oct 01 Monday
275	3	4	0	6	3	6	4	5	11	19	4	5	9	14	15	17	14	15	8	16	5	0	6	2	191	Oct 02 Tuesday
276	9	4	1	6	6	6	4	19	10	28	19	12	11	13	10	5	9	17	11	8	3	1	4	5	221	Oct 03 Wednesday
277	8	4	3	2	5	2	2	3	8	11	2	4	12	12	5	8	9	12	6	9	1	0	1	2	131	Oct 04 Thursday
278	11	2	1	12	6	3	5	3	5	5	8	17	5	13	4	12	6	11	15	8	1	5	3	4	165	Oct 05 Friday
279	9	3	4	13	5	2	5	5	1	9	10	7	8	6	23	19	5	8	1	5	6	4	1	6	165	Oct 06 Saturday
280	5	1	5	7	13	19	8	8	10	11	4	5	3	3	4	6	6	14	14	4	2	2	1	7	162	Oct 07 Sunday
281	5	11	2	1	8	4	2	6	6	4	6	3	21	12	12	17	7	9	17	5	5	14	6	5	188	Oct 08 Monday
282	4	6	7	4	6	5	2	6	7	10	11	4	11	23	13	1	8	11	16	9	2	1	2	5	174	Oct 09 Tuesday
283	10	6	0	6	2	6	8	4	12	5	11	12	11	21	8	4	6	13	6	12	2	3	1	1	170	Oct 10 Wednesday
284	7	5	3	3	3	2	1	3	2	10	7	14	14	11	11	10	3	9	6	8	0	0	0	6	138	Oct 11 Thursday
285	9	4	2	23	1	10	2	4	4	18	9	19	13	15	0	0	0	10	16	23	4	0	3	6	185	Oct 12 Friday
286	15	2	1	5	12	0	5	6	2	7	4	3	1	19	12	3	3	2	5	1	2	2	2	4	118	Oct 13 Saturday
287	1	1	7	4	3	7	12	1	8	6	4	3	3	17	3	7	5	15	15	0	3	5	2	3	135	Oct 14 Sunday
288	16	7	9	17	4	8	6	1	7	20	8	5	13	23	10	4	7	11	11	4	9	16	2	4	222	Oct 15 Monday
289	12	3	5	6	6	8	5	3	12	9	9	3	18	11	24	2	2	8	12	15	1	0	1	4	179	Oct 16 Tuesday
290	10	1	2	10	2	2	3	6	0	13	2	2	28	15	22	38	7	9	3	2	5	16	6	6	190	Oct 17 Wednesday
291	26	2	3	1	9	11	17	2	14	16	18	14	28	40	33	15	3	14	7	14	21	12	20	15	355	Oct 18 Thursday
292	8	1	2	6	3	4	4	15	22	18	15	13	32	10	8	0	10	17	7	10	15	6	3	3	232	Oct 19 Friday
293	12	2	0	16	1	8	6	13	14	3	8	15	5	9	7	5	3	9	0	1	3	9	2	1	152	Oct 20 Saturday
294	6	1	3	2	2	5	4	2	1	6	7	9	2	2	5	5	8	19	18	7	1	4	2	3	124	Oct 21 Sunday
295	20	4	10	14	1	15	11	16	1	22	14	6	24	17	25	12	12	10	12	1	0	16	1	1	265	Oct 22 Monday
296	13	26	14	11	16	12	7	19	1	21	1	22	17	22	5	20	6	26	10	10	17	6	2	2	306	Oct 23 Tuesday
297	9	3	0	11	4	6	9	3	8	6	7	13	26	12	9	25	11	16	6	1	13	6	2	11	217	Oct 24 Wednesday
298	15	8	7	14	4	10	6	1	4	8	7	24	12	16	18	7	6	11	3	5	10	10	9	6	221	Oct 25 Thursday
299	21	3	6	19	2	16	4	8	8	10	12	12	9	18	14	7	2	14	30	9	9	19	5	5	262	Oct 26 Friday
300	21	7	8	12	7	1	3	8	4	9	2	5	7	6	5	6	11	6	1	3	6	9	4	2	153	Oct 27 Saturday
301	1	4	5	5	1	7	3	6	6	6	8	27	25	17	7	15	9	13	17	2	13	2	4	6	209	Oct 28 Sunday
302	9	2	8	15	0	3	4	1	7	14	4	3	3	10	9	15	6	65	19	0	3	0	3	1	204	Oct 29 Monday
303	16	11	21	44	56	16	4	5	11	15	10	2	13	14	23	8	2	11	6	3	12	3	0	7	313	Oct 30 Tuesday
304	6	1	0	16	4	5	8	3	5	10	28	9	12	32	9	18	5	23	19	2	4	17	1	2	239	Oct 31 Wednesday
305	10	4	0	12	3	4	3	2	11	6	7	5	7	8	14	9	2	13	18	2	15	1	4	1	161	Nov 01 Thursday
306	8	7	1	6	4	8	9	11	13	7	14	13	8	22	11	8	3	12	15	5	5	3	15	1	209	Nov 02 Friday
307	13	9	1	8	7	1	9	24	4	3	8	11	5	10	7	5	10	7	5	0	5	1	4	6	163	Nov 03 Saturday
308	3	3	3	2	4	3	4	2	3	5	11	6	4	1	10	12	6	9	19	3	5	7	6	4	135	Nov 04 Sunday
309	9	4	5	14	3	4	7	1	6	5	1	6	16	17	14	5	4	15	9	8	8	20	1	4	186	Nov 05 Monday
310	14	2	1	13	4	7	2	1	56	34	6	17	19	19	7	24	7	15	19	20	25	5	11	7	335	Nov 06 Tuesday
311	19	4	6	11	5	9	3	3	3	4	1	8	7	17	12	10	4	15	4	7	16	2	1	1	172	Nov 07 Wednesday
312	9	0	0	7	0	7	7	2	8	8	13	5	8	28	15	13	8	18	7	3	13	5	4	7	193	Nov 08 Thursday
313	14	6	4	21	8	9	6	2	6	9	3	4	21	21	15	6	0	15	5	24	2	18	2	3	224	Nov 09 Friday
314	7	7	2	3	11	1	15	16	4	7	5	27	8	15	11	10	6	13	19	8	8	8	10	7	228	Nov 10 Saturday
315	3	20	27	23	23	0	10	13	4	8	18	21	13	13	10	11	2	17	15	7	4	7	7	8	284	Nov 11 Sunday
316	13	5	1	21	5	4	8	3	8	4	3	9	20	23	10	14	22	9	13	2	2	13	0	1	213	Nov 12 Monday
317	10	2	6	12	3	4	9	2	6	7	8	10	19	28	21	25	9	9	5	6	8	9	3	1	221	Nov 13 Tuesday
318	8	3	5	7	4	3	4	5	7	8	12	16	26	26	23	20	6	8	18	6	6	8	2	5	236	Nov 14 Wednesday
319	6	3	8	21	7	16	12	8	16	12	6	17	16	22	16	16	8	15	6	3	6	18	11	3	272	Nov 15 Thursday
320	7	9	5	13	4	3	6	9	9	9	7	5	23	11	12	12	5	6	15	18	8	12	3	12	223	Nov 16 Friday
321	6	2	5	9	1	1	6	13	4	11	2	3	9	6	6	11	2	1	3	3	3	3	5	6	121	Nov 17 Saturday
322	4	5	2	2	4	6	10	16	5	6	3	13	6	0	10	10	9	17	9	8	10	6	4	3	168	Nov 18 Sunday
323	29	13	9	19	7	12	18	9	5	8	10	10	13	20	18	1	14	20	24	18	23	14	0	4	318	Nov 19 Monday
324	10	8	1	21	8	8	5	6	2	8	7	4	16	16	5	12	1	14	11	8	8	10	16	8	213	Nov 20 Tuesday
325	11	7	2	11	1	5	5	4	9	13	5	5	18	21	12	7	16	18	8	4	9	9	26	7	233	Nov 21 Wednesday
326	8	3	3	9	7	11	11	8	11	8	3	9	7	17	23	14	11	14	9	10	6	19	4	16	241	Nov 22 Thursday
327	11	10	14	12	8	15	10	13	13	26	6	9	11	18	16	18	15	27	32	31	34	33	43	6	431	Nov 23 Friday
328	21	6	4	17	2	2	5	10	11	11	9	12	7	4	11	4	0	3	4	4	7	7	8	5	174	Nov 24 Saturday
329	6	3	13	11	11	11	1	2	5	7	7	6	6	3	5	4	6	12	13	1	3	2	3	1	142	Nov 25 Sunday

Table 3.4.1. (Page 1 of 4)

NRS .FKX Hourly distribution of detections

Day	00	01	02	03	04	05	06	07	08	09	10	11	12	13	14	15	16	17	18	19	20	21	22	23	Sum	Date		
330	6	2	0	13	3	3	2	5	6	10	5	9	12	3	20	14	5	4	13	6	2	0	5	0	148	Nov 26	Monday	
331	0	0	0	0	0	0	2	7	5	4	19	13	30	20	14	20	6	12	9	3	8	7	1	9	189	Nov 27	Tuesday	
332	13	0	3	7	6	15	6	2	4	13	16	20	0	0	4	0	0	6	7	8	3	13	5	0	151	Nov 28	Wednesday	
333	10	17	26	26	15	5	5	3	7	3	7	6	22	10	13	5	1	11	7	3	1	6	1	1	211	Nov 29	Thursday	
334	6	0	2	8	11	3	2	2	5	4	12	10	19	7	17	9	4	4	12	6	19	31	13	4	210	Nov 30	Friday	
335	18	3	4	9	18	21	16	21	16	10	11	7	6	6	5	5	2	11	47	32	28	1	5	3	305	Dec 01	Saturday	
336	1	3	3	1	0	6	4	14	14	6	8	2	3	3	11	3	3	4	4	1	1	3	3	8	109	Dec 02	Sunday	
337	6	7	4	11	1	3	7	3	3	4	2	0	8	5	13	25	39	27	10	9	3	7	5	6	208	Dec 03	Monday	
338	9	8	9	4	3	8	6	7	36	33	13	20	24	13	19	15	6	7	4	11	19	30	20	31	355	Dec 04	Tuesday	
339	26	18	19	31	29	24	10	15	6	15	14	12	14	8	5	5	11	3	10	17	32	40	37	21	422	Dec 05	Wednesday	
340	12	4	3	0	10	3	5	2	5	4	9	10	9	10	12	7	4	7	2	5	1	4	4	3	135	Dec 06	Thursday	
341	4	1	2	2	2	3	4	3	16	14	30	18	10	16	13	7	20	27	15	33	29	20	7	6	302	Dec 07	Friday	
342	7	5	0	7	9	5	8	8	2	8	7	11	11	6	23	4	4	8	29	28	47	50	51	48	386	Dec 08	Saturday	
343	17	9	11	[illegible]	8	[illegible]	[illegible]	6	1	7	6	16	8	14	11	4	4	11	8	0	2	4	3	3	176	Dec 09	Sunday	
344	12	7	1	8	8	1	3	5	1	4	6	6	16	24	12	12	9	34	13	12	5	1	0	11	213	Dec 10	Monday	
345	27	34	44	96	33	3	10	6	6	7	6	4	7	27	24	6	4	10	9	2	10	1	3	3	402	Dec 11	Tuesday	
346	9	1	[illegible]	4	1	3	2	14	8	35	1	21	19	23	7	11	3	8	7	1	7	12	6	8	211	Dec 12	Wednesday	
347	11	25	15	[illegible]	2	12	28	12	13	12	10	20	17	17	22	10	8	11	9	0	26	6	9	9	329	Dec 13	Thursday	
348	6	5	8	10	2	13	8	17	5	7	16	23	53	23	7	8	5	12	11	10	1	18	6	3	277	Dec 14	Friday	
349	9	4	4	9	9	3	4	3	10	10	14	8	14	2	14	5	13	14	4	8	9	9	4	3	186	Dec 15	Saturday	
350	4	7	5	2	10	5	7	8	9	13	16	11	8	20	17	18	20	23	24	15	9	8	13	19	291	Dec 16	Sunday	
351	12	7	11	11	13	18	15	23	12	12	11	13	17	16	17	18	23	26	8	2	2	11	4	1	303	Dec 17	Monday	
352	6	6	6	7	6	4	7	8	16	0	10	7	19	16	17	10	2	6	11	5	14	2	4	6	195	Dec 18	Tuesday	
353	7	5	0	10	4	1	6	3	20	23	15	23	27	27	15	13	6	7	2	11	12	13	13	21	284	Dec 19	Wednesday	
354	5	4	0	7	6	7	2	20	17	15	16	18	24	34	36	7	11	16	10	11	6	7	10	4	293	Dec 20	Thursday	
355	14	4	9	8	14	9	6	8	6	8	14	10	30	29	10	11	15	18	23	10	11	7	5	4	283	Dec 21	Friday	
356	16	9	3	4	1	1	4	8	6	8	13	10	12	16	8	8	11	8	14	9	7	5	3	12	196	Dec 22	Saturday	
357	6	4	4	7	4	9	4	0	6	3	0	1	0	7	6	7	2	9	12	1	2	7	3	1	105	Dec 23	Sunday	
358	2	0	8	3	2	3	10	6	7	5	4	4	14	4	6	2	6	4	12	7	6	4	8	4	131	Dec 24	Monday	
359	4	7	4	4	13	9	2	3	9	4	6	*10*	*17*	*6*	*8*	*4*	*3*	*5*	*0*	2	6	2	3	6	137	*Dec 25*	*Tuesday*	*F:rste*
360	6	5	3	2	2	3	5	8	11	12	20	12	22	10	10	22	8	11	13	9	5	2	11	3	215	Dec 26	Wednesday	*Andre*
361	14	1	6	2	2	6	8	9	16	8	14	17	10	10	5	2	4	15	7	1	5	2	0	3	167	Dec 27	Thursday	
362	7	6	6	7	4	1	6	5	3	11	18	21	12	8	9	9	6	12	4	5	4	1	8	7	180	Dec 28	Friday	
363	13	3	10	7	9	5	5	8	6	10	9	17	9	7	5	8	2	3	3	12	3	12	7	4	177	Dec 29	Saturday	
364	3	3	3	10	20	20	15	18	7	14	3	7	7	6	1	2	1	9	13	31	13	9	5	8	228	Dec 30	Sunday	
365	8	25	42	39	21	24	16	33	27	17	13	22	19	30	20	20	20	30	35	27	34	28	21	44	615	Dec 31	Monday	
1	33	14	10	4	8	16	4	16	5	5	5	3	5	5	4	18	12	15	12	18	6	9	1	10	238	Jan 01	Tuesday	F:rste
2	9	8	4	7	5	2	1	3	7	8	2	7	5	8	6	4	1	11	14	8	2	1	0	0	123	Jan 02	Wednesday	
3	9	2	1	0	5	3	6	7	5	14	4	15	7	11	8	7	0	7	6	8	2	2	4	3	136	Jan 03	Thursday	
4	6	2	4	5	5	5	10	6	5	4	11	10	9	16	10	3	10	5	4	6	6	1	2	1	146	Jan 04	Friday	
5	5	2	4	3	2	2	1	7	1	3	4	4	10	4	10	19	12	2	8	11	3	6	3	3	129	Jan 05	Saturday	
6	4	4	3	8	1	2	14	2	1	7	3	5	2	9	5	3	2	14	5	0	0	1	10	2	107	Jan 06	Sunday	
7	10	5	2	16	5	4	6	18	11	11	13	20	13	21	20	17	15	7	11	1	1	3	19	25	274	Jan 07	Monday	
8	11	57	4	6	2	4	5	7	8	16	25	5	7	22	12	4	3	10	8	19	2	1	17	5	260	Jan 08	Tuesday	
9	6	12	4	6	17	7	7	19	16	18	10	11	13	32	22	12	3	7	8	5	1	2	0	3	241	Jan 09	Wednesday	
10	5	6	0	4	4	3	12	15	8	25	18	10	8	22	15	0	7	8	3	11	9	2	2	4	201	Jan 10	Thursday	
11	6	4	6	6	6	5	10	6	11	12	15	12	11	3	7	3	8	7	6	15	6	7	1	2	175	Jan 11	Friday	
12	5	4	3	8	1	10	10	20	4	5	10	10	24	7	14	9	17	14	13	11	14	19	20	17	269	Jan 12	Saturday	
13	19	21	31	23	26	16	34	41	28	11	11	5	13	5	17	23	29	30	23	13	15	13	22	14	483	Jan 13	Sunday	
14	12	7	11	17	13	18	8	19	12	5	6	5	9	8	16	24	14	21	28	19	10	10	9	7	308	Jan 14	Monday	
15	7	9	4	8	5	6	6	1	0	12	3	19	24	8	18	7	12	14	6	5	3	6	9	4	196	Jan 15	Tuesday	
16	3	2	7	18	16	12	11	17	6	8	16	13	22	9	15	6	2	7	3	3	7	2	3	2	210	Jan 16	Wednesday	
17	4	5	3	4	8	0	4	2	15	17	17	45	11	14	20	5	2	10	6	5	10	3	4	2	214	Jan 17	Thursday	
18	9	6	1	1	0	6	4	0	7	9	10	17	18	10	8	10	1	14	5	14	4	3	2	4	165	Jan 18	Friday	
19	7	4	1	7	3	1	1	8	3	4	6	6	8	5	3	1	6	5	12	4	6	26	16	13	156	Jan 19	Saturday	
20	8	4	5	3	6	4	3	4	8	5	12	18	6	4	5	12	1	7	5	9	7	4	9	16	165	Jan 20	Sunday	

Table 3.4.1. (Page 2 of 4)

NHS FKX hourly distribution of detections

Day	00	01	02	03	04	05	06	07	08	09	10	11	12	13	14	15	16	17	18	19	20	21	22	23	Sum	Date
21	10	16	34	31	19	21	14	13	11	13	18	9	13	35	19	10	20	39	21	22	10	7	3	4	412	Jan 21 Monday
22	10	7	6	10	8	8	9	6	3	5	9	4	16	10	20	19	2	9	7	9	1	3	11	8	200	Jan 22 Tuesday
23	8	23	41	20	16	9	13	2	2	4	8	5	21	11	14	12	1	5	3	9	1	1	3	5	226	Jan 23 Wednesday
24	22	18	19	16	11	3	7	4	6	13	6	6	25	16	12	9	6	13	11	5	9	15	14	10	276	Jan 24 Thursday
25	8	7	5	23	11	25	17	4	10	5	4	16	12	18	8	4	4	5	4	9	4	5	2	4	214	Jan 25 Friday
26	11	10	7	14	22	28	23	17	13	13	9	16	4	4	5	7	8	8	11	6	4	10	6	18	274	Jan 26 Saturday
27	21	29	26	34	39	56	43	39	28	12	14	16	10	9	5	13	14	8	17	6	13	2	5	5	464	Jan 27 Sunday
28	8	4	5	16	8	3	7	8	8	12	5	8	11	18	8	7	9	6	12	18	24	21	38	29	293	Jan 28 Monday
29	44	31	25	25	8	7	2	3	6	9	7	16	13	7	14	8	2	2	7	4	8	10	12	0	270	Jan 29 Tuesday
30	2	2	3	2	0	3	4	4	4	16	6	2	3	16	15	5	0	4	7	5	12	4	2	5	126	Jan 30 Wednesday
31	4	3	9	4	1	6	3	2	9	6	7	11	18	24	16	5	9	7	10	16	11	11	13	15	220	Jan 31 Thursday
32	11	12	14	9	7	4	4	2	2	9	14	21	25	8	9	4	9	0	1	1	12	3	1	2	184	Feb 01 Friday
33	3	0	2	2	7	3	8	6	0	12	4	12	4	3	11	4	1	3	10	5	0	5	3	6	109	Feb 02 Saturday
34	1	2	2	2	5	8	5	2	3	3	5	5	2	2	4	0	9	5	2	3	3	0	2	11	86	Feb 03 Sunday
35	10	12	12	13	15	5	6	2	6	3	7	12	8	18	10	5	7	15	11	17	20	8	11	16	239	Feb 04 Monday
36	13	7	7	10	21	18	6	12	7	18	14	7	6	16	8	3	2	5	5	7	12	14	27	38	283	Feb 05 Tuesday
37	35	45	53	67	56	39	21	10	14	7	14	13	10	38	35	6	1	2	7	5	7	14	30	30	559	Feb 06 Wednesday
38	26	51	62	57	69	49	35	29	53	23	68	46	3	38	41	12	2	12	3	20	28	44	50	84	905	Feb 07 Thursday
39	57	[illegible]	[illegible]	95	88	69	56	49	41	25	55	39	12	9	5	6	6	1	1	5	13	4	3	4	840	Feb 08 Friday
40	5	9	6	2	3	4	4	2	7	3	8	4	2	5	5	1	11	7	2	3	5	3	2	6	109	Feb 09 Saturday
41	6	19	6	4	5	2	1	4	5	3	5	1	6	4	13	1	2	5	3	8	8	5	0	9	116	Feb 10 Sunday
42	9	4	2	2	2	2	0	30	13	28	44	24	34	54	46	16	7	3	1	5	3	4	1	3	337	Feb 11 Monday
43	5	1	2	2	11	4	3	41	39	51	74	57	17	59	51	15	2	0	1	4	1	6	6	5	458	Feb 12 Tuesday
44	6	1	1	2	4	7	7	28	18	35	46	31	19	43	25	14	7	9	2	8	4	10	4	9	340	Feb 13 Wednesday
45	9	14	15	13	18	15	8	25	17	15	21	19	21	33	21	4	9	0	2	14	1	0	3	3	300	Feb 14 Thursday
46	10	4	13	5	17	12	9	32	24	39	48	29	19	16	14	2	5	14	4	14	5	12	2	2	350	Feb 15 Friday
47	4	7	9	6	4	1	4	3	4	7	8	13	13	21	2	7	9	10	4	3	7	4	1	1	152	Feb 16 Saturday
48	3	7	6	12	7	1	11	10	6	6	11	7	9	10	6	2	1	2	2	2	9	5	3	5	143	Feb 17 Sunday
49	10	1	15	13	8	3	7	14	30	12	21	10	17	10	29	1	15	2	4	0	1	7	2	9	243	Feb 18 Monday
50	4	3	4	11	2	9	5	8	6	6	15	20	7	9	18	5	15	1	1	12	0	0	3	3	167	Feb 19 Tuesday
51	7	3	0	0	13	12	2	4	1	8	19	9	14	18	12	4	11	1	0	7	6	10	7	3	171	Feb 20 Wednesday
52	1	4	14	3	7	2	4	0	5	5	2	13	25	16	7	11	0	1	2	5	2	2	4	5	140	Feb 21 Thursday
53	6	10	1	2	14	0	0	1	7	6	9	22	11	8	11	8	4	3	5	12	4	6	4	1	155	Feb 22 Friday
54	4	0	2	1	3	2	9	2	7	8	5	3	14	5	3	5	4	4	3	3	5	0	7	2	101	Feb 23 Saturday
55	12	8	3	1	5	3	1	1	9	1	4	7	5	6	2	1	2	2	5	7	2	2	4	2	95	Feb 24 Sunday
56	2	4	3	5	1	2	5	5	1	3	27	6	12	12	14	12	4	8	7	10	6	6	9	9	173	Feb 25 Monday
57	9	12	16	8	13	5	3	9	7	3	1	16	7	9	7	8	10	9	5	14	7	20	17	25	240	Feb 26 Tuesday
58	27	28	34	22	30	13	6	6	9	11	14	11	24	10	10	12	7	13	4	8	3	7	6	5	320	Feb 27 Wednesday
59	2	8	9	5	5	9	3	5	5	5	4	13	14	11	20	9	3	7	5	9	16	4	3	3	177	Feb 28 Thursday
60	3	1	4	7	3	2	5	2	8	11	10	9	14	14	13	6	4	13	6	14	4	13	2	6	174	Mar 01 Friday
61	7	0	0	0	0	0	0	0	0	0	0	0	0	0	0	5	7	3	3	3	3	2	2	9	44	Mar 02 Saturday
62	2	4	3	0	0	1	5	3	8	9	7	1	3	4	6	7	5	3	6	17	17	2	0	6	119	Mar 03 Sunday
63	3	2	4	2	3	1	1	6	6	6	6	12	9	5	5	10	5	5	6	9	7	9	2	10	134	Mar 04 Monday
64	10	6	3	9	8	9	1	5	5	14	9	6	25	22	22	4	10	6	6	11	6	3	10	6	216	Mar 05 Tuesday
65	4	2	8	3	4	6	5	2	1	7	6	13	20	19	12	4	12	4	3	2	4	3	10	2	156	Mar 06 Wednesday
66	5	11	2	3	6	2	0	5	5	1	6	17	13	0	7	12	4	2	3	5	6	7	0	6	128	Mar 07 Thursday
67	7	12	1	5	8	1	2	3	6	4	4	18	23	24	22	11	7	3	10	11	5	9	5	9	210	Mar 08 Friday
68	11	11	1	7	11	8	9	3	4	8	8	6	3	6	1	4	18	6	6	4	5	2	2	3	147	Mar 09 Saturday
69	5	16	2	10	6	0	6	4	3	1	0	5	7	8	4	5	5	3	3	11	2	5	10	5	126	Mar 10 Sunday
70	3	1	0	10	6	5	6	3	6	4	4	11	4	4	10	7	1	7	9	5	2	19	0	3	130	Mar 11 Monday
71	4	6	1	8	2	4	9	6	8	17	7	8	9	20	5	4	3	7	10	8	4	8	1	1	160	Mar 12 Tuesday
72	2	5	4	7	7	2	4	2	10	6	8	5	16	4	21	7	5	7	2	14	3	2	3	5	151	Mar 13 Wednesday
73	5	3	0	5	2	2	2	0	2	6	5	13	9	11	10	8	13	11	3	11	3	16	9	15	164	Mar 14 Thursday
74	12	9	5	7	3	13	6	9	4	14	10	18	15	12	14	8	2	0	4	13	5	3	4	3	193	Mar 15 Friday
75	15	2	7	12	6	3	7	2	4	2	3	4	12	10	8	8	5	1	3	4	2	4	1	1	126	Mar 16 Saturday
76	10	2	1	11	3	2	4	6	3	0	2	1	1	9	5	3	6	3	0	9	6	4	4	2	97	Mar 17 Sunday

Table 3.4.1. (Page 3 of 4)

NRS .FKX Hourly distribution of detections

Day	00	01	02	03	04	05	06	07	08	09	10	11	12	13	14	15	16	17	18	19	20	21	22	23	Sum	Date	
77	6	4	3	9	2	2	3	4	6	5	2	6	5	4	12	7	9	7	12	8	2	2	1	4	125	Mar 18 Monday	
78	7	2	11	4	2	4	5	5	2	6	7	15	23	18	11	6	2	4	2	8	11	7	8	5	175	Mar 19 Tuesday	
79	4	1	6	1	6	0	0	2	1	3	10	7	14	10	16	4	9	8	7	11	6	5	2	0	133	Mar 20 Wednesday	
80	10	1	18	6	2	3	4	4	3	2	12	17	29	12	12	6	5	9	11	3	7	5	3	2	186	Mar 21 Thursday	
81	5	1	4	8	0	2	2	4	14	13	11	20	16	6	4	1	3	7	5	6	5	13	12	4	166	Mar 22 Friday	
82	13	4	1	12	2	3	8	7	4	7	5	6	10	3	8	3	7	4	3	6	10	3	1	1	131	Mar 23 Saturday	
83	4	3	0	1	14	1	2	2	0	1	5	6	5	20	2	3	6	3	5	3	2	7	4	8	107	Mar 24 Sunday	
84	12	6	6	9	11	3	2	3	16	12	2	6	3	5	4	10	6	6	4	9	25	7	10	4	181	Mar 25 Monday	
85	5	3	4	3	13	8	5	6	5	0	14	9	19	28	15	9	8	4	11	18	11	8	9	5	220	Mar 26 Tuesday	
86	3	18	10	9	4	15	6	5	5	15	11	12	18	32	10	4	3	8	20	11	4	7	19	4	253	Mar 27 Wednesday	
87	6	4	7	15	2	5	5	5	4	11	1	9	15	10	11	4	1	12	15	6	4	7	5	3	167	Mar 28 Thursday	Skj(rt
88	10	19	26	19	21	14	3	12	8	12	12	16	20	14	8	5	11	8	4	8	3	6	2	12	273	Mar 29 Friday	Langfr
89	7	10	5	6	0	3	6	6	4	5	9	12	9	18	10	13	5	7	9	5	5	9	18	10	191	Mar 30 Saturday	
90	9	19	15	14	10	10	13	3	5	9	3	0	2	1	4	3	5	2	5	1	0	3	1	10	147	Mar 31 Sunday	F:rste

NRS	00	01	02	03	04	05	06	07	08	09	10	11	12	13	14	15	16	17	18	19	20	21	22	23		
Sum	1795	1396	1393	1967	1527	1388	1279	1487	1568	1833	1898	2094	2368	2574	2234	1576	1258	1833	1647	1521	1382	1438	1238	1296	39990	Total sum
182	10	8	8	11	8	8	7	8	9	10	10	12	13	14	12	9	7	10	9	8	8	8	7	7	220	Total average
125	10	8	8	12	9	8	7	8	10	12	12	13	15	17	14	9	7	11	9	9	8	9	7	7	240	Average workdays
57	9	6	6	8	7	7	8	9	6	7	7	9	8	8	8	7	7	8	9	7	7	6	6	7	176	Average weekends

Table 3.4.1. Daily and hourly distribution of NORESS detections. For each day is shown number of detections within each hour of the day, and number of detections for that day. The end statistics give total number of detections distributed for each hour and the total sum of detections during the period. The averages show number of processed days, hourly distribution and average per processed day. (Page 4 of 4)

ARC .FKX Hourly distribution of detections

Day	00	01	02	03	04	05	06	07	08	09	10	11	12	13	14	15	16	17	18	19	20	21	22	23	Sum	Date
274	5	7	10	3	7	14	10	17	24	34	22	23	21	34	33	31	22	32	27	17	6	9	22	23	453	Oct 01 Monday
275	3	4	10	8	18	12	14	10	33	20	23	32	45	28	42	37	18	9	22	14	18	16	24	19	479	Oct 02 Tuesday
276	10	5	6	8	10	31	0	0	0	0	0	0	0	0	0	0	0	0	0	9	11	1	23	15	129	Oct 03 Wednesday
277	7	10	12	6	11	30	13	7	26	15	29	30	25	40	21	11	15	20	8	18	25	16	12	23	430	Oct 04 Thursday
278	27	19	16	36	10	10	13	14	27	28	29	29	37	10	0	0	3	18	15	11	8	0	2	8	373	Oct 05 Friday
279	13	4	9	8	6	13	12	11	16	15	32	18	30	13	33	15	3	10	12	17	14	3	4	26	337	Oct 06 Saturday
280	10	8	5	5	16	11	4	3	5	6	2	10	29	12	22	22	20	17	17	15	19	3	9	20	290	Oct 07 Sunday
281	5	10	9	6	12	10	21	5	16	15	6	11	16	18	27	15	20	17	5	10	13	25	26	31	349	Oct 08 Monday
282	34	38	44	54	61	53	24	8	27	8	26	32	23	16	10	10	6	12	8	4	8	6	17	22	551	Oct 09 Tuesday
283	7	21	3	7	5	11	16	15	8	15	25	16	18	28	23	19	6	11	9	19	14	7	10	7	320	Oct 10 Wednesday
284	2	2	6	10	12	9	22	10	7	10	14	22	27	7	32	21	17	14	3	9	4	19	10	30	319	Oct 11 Thursday
285	4	11	5	9	8	10	5	9	10	38	18	16	35	26	13	8	15	11	10	11	6	10	23	22	333	Oct 12 Friday
286	44	8	23	30	40	36	5	13	9	5	14	22	8	18	6	12	2	1	14	1	9	4	4	21	349	Oct 13 Saturday
287	12	1	9	1	3	7	19	2	5	7	8	5	6	14	7	7	13	13	6	18	24	6	12	32	237	Oct 14 Sunday
288	18	11	5	4	5	12	11	10	16	12	3	6	24	21	14	18	17	9	7	12	16	11	15	18	295	Oct 15 Monday
289	3	11	2	12	8	7	10	10	8	22	11	30	46	26	11	20	14	7	24	19	13	8	24	18	354	Oct 16 Tuesday
290	16	3	5	8	6	11	12	12	10	20	16	36	33	11	36	18	9	8	1	10	17	19	7	13	337	Oct 17 Wednesday
291	9	6	43	40	46	20	40	16	13	11	18	26	21	30	54	116	76	50	23	53	53	62	88	71	985	Oct 18 Thursday
292	52	12	18	90	42	23	13	24	16	29	15	18	31	30	18	11	9	8	10	11	6	11	6	17	520	Oct 19 Friday
293	7	11	9	3	4	9	19	71	16	20	14	75	35	9	19	29	8	17	14	31	166	14	19	22	641	Oct 20 Saturday
294	5	11	23	5	8	13	17	12	5	9	6	7	7	17	8	11	20	6	10	18	11	10	5	10	254	Oct 21 Sunday
295	5	1	3	10	3	3	16	19	10	11	17	15	18	0	0	3	3	3	15	7	12	8	10	21	213	Oct 22 Monday
296	8	12	7	4	9	12	2	6	18	10	14	24	24	26	34	11	10	9	3	18	14	11	6	12	304	Oct 23 Tuesday
297	13	4	13	4	6	11	7	24	19	15	19	18	29	23	14	38	17	17	11	14	20	14	11	20	381	Oct 24 Wednesday
298	3	6	9	3	11	14	10	13	4	15	12	33	13	10	15	9	29	40	14	15	11	7	16	25	337	Oct 25 Thursday
299	26	7	11	13	12	12	15	10	16	12	19	10	21	36	10	7	4	9	10	8	10	8	12	12	310	Oct 26 Friday
300	7	7	5	10	10	21	19	20	12	14	12	36	51	72	45	28	16	3	4	17	3	2	13	8	435	Oct 27 Saturday
301	3	5	10	3	4	10	17	16	23	44	54	31	11	7	8	9	9	9	10	7	7	4	13	11	325	Oct 28 Sunday
302	13	7	8	6	3	7	9	6	6	3	4	12	14	17	14	8	2	8	9	7	5	7	10	19	204	Oct 29 Monday
303	64	26	5	9	7	4	6	16	6	14	8	14	24	21	41	23	24	18	12	9	18	13	13	19	414	Oct 30 Tuesday
304	11	6	10	11	11	9	20	12	8	22	24	18	20	9	18	26	8	7	2	5	8	11	13	20	309	Oct 31 Wednesday
305	4	2	8	10	9	8	7	5	23	18	18	16	15	22	21	16	12	8	6	8	7	7	13	19	282	Nov 01 Thursday
306	13	8	15	9	4	7	6	15	8	18	18	32	32	23	12	11	10	8	5	12	19	16	15	10	326	Nov 02 Friday
307	3	4	4	5	9	4	10	11	9	8	5	21	13	7	15	12	4	5	11	8	15	4	2	14	205	Nov 03 Saturday
308	3	9	6	2	2	9	7	4	4	7	9	7	9	2	3	5	6	8	6	13	7	10	14	20	172	Nov 04 Sunday
309	10	16	7	4	9	3	4	7	20	16	5	15	14	22	16	5	10	11	17	13	3	11	6	14	258	Nov 05 Monday
310	9	9	10	4	16	7	12	1	3	18	20	7	29	6	9	6	12	8	10	18	19	9	17	22	281	Nov 06 Tuesday
311	8	8	9	3	6	6	18	4	13	6	19	13	14	3	19	13	9	15	12	20	12	9	8	14	261	Nov 07 Wednesday
312	5	6	7	4	3	3	14	12	9	4	12	8	11	9	14	22	13	16	7	1	1	10	12	20	223	Nov 08 Thursday
313	4	4	1	2	4	8	9	5	5	4	3	7	14	11	14	14	4	2	12	23	10	7	17	16	200	Nov 09 Friday
314	10	8	1	2	8	11	19	16	9	17	16	19	4	10	8	6	6	5	20	18	23	27	13	21	297	Nov 10 Saturday
315	10	3	11	4	9	2	3	21	16	13	22	14	17	16	16	9	8	10	9	20	32	15	23	29	332	Nov 11 Sunday
316	10	4	5	3	6	7	9	6	3	3	11	11	29	6	6	15	27	20	7	11	5	7	4	10	225	Nov 12 Monday
317	1	2	9	4	2	4	2	4	3	5	5	14	20	9	12	10	3	9	12	7	6	4	5	8	160	Nov 13 Tuesday
318	2	5	0	6	17	16	32	27	9	21	22	21	21	25	29	20	21	13	9	12	9	24	28	44	433	Nov 14 Wednesday
319	38	29	39	40	29	26	15	16	33	15	13	18	30	48	55	29	28	33	26	14	12	16	13	26	641	Nov 15 Thursday
320	7	27	13	4	8	6	12	24	26	21	38	21	39	22	31	19	9	14	13	16	6	10	12	20	418	Nov 16 Friday
321	3	4	8	3	15	17	15	27	13	12	25	15	15	22	9	10	2	1	15	12	14	7	14	19	297	Nov 17 Saturday
322	6	4	12	2	3	8	16	9	13	9	9	9	4	9	11	11	15	12	7	14	4	6	2	10	205	Nov 18 Sunday
323	12	4	6	9	10	8	9	7	6	15	21	15	23	22	8	16	10	23	42	44	47	41	54	46	498	Nov 19 Monday
324	27	27	22	15	3	9	8	12	21	20	23	9	40	52	46	22	29	18	14	17	17	21	18	16	506	Nov 20 Tuesday
325	8	6	8	19	4	6	11	15	18	17	14	11	34	33	14	8	6	12	10	25	10	9	14	10	322	Nov 21 Wednesday
326	18	7	9	14	4	11	16	12	17	11	12	21	31	23	14	12	14	8	9	7	11	20	11	21	333	Nov 22 Thursday
327	4	6	3	1	4	4	8	5	18	19	5	21	18	20	7	15	8	6	11	19	21	13	23	24	283	Nov 23 Friday
328	9	22	14	26	12	9	8	6	13	10	14	22	14	6	12	1	4	8	6	6	0	9	5	14	256	Nov 24 Saturday
329	3	4	2	6	14	4	15	5	2	10	11	9	7	4	10	6	3	12	9	8	3	4	20	15	186	Nov 25 Sunday

Table 3.4.2. (Page 1 of 4)

ARC .PKX Hourly distribution of detections

Day	00	01	02	03	04	05	06	07	08	09	10	11	12	13	14	15	16	17	18	19	20	21	22	23	Sum	Date	
330	4	11	7	7	6	9	10	6	11	7	17	14	27	19	14	8	15	7	10	17	11	12	9	20	278	Nov 26 Monday	
331	13	9	0	6	14	7	7	9	11	14	9	2	25	19	16	13	2	13	5	9	12	4	18	14	251	Nov 27 Tuesday	
332	7	5	3	2	7	4	8	6	10	24	18	19	29	18	9	11	5	1	10	11	3	7	13	10	240	Nov 28 Wednesday	
333	11	18	2	6	14	12	19	7	6	26	12	8	31	24	11	12	3	1	9	4	12	14	1	18	281	Nov 29 Thursday	
334	1	5	4	10	12	5	8	5	11	19	33	14	8	22	15	17	11	6	17	8	9	6	10	11	267	Nov 30 Friday	
335	4	4	7	6	1	13	4	1	13	18	14	16	12	7	17	7	6	9	23	18	12	17	29	22	280	Dec 01 Saturday	
336	9	8	2	4	5	5	5	6	13	9	9	16	10	8	6	11	7	6	12	8	1	8	8	7	183	Dec 02 Sunday	
337	10	6	6	9	6	8	14	12	15	10	6	16	8	18	19	9	6	19	15	7	15	10	12	9	265	Dec 03 Monday	
338	7	4	5	2	3	4	12	14	19	16	10	29	25	11	13	7	5	8	7	6	7	10	4	25	253	Dec 04 Tuesday	
339	4	7	7	4	4	1	4	11	9	18	8	22	8	22	10	5	17	9	9	5	13	13	6	15	231	Dec 05 Wednesday	
340	11	3	8	8	3	9	7	10	7	13	14	14	11	14	9	18	5	11	4	6	7	1	12	14	219	Dec 06 Thursday	
341	14	5	8	4	10	1	4	7	15	21	28	29	41	47	16	13	16	42	18	12	3	7	3	19	383	Dec 07 Friday	
342	4	8	7	2	9	5	8	5	13	18	11	47	47	26	18	33	45	40	42	39	47	23	16	22	535	Dec 08 Saturday	
343	5	6	2	7	10	18	13	8	6	8	3	9	6	4	5	7	10	3	5	7	2	12	8	8	172	Dec 09 Sunday	
344	2	12	5	5	6	5	7	7	8	14	42	82	76	50	39	57	26	24	31	54	36	24	49	91	752	Dec 10 Monday	
345	94	70	16	16	121	100	65	80	60	78	101	63	66	60	43	24	13	13	7	7	19	22	17	14	1169	Dec 11 Tuesday	
346	15	4	6	14	14	14	8	22	24	18	11	13	21	10	12	17	7	14	10	9	10	6	13	15	307	Dec 12 Wednesday	
347	7	9	2	5	17	15	21	22	25	19	18	14	18	12	8	7	11	21	24	32	62	41	44	55	509	Dec 13 Thursday	
348	60	78	104	25	0	0	0	0	0	0	0	0	0	0	0	0	0	0	3	14	31	8	9	9	341	Dec 14 Friday	
349	5	4	6	6	2	5	7	4	4	16	10	6	14	3	3	2	5	1	1	0	3	5	2	6	120	Dec 15 Saturday	
350	8	2	5	2	4	5	2	5	7	5	9	6	5	2	4	7	7	9	8	2	5	4	23	21	157	Dec 16 Sunday	
351	6	9	20	4	13	11	18	4	4	13	24	22	10	12	17	5	18	11	4	10	12	10	14	16	287	Dec 17 Monday	
352	6	10	6	7	8	11	4	7	4	8	12	11	15	11	10	12	10	5	5	17	12	22	14	9	236	Dec 18 Tuesday	
353	13	5	8	5	6	15	11	9	18	16	9	13	42	40	57	41	63	35	11	13	21	15	24	21	511	Dec 19 Wednesday	
354	23	51	84	94	90	84	79	58	81	64	62	32	38	26	19	9	11	17	18	4	7	8	8	19	986	Dec 20 Thursday	
355	7	7	12	10	1	3	8	22	18	45	22	21	29	45	7	5	6	14	8	10	18	6	7	17	348	Dec 21 Friday	
356	9	6	15	13	23	27	21	35	60	72	72	78	76	66	53	31	36	36	11	13	9	10	5	19	796	Dec 22 Saturday	
357	7	6	8	3	8	11	11	2	8	7	10	17	24	39	37	41	17	13	16	14	8	13	9	13	342	Dec 23 Sunday	
358	9	3	4	5	9	11	10	8	15	9	12	8	11	6	6	5	8	3	8	9	13	9	9	6	196	Dec 24 Monday	
359	5	8	8	9	5	4	6	2	2	13	7	8	14	5	19	5	7	1	3	6	18	5	7	9	176	Dec 25 Tuesday	F:rste
360	5	6	5	2	6	1	1	6	5	5	9	14	15	17	12	19	15	7	3	7	5	10	8	11	194	Dec 26 Wednesday	Andre
361	4	2	4	2	5	15	6	5	9	8	14	34	24	8	12	7	11	13	10	8	11	9	11	7	239	Dec 27 Thursday	
362	8	8	9	7	11	4	14	8	6	30	21	18	28	9	11	16	5	3	7	8	2	4	16	14	267	Dec 28 Friday	
363	5	5	8	8	10	5	16	8	11	14	8	24	15	12	5	12	4	2	7	13	5	11	8	8	224	Dec 29 Saturday	
364	7	11	5	6	3	9	11	7	6	16	5	11	11	12	11	3	1	11	37	50	29	31	78	45	416	Dec 30 Sunday	
365	14	7	22	35	27	16	19	46	54	49	39	20	10	6	7	4	11	3	7	5	12	5	7	1	426	Dec 31 Monday	
1	14	5	4	6	11	9	5	5	6	7	5	8	8	4	15	12	3	8	21	73	107	140	135	146	757	Jan 01 Tuesday	F:rste
2	120	114	109	117	114	139	132	123	54	18	23	17	32	23	12	5	6	13	11	8	9	6	23	12	1240	Jan 02 Wednesday	
3	7	6	5	2	4	13	7	5	9	15	17	11	16	26	15	19	15	24	19	8	4	17	24	21	309	Jan 03 Thursday	
4	12	22	29	24	23	26	33	14	16	14	13	19	27	21	19	22	22	37	39	38	36	49	79	54	688	Jan 04 Friday	
5	80	69	19	26	30	10	17	14	17	20	19	29	45	40	17	18	16	11	8	16	7	27	8	21	584	Jan 05 Saturday	
6	4	8	11	13	12	9	6	9	17	8	14	24	19	20	21	15	18	22	25	33	28	24	24	30	414	Jan 06 Sunday	
7	12	11	19	8	11	13	11	13	12	21	28	18	18	12	16	12	16	10	8	20	11	5	18	21	344	Jan 07 Monday	
8	11	9	10	9	12	5	16	3	6	11	25	14	19	17	10	14	7	19	16	13	15	13	15	15	304	Jan 08 Tuesday	
9	5	6	4	4	11	4	9	6	19	5	13	27	25	28	13	20	9	6	9	18	8	13	12	18	292	Jan 09 Wednesday	
10	5	16	6	12	8	8	7	8	7	22	7	10	30	9	19	15	6	10	14	13	15	28	44	46	365	Jan 10 Thursday	
11	42	63	63	71	64	63	74	58	72	71	57	67	67	56	44	42	35	35	31	28	18	23	28	23	1195	Jan 11 Friday	
12	18	14	13	17	20	15	24	6	18	15	9	6	31	10	4	5	7	7	4	5	7	8	9	11	283	Jan 12 Saturday	
13	7	5	11	11	8	3	6	10	5	4	6	5	14	9	6	4	5	11	8	11	7	9	2	11	178	Jan 13 Sunday	
14	8	12	14	20	11	22	18	16	15	30	19	18	10	4	21	29	11	24	9	5	6	19	10	22	373	Jan 14 Monday	
15	10	7	8	4	4	7	10	3	7	12	9	10	4	8	3	3	3	9	7	5	5	10	10	9	175	Jan 15 Tuesday	
16	7	9	8	6	4	6	11	10	4	7	13	18	27	20	6	13	3	8	7	10	11	13	17	10	248	Jan 16 Wednesday	
17	0	10	1	4	9	6	5	1	20	32	22	22	19	18	13	8	22	11	13	10	19	15	8	9	297	Jan 17 Thursday	
18	6	16	6	13	6	3	11	2	7	15	21	28	41	6	10	11	7	9	10	13	8	6	9	13	277	Jan 18 Friday	
19	5	5	8	11	5	5	10	5	9	15	17	19	22	10	6	2	6	7	10	3	4	15	7	21	227	Jan 19 Saturday	
20	12	9	13	10	8	8	14	7	11	2	8	13	9	4	6	8	7	7	8	20	6	3	3	10	206	Jan 20 Sunday	

Table 3.4.2. (Page 2 of 4)

ARC .FKX Hourly distribution of detections

Day	00	01	02	03	04	05	06	07	08	09	10	11	12	13	14	15	16	17	18	19	20	21	22	23	Sum	Date
21	3	7	2	4	9	4	2	5	1	5	5	5	5	3	13	6	4	9	9	1	3	6	7	15	133	Jan 21 Monday
22	3	8	7	4	0	2	7	8	4	4	0	7	29	9	6	8	7	8	6	1	9	4	2	9	152	Jan 22 Tuesday
23	4	11	7	6	2	7	12	0	4	15	4	0	18	17	8	6	3	6	7	7	6	0	7	10	167	Jan 23 Wednesday
24	4	7	10	8	1	3	10	2	14	26	13	22	29	13	10	7	17	5	13	9	15	5	4	6	253	Jan 24 Thursday
25	7	6	3	13	3	3	4	4	16	14	4	20	11	15	8	3	6	16	8	9	7	6	9	15	210	Jan 25 Friday
26	13	3	9	2	5	7	11	5	16	9	11	27	8	9	9	16	16	13	27	30	32	35	29	38	380	Jan 26 Saturday
27	16	20	11	13	6	5	15	17	6	9	9	10	11	6	16	7	12	3	6	19	10	7	4	14	252	Jan 27 Sunday
28	4	7	10	8	12	3	7	4	10	10	12	19	27	17	21	6	16	12	13	14	10	8	21	8	279	Jan 28 Monday
29	2	11	1	5	13	10	8	5	19	15	20	25	33	17	20	20	9	13	11	10	14	12	19	18	330	Jan 29 Tuesday
30	11	9	7	8	7	7	13	16	17	14	19	18	22	11	5	5	9	6	7	9	8	6	10	14	258	Jan 30 Wednesday
31	5	8	7	8	6	8	13	12	23	20	30	14	44	22	12	20	11	16	11	26	18	14	14	34	396	Jan 31 Thursday
32	21	10	16	16	16	35	16	19	24	38	39	40	34	22	23	16	6	16	16	21	21	15	26	18	524	Feb 01 Friday
33	21	25	31	32	40	33	37	31	36	27	15	40	16	13	6	9	5	7	2	6	14	11	7	18	482	Feb 02 Saturday
34	4	5	6	4	13	8	13	3	7	10	11	12	5	10	13	8	9	22	12	34	25	20	37	34	325	Feb 03 Sunday
35	43	29	25	54	41	48	38	42	57	48	44	40	40	27	22	25	20	15	15	12	13	5	11	22	736	Feb 04 Monday
36	5	9	6	11	6	7	8	13	3	16	11	10	22	18	16	11	13	6	5	16	13	5	16	20	266	Feb 05 Tuesday
37	10	5	3	9	7	4	10	9	11	11	22	22	31	21	10	15	9	5	4	13	4	5	6	18	264	Feb 06 Wednesday
38	9	5	4	7	17	6	11	11	8	12	9	26	25	7	16	17	10	9	11	6	6	10	14	20	276	Feb 07 Thursday
39	7	5	9	10	11	8	5	10	30	14	15	21	29	27	6	8	8	8	9	4	9	11	16	17	297	Feb 08 Friday
40	6	9	9	3	5	2	6	7	10	14	11	28	18	9	8	9	13	4	0	18	6	5	9	13	216	Feb 09 Saturday
41	11	6	5	11	4	4	6	8	8	11	12	7	12	15	21	17	13	11	11	17	30	13	2	7	260	Feb 10 Sunday
42	3	4	2	4	1	6	6	9	7	31	13	31	25	31	16	16	15	8	8	14	10	4	6	24	294	Feb 11 Monday
43	7	5	5	7	5	1	9	9	25	30	17	34	30	20	29	14	7	11	6	8	7	6	24	10	326	Feb 12 Tuesday
44	9	1	1	4	1	4	15	3	10	15	12	18	19	13	26	17	19	27	6	13	15	15	13	21	297	Feb 13 Wednesday
45	13	33	31	34	38	54	48	54	58	68	38	59	54	57	58	57	69	86	80	71	96	61	34	89	1340	Feb 14 Thursday
46	77	88	69	60	71	67	70	63	79	70	68	71	61	54	42	43	53	54	55	59	60	70	54	55	1513	Feb 15 Friday
47	27	17	35	37	21	12	13	6	8	14	9	32	15	7	5	8	6	4	7	2	9	9	8	6	317	Feb 16 Saturday
48	5	1	5	8	8	1	7	8	2	7	7	8	4	4	15	6	0	6	6	3	20	17	9	12	169	Feb 17 Sunday
49	3	3	12	11	13	6	22	3	3	8	10	20	19	20	14	5	9	9	11	11	10	12	15	29	278	Feb 18 Monday
50	15	6	14	9	4	10	9	10	17	14	17	21	8	0	0	0	0	0	4	0	0	0	0	0	158	Feb 19 Tuesday
51	0	0	0	0	0	0	0	0	0	2	17	14	44	16	13	10	8	3	5	5	13	6	16	11	183	Feb 20 Wednesday
52	10	8	26	5	6	4	15	11	12	8	15	18	29	10	25	18	21	8	9	10	10	7	16	1	302	Feb 21 Thursday
53	0	0	0	0	0	0	0	12	10	19	6	11	9	13	10	4	7	9	7	19	10	5	16	18	185	Feb 22 Friday
54	10	5	3	3	2	6	17	9	19	12	20	16	21	9	3	8	6	8	6	10	17	11	18	13	252	Feb 23 Saturday
55	4	14	2	9	9	2	7	2	13	12	4	18	6	7	7	10	5	1	3	11	1	14	19	11	191	Feb 24 Sunday
56	7	2	9	2	8	7	10	12	12	27	7	6	8	17	19	12	13	13	24	12	15	13	11	18	284	Feb 25 Monday
57	4	7	5	8	5	5	7	5	15	17	11	15	14	25	15	16	11	6	7	12	10	8	22	24	274	Feb 26 Tuesday
58	13	8	6	12	8	6	18	21	15	22	20	31	33	19	34	25	37	33	37	40	68	38	45	42	631	Feb 27 Wednesday
59	53	40	41	45	48	46	44	45	33	23	24	32	34	31	21	20	18	7	29	23	22	18	12	22	731	Feb 28 Thursday
60	21	18	14	6	8	14	15	30	38	32	61	70	84	92	53	19	12	12	11	7	11	10	12	15	665	Mar 01 Friday
61	4	11	8	19	22	19	21	15	28	13	25	32	30	30	17	9	9	7	8	22	8	10	18	18	403	Mar 02 Saturday
62	16	9	11	19	21	14	18	4	8	3	10	5	6	13	10	11	7	3	7	21	15	10	2	11	254	Mar 03 Sunday
63	6	1	10	4	2	9	6	11	10	17	27	19	21	22	12	13	13	12	1	11	11	5	17	10	270	Mar 04 Monday
64	7	9	3	6	3	1	5	7	16	37	15	20	24	21	28	9	19	10	20	11	7	10	18	17	323	Mar 05 Tuesday
65	8	3	12	4	6	20	26	2	11	17	21	17	0	12	6	14	21	3	10	13	11	4	15	11	267	Mar 06 Wednesday
66	2	7	4	7	9	7	15	15	23	21	12	27	24	20	16	16	19	5	10	14	5	6	23	17	324	Mar 07 Thursday
67	8	10	5	7	12	17	11	2	9	24	16	29	56	19	22	10	9	4	13	11	9	11	11	16	341	Mar 08 Friday
68	10	7	2	2	7	3	3	2	8	10	4	13	10	6	7	6	5	11	20	8	12	8	5	22	191	Mar 09 Saturday
69	12	19	13	10	8	4	11	23	14	10	11	10	17	18	8	21	11	16	9	12	17	17	8	15	314	Mar 10 Sunday
70	7	6	10	6	4	15	20	18	16	28	16	13	21	11	19	12	10	18	15	11	13	21	12	19	341	Mar 11 Monday
71	3	5	8	10	6	7	8	11	7	16	21	20	24	21	21	19	6	9	15	13	19	23	17	15	324	Mar 12 Tuesday
72	4	6	4	2	9	11	12	17	11	8	28	20	32	22	10	5	11	12	7	7	12	9	13	14	286	Mar 13 Wednesday
73	8	5	2	4	4	7	7	4	10	11	10	16	29	36	24	8	12	12	15	11	8	3	8	31	285	Mar 14 Thursday
74	11	3	5	12	5	10	25	10	17	23	22	18	34	17	17	11	12	2	15	7	12	5	10	18	321	Mar 15 Friday
75	14	7	11	9	11	7	17	17	9	6	7	5	29	12	10	8	4	7	7	8	8	5	8	17	243	Mar 16 Saturday
76	18	10	12	7	15	12	25	6	8	11	12	7	8	11	9	11	11	12	22	14	17	7	7	18	290	Mar 17 Sunday

Table 3.4.2. (Page 3 of 4)

ARC .FKX Hourly distribution of detections

Day	00	01	02	03	04	05	06	07	08	09	10	11	12	13	14	15	16	17	18	19	20	21	22	23	Sum	Date	
77	7	12	4	7	19	6	12	19	3	14	10	15	23	17	11	8	8	8	8	9	8	2	17	17	264	Mar 18 Monday	
78	7	4	11	9	7	6	5	16	11	12	18	31	38	30	32	9	8	3	24	18	20	12	26	23	380	Mar 19 Tuesday	
79	15	11	3	3	8	6	6	16	12	25	8	16	39	25	21	10	15	13	17	17	8	7	18	16	335	Mar 20 Wednesday	
80	4	3	12	7	18	5	9	17	23	26	16	28	26	25	14	20	17	20	14	9	12	5	17	25	372	Mar 21 Thursday	
81	14	6	4	9	8	6	4	12	27	23	23	34	40	26	12	17	13	27	13	28	11	9	10	19	395	Mar 22 Friday	
82	20	11	4	8	13	8	6	14	9	17	17	13	39	17	18	9	8	21	4	10	17	11	19	23	336	Mar 23 Saturday	
83	8	7	4	4	17	5	9	4	14	4	2	18	8	11	9	6	13	3	5	7	6	12	2	18	196	Mar 24 Sunday	
84	11	6	10	4	9	3	11	14	16	22	9	24	10	16	16	17	10	15	13	16	19	9	19	16	315	Mar 25 Monday	
85	5	3	2	4	9	5	16	3	11	12	25	15	25	20	20	11	10	14	14	23	8	6	28	14	303	Mar 26 Tuesday	
86	5	10	12	8	9	9	9	12	19	19	43	10	33	26	23	16	24	21	15	3	7	9	24	12	378	Mar 27 Wednesday	
87	6	6	14	3	1	7	3	9	13	12	2	9	16	15	17	2	2	9	6	5	5	5	12	13	192	Mar 28 Thursday	Skj{rt
88	5	3	5	6	8	5	5	9	12	35	12	16	27	11	2	1	13	9	14	6	10	13	12	0	239	Mar 29 Friday	Langfr
89	7	3	6	4	4	7	8	4	16	4	8	8	21	10	1	5	3	7	7	6	6	2	0	3	150	Mar 30 Saturday	
90	7	4	6	5	3	1	10	2	0	2	5	3	3	8	5	8	8	10	5	10	3	5	4	4	121	Mar 31 Sunday	F:rste

ARC	00	01	02	03	04	05	06	07	08	09	10	11	12	13	14	15	16	17	18	19	20	21	22	23		
Sum	2232	2032	2056	2084	2249	2211	2527	2349	2743	3155	3085	3653	4271	3417	2996	2552	2240	2255	2209	2588	2722	2314	2878	3541	64359	Total sum
182	12	11	11	11	12	12	14	13	15	17	17	20	23	19	16	14	12	12	12	14	15	13	16	19	354	Total average
125	13	12	12	13	13	14	15	14	17	19	19	21	26	21	18	15	14	14	13	14	14	13	17	20	380	Average workdays
57	11	9	9	9	10	9	12	11	12	13	13	18	17	14	13	11	9	10	11	15	17	13	14	19	295	Average weekends

Table 3.4.2. Daily and hourly distribution of ARCESS detections. For each day is shown number of detections within each hour of the day, and number of detections for that day. The end statistics give total number of detections distributed for each hour and the total sum of detections during the period. The averages show number of processed days, hourly distribution and average per processed day. (Page 4 of 4)

FIN .FKX Hourly distribution of detections

Day	00	01	02	03	04	05	06	07	08	09	10	11	12	13	14	15	16	17	18	19	20	21	22	23	Sum	Date
274	7	7	12	12	3	2	2	7	8	12	19	16	25	9	12	16	7	4	12	5	6	5	8	3	219	Oct 01 Monday
275	13	10	8	5	3	6	1	11	9	8	16	24	14	21	15	19	6	10	3	6	2	6	6	3	225	Oct 02 Tuesday
276	9	3	4	6	3	7	6	20	16	10	5	18	18	15	12	5	3	4	1	6	2	6	8	8	195	Oct 03 Wednesday
277	6	7	10	5	5	2	3	8	15	16	17	6	0	0	0	0	0	0	0	0	0	0	0	0	100	Oct 04 Thursday
278	0	0	0	0	0	0	1	6	6	13	21	17	29	15	4	13	3	1	4	5	4	0	6	2	150	Oct 05 Friday
279	3	1	1	4	9	6	1	4	1	6	4	4	6	3	13	2	5	6	2	6	8	4	1	5	105	Oct 06 Saturday
280	4	1	5	2	6	20	14	16	21	19	18	21	18	16	4	9	8	11	14	11	9	11	11	15	284	Oct 07 Sunday
281	7	13	7	9	5	0	1	8	6	10	10	12	16	12	13	12	7	2	4	4	4	5	5	9	181	Oct 08 Monday
282	9	5	8	11	4	2	2	7	8	23	22	26	32	18	14	19	23	19	18	8	9	12	7	9	315	Oct 09 Tuesday
283	15	14	11	4	26	20	29	28	27	36	46	53	61	41	22	20	15	12	6	6	5	6	7	5	515	Oct 10 Wednesday
284	7	8	11	4	5	4	2	14	25	48	33	34	35	15	12	19	4	7	5	6	3	6	7	12	326	Oct 11 Thursday
285	6	3	6	4	8	11	8	9	9	27	31	19	45	23	11	11	6	2	6	3	3	2	2	9	264	Oct 12 Friday
286	14	3	4	3	13	2	4	7	3	4	4	7	3	5	4	5	13	33	23	34	10	3	6	17	224	Oct 13 Saturday
287	13	24	30	21	22	31	30	27	30	19	28	24	11	18	2	19	12	5	6	6	14	4	10	7	413	Oct 14 Sunday
288	4	10	14	5	6	8	7	5	4	12	9	20	22	24	15	7	1	11	7	8	5	1	6	5	216	Oct 15 Monday
289	3	3	9	11	6	2	5	4	6	14	8	16	25	17	16	12	5	3	2	5	5	5	8	7	197	Oct 16 Tuesday
290	2	10	8	6	5	4	6	5	5	26	17	21	23	25	25	6	6	12	7	7	4	6	10	3	249	Oct 17 Wednesday
291	3	7	5	7	3	3	2	7	2	10	15	24	27	11	12	6	1	9	3	14	4	11	7	15	208	Oct 18 Thursday
292	5	0	7	8	6	0	9	12	13	16	25	17	27	18	4	3	6	5	5	6	6	7	11	6	222	Oct 19 Friday
293	3	18	19	35	44	39	36	34	24	9	18	14	13	16	3	16	57	50	51	49	63	71	51	57	790	Oct 20 Saturday
294	54	44	14	14	16	8	13	9	14	15	25	33	23	11	9	5	7	2	6	17	9	15	8	7	378	Oct 21 Sunday
295	3	7	8	8	4	3	1	6	3	7	10	18	21	9	6	6	3	3	3	7	4	5	5	3	153	Oct 22 Monday
296	3	4	5	2	6	2	10	5	8	15	7	20	30	16	22	14	4	6	4	7	15	6	8	6	225	Oct 23 Tuesday
297	5	4	9	4	3	1	7	5	6	13	17	24	33	12	18	11	10	5	9	8	9	9	8	18	248	Oct 24 Wednesday
298	4	8	8	8	12	9	2	11	9	14	8	29	30	12	15	7	4	11	6	3	6	2	11	12	241	Oct 25 Thursday
299	12	4	10	7	3	3	2	7	15	10	11	16	32	16	15	9	3	3	11	5	3	11	11	4	223	Oct 26 Friday
300	4	4	3	2	7	9	36	81	83	4	17	33	17	22	35	18	28	78	67	28	1	7	4	1	589	Oct 27 Saturday
301	2	1	3	7	26	111	43	34	5	37	15	6	53	39	28	24	13	5	5	24	38	39	5	6	569	Oct 28 Sunday
302	10	6	5	4	8	3	1	8	15	6	17	21	35	28	20	7	4	5	4	7	4	6	7	9	240	Oct 29 Monday
303	5	10	11	19	11	12	11	14	10	20	21	29	20	22	15	16	8	12	17	15	17	7	19	23	364	Oct 30 Tuesday
304	24	15	18	25	28	14	17	23	20	22	24	17	32	16	14	11	7	5	6	5	9	7	4	4	367	Oct 31 Wednesday
305	0	0	0	0	0	5	0	2	7	5	7	16	19	14	20	2	2	4	5	5	7	6	10	5	141	Nov 01 Thursday
306	5	5	11	11	2	6	8	7	8	19	18	29	22	21	7	5	8	3	5	1	5	6	3	4	219	Nov 02 Friday
307	7	14	5	1	9	3	8	6	0	4	7	15	24	17	14	54	18	29	43	41	30	10	16	7	382	Nov 03 Saturday
308	6	2	0	2	8	10	14	55	34	23	27	35	34	21	5	9	5	2	9	8	9	10	5	7	340	Nov 04 Sunday
309	10	4	9	8	9	1	3	6	4	13	2	15	20	15	19	6	3	3	6	4	7	7	5	0	179	Nov 05 Monday
310	9	11	7	6	10	2	3	6	8	17	20	24	24	24	28	15	5	6	10	8	10	3	18	13	287	Nov 06 Tuesday
311	13	7	12	14	3	3	3	6	3	6	10	12	8	10	18	5	5	8	1	12	8	4	6	5	182	Nov 07 Wednesday
312	11	3	3	8	5	6	0	8	2	14	13	16	16	13	13	0	8	8	1	5	8	4	6	8	179	Nov 08 Thursday
313	7	5	1	7	7	0	4	6	20	7	5	12	30	20	7	6	11	12	13	24	17	10	11	44	286	Nov 09 Friday
314	16	12	46	8	39	22	9	14	7	5	6	28	21	4	8	15	12	9	13	12	4	5	2	1	318	Nov 10 Saturday
315	1	0	17	27	15	2	2	10	4	9	13	24	10	4	2	4	2	8	4	5	8	8	11	9	199	Nov 11 Sunday
316	11	8	6	10	5	1	2	5	3	8	2	21	36	21	12	4	9	5	3	5	3	6	11	5	202	Nov 12 Monday
317	11	4	8	7	6	6	3	7	1	9	9	20	46	26	10	6	2	2	5	1	10	9	6	7	221	Nov 13 Tuesday
318	9	6	5	2	5	5	7	9	11	13	12	31	30	24	22	19	24	29	39	28	38	41	32	52	493	Nov 14 Wednesday
319	38	59	73	58	16	9	3	9	9	13	9	15	28	21	16	5	8	6	5	9	3	7	13	30	462	Nov 15 Thursday
320	8	8	3	1	3	2	1	5	4	22	18	22	29	6	7	6	6	4	2	3	7	4	2	4	177	Nov 16 Friday
321	0	4	7	1	1	6	7	7	7	8	16	20	9	9	5	8	11	14	17	21	12	23	33	33	279	Nov 17 Saturday
322	38	23	11	9	13	11	5	4	2	2	8	5	3	7	3	7	10	7	7	5	5	6	9	6	206	Nov 18 Sunday
323	13	11	8	3	9	3	2	4	5	11	15	11	10	17	13	5	4	2	3	3	5	10	5	12	184	Nov 19 Monday
324	5	19	9	5	10	3	12	9	2	14	12	20	34	26	31	19	21	18	16	20	3	7	7	27	349	Nov 20 Tuesday
325	44	44	36	38	35	20	11	7	11	8	12	9	37	28	39	28	27	45	40	45	27	51	48	51	741	Nov 21 Wednesday
326	59	66	94	88	72	46	37	32	10	9	16	27	18	17	28	5	10	7	4	7	3	8	4	5	672	Nov 22 Thursday
327	2	5	5	6	5	2	4	6	3	21	24	18	22	17	36	38	31	45	51	28	16	11	20	9	425	Nov 23 Friday
328	4	11	17	83	94	89	68	68	27	19	7	10	16	42	60	44	19	22	17	11	7	8	0	2	745	Nov 24 Saturday
329	1	6	5	2	15	2	8	4	1	6	6	4	6	5	2	10	7	6	3	7	4	9	9	8	136	Nov 25 Sunday

Table 3.4.3. (Page 1 of 4)

FIN .FKX Hourly distribution of detections

Day	00	01	02	03	04	05	06	07	08	09	10	11	12	13	14	15	16	17	18	19	20	21	22	23	Sum	Date		
330	7	6	9	5	2	6	3	4	3	5	5	19	30	30	8	7	6	3	4	8	9	9	12	8	208	Nov 26	Monday	
331	12	8	7	13	12	1	4	5	5	5	15	29	37	24	9	2	3	5	5	2	10	6	6	8	233	Nov 27	Tuesday	
332	3	5	4	3	5	3	1	5	12	7	12	23	29	24	9	4	4	4	4	3	5	3	1	3	164	Nov 28	Wednesday	
333	5	2	7	3	10	0	4	6	12	28	21	17	36	16	6	18	2	6	10	6	13	15	17	8	268	Nov 29	Thursday	
334	12	6	5	7	9	4	3	6	11	16	21	21	24	14	5	13	5	4	11	7	8	7	7	3	229	Nov 30	Friday	
335	4	9	6	3	6	4	4	6	10	8	11	16	8	3	16	31	34	44	46	44	27	28	25	12	405	Dec 01	Saturday	
336	13	12	18	25	49	26	6	14	16	13	8	12	7	4	5	5	8	16	9	8	11	15	16	41	357	Dec 02	Sunday	
337	50	58	58	65	75	49	48	42	34	22	18	14	28	29	23	22	17	24	14	16	22	33	35	34	830	Dec 03	Monday	
338	26	20	19	11	6	2	0	6	6	15	13	10	22	13	12	8	9	32	7	8	3	7	8	14	277	Dec 04	Tuesday	
339	31	11	31	29	18	21	27	24	18	20	23	31	36	35	25	35	51	45	57	41	10	7	6	13	651	Dec 05	Wednesday	
340	11	8	10	11	17	30	19	7	5	15	18	23	13	14	31	41	24	19	10	7	8	9	12	9	371	Dec 06	Thursday	
341	4	4	5	8	4	8	7	16	37	63	57	40	40	47	23	6	5	3	4	4	3	2	4	3	397	Dec 07	Friday	
342	2	3	3	0	5	8	3	6	5	11	3	13	8	10	4	2	2	3	2	0	2	2	2	8	107	Dec 08	Saturday	
343	12	10	4	5	13	17	5	23	27	24	26	28	47	32	59	53	70	35	12	1	7	6	7	5	528	Dec 09	Sunday	
344	7	7	11	13	3	4	3	7	5	13	11	13	26	17	10	7	2	4	6	3	2	3	7	8	192	Dec 10	Monday	
345	3	7	9	3	3	3	2	4	4	6	14	10	26	15	6	8	9	7	8	1	3	3	5	6	165	Dec 11	Tuesday	
346	4	5	4	5	5	6	3	7	7	9	3	15	21	20	11	18	17	14	9	8	19	18	32	15	275	Dec 12	Wednesday	
347	17	19	11	5	7	4	2	7	10	9	18	19	34	23	49	54	49	47	42	12	54	39	42	53	626	Dec 13	Thursday	
348	14	9	9	12	5	5	2	4	6	16	29	27	43	45	44	52	63	52	52	58	58	58	56	51	770	Dec 14	Friday	
349	41	42	47	39	23	16	15	12	10	6	9	6	6	6	3	10	8	8	16	11	17	18	18	22	409	Dec 15	Saturday	
350	14	6	13	8	10	14	6	4	6	8	2	2	1	7	6	6	5	3	10	1	8	5	7	15	167	Dec 16	Sunday	
351	8	10	7	6	9	10	9	7	1	3	10	15	14	22	2	6	7	5	4	6	6	9	5	3	184	Dec 17	Monday	
352	4	11	9	7	12	7	1	4	5	12	7	21	30	19	6	4	3	6	2	4	8	4	6	7	201	Dec 18	Tuesday	
353	8	4	5	2	0	1	4	5	11	9	23	18	34	20	7	7	4	2	3	6	7	7	7	13	207	Dec 19	Wednesday	
354	8	13	22	19	12	13	6	6	5	15	10	23	43	12	10	2	3	4	5	4	9	5	6	1	256	Dec 20	Thursday	
355	6	9	7	10	4	9	4	7	10	11	27	36	44	26	11	8	10	12	4	4	7	3	3	4	276	Dec 21	Friday	
356	4	6	6	13	8	34	53	40	13	11	11	6	7	25	5	4	6	8	7	5	5	6	5	2	290	Dec 22	Saturday	
357	3	2	5	4	3	3	0	6	7	3	4	1	0	3	1	4	10	0	5	2	4	10	1	1	82	Dec 23	Sunday	
358	5	3	4	3	6	5	8	10	6	8	10	6	9	4	6	2	7	1	3	8	5	11	13	6	149	Dec 24	Monday	
359	9	9	4	4	5	10	11	6	9	3	10	5	14	8	13	3	4	2	2	6	15	34	20	47	236	Dec 25	Tuesday	F:rste
360	44	56	51	63	66	72	76	57	41	49	65	[illegible]	85	53	22	16	10	3	5	5	3	3	6	5	934	Dec 26	Wednesday	Andre
361	12	2	2	3	2	4	2	7	2	7	13	15	20	9	5	3	5	8	10	2	11	4	4	6	158	Dec 27	Thursday	
362	4	6	3	11	11	11	6	8	9	17	15	18	30	15	6	7	5	6	4	6	4	3	11	6	222	Dec 28	Friday	
363	7	7	12	9	7	4	1	13	8	20	10	32	32	26	51	49	47	57	66	68	71	63	59	56	775	Dec 29	Saturday	
364	60	43	46	43	34	15	8	4	10	16	9	11	7	5	4	3	6	5	3	14	2	6	5	9	368	Dec 30	Sunday	
365	3	4	7	6	5	2	3	11	4	2	3	6	4	5	4	8	9	6	3	8	6	4	8	4	125	Dec 31	Monday	
1	7	1	7	4	3	2	5	4	6	8	9	16	39	11	8	5	4	6	5	15	13	25	34	26	263	Jan 01	Tuesday	F:rste
2	15	12	12	34	29	10	5	15	10	24	10	14	20	30	10	1	7	3	8	4	5	5	10	14	307	Jan 02	Wednesday	
3	11	16	24	17	14	7	9	23	10	9	9	24	27	30	11	6	8	9	6	11	5	2	4	5	297	Jan 03	Thursday	
4	4	4	6	7	19	3	5	7	5	15	24	30	25	21	6	9	2	6	4	5	2	3	2	7	221	Jan 04	Friday	
5	7	3	9	4	4	7	5	5	7	10	5	15	10	2	11	17	9	1	6	3	2	6	5	2	155	Jan 05	Saturday	
6	0	4	3	4	1	2	4	2	4	5	1	7	6	6	10	4	5	2	6	3	5	8	7	5	104	Jan 06	Sunday	
7	15	8	7	4	6	6	6	8	4	9	14	18	21	15	16	12	5	8	7	7	2	2	9	6	215	Jan 07	Monday	
8	4	4	4	2	4	6	11	17	12	19	25	20	28	15	4	6	10	6	5	10	7	7	8	4	238	Jan 08	Tuesday	
9	3	5	6	8	2	2	5	6	13	5	11	21	34	16	10	7	5	9	15	24	18	15	4	7	251	Jan 09	Wednesday	
10	5	7	2	9	15	3	2	9	7	17	11	19	28	27	4	7	6	2	7	24	33	50	59	30	383	Jan 10	Thursday	
11	24	38	41	24	41	39	16	13	32	10	18	29	27	19	5	8	8	10	7	7	6	8	8	6	444	Jan 11	Friday	
12	6	5	15	11	3	3	7	7	3	6	7	3	7	6	6	3	3	5	2	15	10	7	5	4	149	Jan 12	Saturday	
13	2	0	4	7	7	4	5	6	2	2	3	2	11	3	1	7	2	4	4	4	4	10	3	8	105	Jan 13	Sunday	
14	12	4	5	7	4	6	7	8	6	8	13	10	29	20	17	4	6	5	5	7	6	11	4	8	212	Jan 14	Monday	
15	4	4	6	7	3	4	7	3	2	7	14	16	37	18	9	8	5	3	2	6	4	4	3	8	189	Jan 15	Tuesday	
16	7	6	2	5	0	3	6	4	4	10	15	19	19	16	13	9	2	9	2	9	10	7	6	4	187	Jan 16	Wednesday	
17	5	3	6	6	5	4	2	4	14	6	16	21	25	24	7	12	7	3	5	7	10	4	9	11	216	Jan 17	Thursday	
18	4	8	4	9	4	2	6	7	7	17	21	31	29	2	3	6	6	7	7	6	5	5	3	4	208	Jan 18	Friday	
19	3	7	4	3	10	2	3	8	1	7	7	10	10	6	2	6	3	3	7	2	2	10	9	10	135	Jan 19	Saturday	
20	6	7	4	5	3	11	0	5	22	24	15	23	26	24	38	43	27	19	27	27	13	15	8	3	393	Jan 20	Sunday	

Table 3.4.3. (Page 2 of 4)

PIN .FXX Hourly distribution of detections

Day	00	01	02	03	04	05	06	07	08	09	10	11	12	13	14	15	16	17	18	19	20	21	22	23	Sum	Date
21	0	1	4	4	6	8	4	7	7	7	10	22	22	13	12	5	7	14	7	3	5	14	15	11	208	Jan 21 Monday
22	15	8	7	8	2	3	9	5	9	11	9	16	30	17	6	4	7	4	12	15	17	27	13	15	260	Jan 22 Tuesday
23	16	12	11	13	22	10	41	25	41	35	71	89	95	70	57	67	53	70	50	63	57	35	36	46	1085	Jan 23 Wednesday
24	49	16	0	0	0	0	0	0	5	14	8	37	28	22	18	13	10	6	6	9	5	3	6	3	258	Jan 24 Thursday
25	6	2	10	4	8	3	5	9	21	30	19	39	55	46	60	49	16	37	53	59	49	65	78	62	785	Jan 25 Friday
26	47	49	71	61	43	26	9	7	8	6	3	12	16	17	13	5	5	10	12	14	13	18	13	11	489	Jan 26 Saturday
27	19	29	34	42	27	47	48	52	33	7	13	6	19	9	5	14	11	10	16	11	9	5	9	11	486	Jan 27 Sunday
28	9	7	6	8	6	4	1	10	2	7	9	21	22	17	16	4	9	2	5	10	6	10	8	10	209	Jan 28 Monday
29	1	3	7	6	3	7	7	8	13	6	22	25	30	14	18	21	22	21	20	28	31	37	34	28	412	Jan 29 Tuesday
30	43	39	40	45	50	37	42	41	36	15	15	22	28	14	10	14	3	13	16	12	9	10	18	10	582	Jan 30 Wednesday
31	6	6	7	8	4	3	2	6	9	14	17	26	30	16	17	7	6	1	7	5	6	7	9	14	233	Jan 31 Thursday
32	5	3	4	6	4	3	2	4	4	21	28	29	30	7	6	7	6	6	5	12	9	16	13	13	249	Feb 01 Friday
33	10	5	4	1	3	8	5	6	9	19	14	19	26	39	24	20	21	26	19	27	42	66	68	74	556	Feb 02 Saturday
34	67	75	71	54	66	75	59	43	33	21	3	2	7	0	5	2	8	7	11	4	12	11	9	11	658	Feb 03 Sunday
35	4	9	3	8	3	4	2	5	4	11	9	16	20	12	7	10	13	18	9	14	6	23	49	51	310	Feb 04 Monday
36	53	58	55	47	31	26	30	24	26	19	22	28	23	22	9	7	8	8	10	5	15	18	40	50	634	Feb 05 Tuesday
37	61	55	53	62	35	35	30	37	23	20	18	22	26	20	6	9	5	7	3	10	17	10	15	14	593	Feb 06 Wednesday
38	20	16	25	50	43	37	23	33	15	8	14	20	25	19	12	13	10	7	4	17	13	10	5	11	450	Feb 07 Thursday
39	1	9	5	10	5	3	1	2	9	16	22	19	14	19	5	6	7	5	4	5	4	13	10	7	201	Feb 08 Friday
40	7	7	8	6	3	8	4	9	10	20	11	6	2	6	4	4	13	7	2	4	3	2	8	4	148	Feb 09 Saturday
41	3	8	4	4	8	4	10	7	5	8	4	3	8	8	7	0	3	10	5	11	7	5	7	11	150	Feb 10 Sunday
42	8	14	6	6	3	6	2	7	9	11	15	15	21	23	8	11	10	4	9	11	13	15	25	40	292	Feb 11 Monday
43	46	57	41	45	36	24	30	26	11	9	18	20	26	24	22	6	7	4	3	14	10	8	14	10	511	Feb 12 Tuesday
44	6	10	3	12	7	8	4	5	4	13	16	16	34	20	12	15	7	10	7	5	1	4	4	4	227	Feb 13 Wednesday
45	6	11	8	8	3	4	6	7	10	23	23	23	25	16	12	5	5	6	5	11	11	7	4	9	248	Feb 14 Thursday
46	6	8	7	7	10	2	7	7	3	22	23	21	29	20	11	8	5	8	10	2	2	8	8	8	242	Feb 15 Friday
47	4	9	16	13	2	7	6	2	6	5	6	9	3	0	3	3	8	2	2	4	7	1	4	0	122	Feb 16 Saturday
48	4	0	2	7	4	3	4	10	3	6	6	3	4	4	3	5	7	2	7	8	7	6	3	5	113	Feb 17 Sunday
49	8	7	14	15	11	6	7	6	11	14	14	27	40	26	21	2	15	8	3	10	5	12	10	14	306	Feb 18 Monday
50	7	10	8	5	5	6	3	6	4	24	17	20	20	24	14	9	10	11	4	9	9	3	5	10	243	Feb 19 Tuesday
51	3	7	7	5	6	4	2	6	5	16	16	19	40	19	5	9	3	6	1	5	10	6	4	5	209	Feb 20 Wednesday
52	3	8	6	3	4	2	4	7	9	25	7	24	43	57	27	12	2	5	3	10	9	4	11	4	289	Feb 21 Thursday
53	11	1	6	7	5	3	3	4	6	18	21	23	20	15	13	3	5	2	3	4	8	4	8	7	200	Feb 22 Friday
54	4	2	7	4	0	5	9	5	18	29	27	10	12	4	4	6	5	9	4	4	9	5	10	5	197	Feb 23 Saturday
55	7	9	5	10	4	3	16	9	9	1	4	10	3	7	4	1	5	5	2	6	6	4	5	5	140	Feb 24 Sunday
56	7	7	4	4	6	4	6	6	1	15	9	6	19	18	19	12	7	9	8	5	15	6	8	8	209	Feb 25 Monday
57	8	8	21	19	30	25	26	23	24	32	28	19	18	14	11	12	24	21	36	42	26	8	9	7	491	Feb 26 Tuesday
58	18	22	14	49	53	36	11	17	26	36	28	57	54	34	37	14	17	20	35	25	14	14	31	27	689	Feb 27 Wednesday
59	22	39	24	46	39	25	16	20	14	26	18	16	30	20	23	28	40	31	41	35	43	48	59	37	740	Feb 28 Thursday
60	53	58	55	53	54	38	31	37	27	38	29	24	21	25	20	7	5	16	15	12	19	43	37	35	752	Mar 01 Friday
61	45	53	58	66	62	67	70	63	61	77	51	34	17	5	21	30	27	27	54	36	43	51	78	80	1176	Mar 02 Saturday
62	71	49	72	63	49	81	91	110	101	85	51	20	15	7	40	43	2	7	13	11	11	11	15	13	1031	Mar 03 Sunday
63	17	10	4	3	5	2	3	7	10	7	12	18	22	20	15	17	15	8	8	9	16	17	6	14	265	Mar 04 Monday
64	9	20	12	8	3	6	1	4	5	13	12	21	23	22	14	15	8	17	33	23	10	8	9	14	310	Mar 05 Tuesday
65	10	6	12	12	2	8	2	10	13	18	18	27	43	15	8	12	13	6	3	7	5	9	6	13	278	Mar 06 Wednesday
66	6	13	6	16	9	6	0	10	14	27	29	23	25	26	9	12	11	13	10	17	8	9	7	12	318	Mar 07 Thursday
67	16	11	12	10	11	17	4	11	5	13	20	21	27	11	18	13	10	17	25	16	14	31	17	6	356	Mar 08 Friday
68	30	20	14	25	15	20	6	13	12	14	17	24	28	7	5	20	20	25	7	15	22	19	3	11	392	Mar 09 Saturday
69	39	29	26	34	34	20	16	15	8	11	20	15	29	4	17	18	12	10	10	14	8	11	11	7	418	Mar 10 Sunday
70	11	8	3	12	6	3	7	4	9	8	12	17	20	12	12	15	6	3	13	8	7	14	6	4	220	Mar 11 Monday
71	7	7	9	5	4	8	11	12	9	27	12	11	25	17	17	11	17	15	15	12	7	10	13	11	292	Mar 12 Tuesday
72	15	9	12	12	10	9	9	9	8	29	11	31	26	28	22	10	13	17	8	19	21	13	25	30	396	Mar 13 Wednesday
73	32	38	24	43	36	13	20	35	26	31	25	28	18	23	15	9	16	26	23	19	12	33	39	44	628	Mar 14 Thursday
74	36	18	8	20	21	17	9	12	18	18	32	29	31	19	11	25	25	15	6	28	31	25	23	31	508	Mar 15 Friday
75	39	19	27	23	32	24	25	30	21	22	24	23	25	30	19	26	30	35	30	23	51	9	27	36	650	Mar 16 Saturday
76	54	38	32	19	17	12	13	27	25	21	27	29	32	46	27	16	22	14	8	12	19	14	18	17	559	Mar 17 Sunday

Table 3.4.3. (Page 3 of 4)

FIN .FKX Hourly distribution of detections

Day	00	01	02	03	04	05	06	07	08	09	10	11	12	13	14	15	16	17	18	19	20	21	22	23	Sum	Date	
77	19	29	15	18	8	7	10	11	8	11	9	19	17	23	20	14	14	19	14	20	9	12	14	15	355	Mar 18 Monday	
78	8	7	13	23	11	10	8	6	9	15	11	26	33	25	15	15	11	9	11	12	13	9	17	23	340	Mar 19 Tuesday	
79	17	9	12	16	13	3	12	10	10	16	14	12	24	24	10	10	9	8	11	9	4	5	6	8	272	Mar 20 Wednesday	
80	4	5	6	7	4	4	5	5	7	11	19	11	15	23	11	8	4	12	9	4	8	4	8	3	197	Mar 21 Thursday	
81	1	2	7	3	8	2	2	2	8	12	15	20	42	14	13	18	15	18	15	22	28	21	31	14	333	Mar 22 Friday	
82	14	13	12	11	5	5	3	8	3	5	6	11	9	10	3	12	3	20	19	2	8	2	1	2	187	Mar 23 Saturday	
83	2	5	2	4	14	1	5	3	0	2	6	5	4	17	2	9	10	4	1	6	3	8	4	4	121	Mar 24 Sunday	
84	9	5	7	5	2	3	4	5	1	8	8	10	19	13	6	6	5	6	3	3	12	3	6	5	154	Mar 25 Monday	
85	9	4	2	6	7	3	0	0	0	0	0	0	0	0	0	0	0	1	5	15	4	6	8	10	80	Mar 26 Tuesday	
86	5	9	6	8	10	9	0	0	20	7	14	0	0	4	10	11	6	7	13	14	20	15	37	38	263	Mar 27 Wednesday	
87	34	31	44	35	16	13	8	5	12	18	17	22	19	14	7	5	6	7	9	6	8	6	10	11	365	Mar 28 Thursday	Skj(rt
88	18	21	40	35	31	27	11	3	8	14	12	15	19	18	6	6	13	3	1	4	4	9	4	4	326	Mar 29 Friday	Langfr
89	2	2	4	7	4	6	12	9	30	44	44	24	23	15	17	19	31	12	15	56	32	40	13	10	471	Mar 30 Saturday	
90	10	14	18	17	4	8	16	8	14	10	17	17	20	17	24	18	7	2	2	3	7	17	29	48	347	Mar 31 Sunday	F:rste

FIN	00	01	02	03	04	05	06	07	08	09	10	11	12	13	14	15	16	17	18	19	20	21	22	23		
Sum	2476	2399	2524	2651	2459	2141	1912	2308	2176	2771	2880	3522	4349	3231	2543	2272	2017	2119	2108	2237	2165	2259	2458	2570	60547	Total sum
182	14	13	14	15	14	12	11	13	12	15	16	19	24	18	14	12	11	12	12	12	12	12	14	14	333	Total average
125	12	12	12	13	11	8	8	10	10	15	17	21	27	20	15	12	10	11	11	11	11	12	13	14	316	Average workdays
57	17	16	18	18	18	19	17	18	16	15	14	16	16	13	13	14	13	13	14	14	14	14	14	15	369	Average weekends

Table 3.4.3. Daily and hourly distribution of FINESA detections. For each day is shown number of detections within each hour *of the day, and number of detections for that day. The end statistics give total number of detections distributed for each hour and* the total sum of detections during the period. The averages show number of processed days, hourly distribution and average per processed day. (Page 4 of 4)

GIR .FKX Hourly distribution of detections

Day	00	01	02	03	04	05	06	07	08	09	10	11	12	13	14	15	16	17	18	19	20	21	22	23	Sum	Date
274	0	0	0	0	0	0	0	0	0	0	0	0	0	0	0	0	0	0	0	0	0	0	0	0	0	Oct 01 Monday
275	0	0	0	0	0	0	0	0	0	0	0	0	0	0	0	0	0	0	0	0	0	0	0	0	0	Oct 02 Tuesday
276	0	0	0	0	0	0	0	0	0	0	0	0	0	0	0	0	0	0	0	0	0	0	0	0	0	Oct 03 Wednesday
277	0	0	0	0	0	0	0	0	0	0	0	0	0	0	0	0	0	0	0	0	0	0	0	0	0	Oct 04 Thursday
278	0	0	0	0	0	0	0	0	0	0	0	0	0	0	0	0	0	0	0	0	0	0	0	0	0	Oct 05 Friday
279	0	0	0	0	0	0	0	0	0	0	0	0	0	0	0	0	0	0	0	0	0	0	0	0	0	Oct 06 Saturday
280	0	0	0	0	0	0	0	0	0	0	0	0	0	0	0	0	0	0	0	0	0	0	0	0	0	Oct 07 Sunday
281	0	0	0	0	0	0	0	0	0	0	0	0	0	0	0	0	0	0	0	0	0	0	0	0	0	Oct 08 Monday
282	0	0	0	0	0	0	0	0	0	0	0	0	0	0	0	0	0	0	0	0	0	0	0	0	0	Oct 09 Tuesday
283	0	0	0	0	0	0	0	0	0	0	0	0	0	0	0	0	0	0	0	0	0	0	0	0	0	Oct 10 Wednesday
284	0	0	0	0	0	0	0	0	0	0	0	0	0	0	0	0	0	0	0	0	0	0	0	0	0	Oct 11 Thursday
285	0	0	0	0	0	0	0	0	0	0	0	0	0	0	0	0	0	0	0	0	0	0	0	0	0	Oct 12 Friday
286	0	0	0	0	0	0	0	0	0	0	0	0	0	0	0	0	0	0	0	0	0	0	0	0	0	Oct 13 Saturday
287	0	0	0	0	0	0	0	0	0	0	0	0	0	0	0	0	0	0	0	0	0	0	0	0	0	Oct 14 Sunday
288	0	0	0	0	0	0	0	0	0	0	0	0	0	0	0	0	0	0	0	0	0	0	0	0	0	Oct 15 Monday
289	0	0	0	0	0	0	0	0	0	0	0	0	0	0	0	0	0	0	0	0	0	0	0	0	0	Oct 16 Tuesday
290	0	0	0	0	0	0	0	0	0	0	0	5	12	9	18	14	4	8	4	4	12	10	7	5	112	Oct 17 Wednesday
291	9	3	5	8	13	4	1	4	4	13	17	21	24	23	48	12	1	6	12	14	5	5	6	5	263	Oct 18 Thursday
292	2	2	4	5	6	0	2	9	6	11	8	23	20	11	12	2	6	4	6	4	5	8	2	6	164	Oct 19 Friday
293	0	2	2	1	3	2	2	3	7	4	5	11	24	15	17	8	10	5	7	8	5	3	2	3	149	Oct 20 Saturday
294	1	2	1	1	2	7	2	4	2	5	8	11	3	11	20	12	3	5	7	14	6	2	0	1	130	Oct 21 Sunday
295	2	3	9	4	2	4	8	8	9	22	26	14	20	20	32	7	5	18	25	12	26	11	13	3	303	Oct 22 Monday
296	11	9	29	6	12	0	1	2	11	10	23	19	12	9	20	9	7	13	24	49	39	15	7	2	339	Oct 23 Tuesday
297	5	4	0	8	3	2	2	6	13	23	29	26	28	27	18	16	9	11	19	21	6	9	5	13	303	Oct 24 Wednesday
298	5	5	2	2	9	9	1	1	18	21	29	44	24	43	40	12	10	29	19	22	33	10	7	7	402	Oct 25 Thursday
299	15	2	3	4	8	1	1	6	0	0	70	36	20	17	19	8	12	22	19	6	4	8	8	2	291	Oct 26 Friday
300	4	5	9	5	1	1	2	2	1	4	9	5	16	16	14	3	9	11	4	16	4	0	15	5	161	Oct 27 Saturday
301	6	0	1	0	1	1	1	3	5	5	1	7	6	11	5	4	3	3	3	1	5	6	3	0	81	Oct 28 Sunday
302	0	0	0	0	0	0	0	0	0	0	0	0	0	0	0	0	0	0	0	0	0	0	0	0	0	Oct 29 Monday
303	0	0	0	0	0	0	0	0	34	5	10	18	36	14	23	13	13	6	5	7	8	7	5	6	210	Oct 30 Tuesday
304	4	5	2	1	7	0	1	3	16	13	42	21	25	5	20	11	7	2	7	9	11	2	10	3	227	Oct 31 Wednesday
305	8	5	7	5	2	11	8	26	11	13	15	21	14	8	8	6	3	1	7	2	2	4	2	4	193	Nov 01 Thursday
306	1	2	1	0	2	0	1	9	24	2	7	0	0	0	0	8	4	6	3	4	1	3	3	1	82	Nov 02 Friday
307	3	1	1	2	5	1	3	0	1	2	0	0	0	0	0	0	0	0	0	0	0	0	0	0	19	Nov 03 Saturday
308	0	0	0	0	0	0	0	0	0	0	0	4	4	3	1	1	12	5	2	1	2	4	4	1	44	Nov 04 Sunday
309	4	2	1	1	3	0	3	3	6	7	15	0	0	0	31	15	7	7	20	1	28	50	34	12	250	Nov 05 Monday
310	11	8	4	6	9	0	7	7	14	23	20	29	25	34	31	27	15	18	45	36	44	51	16	6	486	Nov 06 Tuesday
311	1	3	5	2	4	5	1	9	10	8	16	15	26	26	7	19	14	14	18	28	18	9	36	7	301	Nov 07 Wednesday
312	4	2	1	9	2	1	5	8	18	6	22	17	20	20	19	9	9	2	0	0	0	0	0	0	174	Nov 08 Thursday
313	0	0	0	0	0	0	0	0	0	0	0	0	0	0	0	0	0	0	0	0	0	0	0	0	0	Nov 09 Friday
314	0	0	0	0	0	0	0	0	0	0	0	0	0	0	0	0	0	0	0	0	0	0	0	0	0	Nov 10 Saturday
315	0	0	0	0	0	0	0	0	0	0	0	0	0	0	0	0	0	0	0	0	0	0	0	0	0	Nov 11 Sunday
316	0	0	0	0	0	0	0	0	14	23	32	38	28	17	3	4	12	16	9	10	3	8	5	4	226	Nov 12 Monday
317	4	7	3	2	2	1	1	3	9	14	11	23	19	6	3	0	0	0	0	0	0	0	0	0	108	Nov 13 Tuesday
318	0	0	0	0	0	0	0	0	0	0	0	0	0	0	0	0	0	0	0	0	0	0	0	0	0	Nov 14 Wednesday
319	0	0	0	0	0	0	0	0	0	0	0	0	0	0	6	4	11	2	12	6	5	7	7	7	67	Nov 15 Thursday
320	2	3	1	2	2	3	3	2	9	4	12	15	19	11	7	8	12	8	11	1	2	1	2	4	144	Nov 16 Friday
321	2	2	5	14	9	3	11	3	2	2	5	7	7	1	10	19	7	22	31	35	20	38	44	31	330	Nov 17 Saturday
322	28	19	22	19	8	8	13	20	36	32	45	38	37	8	15	14	9	7	11	7	6	7	2	4	415	Nov 18 Sunday
323	2	6	9	4	4	5	9	5	11	8	10	12	13	4	4	6	3	0	0	3	3	0	2	4	127	Nov 19 Monday
324	0	3	5	1	2	0	0	4	77	61	18	18	18	7	3	8	2	2	6	6	6	3	0	6	256	Nov 20 Tuesday
325	3	7	13	6	4	4	10	17	6	2	17	10	20	6	4	4	1	2	11	5	12	4	5	6	179	Nov 21 Wednesday
326	2	5	1	5	1	3	2	5	2	6	16	21	5	11	6	12	8	3	1	11	11	5	5	3	150	Nov 22 Thursday
327	0	4	2	3	5	2	4	6	6	4	12	16	21	7	5	4	1	1	4	4	6	3	8	5	133	Nov 23 Friday
328	3	3	1	1	1	2	1	2	3	0	4	8	11	19	15	4	2	17	37	32	18	21	32	26	263	Nov 24 Saturday
329	38	34	37	25	5	2	1	7	21	29	31	13	20	22	32	10	2	32	34	43	38	41	29	25	571	Nov 25 Sunday

Table 3.4.4. (Page 1 of 4)

GER .FKX Hourl/ distribution of detections

Day	00	01	02	03	04	05	06	07	08	09	10	11	12	13	14	15	16	17	18	19	20	21	22	23	Sum	Date		
330	30	28	13	1	0	0	1	4	14	15	16	25	9	12	10	6	4	4	3	3	4	4	2	3	211	Nov 26	Monday	
331	7	11	5	0	11	20	7	8	15	18	14	19	13	10	8	18	1	2	9	9	8	3	7	1	224	Nov 27	Tuesday	
332	3	7	4	1	4	2	5	3	14	13	12	10	19	18	10	4	2	1	7	10	3	7	6	6	171	Nov 28	Wednesday	
333	9	4	12	6	5	0	1	3	7	14	12	16	13	5	10	9	6	2	2	2	5	5	3	3	154	Nov 29	Thursday	
334	0	1	5	1	3	0	2	0	5	9	16	15	22	7	5	7	2	1	8	2	3	3	2	1	120	Nov 30	Friday	
335	5	2	7	5	3	7	4	5	9	9	18	8	14	10	17	7	1	10	9	3	18	5	3	2	181	Dec 01	Saturday	
336	6	5	5	10	5	5	6	6	6	13	9	8	4	0	3	6	1	2	0	2	1	2	1	4	110	Dec 02	Sunday	
337	3	1	1	5	2	5	4	8	8	6	5	0	0	0	0	0	0	0	0	0	0	0	0	0	48	Dec 03	Monday	
338	0	0	0	0	0	0	0	0	0	0	0	0	0	0	0	0	0	0	0	0	0	0	0	0	0	Dec 04	Tuesday	
339	0	0	0	0	0	0	0	0	0	0	13	11	20	6	12	3	5	3	6	4	5	6	5	7	106	Dec 05	Wednesday	
340	4	2	1	2	0	4	1	1	6	10	25	18	5	16	15	3	2	5	10	9	10	8	17	14	188	Dec 06	Thursday	
341	7	5	1	6	5	0	2	5	11	13	0	0	0	0	0	0	0	0	0	0	0	0	0	0	55	Dec 07	Friday	
342	0	0	0	0	0	0	0	0	0	0	0	0	0	0	0	0	0	0	0	0	0	0	0	0	0	Dec 08	Saturday	
343	0	0	0	0	0	0	0	0	0	0	0	0	0	0	0	0	0	0	0	0	0	0	0	0	0	Dec 09	Sunday	
344	0	0	0	0	0	0	0	0	0	0	0	0	0	0	0	0	0	0	0	0	0	0	0	0	0	Dec 10	Monday	
345	0	0	0	0	0	0	0	0	0	0	0	0	0	0	0	0	0	0	0	0	0	0	0	0	0	Dec 11	Tuesday	
346	0	0	0	0	0	0	0	0	0	0	0	0	0	0	0	0	0	0	0	0	0	0	0	0	0	Dec 12	Wednesday	
347	0	0	0	0	0	0	0	0	0	0	0	0	0	0	0	0	0	0	0	0	0	0	0	0	0	Dec 13	Thursday	
348	0	0	0	0	0	0	0	0	0	0	0	0	0	0	0	0	0	0	0	0	0	0	0	0	0	Dec 14	Friday	
349	0	0	0	0	0	0	0	0	0	0	0	0	0	0	0	0	0	0	0	0	0	0	0	0	0	Dec 15	Saturday	
350	0	0	0	0	0	0	0	0	0	0	0	0	0	0	0	0	0	0	0	0	0	0	0	0	0	Dec 16	Sunday	
351	0	0	0	0	0	0	0	0	0	0	0	0	0	0	0	0	0	0	0	0	0	0	0	0	0	Dec 17	Monday	
352	0	0	0	0	0	0	0	0	0	0	0	0	0	0	0	0	0	0	0	0	0	0	0	0	0	Dec 18	Tuesday	
353	0	0	0	0	0	0	0	0	0	0	0	0	0	0	0	0	0	0	0	0	0	0	0	0	0	Dec 19	Wednesday	
354	0	0	0	0	0	0	0	0	0	0	0	0	0	0	0	0	0	0	0	0	0	0	0	0	0	Dec 20	Thursday	
355	0	0	0	0	0	0	0	0	0	0	0	0	0	0	0	0	0	0	0	0	0	0	0	0	0	Dec 21	Friday	
356	0	0	0	0	0	0	0	0	0	0	0	0	0	0	0	0	0	0	0	0	0	0	0	0	0	Dec 22	Saturday	
357	0	0	0	0	0	0	0	0	0	0	0	0	0	0	0	0	0	0	0	0	0	0	0	0	0	Dec 23	Sunday	
358	0	0	0	0	0	0	0	0	0	0	0	0	0	0	0	0	0	0	0	0	0	0	0	0	0	Dec 24	Monday	
359	0	0	0	0	0	0	0	0	0	0	0	0	0	0	0	0	0	0	0	0	0	0	0	0	0	Dec 25	Tuesday	F:rste
360	0	0	0	0	0	0	0	0	0	0	0	0	0	0	0	0	0	0	0	0	0	0	0	0	0	Dec 26	Wednesday	Andre
361	0	0	0	0	0	0	0	0	0	0	0	0	0	0	0	0	0	0	0	0	0	0	0	0	0	Dec 27	Thursday	
362	0	0	0	0	0	0	0	0	0	0	0	0	0	0	0	0	0	0	0	0	0	0	0	0	0	Dec 28	Friday	
363	0	0	0	0	0	0	0	0	0	0	0	0	0	0	0	0	0	0	0	0	0	0	0	0	0	Dec 29	Saturday	
364	0	0	0	0	0	0	0	0	0	0	0	0	0	0	0	0	0	0	0	0	0	0	0	0	0	Dec 30	Sunday	
365	0	0	0	0	0	0	0	0	0	0	0	0	0	0	0	0	0	0	0	0	0	0	0	0	0	Dec 31	Monday	
1	0	0	0	0	0	0	0	0	0	0	0	0	0	0	0	0	0	0	0	0	0	0	0	0	0	Jan 01	Tuesday	F:rste
2	0	0	0	0	0	0	0	0	0	0	0	0	0	0	0	0	0	0	0	0	0	0	0	0	0	Jan 02	Wednesday	
3	0	0	0	0	0	0	0	0	0	0	0	0	0	0	0	0	0	0	0	0	0	0	0	0	0	Jan 03	Thursday	
4	0	0	0	0	0	0	0	0	0	0	0	0	0	0	0	0	0	0	0	0	0	0	0	0	0	Jan 04	Friday	
5	0	0	0	0	0	0	0	0	0	0	0	0	0	0	0	0	0	0	0	0	0	0	0	0	0	Jan 05	Saturday	
6	0	0	0	0	0	0	0	0	0	0	0	0	0	0	0	0	0	0	0	0	0	0	0	0	0	Jan 06	Sunday	
7	0	0	0	0	0	0	0	0	6	4	19	9	10	3	9	3	3	3	1	3	2	8	1	5	89	Jan 07	Monday	
8	2	3	4	5	6	4	2	3	13	13	11	15	17	6	14	7	13	7	2	4	3	4	9	2	169	Jan 08	Tuesday	
9	0	1	0	1	9	0	1	8	13	16	14	14	13	5	15	12	9	9	1	3	2	5	3	2	156	Jan 09	Wednesday	
10	5	2	2	2	10	4	12	5	10	0	0	0	0	0	0	0	0	0	0	0	0	0	0	0	52	Jan 10	Thursday	
11	0	0	0	0	0	0	0	0	7	2	0	0	0	0	0	0	0	0	0	0	0	0	0	0	9	Jan 11	Friday	
12	0	0	0	0	0	0	0	0	0	0	0	0	0	0	0	0	0	0	0	0	0	0	0	0	0	Jan 12	Saturday	
13	0	0	0	0	0	0	0	0	0	0	0	0	0	0	0	0	0	0	0	0	0	0	0	0	0	Jan 13	Sunday	
14	0	0	0	0	0	0	0	0	0	1	20	5	10	7	8	4	13	15	5	6	22	15	21	7	159	Jan 14	Monday	
15	4	15	11	10	5	1	1	6	8	3	12	22	14	9	3	2	4	6	1	2	6	3	2	4	154	Jan 15	Tuesday	
16	3	10	48	37	36	3	9	6	20	11	9	4	23	10	6	10	7	13	15	5	5	5	2	1	298	Jan 16	Wednesday	
17	3	1	0	0	7	2	2	1	2	5	20	11	15	11	2	6	0	4	5	1	5	1	0	6	110	Jan 17	Thursday	
18	0	5	2	5	4	0	0	2	9	16	10	17	5	3	10	3	4	3	3	2	4	2	0	3	112	Jan 18	Friday	
19	1	3	8	6	4	2	0	6	1	20	28	18	8	13	6	2	5	1	3	6	1	1	2	6	151	Jan 19	Saturday	
20	9	8	6	2	1	2	2	1	0	2	9	12	8	16	8	0	4	4	4	8	4	6	1	2	119	Jan 20	Sunday	

Table 3.4.4. (Page 2 of 4)

GER .FKX hourly distribution of detections

Day	00	01	02	03	04	05	06	07	08	09	10	11	12	13	14	15	16	17	18	19	20	21	22	23	Sum	Date
21	4	3	3	2	5	1	3	5	12	10	11	4	28	12	13	4	4	9	4	3	10	6	6	5	167	Jan 21 Monday
22	4	6	4	4	12	16	22	1	0	0	0	0	0	0	0	0	0	0	0	0	0	0	0	0	69	Jan 22 Tuesday
23	0	0	0	0	0	0	0	0	0	0	0	0	0	0	0	0	0	0	0	0	0	0	0	0	0	Jan 23 Wednesday
24	0	0	0	0	0	0	0	0	0	0	0	0	0	0	0	0	0	0	0	0	0	0	0	0	0	Jan 24 Thursday
25	0	0	0	0	0	0	0	0	0	0	0	0	0	0	0	0	0	0	0	0	0	0	0	0	0	Jan 25 Friday
26	0	0	0	0	0	0	0	0	0	0	0	0	0	0	0	0	0	0	0	0	0	0	0	0	0	Jan 26 Saturday
27	0	0	0	0	0	0	0	0	0	0	0	0	0	0	0	0	0	0	0	0	0	0	0	0	0	Jan 27 Sunday
28	0	0	0	0	0	0	0	0	0	0	0	0	0	0	0	0	0	0	0	0	0	0	0	0	0	Jan 28 Monday
29	6	4	7	4	7	3	2	4	9	5	10	22	22	7	13	3	3	12	5	6	9	13	10	6	192	Jan 29 Tuesday
30	3	3	6	6	6	2	1	5	11	15	15	9	5	6	6	2	3	6	7	9	5	6	0	6	143	Jan 30 Wednesday
31	2	3	9	2	1	3	5	2	8	5	9	12	18	14	7	2	1	3	5	6	2	6	2	10	137	Jan 31 Thursday
32	5	1	4	3	7	6	3	2	8	8	15	18	23	7	4	7	6	10	9	5	10	2	2	3	168	Feb 01 Friday
33	7	2	3	1	7	1	4	4	7	7	5	10	9	5	14	6	6	9	8	1	7	6	1	0	130	Feb 02 Saturday
34	3	4	1	2	3	2	1	0	3	12	8	16	26	45	33	6	6	5	3	4	7	2	3	4	199	Feb 03 Sunday
35	1	4	3	4	6	4	2	3	6	4	19	12	17	12	10	8	7	5	10	4	0	6	5	1	153	Feb 04 Monday
36	1	4	2	3	2	3	1	2	13	6	12	12	18	3	4	6	5	4	3	7	6	9	3	1	130	Feb 05 Tuesday
37	5	3	5	1	1	3	5	7	12	6	13	14	19	8	6	3	3	2	8	18	20	34	21	8	225	Feb 06 Wednesday
38	6	3	4	2	6	0	1	8	11	3	7	6	6	14	3	2	3	3	3	7	34	34	37	14	217	Feb 07 Thursday
39	1	3	13	13	10	7	2	0	3	13	11	10	14	6	3	3	2	0	1	1	1	7	1	3	128	Feb 08 Friday
40	2	2	4	1	2	1	2	3	4	1	1	0	10	5	2	1	7	1	0	0	2	1	1	2	55	Feb 09 Saturday
41	1	2	1	0	1	3	0	1	3	0	1	4	10	3	3	1	4	1	0	2	4	16	17	9	87	Feb 10 Sunday
42	15	14	5	5	2	3	0	4	9	8	9	2	10	6	5	6	5	7	1	1	2	1	1	2	123	Feb 11 Monday
43	0	7	3	2	0	1	1	1	2	11	12	11	15	11	9	10	3	2	3	4	3	4	5	0	120	Feb 12 Tuesday
44	5	1	2	3	2	3	1	3	4	4	13	5	25	7	10	11	10	4	4	3	3	3	2	1	129	Feb 13 Wednesday
45	2	5	3	8	3	2	3	2	8	11	17	16	13	8	4	8	12	6	1	5	5	3	6	3	154	Feb 14 Thursday
46	3	3	0	7	1	5	2	1	6	1	9	10	15	11	14	2	2	9	3	7	10	6	5	4	136	Feb 15 Friday
47	4	4	1	2	1	1	2	2	4	3	4	12	11	9	9	1	4	2	2	2	5	3	2	1	91	Feb 16 Saturday
48	0	2	1	4	2	1	4	3	0	10	3	6	4	4	1	3	1	4	5	3	3	2	6	8	80	Feb 17 Sunday
49	4	9	9	4	10	1	5	1	4	10	21	11	17	10	4	5	6	1	3	12	6	5	11	10	179	Feb 18 Monday
50	3	2	7	2	4	2	1	5	10	12	19	31	22	26	24	0	4	10	46	14	5	3	1	11	264	Feb 19 Tuesday
51	31	1	2	5	18	5	4	46	22	15	22	17	21	17	9	10	20	24	17	18	41	42	4	3	414	Feb 20 Wednesday
52	0	4	7	2	2	0	2	11	71	22	25	38	46	0	0	0	1	7	10	8	2	0	0	0	258	Feb 21 Thursday
53	0	0	0	0	0	0	0	0	0	0	0	1	14	12	5	3	10	4	4	8	4	5	3	3	76	Feb 22 Friday
54	3	11	2	3	4	6	6	3	4	6	8	12	16	6	8	8	3	4	7	7	8	3	11	6	155	Feb 23 Saturday
55	3	3	5	2	11	5	2	0	4	7	10	22	6	19	19	2	4	0	5	5	3	10	3	4	154	Feb 24 Sunday
56	4	3	5	7	3	1	4	3	5	9	20	13	14	4	9	8	6	3	4	5	11	4	8	11	164	Feb 25 Monday
57	4	1	2	2	4	4	1	7	9	14	16	13	19	5	16	8	4	6	11	8	10	4	13	4	185	Feb 26 Tuesday
58	13	5	8	6	5	2	4	4	7	13	13	19	24	13	10	8	7	3	11	12	15	7	18	8	235	Feb 27 Wednesday
59	2	6	9	4	4	9	9	2	10	22	25	7	18	16	11	12	10	4	11	12	12	23	6	7	251	Feb 28 Thursday
60	5	4	9	6	5	1	3	5	14	16	22	7	25	15	17	5	10	14	12	2	9	11	12	4	233	Mar 01 Friday
61	8	6	5	9	13	6	6	4	5	16	16	27	23	9	3	3	4	10	12	7	4	3	7	10	216	Mar 02 Saturday
62	8	7	5	4	3	1	7	1	8	6	2	10	11	13	9	9	9	8	12	6	6	5	5	10	165	Mar 03 Sunday
63	10	1	2	8	2	2	5	5	10	11	17	12	15	13	10	6	5	9	2	3	10	4	5	2	169	Mar 04 Monday
64	9	5	9	5	7	2	3	5	10	14	23	20	23	15	20	15	3	6	7	3	25	13	26	9	277	Mar 05 Tuesday
65	8	4	10	9	5	4	2	2	28	19	32	30	0	0	7	8	6	8	4	6	10	6	4	7	219	Mar 06 Wednesday
66	6	12	8	5	7	2	2	1	13	16	23	18	27	15	26	24	36	6	8	19	10	7	13	5	309	Mar 07 Thursday
67	4	7	2	0	8	1	8	2	12	23	31	54	36	16	16	10	7	10	6	15	25	7	7	1	308	Mar 08 Friday
68	3	7	2	4	4	3	11	19	6	0	9	4	5	5	6	2	10	11	7	3	5	2	3	4	135	Mar 09 Saturday
69	6	9	1	4	5	5	2	4	5	0	2	9	12	3	1	21	5	31	4	10	4	5	16	7	171	Mar 10 Sunday
70	7	4	5	10	8	2	5	4	7	4	15	10	17	6	14	36	23	15	12	6	6	21	19	7	263	Mar 11 Monday
71	14	4	11	6	4	2	8	9	12	17	24	25	16	27	21	27	28	9	4	9	9	5	3	4	298	Mar 12 Tuesday
72	1	2	6	7	2	3	3	7	15	9	33	17	18	18	27	20	38	9	19	20	7	3	6	10	300	Mar 13 Wednesday
73	2	0	0	0	0	0	0	0	0	0	0	0	0	0	0	0	0	0	0	0	0	0	0	0	2	Mar 14 Thursday
74	0	0	0	0	0	0	0	0	0	0	0	0	0	0	0	0	0	0	0	0	0	0	0	0	0	Mar 15 Friday
75	0	0	0	0	0	0	0	0	0	0	0	0	0	0	0	0	0	0	0	0	0	0	0	0	0	Mar 16 Saturday
76	0	0	0	0	0	0	0	0	0	0	0	0	0	0	0	0	0	0	0	0	0	0	0	0	0	Mar 17 Sunday

Table 3.4.4. (Page 3 of 4)

GER .FKX Hourly distribution of detections

Day	00	01	02	03	04	05	06	07	08	09	10	11	12	13	14	15	16	17	18	19	20	21	22	23	Sum	Date	
77	0	0	0	0	0	0	0	0	0	0	0	0	0	0	0	0	0	0	0	0	0	0	0	0	0	Mar 18 Monday	
78	0	0	0	0	0	0	0	0	0	0	0	0	0	0	0	0	0	0	0	0	0	0	0	0	0	Mar 19 Tuesday	
79	0	0	0	0	0	0	0	0	0	0	0	0	0	0	0	0	0	0	0	0	0	0	0	0	0	Mar 20 Wednesday	
80	0	0	2	3	5	3	0	4	16	9	20	26	28	16	22	3	17	11	5	3	10	3	8	2	216	Mar 21 Thursday	
81	6	6	6	5	4	5	3	1	5	7	23	14	14	14	3	4	9	10	2	4	2	9	1	6	163	Mar 22 Friday	
82	12	3	2	6	4	6	2	6	3	1	8	11	9	9	8	4	7	9	4	1	20	20	26	11	192	Mar 23 Saturday	
83	7	2	0	6	4	9	8	1	5	22	19	14	17	9	16	22	11	0	0	0	0	0	0	0	172	Mar 24 Sunday	
84	0	0	0	0	0	0	0	0	0	3	15	12	10	6	15	6	7	13	22	7	3	13	10	3	145	Mar 25 Monday	
85	8	5	5	4	7	8	4	1	18	14	20	15	19	7	10	10	13	4	8	11	9	6	8	10	224	Mar 26 Tuesday	
86	10	8	2	2	8	6	3	0	19	23	29	23	15	14	9	10	13	10	3	7	13	6	12	15	260	Mar 27 Wednesday	
87	5	7	5	5	8	13	25	9	20	1	18	18	17	7	9	11	7	5	5	7	14	17	16	11	260	Mar 28 Thursday	Skj(rt
88	6	8	2	7	3	1	4	5	25	7	31	19	10	15	7	17	6	12	1	7	14	10	13	15	245	Mar 29 Friday	Langfr
89	3	1	1	8	5	4	7	5	7	9	13	13	12	6	16	21	18	9	8	13	30	25	21	10	265	Mar 30 Saturday	
90	5	5	2	5	4	4	1	8	2	2	14	4	4	0	3	7	3	7	3	5	6	7	5	0	106	Mar 31 Sunday	F:rste
GER	00	01	02	03	04	05	06	07	08	09	10	11	12	13	14	15	16	17	18	19	20	21	22	23			
Sum	581	517	563	501	534	342	396	521	1144	1117	1719	1630'	1737	1197	1270	885	786	809	901	887	1021	932	873	617	21480	Total sum	
116	5	4	5	4	5	3	3	4	10	10	15	14	15	10	11	8	7	7	8	8	9	8	8	5	185	Total average	
84	5	4	5	4	5	3	3	5	11	10	16	15	16	10	11	8	7	7	8	7	9	8	7	5	189	Average workdays	
32	6	5	5	5	4	4	4	4	7	7	11	11	12	10	10	7	6	8	7	8	8	9	9	7	175	Average weekends	

Table 3.4.4. Daily and hourly distribution of GERESS detections. For each day is shown number of detections within each hour of the day, and number of detections for that day. The end statistics give total number of detections distributed for each hour and the total sum of detections during the period. The averages show number of processed days, hourly distribution and average per processed day. (Page 4 of 4)

3.5 IMS operation

The Intelligent Monitoring System (IMS) was installed at NORSAR in December 1989 and has been operated experimentally since 1 January 1990 for automatic processing of multiple-array data. The current version of IMS processes data from the two-array network consisting of NORESS and ARCESS. An upgrade of IMS scheduled for mid-91 will allow data from additional arrays and single stations to be incorporated.

In general, our routine operation of the IMS during the reporting period has progressed well, and the system has proved to be very powerful and flexible. The well-developed automatic processing combined with very versatile interactive tools has kept the analyst workload at a low level, and in fact only one analyst has been required to handle the regular processing at any time.

Since the IMS is still in an initial stage, there have naturally been some problems of a technical nature, but these have diminished considerably as the system has matured.

Table 3.5.1 presents an overview of IMS event processor downtimes. Table 3.5.2 gives a summary of phase detections and processed regional events by IMS. From top to bottom, the table gives the total number of detections by the IMS, the detections that are associated with regional events declared by the IMS, the number of detections that are not associated with such events, the number of regional events declared by the IMS, the number of such events rejected by the analyst, the number of events accepted by the analyst, the number of events accepted by the analyst without any changes, and finally the number of events accepted after some sort of modification by the analyst. This last category is divided into two classes: Events where phases (not detected by the IMS) have been added by the analyst and events for which the phase assignments by the IMS have been changed or one or more phase detections have been removed.

From initial review of the IMS bulletin, it is clear that the final output is of very high quality from a seismological point of view. More detailed evaluation will be conducted at a later stage.

B.Kr. Hokland
U. Baadshaug
S. Mykkeltveit

```
1990 Oct  1 00:00:00.000 - 1990 Oct  2 00:00:00.000
1990 Dec 11 05:52:10.200 - 1990 Dec 11 14:34:29.600
1991 Feb  7 22:00:00.000 - 1991 Feb  8 08:00:00.000
1991 Feb 13 12:00:00.000 - 1991 Feb 14 10:00:00.000
1991 Feb 14 23:00:00.000 - 1991 Feb 16 03:00:00.000
```

Table 3.5.1. IMS event processor (pipeline) downtimes.

	Oct 90	Nov 90	Dec 90	Jan 91	Feb 91	Mar 91	Total
Phase detections	18011	15578	18127	19042	15652	13854	100264
- Associated phases	2618	2664	2325	2715	2255	2943	15520
- Unassociated phases	15393	12914	15802	16327	13397	10911	84744
Events declared	991	1048	913	1156	957	1126	6191
- Rejected events	192	229	215	246	213	174	1269
- Accepted events	799	819	698	910	744	952	4922
Unchanged events	239	227	166	262	227	263	1384
Modified events	560	592	532	648	517	689	3538
Phases added	39	48	41	48	54	61	291
Phases changed or removed	521	544	491	600	463	628	3247

Table 3.5.2. IMS phase detections and events summary.

4 Improvements and Modifications

4.1 NORSAR

NORSAR data acquisition

No modification has been made to the NORSAR data acquisition system.

NORSAR detection processing

The NORSAR detection processor has been running satisfactorily on the IBM during this reporting period.

Detection statistics are given in section 2.

NORSAR event processing

There are no changes in the routine processing of NORSAR events, using the IBM system.

NORSAR upgrade

Testing of new digitizer systems has been going on. It is now clear that it will be possible to transmit sufficient DC power through existing cables to operate modern 24 bit digitizers at the remote sites.

The strategy for upgrading the NORSAR system is to continue testing of available 24 bit digitizer systems to evaluate their performance, and within the coming year to acquire continuous data from one subarray.

In parallel with hardware testing, there is a need to reanalyze NORSAR master events to generate a new data base of time delay corrections.

4.2 NORESS/ARCESS/FINESA/GERESS

Detection processing

The routine detection processing of the array data is running satisfactorily on each of the arrays' SUN-3/280 acquisition systems. The same program is used for NORSAR, NORESS, ARCESS, FINESA, and GERESS, but with different recipes. The beam tables for NORESS and ARCESS are found in NORSAR Sci. Rep. No. 1-89/90. The beam table for FINESA/GERESS is found in NORSAR Sci. Rep. No. 1-90/91.

Detection statistics are given in section 3.

During this reporting period, two new three-component stations have been installed in Poland. KSP is located at Ksiaz (50.8°N, 16.3°E), and SFP is located at Stary Folwark (54.3°N, 23.3°E).

Data acquisition for the two stations in Poland has been running during test periods along with detection processing. Detection (STA/LTA) processing is performed on the vertical component using 13 different filter bands. Incoherent detection processing has been tested on the horizontal components. The subsequent signal processing is still in an experimental mode and is focusing on the difficult problem of phase identification.

Event processing. Phase estimation

This process performs F-K and polarization analysis for each detection to identify phase velocity, azimuth and type of phase, and the results are put into the ORACLE detection data base for use by IAS.

Plot and epicenter determination

Descriptions of single array event processing are found in NORSAR Sci. Rep. No. 2-88/89 and NORSAR Sci. Rep. No. 2-89/90.

J. Fyen

5 Maintenance Activities

5.1 Activities in the field and at the Maintenance Center

This section summarizes the activities in the field, at the Maintenance Center (NMC) Hamar and NDPC activities related to monitoring and control of the NORSAR, NORESS, ARCESS, FINESA and GERESS arrays. The recently installed stations in Poland were not fully operational by the end of March 1991, but data from these stations have been subjected to NDPC monitoring during selected time intervals.

Activities involve preventive and corrective maintenance, and in addition installation and testing of new equipment related to satellite communication (P.W. Larsen, Poland, October 1990) and installation and testing of a new UPS system (ARCESS, October 1990).

NORSAR

This array was visited in October and November 1990 and in January and March 1991. Activities related to this array have been diverse, involving: preventive maintenance, cable splicing/location of cables, adjustment of Channel gain and DC offset, RA-5 amplifier replacements, work on 02B (tel) including channel VCO adjustment, battery replacement, SP/LP instrument adjustments, and SLEM reset after power outages. Finnaly, there was work in connection with testing of an RD-3 (Remote Digitizer) in conjunction with the NORSAR upgrade activities.

NORESS

The NORESS array was visited in November 1990 and January 1991. The satellite clock was replaced, the UPS reset and a test of the Megamux multiplexer was carried out.

ARCESS

This array was visited in October and December 1990 in connection with installation of a new UPS (Uninterrupted Power Supply), replacement of a seismometer cable, adjustment of fiber optic links between the hub and remote sites, and restart and check of UPS equipment (Dec 1990).

FINESA

There were no visits in the period.

Poland

Satellite communication equipment was installed (October 1990).

Details on all actitivites are presented in Table 5.1.

Subarray/ area	Task	Date
NORSAR:		
01A	Preventive maintenance including adjustment of channel gain, DC offset. Also cable work SP02 carried out.	25 Oct
01B	Preventive maintenance. Cable splicing SP04	9 Oct
02B	Preventive maintenance.	26 Oct
02C	Preventive maintenance.	24 Oct
03C	Preventive maintenance.	26 Oct
04C	Preventive maintenance.	29 Oct
06C	Preventive maintenance. In addition, splicing of cable SP02, 04 05.	10 Oct
ARCESS:	Installed a new UPS. Replaced defective seismometer cable at site B5. Adjusted all fiber links between the hub and remote sites.	1-7 Oct
Poland:	P.W. Larsen installed satellite communication equipment.	23-30 Oct
NDPC:	Daily status check of all arrays Weekly calibration of NORSAR SP/LP instruments Continuous measurement of Mass Position and Free Period. Adjusted when outside tolerances	Oct
NORSAR:		
01A	Cable splicing, SP02	2 Nov
	Cable splicing, SP05	5 Nov
06C	Replaced RA-5 amplifier SP01	8 Nov
02C	Visited the subarray in connection with communication cable damage	12 Nov
02B(tel)	Station 05 work, channel inoperative	28 Nov
NORESS:	Replaced satellite clock. UPS reset.	13,19 Nov
NDPC:	Daily status check of all arrays. Weekly calibration of NORSAR SP/LP instruments Continuous measurement of Mass Position and Free Period	Nov

Table 5.1 Activities in the field and the NORSAR Maintenance Center, including NDPC activities related to the NORSAR, NORESS, ARCESS and FINESA arrays, 1 October 1990 – 31 March 1991.

Subarray/ area	Task	Date
ARCESS:	Restart of UPS equipment	14,15 Dec
NDPC:	Daily status check of all arrays. Weekly calibration of NORSAR SP/LP instruments Continuous measurement of Mass Position and Free Period Adjustment of Mass Position and Free Period when outside tolerances	Dec
NORSAR:		
02B(tel)	Adjusted VCO, ch. 5	4 Jan
06C	Adjusted SP/LP instruments	7 Jan
02B	SLEM restart after power outage.	23 Jan
NORESS:	Megamux installed in connection with a test.	9 Jan
	Megamux disconnected after test completed.	11 Jan
NDPC:	Daily status check of all arrays. Weekly calibration of NORSAR SP/LP instruments Continuous measurement of Mass Position and Free Period Adjustment of Mass Position and Free Period when *outside tolerances*	Jan 1991
NMC:	Work in connection with NORSAR upgrading	Feb
NDPC:	Daily status check of all arrays. Weekly calibration of NORSAR SP/LP instruments Continuous measurement of Mass Position and Free Period Adjustment of Mass Position and Free Period when outside tolerances	Feb

Table 5.1 (cont.)

Subarray/ area	Task	Date
NORSAR:		
06C	An RD-3 (Remote Digitizer) was tested on channel 01	6,10 Mar
06C	Replaced RA-5 amplifier ch 03	14 Mar
02B(tel)	Replaced channel 4 battery.	7 Mar
NDPC:	Daily status check of all arrays.	Mar
	Weekly calibration of NORSAR SP/LP instruments	
	Continuous measurement of Mass Position and Free Period	
	Adjustment of Mass Position and Free Period when outside tolerances	

Table 5.1 (cont.)

5.2 Array status

As of 31 March 1991 the following NORSAR channels deviated from tolerances.

01A 01 8 Hz filter
02 8 Hz filter
04 30 dB attenuator

O.A. Hansen

6 Documentation Developed

Bannister, S.C., E.S. Husebye and B.O. Ruud: Teleseismic P coda analyzed by three-component and array techniques: Deterministic location of topographic P-to-Rg scattering near the NORESS array, *Bull. Seism. Soc. Am.*, 80, 1969–1986, 1990.

Dahle, A., H. Bungum and L.B. Kvamme: Empirically derived PSV spectral attenuation models for intraplate conditions, *European Earthq. Eng.*, submitted for publication.

Havskov, J., L.B. Kvamme, R.A. Hansen, H. Bungum and C.D. Lindholm: The Northern Norway Seismic Network: Design, operation and results, *Bull. Seism. Soc. Am.*, in press.

Kværna, T. and D.J. Doornbos: Scattering of regional P_n by Moho topography, *Geophys. Res. Lett.*, in press.

Mykkeltveit, S. (Ed.): *Basic Seismological Research, 1 October 1989 – 30 September 1990.* Final Report, Kjeller, Norway.

Semiannual Tech. Summary, 1 Apr – 30 Sep 1990, NORSAR Sci. Rep. No. 1-90/91, Kjeller, Norway.

L.B. Loughran

7 Summary of Technical Reports / Papers Published

7.1 RMS Lg analysis of Novaya Zemlya explosion recordings

Introduction

In recent years, much attention has focused upon the use of the seismic Lg phase to determine the yield of underground nuclear explosions. In the first of a number of Lg studies undertaken by the NORSAR staff during the 1980s, Ringdal (1983) analyzed digital NORSAR Lg data of selected Semipalatinsk events. He found that, when using NORSAR RMS Lg instead of P waves recorded at NORSAR to estimate source size, it was possible to eliminate effectively the magnitude bias relative to worldwide m_b observed at NORSAR between Degelen and Shagan River explosions. The method consisted of averaging log(RMS) values of individual NORSAR channels, filtered in a band of 0.6 to 3.0 Hz in order to enhance Lg signal-to-noise ratio. Ringdal and Hokland (1987) expanded the data base and introduced a noise compensation procedure to improve the reliability of measurement at low SNR values. They were able to identify a distinct P-Lg bias between the Northeast and Southwest portions of the Shagan River Test Site, a feature that was confirmed by Ringdal and Fyen (1988) using Gräfenberg array data. Ringdal and Marshall (1989) combined P- and Lg-based source size estimators to estimate the yields of 96 Shagan River explosions from 1965 to 1988, using data on the cratering explosion of 15 January 1965 as a reference for the yield calculations.

Hansen, Ringdal and Richards (1990) analyzed available data from stations in China and the Soviet Union, and found that RMS Lg of Semipalatinsk explosions measured at these stations showed excellent consistency. They concluded that for explosions at Semipalatinsk with good signal-to-noise ratio, $m_b(Lg)$ may be estimated at single stations with an accuracy (one standard deviation) of about 0.03 magnitude unit. It is noteworthy that this accuracy was consistently obtained for a variety of stations at very different azimuths and distances, even though the basic parameters remained exactly as originally proposed by Ringdal for NORSAR recordings (0.6–3.0 Hz bandpass filter, RMS window length of 2 minutes, centered at a time corresponding to a group velocity of 3.5 km/s).

In this paper we apply Ringdal's method to NORSAR and Gräfenberg recordings of Novaya Zemlya explosions. This initial study focuses on the Northern Novaya Zemlya test site, and we will only consider explosions occurring after 1976.

Data

The data base for this study comprises seismic recordings at NORSAR and Gräfenberg for 18 presumed underground nuclear explosions at Novaya Zemlya from 1976 through 1990.

The NORSAR array (Bungum, Husebye and Ringdal, 1971) was established in 1970, and originally comprised 22 subarrays, deployed over an area of 100 km diameter. Since 1976 the number of operational subarrays has been 7, comprising altogether 42 vertical-component SP sensors (type HS-10). In this paper, analysis has been conducted using data from these 7 subarrays. Sampling rate for the NORSAR SP data is 20 samples per second, and all data are recorded on digital magnetic tape.

The Gräfenberg array (Harjes and Seidl, 1978) was established in 1976, and today comprises 13 broadband seismometer sites, three of which are 3-component systems. The instrument response is flat to velocity from about 20 second period to 5 Hz. Sampling rate is 20 samples per second, and the data are recorded on digital magnetic tape.

Fig. 7.1.1 shows the Lg propagation paths from Novaya Zemlya to the two arrays. The distance and azimuth are 2200 km and 256 degrees to NORSAR, compared to 3300 km and 213 degrees to Gräfenberg. Both paths cross the Barents Sea, and as observed by several authors (see Baumgardt, 1990), this implies significant Lg blockage effects. The result is particularly visible on NORSAR records, which show relatively weak Lg energy compared to the P and Sn phases.

Examples of NORSAR recordings of one of the explosions are shown in Fig. 7.1.2. We note that this (as well as most of the other events analyzed) exhibits signal clipping of both P and Sn. This is a result of the very strong seismic signals recorded at NORSAR for Novaya Zemlya explosions, in combination with the limited dynamic range of the digital recording system. For this reason, we have chosen to measure the RMS Lg at NORSAR by selecting a 2-minute window in the Lg coda, starting at 10 1/2 min after the origin time of the event (see the figure). Previous studies of Semipalatinsk explosions have shown that the RMS method is not very sensitive to the exact positioning of the time window, as long as it is kept the same for all events analyzed.

On Fig. 7.1.2, we have also indicated a two-minute P coda window, which we have used to calculate NORSAR P coda magnitudes for the explosions, using the array RMS method. The P coda window starts 6 minutes after the event origin time.

In Fig. 7.1.3 we show an example of GRF recordings of one of the explosions. Here, the dynamic range is sufficient to avoid any clipping, and we have selected a two-minute window which includes the main Lg energy, starting 16 minutes after event origin time.

Analysis results

Applying the RMS measurement technique using our standard filter band (0.6-3.0 Hz) and averaging over array elements as described by Ringdal and Hokland (1987), we arrive at results listed in Tables 7.1.1 through 7.1.3.

Table 7.1.1 gives our results for NORSAR P-coda magnitudes, using the time window indicated on Fig. 7.1.2. A constant correction factor has been added to the log(RMS) values to make these coda magnitudes consistent, on the average, with world-wide m_b.

Table 7.1.2 covers the NORSAR Lg results, and shows that RMS Lg can be estimated for all the events processed, including two events below $m_b = 5.0$ (events 2 and 4). (For the 27 Sep 78 explosion, no NORSAR data are available.)

Table 7.1.3 gives corresponding Lg results for the Gräfenberg array. Here, the smallest of the events (Event 4) had too low SNR to allow reliable measurements.

The m_b values listed in Tables 7.1.1 through 7.1.3 are taken from Lilwall and Marshall (1986) for events up to 1984, and have been calculated from NEIC station reports for later events.

Fig. 7.1.4 shows a comparison of world-wide m_b and NORSAR P coda magnitudes. We note that the correspondence is excellent (orthogonal standard deviation is only 0.027). Thus the NORSAR recordings appear to provide a very stable measure of m_b for events from this test site.

Figs. 7.1.5 and 7.1.6 are scatter plots comparing world-wide m_b to NORSAR and Gräfenberg RMS Lg magnitudes. We note that there is a considerable scatter in both of these plots. In particular, it appears that the majority of events have almost the same M(Lg), whereas the m_b values vary from below 5.7 to above 6.0 for this group.

It is especially interesting to note that NORSAR M(Lg) deviates significantly from m_b, whereas NORSAR P coda corresponds very closely to m_b.

Fig. 7.1.7 shows a scatter plot of Gräfenberg versus NORSAR M(Lg). The correspondence is excellent, with an orthogonal standard deviation of only 0.035. The scatter is further reduced (to 0.025) if we consider only events with at least 5 available GRF channels (Fig. 7.1.8). Thus, we obtain the same close correspondence between Lg observations from these two arrays for Novaya Zemlya explosions as has previously been observed for Semipalatinsk events.

With the current lack of independently obtained calibration data, it would be premature to draw any firm conclusions as to the relative accuracy of m_b and M(Lg) in estimating yields of these explosions. Nevertheless, it would appear that the close grouping in M(Lg), especially seen for the NORSAR data, is unlikely to be a coincidence. It would seem reasonable to conclude that this group of explosions has very nearly the same yield, in spite of the divergence in m_b estimates. However, additional analysis, in particular including available Lg data from Soviet stations for this event set, should be performed in order to further test this hypothesis.

F. Ringdal
J. Fyen

References

Baumgardt, D. (1990): Investigation of teleseismic Lg blockage and scattering using regional arrays, *Bull. Seism. Soc. Am.*, Vol. 80, Special Issue, 2261–2281.

Bungum, H., E.S. Husebye and F. Ringdal (1971): The NORSAR array and preliminary results of data analysis, *Gepohys. J.*, Vol. 25, 115–126.

Hansen, R.A., F. Ringdal and P.G. Richards (1990): The stability of RMS Lg measurements and their potential for accurate estimation of the yields of Soviet underground nuclear explosions, *Bull. Seism. Soc. Am.*, Vol. 80, Special Issue, 2106–2126.

Harjes, H.P. and D. Seidl (1978): Digital recording and analysis of broadband seismic data at the Gräfenberg (GRF) array, *J. Geophys. Res.*, Vol. 44, 511–523.

Lilwall, R.C. and P.D. Marshall (1986): Body wave magnitudes and locations of Soviet underground explosions at the Novaya Zemlya test site, *AWRE Report No. O 17/86*, HMSO, London.

Ringdal, F. (1983): Magnitudes from P coda and Lg using NORSAR data, in *NORSAR Semiannual Technical Summary, 1 Oct 82 - 31 Mar 83*, NORSAR Sci. Rep. 2-82/83, NORSAR, Kjeller, Norway.

Ringdal, F. and B.Kr. Hokland (1987): Magnitudes of large Semipalatinsk explosions using P coda and Lg measurements at NORSAR, in *NORSAR Semiannual Technical Summary, 1 Apr - 30 Sep 87*, NORSAR Sci. Rep. 1-87/88, NORSAR, Kjeller, Norway.

Ringdal, F. and J. Fyen (1988): Comparative analysis of NORSAR and Gräfenberg Lg magnitudes for Shagan River explosions, in *NORSAR Semiannual Technical Summary, 1 Apr - 30 Sep 88*, NORSAR Sci. Rep. 1-88/89, NORSAR, Kjeller, Norway.

Ringdal, F. and P.D. Marshall (1989): Yield determination of Soviet underground nuclear explosions at the Shagan River Test Site, in *NORSAR Semiannual Technical Summary, 1 Oct 88 - 31 Mar 89*, NORSAR Sci. Rep. 2-88/89, NORSAR, Kjeller, Norway.

Ev	Date	Origin time	mb	NCH	Noise	STD	Pcoda	STD	CORR	m(Pcoda)
01	29/09/76-273	03.00.00.00	5.77	40/42	1.867	0.064	3.133	0.049	3.132	5.732
02	20/10/76-294	08.00.00.00	4.89	40/42	1.933	0.066	2.405	0.048	2.378	4.978
03	01/09/77-244	03.00.00.00	5.71	34/41	1.777	0.062	3.151	0.045	3.150	5.750
04	09/10/77-282	11.00.00.00	4.51	40/41	1.908	0.066	2.139	0.047	2.046	4.646
05	10/08/78-222	08.00.00.00	6.04	33/39	1.862	0.066	3.352	0.046	3.352	5.952
06	27/09/78-270	02.05.00.00	5.68	*00/00	0.000	0.000	0.000	0.000	0.000	0.000
07	24/09/79-267	03.30.00.00	5.80	38/39	1.852	0.059	3.182	0.050	3.182	5.782
08	18/10/79-291	07.10.00.00	5.85	28/39	1.918	0.050	3.222	0.050	3.221	5.821
09	11/10/80-285	07.10.00.00	5.80	32/38	1.911	0.060	3.176	0.041	3.176	5.776
10	01/10/81-274	12.15.00.00	5.91	20/39	1.959	0.063	3.282	0.037	3.282	5.882
11	11/10/82-284	07.15.00.00	5.52	27/40	1.828	0.085	2.952	0.050	2.951	5.551
12	18/08/83-230	16.10.00.00	5.84	25/39	1.776	0.054	3.170	0.054	3.169	5.769
13	25/09/83-268	13.10.00.00	5.71	24/39	2.148	0.055	3.125	0.052	3.123	5.723
14	25/10/84-299	06.30.00.00	5.77	28/41	1.932	0.063	3.144	0.066	3.143	5.743
15	02/08/87-214	02.00.00.00	5.71	28/40	1.908	0.080	3.170	0.048	3.169	5.769
16	07/05/88-128	22.50.00.00	5.52	27/40	1.478	0.066	3.014	0.038	3.014	5.614
17	04/12/88-339	05.20.00.00	5.79	30/40	2.055	0.061	3.223	0.046	3.222	5.822
18	24/10/90-297	14.58.00.00	5.60	38/40	1.822	0.070	3.019	0.044	3.018	5.618

Table 7.1.1. NORSAR RMS P coda magnitudes for events in the data base. The table lists event number, origin date and time, world-wide m_b and a list of measurements made in this study:

NCH	: Number of NORSAR data channels used, and the total number available
Noise	: Array averaged log RMS values in a noise window
STD	: Corresponding standard deviation across array
Pcoda	: Array averaged log RMS values in the P coda window
STD	: Corresponding standard deviation
CORR	: Noise-corrected log RMS values of the P coda
m(Pcoda)	: P coda magnitude derived by adding a constant term to the noise-corrected values.

Ev	Date Origin time	mb	NCH	Noise	STD	Lg	STD	LgCORR	MLg(NAO)
01	29/09/76-273:03.00.00.00	5.77	40/42	1.867	0.064	3.161	0.065	3.160	5.770
02	20/10/76-294:08.00.00.00	4.89	40/42	1.933	0.066	2.479	0.065	2.461	5.071
03	01/09/77-244:03.00.00.00	5.71	34/41	1.777	0.062	3.147	0.065	3.147	5.757
04	09/10/77-282:11.00.00.00	4.51	40/41	1.906	0.063	2.278	0.059	2.235	4.845
05	10/08/78-222:08.00.00.00	6.04	33/39	1.862	0.066	3.174	0.057	3.173	5.783
06	27/09/78-270:02.05.00.00	5.68	*00/00	0.000	0.000	0.000	0.000	0.000	0.000
07	24/09/79-267:03.30.00.00	5.80	38/39	1.852	0.059	3.170	0.063	3.169	5.779
08	18/10/79-291:07 10.00.00	5.85	28/39	1.918	0.050	3.128	0.060	3.127	5.737
09	11/10/80-285:07 10.00.00	5.80	32/38	1.911	0.060	3.175	0.060	3.174	5.784
10	01/10/81-274:12 15.00.00	5.91	20/39	1.959	0.063	3.173	0.044	3.172	5.782
11	11/10/82-284:07.15.00.00	5.52	27/40	1.828	0.085	2.994	0.074	2.993	5.603
12	18/08/83-230:16.10.00.00	5.84	25/39	1.776	0.054	3.197	0.062	3.197	5.807
13	25/09/83-268:13.10.00.00	5.71	24/39	2.148	0.055	3.189	0.047	3.187	5.797
14	25/10/84-299:06.30.00.00	5.77	28/41	1.932	0.063	3.196	0.075	3.195	5.805
15	02/08/87-214:02.00.00.00	5.71	28/40	1.908	0.080	3.197	0.078	3.196	5.806
16	07/05/88-128:22.50.00.00	5.52	27/40	1.478	0.066	3.109	0.064	3.109	5.719
17	04/12/88-339:05.20.00.00	5.79	30/40	2.055	0.061	3.191	0.053	3.190	5.800
18	24/10/90-297:14.58.00.00	5.60	38/40	1.822	0.070	2.996	0.058	2.995	5.605

NOTE: The M(Lg) values have been obtained by adding a constant correction term (2.610) to the noise corrected log RMS Lg values. This correction term is preliminary, and may be subject to later revision.

Table 7.1.2. NORSAR RMS Lg magnitudes for events in the data base. The structure of the table is analogous to Table 7.1.1. The rightmost column lists the NORSAR M(Lg) values.

Ev	Date	Origin time	mb	NCH	Noise	STD	Lg	STD	LgCORR	MLg(GRF)
01	29/09/76-273	03.00.00.00	5.77	02/04	1.118	0.086	2.025	0.035	2.022	5.799
02	20/10/76-294	08.00.00.00	4.89	03/04	1.318	0.047	1.435	0.041	1.245	5.022
03	01/09/77-244	03.00.00.00	5.71	03/04	1.023	0.007	2.097	0.021	2.095	5.872
04	09/10/77-282	11.00.00.00	4.51	*03/04	1.223	0.008	1.255	0.085	0.000	0.000
05	10/08/78-222	08.00.00.00	6.04	05/13	1.223	0.069	1.988	0.102	1.982	5.759
06	27/09/78-270	02.05.00.00	5.68	06/13	1.270	0.132	1.896	0.114	1.883	5.660
07	24/09/79-267	03.30.00.00	5.80	07/13	1.217	0.097	2.053	0.118	2.048	5.825
08	18/10/79-291	07.10.00.00	5.85	10/13	1.350	0.100	1.905	0.116	1.887	5.664
09	11/10/80-285	07.10.00.00	5.80	13/13	1.350	0.128	1.968	0.115	1.955	5.732
10	01/10/81-274	12.15.00.00	5.91	08/13	1.416	0.069	2.019	0.099	2.006	5.783
11	11/10/82-284	07.15.00.00	5.52	13/13	1.291	0.121	1.828	0.120	1.808	5.585
12	18/08/83-230	16.10.00.00	5.84	12/13	1.214	0.122	2.066	0.135	2.062	5.739
13	25/09/83-268	13.10.00.00	5.71	13/13	1.126	0.103	2.004	0.145	2.000	5.777
14	25/10/84-299	06.30.00.00	5.77	13/13	1.382	0.131	2.069	0.124	2.060	5.837
15	02/08/87-214	02.00.00.00	5.71	12/13	1.033	0.138	2.035	0.147	2.033	5.810
16	07/05/88-128	22.50.00.00	5.52	12/13	1.018	0.162	1.881	0.148	1.877	5.654
17	04/12/88-339	05.20.00.00	5.79	13/13	1.195	0.147	2.038	0.128	2.034	5.811
18	24/10/90-297	14.58.00.00	5.60	08/13	1.452	0.214	1.817	0.150	1.773	5.550

NOTE: The M(Lg) values have been obtained by adding a constant correction term (3.777) to the noise corrected log RMS Lg values. This correction term is preliminary, and may be subject to later revision.

Table 7.1.3. Gräfenberg RMS Lg magnitudes for events in the data base. The structure of the table is analogous to Table 7.1.1. The rightmost column lists the Gräfenberg M(Lg) values.

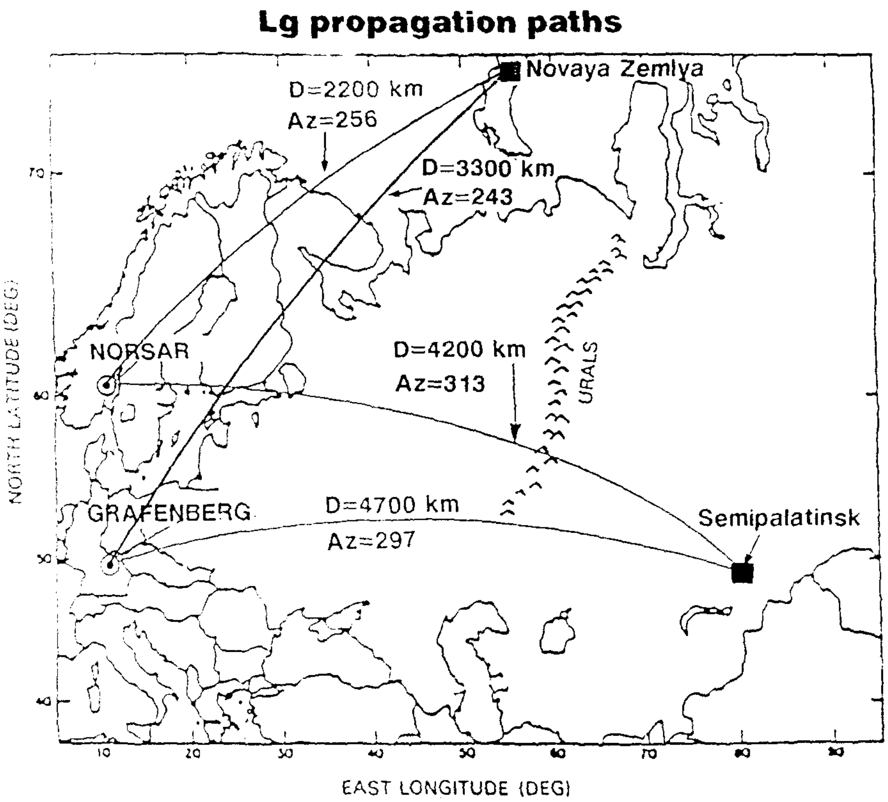

Fig. 7.1.1. Map showing the Lg propagation paths from the main Soviet test sites (Novaya Zemlya and Semipalatinsk) to the NORSAR and Gräfenberg arrays.

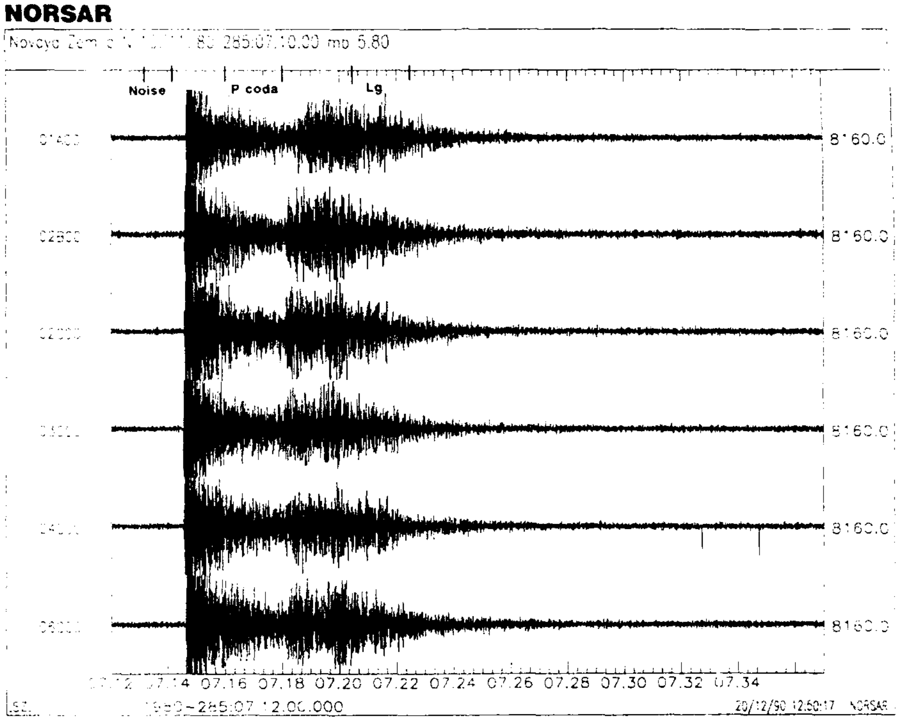

Fig. 7.1.2. Example of NORSAR recordings of a Novaya Zemlya explosion (11 October 1980). The center instrument of each of the 7 subarrays is displayed, covering 25 minutes of unfiltered data. The positioning of time windows used for RMS Lg, Pcoda and noise measurements is indicated. Note the clipping of the initial P and that also the S phase is close to exceeding the dynamic range.

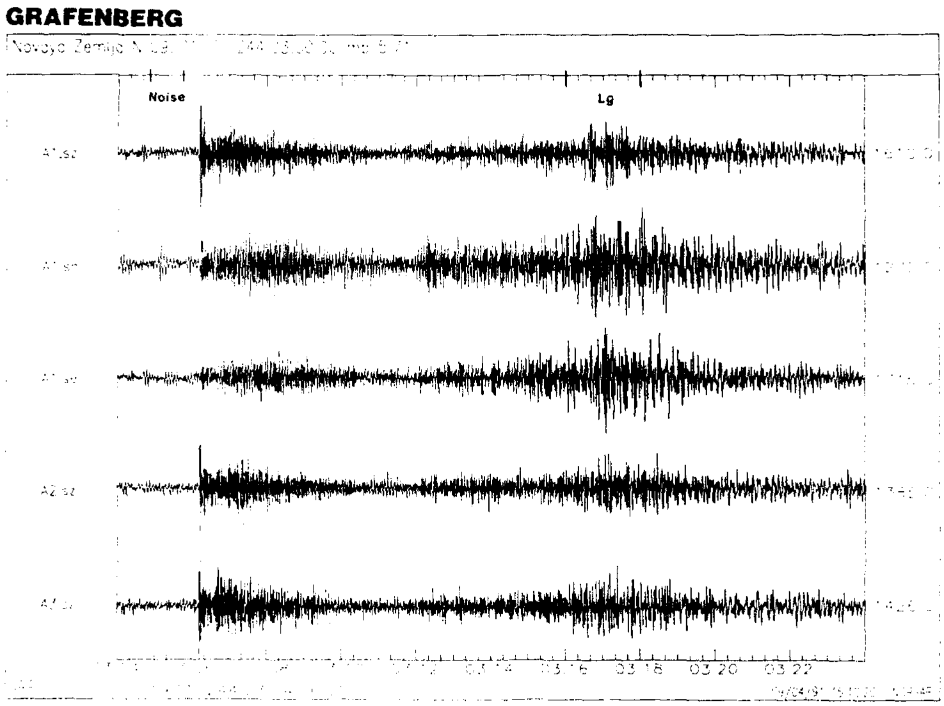

Fig. 7.1.3. Example of Gräfenberg recordings of a Novaya Zemlya explosion (1 September 1977). The figure shows 20 minutes of unfiltered data from the three components of the A1 seismometer site and the vertical-component A2 and A3 instruments. *Note that the horizontal components have not been used in our analysis.* The positioning of time windows used for RMS Lg and noise measurements is indicated.

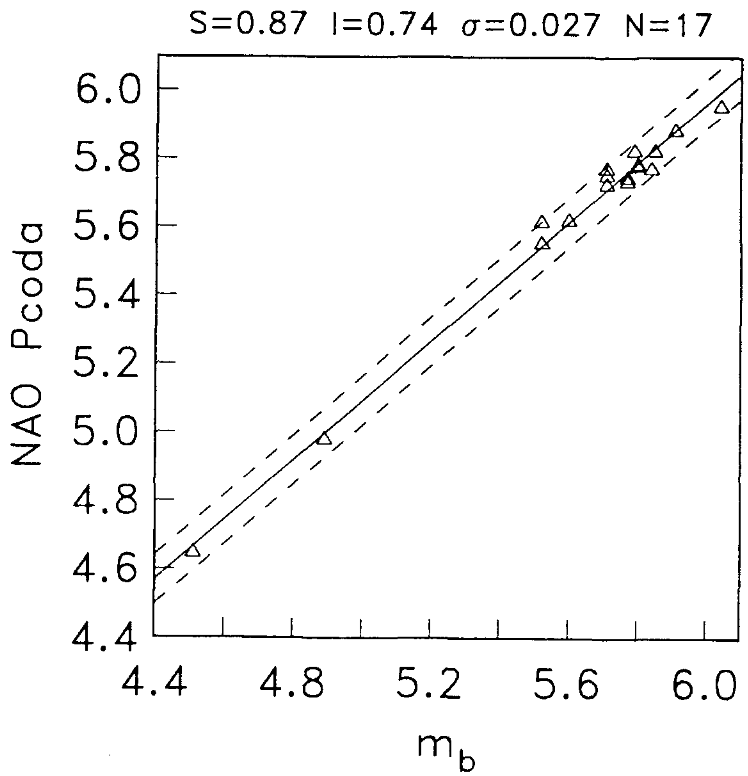

Fig. 7.1.4. Plot of NORSAR RMS P coda m_b versus world-wide m_b for events in the data base. The straight line has been obtained by least-squares regression with respect to the horizontal axis, and the stippled lines correspond to plus/minus two standard deviations. The slope (S), intercept (I), orthogonal standard deviation (σ) and number of data points (N) are listed on the figure. Note the remarkably close correspondence between the two estimators.

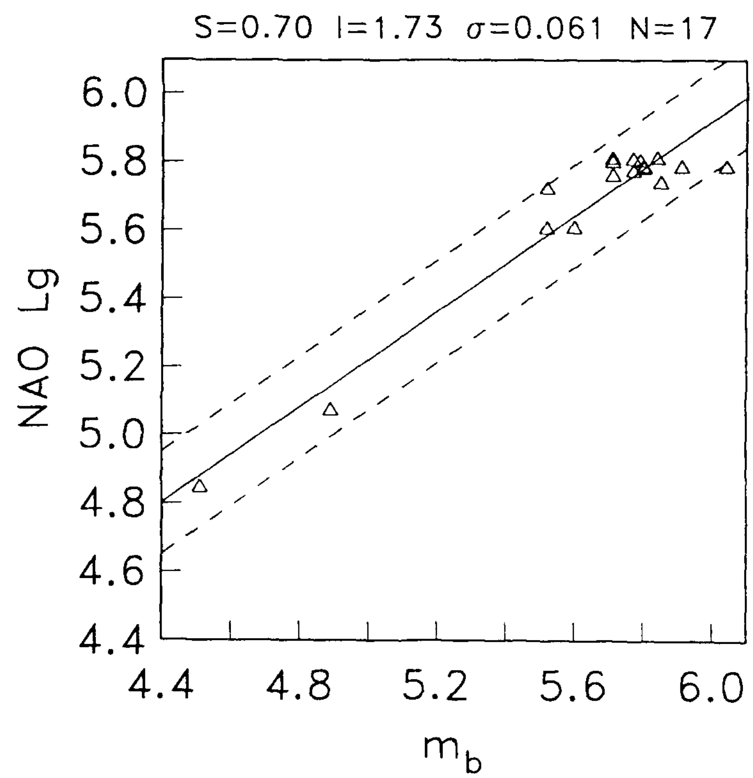

Fig. 7.1.5. Plot of NORSAR RMS Lg magnitude versus world-wide m_b. Note the much greater scatter in this plot compared to Fig. 7.1.4. Notational conventions are as in Fig. 7.1.4.

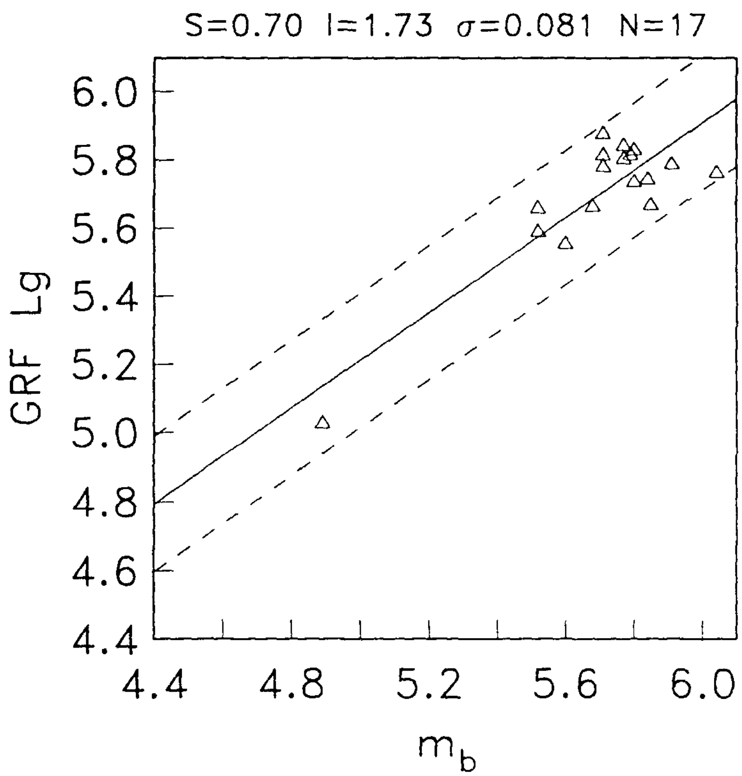

Fig. 7.1.6. Plot of Gräfenberg RMS Lg magnitude versus world-wide m_b. The scatter is comparable to Fig. 7.1.5. Notational conventions are as in Fig. 7.1.4.

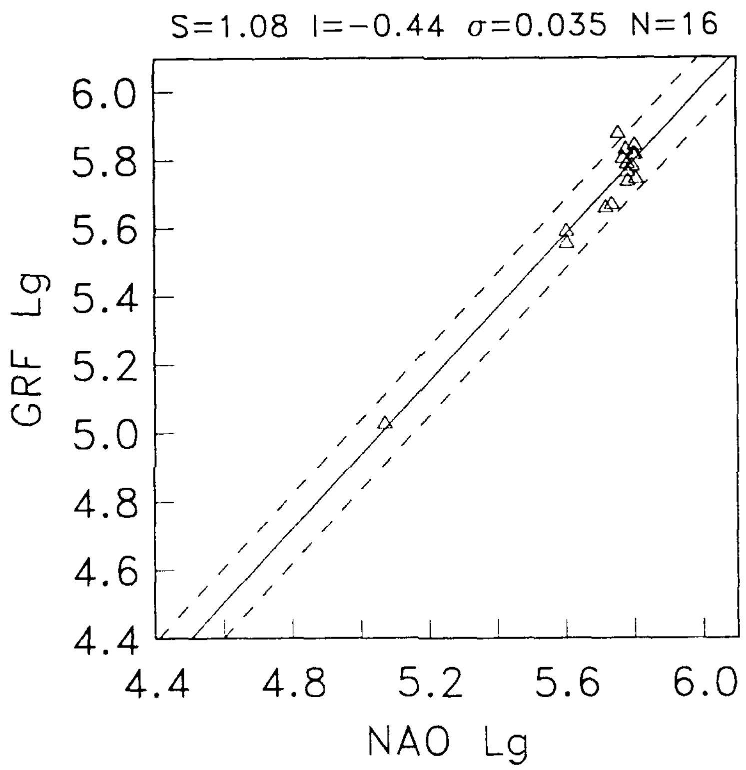

Fig. 7.1.7. Plot of Gräfenberg versus NORSAR RMS Lg magnitudes for all common events. Note the close correspondence, although one point in particular (Event 3) appears to be an outlier. Notational conventions are as in Fig. 7.1.4.

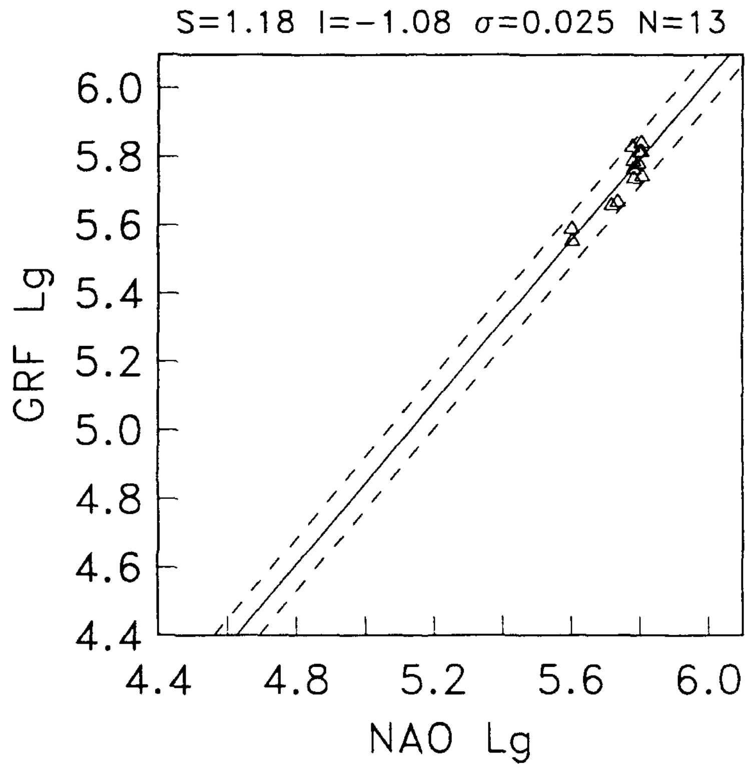

Fig. 7.1.8. Plot of Gräfenberg versus NOPSAR RMS Lg magnitudes, using only events for which at least 5 GRF channels were available. Notational conventions are as in Fig. 7.1.4. Note tha. the orthogonal standard deviation is as low as 0.025. Also note that in spite of the very small range of magnitudes, the two arrays show mutually consistent trends.

7.2 Threshold monitoring of Novaya Zemlya: A scaling experiment

Introduction

In the previous NORSAR Semiannual Technical Summary, Kværna and Ringdal (1990) presented results from a one-week experiment in continuously monitoring the Northern Novaya Zemlya test site. Data from the three regional arrays NORESS, ARCESS, FINESA were used to calculate the thresholds, using the method of Ringdal and Kværna (1989). The location of these three arrays relative to the test site is shown in Fig. 7.2.1.

In that one-week study, it was found that the test site could be consistently monitored at a very low magnitude level (typically $m_b = 2.5$). In fact, every single occurrence of the threshold exceeding $m_b = 2.5$ could be explained as resulting from an interfering event signal either from teleseismic or regional distance.

While these results are very encouraging, there is clearly much work remaining to be done before the concept of threshold monitoring is sufficiently well understood. In this paper, we attempt to illuminate the concept further by describing a simple experiment, involving down-scaling of recorded signal traces of the 24 October 1990 explosion at Novaya Zemlya and simulating what might have been observed on the threshold traces if such a down-scaled event had in fact occurred.

Scaling of the 24 October 1990 explosion

The explosion of 24 October 1990 had a world-wide $m_b = 5.6$. Recorded array traces of this event are shown in Fig. 7.2.2, where also the P-wave SNR (STA/LTA) on each filtered array beam is indicated. Our scaling procedure consisted simply of dividing each trace by a factor of 1000 and adding these down-scaled traces to actually observed recordings at various points in time.

Two examples of such "down-scaled" signals superpositioned on noise are shown in Fig. 7.2.3 and 7.2.4. The first of these figures covers a "low noise" interval (local night time), whereas the second figure corresponds to "high noise" (local day time). In the first case, the P phase is readily seen on all three arrays, and the S phase at ARCESS is also prominent. In the second case, the phases are far less clear, although the ARCESS P and S still have good SNR.

Before proceeding, we pause briefly to note that a down-scaling by a factor of 1000 in effect reduces the event m_b by 3 orders of magnitude. In this sense, the down-scaled event corresponds to $m_b = 2.6$. We have not attempted to apply any source scaling law for signal frequency, partly in order to maintain simplicity. Furthermore, such scaling laws, while certainly important, are not sufficiently well known to apply with any degree of confidence.

Moreover, it should be noted that any shift toward higher signal frequencies, as would be a natural consequence of applying frequency scaling, would only tend to improve the signal-to-noise ratios of these high-frequency arrays. Thus, our procedure can be considered as conservative with respect to estimating detection capability.

Simulation of threshold monitoring

Turning now to tne actual data, we selected a typical 24-hour time period (day 104/1991), and added the down-scaled signal at hourly intervals in order to get a picture of the effect under different noise conditions. A total of 24 identical signals were thus added at different times.

Fig. 7.2.5 shows the "actual" threshold trace (day 104) for Novaya Zemlya, developed exactly as described in detail by Kværna and Ringdal (1990) for the one-week monitoring experiment. We note that there is only one peak significantly exceeding $m_b = 2.5$; this corresponds to a large teleseismic earthquake ($m_b = 6.0$) from the Ryuku Islands.

Fig. 7.2.6 shows the resulting trace for that same day after adding the down-scaled signals and recomputing the threshold trace. We note that all of the 24 occurrences stand out clearly on the plot. Thus, if an explosion of $m_b = 2.6$ had indeed occurred at Novaya Zemlya that day, and assuming that the scaling is representative, there would have been clear indications on the threshold trace of such an explosion.

Discussion

We emphasize that this study is only intended to give an illustration of the potential of the threshold monitoring method, and that clearly more data and additional analysis is required to assess the situation in more detail. With our procedure of scaling by a constant factor in amplitude, we have, for example, not considered signal variance, which might contribute to a greater variability in the size of the amplitude peak, although the effect is not expected to be very significant.

An interesting observation is the way in which threshold monitoring complements the traditional detection/location type monitoring: Let us for a moment assume that an $m_b = 2.6$ explosion had in fact occurred at Novaya Zemlya, and that the resulting signals were similar to the scaled-down signals used here. It might well be that such an explosion would *not* have been detected and located by the regional array network. In fact, during daytime noise conditions (Fig. 7.2.4) there would very likely have been only one or two confident phase detections (Pn and possibly Sn at ARCESS), and this is not sufficient to locate in the traditional network sense.

Nevertheless, as seen in this paper, such an explosion would have been clearly indicated on the network threshold trace. It would not have been possible to explain this peak as resulting from some "different" event (as was always the case for such peaks in the Kværna and Ringdal (1990) study). Thus, a peak of this type would be a prime candidate for further detailed off-line analysis, possibly implying efforts to acquire additional data in order to further elucidate the nature of the event.

T. Kværna
F. Ringdal

References

Kværna, T. and F. Ringdal (1990): Continuous threshold monitoring of the Novaya Zemlya test site, *Semiannual Tech. Summary, 1 Apr - 30 Sep 1990*, NORSAR Sci. Rep. 1-90/91, Kjeller, Norway.

Ringdal, F. and T. Kværna (1989): A multichannel processing approach to real time network detection, phase association and threshold monitoring, *Bull. Seism. Soc. Am.*, Vol. 79, 1927-1940.

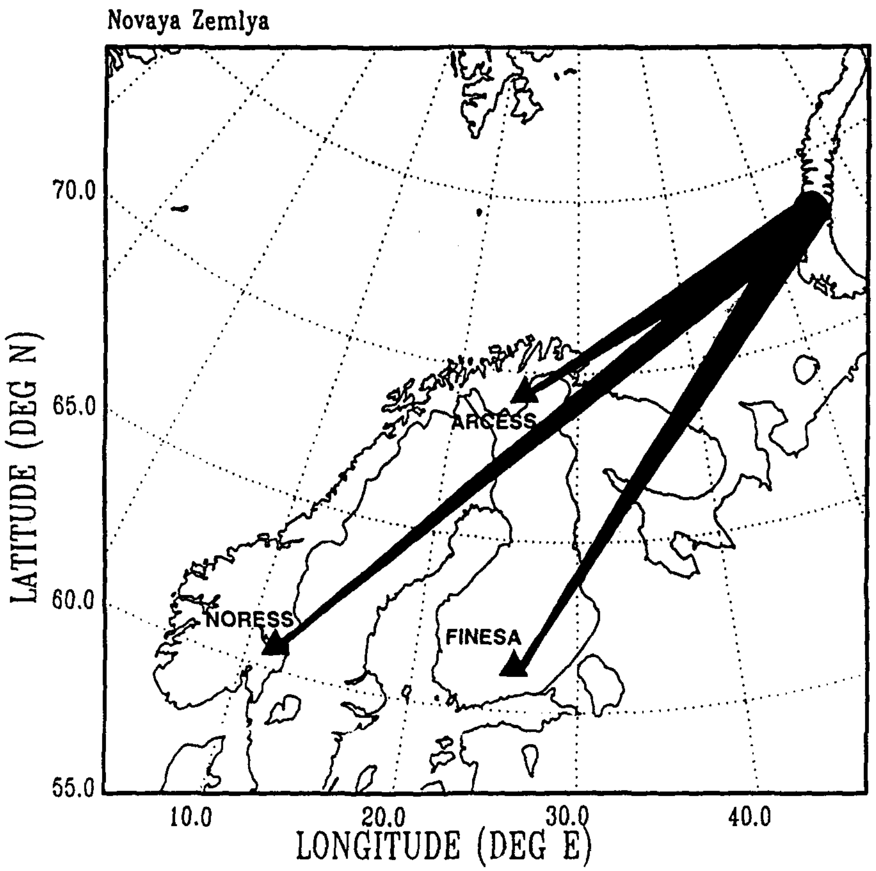

Fig. 7.2.1. Location of the target area (Novaya Zemlya) for the threshold monitoring experiment. The locations of the three arrays NORESS (Δ = 2280 km), ARCESS (Δ = 1110 km) and FINESA (Δ = 1780 km) are indicated.

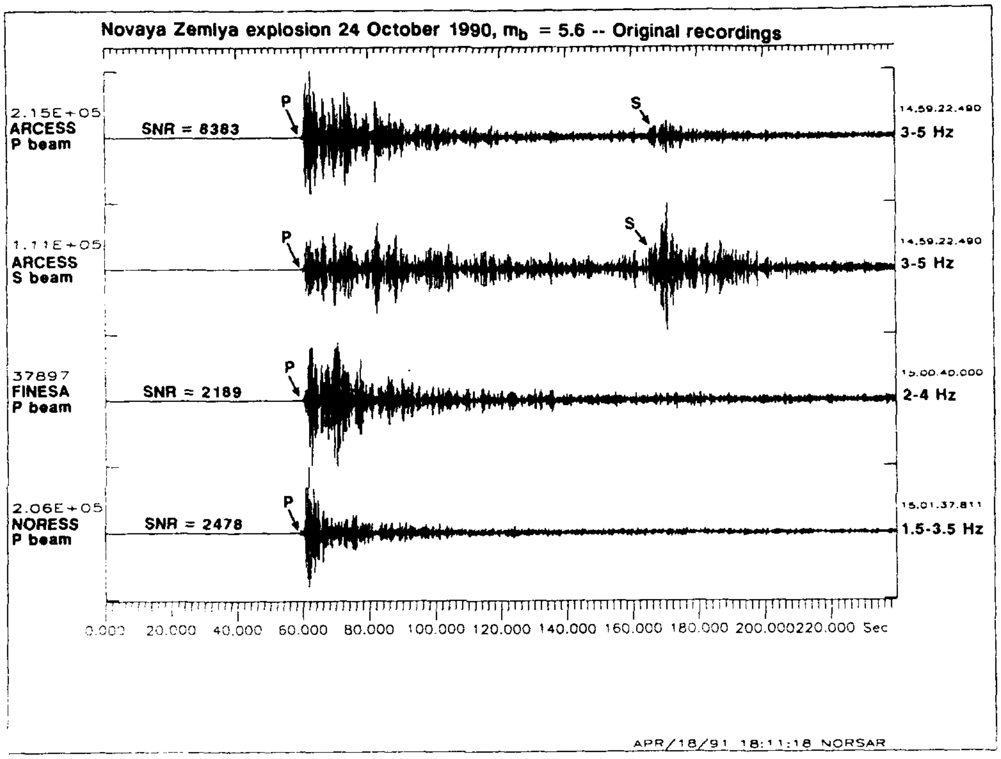

Fig. 7.2.2. P- and S-wave recordings (filtered array beams) at ARCESS, FINESA and NORESS for the Novaya Zemlya nuclear explosion of 24 October 1990. The SNRs of the detecting P-beams are also given.

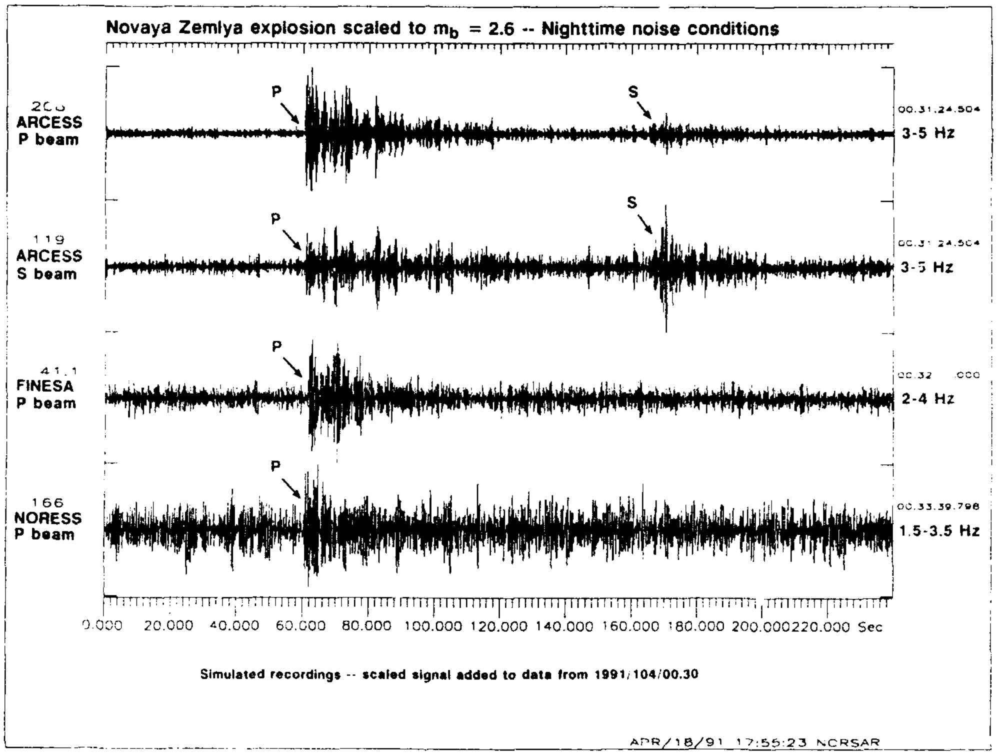

Fig. 7.2.3. "Down-scaled" signals from the Novaya Zemlya nuclear explosion of 24 October 1990 superimposed on noise during a "low noise" interval. The origin time of the simulated "event" is 1991/101/00.30.00.

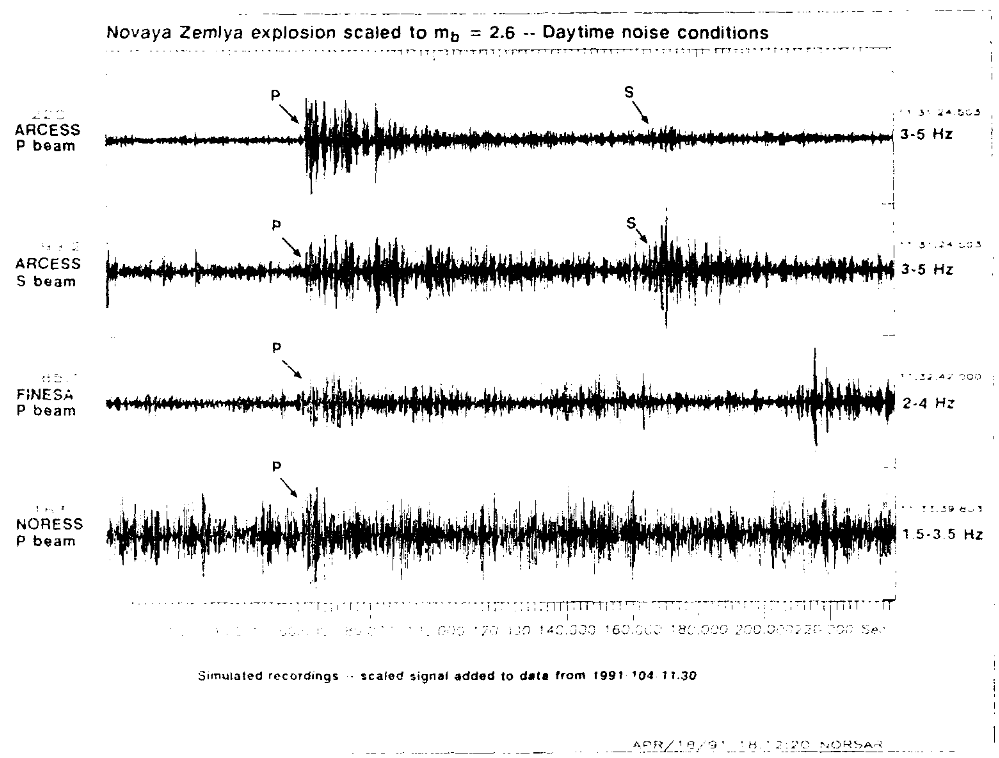

Fig. 7.2.4. Same as Fig. 7.2.3, but for a "high noise" interval. The origin time of the simulated "event" is 1991/101/11.30.00.

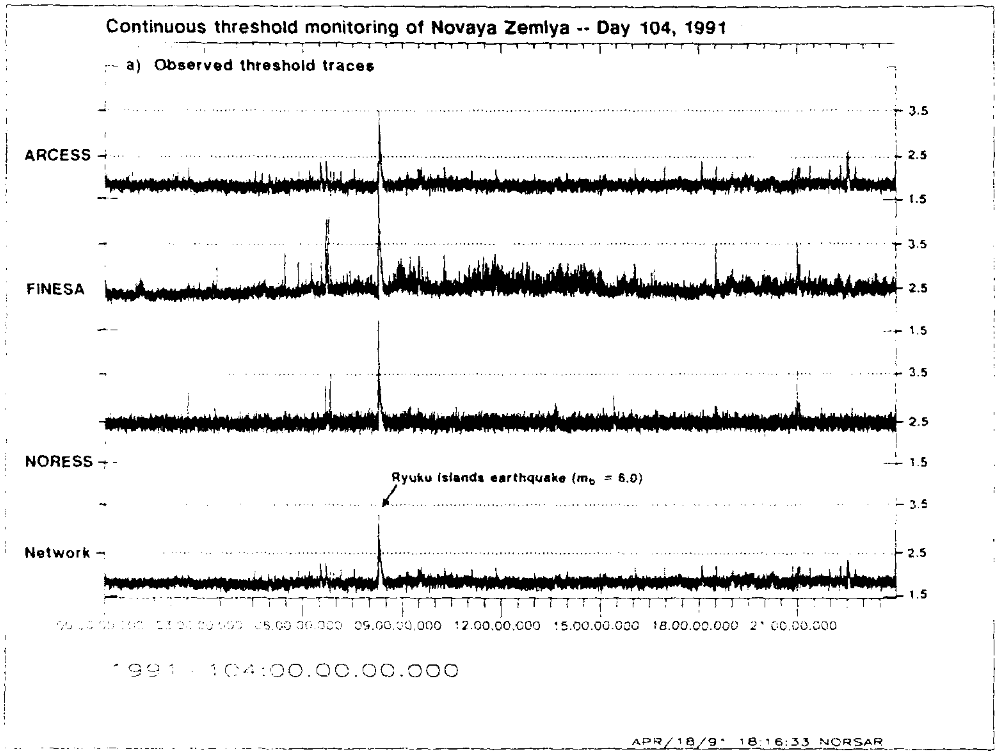

Fig. 7.2.5. Threshold monitoring of the Novaya Zemlya test site for day 1991/104 (14 April 1991). The top three traces represent thresholds (upper 90 per cent magnitude limits) obtained from each of the three arrays (ARCESS, FINESA, NORESS), whereas the bottom trace shows the combined network thresholds. Note that for the network trace there is only one magnitude peak exceeding 2.5.

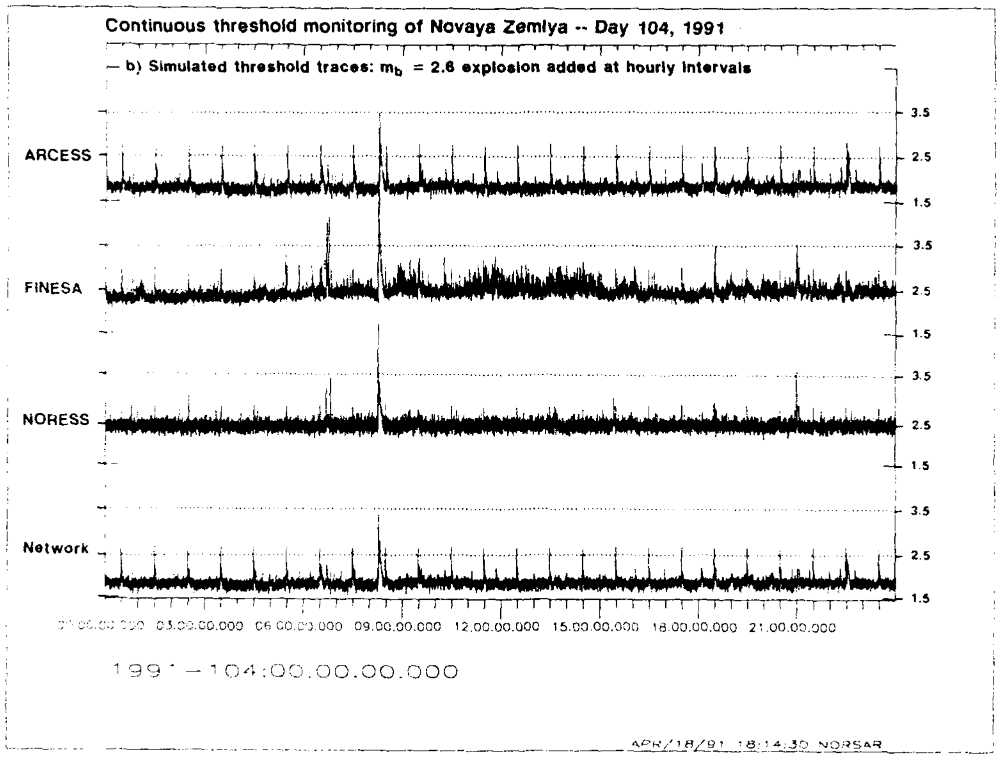

Fig. 7.2.6. Same as Fig. 7.2.5, but with down-scaled signals superimposed on the data at hourly intervals. Note that all occurrences of the simulated $m_b = 2.6$ events clearly stand out on the combined network trace.

7.3 Current status of development of the regional network associated with the NORSAR Data Processing Center

The purpose of this contribution is to summarize the status of development and future plans for the regional network in northern Europe that contributes seismic data in real time to the NORSAR Data Processing Center. The network is shown in Fig. 7.3.1 and currently comprises the NORESS and ARCESS arrays in Norway, the FINESA array in Finland, the GERESS array in Germany, and the two 3-component stations at Ksiaz and Stary Folwark in Poland. Also summarized in this contribution is the current status of development of the Intelligent Monitoring System (IMS) and plans for the near future.

The new 3-component stations in Poland

A description of the two 3-component stations at Ksiaz and Stary Folwark in Poland is given by Mykkeltveit and Paulsen (1990). The current system, comprising field installations in Poland and associated telecommunications arrangements for real time transmission of data to NORSAR, is shown schematically in Fig. 7.3.2. The system is fully operational as of April 1991, and will enable Poland to take an active part in the GSETT-2 (Group of Scientific Experts' Technical Test number 2) experiment during 22 April - 2 June 1991.

During the fall of 1991, the telecommunication links will be rearranged to include also a satellite ground station in Warsaw for real time reception of data from the two stations in Poland. A Sun Sparcstation-based data acquisition and processing system is also planned for installation at the Institute of Geophysics in Warsaw. It is expected that this will effectively contribute to the broadening of the scientific cooperation between NORSAR and the Institute of Geophysics in Warsaw. Such cooperation is needed in order to acquire relevant information on, e.g., seismicity and wave propagation characteristics in Poland and surrounding areas, for integration into the IMS knowledge base.

The NORESS, ARCESS, FINESA and GERESS arrays

A comprehensive description of NORESS and ARCESS is given in Mykkeltveit *et al* (1990). These array have been in stable and continuous operation since they were installed in 1984 and 1987, respectively. The uptime statistics provided in the present and past issues of the NORSAR Semiannual Technical Summaries testify to this. There are no plans for any significant modifications to these arrays.

The performance of the somewhat smaller, technically less sophisticated, yet very powerful FINESA array in Finland has recently been described by Uski (1990). Considering the simplicity of the FINESA field installation, its operational stability since the upgrade of the data acquisition system in December 1989 has been remarkable. There are no immediate plans for modifying the FINESA system.

The GERESS array in German Bavaria has been described by Harjes (1990). Results from the processing of GERESS data at NORSAR have been presented by Fyen (1990). Although the quality of data received at NORSAR is not yet entirely satisfactory, the data are being processed continuously and also used experimentally by IMS (see below). The GERESS field system developer is currently concentrating on solving remaining technical problems. Cooperative efforts between NORSAR personnel and scientists from the Ruhr University in Bochum, Germany, currently focus on optimizing the GERESS beam deployment. Again, active cooperation is needed for the purpose of supplementing the IMS knowledge base.

Data from all four arrays will be contributed to the GSETT-2 experiment, along with data from about 50 other single stations and arrays worldwide. This will provide another excellent opportunity to assess the capability of NORESS-type arrays for detection of weak seismic events at both regional and teleseismic distances.

The Intelligent Monitoring System

IMS is a system for joint processing of data from a regional network of arrays and single 3-component stations. IMS has been described in detail by Bache *et al* (1990), and initial results from operating the system are given by Bratt *et al* (1990). IMS is distributed between NORSAR and the Center for Seismic Studies (CSS) in Arlington, Virginia, as indicated in Fig. 7.3.2.

The first version of IMS provides for joint processing of data from NORESS and ARCESS. This version has been in operation at NORSAR since January 1990, and event statistics are reported in the Semiannual Technical Summaries. The analysis at NORSAR of regional events for the GSETT-2 experiment is carried out using IMS in its current version.

The IMS system developer SAIC is currently operating an upgraded version of IMS at CSS. This new version allows processing of data from an arbitrary number of arrays and single 3-component stations. Since March 1991, data from NORESS, ARCESS, FINESA and GERESS are jointly and experimentally processed at CSS. According to current plans, this new version of IMS will be installed at NORSAR during the summer of 1991.

S. Mykkeltveit

References

Bache, T.C., S.R. Bratt, J. Wang, R.M. Fung, C. Kobryn and J.W. Given (1990): The Intelligent Monitoring System, *Bull. Seism. Soc. Am.*, 80, 1833–1851.

Bratt, S.R., H.J. Swanger, R.J. Stead, F. Ryall and T.C. Bache (1990): Initial results from the Intelligent Monitoring System, *Bull. Seism. Soc. Am.*, 80, 1852–1873.

Fyen, J. (1990): Initial results from real-time processing of GERESS array data, *Semiannual Tech. Summary, 1 April - 30 September 1990)*, NORSAR Sci. Rep. no. 1-90/91, NORSAR, Kjeller, Norway.

Harjes, H.P. (1990): Design and siting of a new regional seismic array in Central Europe, *Bull. Seism. Soc. Am.*, 80, 1801–1817.

Mykkeltveit, S. and R Paulsen (1990): Development of two three-component stations in Poland, *Semiannual Tech. Summary, 1 April - 30 September 1990)*, NORSAR Sci. Rep. no. 1-90/91, NORSAR, Kjeller, Norway.

Mykkeltveit, S., F. Ringdal, T. Kværna and R.W. Alewine (1990): Application of regional arrays in seismic verification, *Bull. Seism. Soc. Am.*, 80, 1777–1800.

Uski, M. (1990): Event detection and location performance of the FINESA array in Finland, *Bull. Seism. Soc. Am.*, 80, 1818–1832.

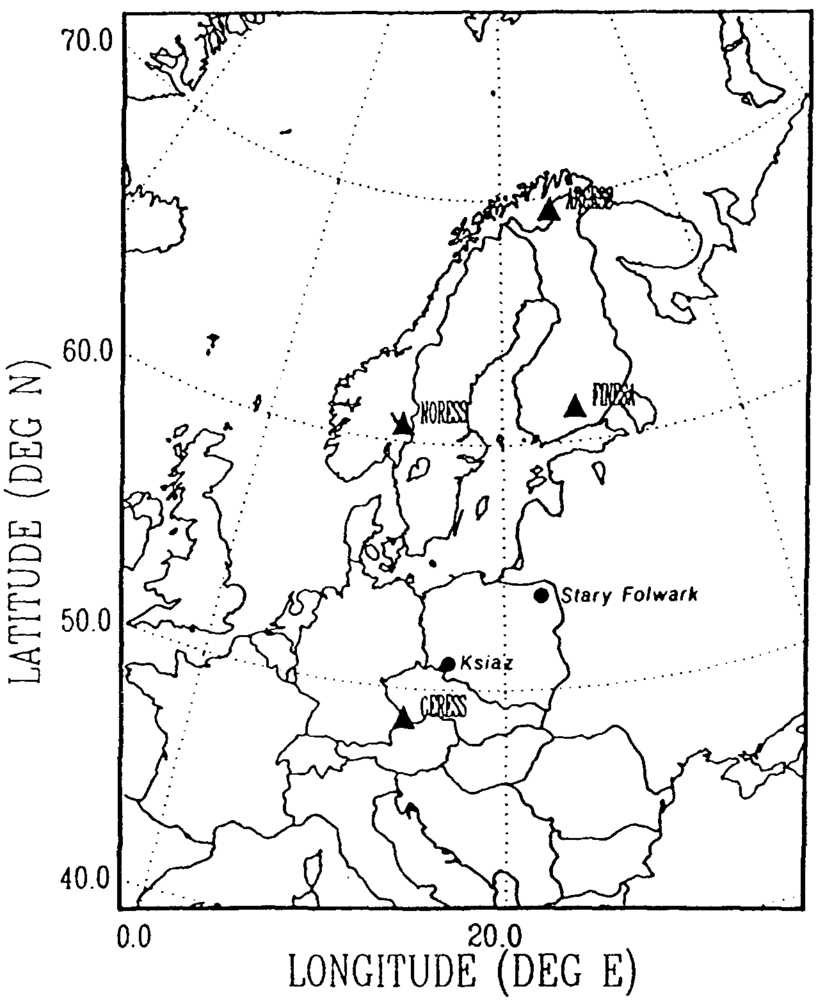

Fig. 7.3.1. The figure shows the network of regional arrays and single 3-component stations in northern Europe contributing real time data to NORSAR.

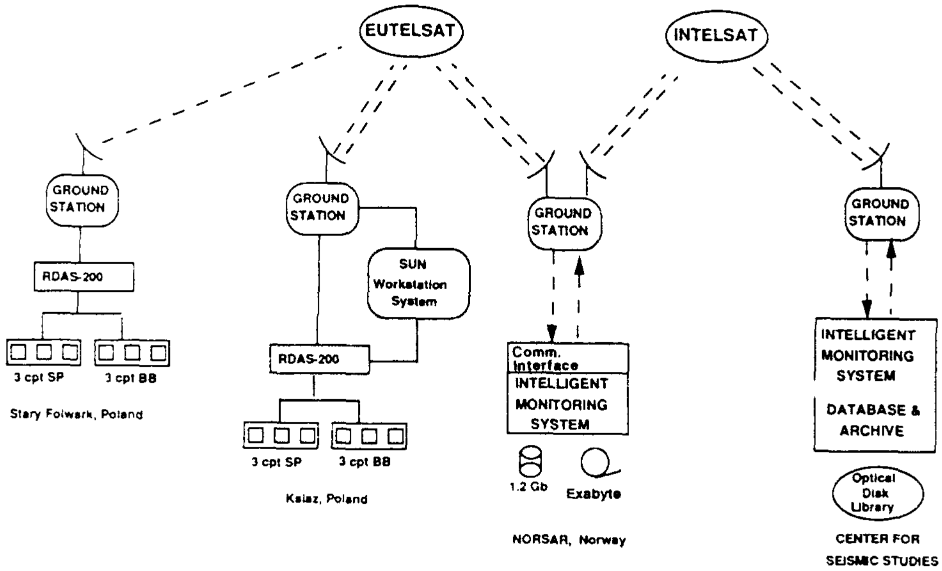

Fig. 7.3.2. The diagram shows the two stations in Poland with associated data communications arrangements. The diagram also shows how data from these stations are made available to the Intelligent Monitoring System, both in Norway and the U.S.

7.4 Multichannel statistical data processing algorithms in the framework of the NORSAR event processing program package

The NORSAR interactive data processing package was developed for the analysis of small aperture seismic array observations. This package, called the Event Processor (EP), has turned out to be a very convenient tool for the daily production of a seismic bulletin. The small aperture seismic arrays NORESS, ARCESS, FINESA and GERESS and their associated data processing facilities are constructed for automatic recording, location and classification of low magnitude regional events and medium magnitude teleseismic events. Signal detection is performed in an online mode, whereas parameter estimation can be performed as an offline procedure using recorded multichannel seismic wavetrains. Now, at NORSAR the automatic system is in full operation, providing seismic signal detection as well as signal parameter estimation. These parameters are: onset time, azimuth, apparent velocity, dominant frequency, signal-to-noise ratio and so on.

This automatic system is operated at a low threshold and inevitably produces numerous "false alarms", i.e., "events" caused by noise bursts. The current seismic bulletin is issued after an interpretation of the detection list, which may be effectively performed using the interactive Event Processing (EP) package. The EP program has a number of graphic routines and interfaces for work with NORSAR data bases. It also comprises some sophisticated and rather time-consuming data processing programs which at present cannot be used in automatic or online processing modes, i.e., without human control. In particular, adaptive statistical multichannel data processing programs have been installed recently in the framework of the EP package. These programs are based on optimal methods of multidimensional time series analysis described in Kushnir *et al* (1983), Kushnir and Lapshin (1984), Pisarenko *et al* (1987) and Kushnir *et al* (1990a, 1990b). They comprise the following procedures of seismic array data processing:

1. Selection of the array instruments and data time interval to be processed.

2. Filtering and resampling of the data.

3. Time-shifting of the channel waveforms with delays corresponding to a given azimuth and apparent velocity of a plane wave propagating across the array.

4. Summing of shifted waveforms, i.e., beamforming for a given azimuth and apparent velocity.

5. Whitening of the background noise by adaptive filtering of the beam output. This procedure provides signal-to-noise ratio (SNR) gain due

to differences in signal and noise frequency contents, but it distorts the signal waveform.

6. Adaptive optimal group filtering (multichannel Wiener filtering) of the array seismograms. This procedure permits high suppression of seismic noise due to its coherency. Theoretically it provides maximum SNR gain without any distortion of seismic signal waveform or frequency contents.

7. Adaptive detection of the distinct phases in single channel seismograms or in the output traces of beamforming and optimal group filtering procedures. The detection procedure takes into account the difference between noise on one hand, and signal plus noise on the other, not only in amplitude values but also in power spectra.

8. Seismic wave onset time estimation by detection of the moment in time when the wavetrain statistical features are abruptly changed.

Array data processing using the procedures listed above is accomplished in the framework of the EP system with the aid of a specially developed set of commands. The major commands are named GRFADAPT, GRFFILT, ESTDET, ESTON1, ESTON3. Description of these commands and examples of performance are given below.

GRFADAPT and GRFFILT commands

The procedures 1–6 are carried out sequentially by each of two EP system commands: GRFADAPT and GRFFILT. The GRFADAPT command, unlike the GRFFILT command, contains additional adaptation algorithms which have not been listed above. These algorithms are used before the execution of procedures 5 and 7 and accomplish adaptation to the current noise of the beam whitening filter and the optimal group filter. During GRFADAPT command execution, the processed data are regarded as "pure" seismic noise and the autoregressive (AR) model of the beam noise time series and the multidimensional AR model of the array noise time series are estimated. Based on these models, the whitening and optimal group filter coefficients are evaluated. They are stored and used later during GRFFILT command execution.

GRFADAPT and GRFFILT command execution produces seven output traces. The first four of them are the main resulting traces and the last three — auxiliary traces — are needed to check the adaptation quality. These seven output traces are placed on top of the EP system data stack (containing all input and output time series during the data processing). The main traces are:

1. Beam waveform composed of filtered and resampled channel traces for a given azimuth and apparent velocity (OGF beam).

2. Whitened beam waveform (OGF Wbeam),

3. Optimal group filter waveform calculated using filtered and resampled channel traces as input for a given azimuth and apparent velocity (OGF t-un),

4. Whitened optimal group filter waveform (OGF th-w).

The GRFADAPT and GRFFILT procedures also calculate the mean values and variances of the listed output traces and of the input channel traces. The important result of these calculations is the value of the ratios of the adapative optimal group filter (AOGF) output variance to the beam waveform variance and AOGF output variance to the averaged channel trace variance. After GRFADAPT command execution the first ratio characterizes the relative noise suppression by beamforming and optimal group filtering. Due to the signal undistorting feature of these procedures (provided a plane seismic signal wave is arriving with the given azimuth and apparent velocity), this ratio also characterizes the relative SNR gain due to beamforming and the AOG filtering.

Using the GRFADAPT and GRFFILT commands, a report file is created containing the input and output numerical parameter values and description of the processed channel traces. Particularly, this report contains the value of AOGF and the beamforming SNR gain ratio. An example of such a report is shown in Fig. 7.4.1.

The format of the GRFADAPT command is given below:

```
grfadapt vel [apparent velocity, km/sec] azi [azimuth, degrees]
{filter type} [cutoff frequencies, Hz] factor [resampling factor]
```

where {filter type} is one of the three character strings: lp, bp, hp, which means low-pass, band-pass and high-pass filter types.

Before the GRFADAPT command is initiated, values of the associated parameters have to be assigned. There are additional numerical parameters which are not specified with the command, and which have the following default vaules:

1. Filter frequency response decay factor: ALPHA = 10^{-4},

2. Filter impulse response one-side length: IRL = 15;

3. Order of beam noise AR model (number of beam-whitening filter coefficients): DARB = 10,

4. Number of input array data matrix autocovariance coefficients: LCRC = 6,

5. Regularizator of matrix autocovariance function: REG $= 10^{-6}$,

6. Order of input array data multidimensional AR model (one-side length of the optimal group filter): DARGRF = 6,

7. Auxiliary parameters: DARARF = 10, DMARF = 20.

Assigning of alternative values for the parameters listed above can be done by the

EP command:

```
gr [parameter name] [parameter value]
```

To check the current parameter setting before GRFADAPT and GRFFILT command execution, one should use the EP command:

```
q gr
```

There is no need to enter any parameter values before the GRFFILT command execution. The computations are carried out with numerical parameter values and whitening and optimal group filter coefficients stored during the previous GRFADAPT command execution.

The numerical results of the GRFADAPT command execution are written to the disk file GRFREPORT.OUTPUT by the command:

```
grfreport
```

The purpose of the array data processing using the GRFADAPT and GRFFILT procedures is to compute the adaptive, statistically optimal beam which suppresses coherent and incoherent array noise, thus providing the maximum SNR gain without distortion of the signal waveform. These procedures are especially efficient in the case when the signal and coherent noise power spectra are overlapping. In this case they can provide much higher SNR gain than bandpass filtering after conventional beamforming.

For this reason, in the first experiments with the GRFADAPT and GRFFILT procedures in the framework of the EP system, we tried to learn how the program parameter values influence the AOGF SNR gain relative to conventional beamforming SNR gain, when data are processed in a broad frequency band. The main program parameters which influence the quality of the optimal group filter adaptation are 1) the order of the input data multidimensional

AR model, 2) the data frequency band and 3) regularizator of the data matrix covariance function. Table 7.4.1 comprises the results of NORESS noise processing. The 120 sec interval of array noise shown in Fig. 7.4.2 has been used for optimal group filter adaptation.

As one can see from this table, increasing the input data multidimensional AR model order leads to a strong increase of AOGF SNR gain. Nevertheless, it does not seem worthwhile to use a multidimensional AR model order greater than 10–12 because the adaptation procedure becomes time consuming and less stable (especially when a large number of array channels are used). Choosing a higher frequency band leads to diminishing of AOGF SNR gain. This can be explained by the strong coherency of the NORESS noise mainly at low frequencies. Varying the regularizator value from 0 to 10^{-4} practically does not affect the AOGF SNR gain.

The GRFADAPT and GRFFILT commands were also tested by processing some low magnitude local event records from the NORESS, ARCESS and FINESA arrays. In these experiments the optimal group and whitening filter adaptations were made using the array noise records preceding the seismic signal wavetrains. The duration of the noise time intervals used for adaptation were from 100 to 150 sec. The main purpose of these experiments was to learn about possible differences in P, S and Lg wave phase extraction by different array data processing algorithms such as conventional beamforming, beam output noise whitening, adaptive optimal group filtering and AOGF output noise whitening. What distinguishes these experiments from those described in our previous reports (Kushnir *et al*, 1990a; Kushnir *et al*, 1990b) is the processing of array data in different frequency bands: 0.2–5 Hz, 0.2–10 Hz, and 0.2–20 Hz. Table 7.4.2 comprises the ratios of AOGF output SNR relative to beamforming output SNR and AOGF output SNR relative to averaged channel SNR for different phases being extracted from 7 small local event records. Each phase has been extracted from the noise by the conventional beam and AOGF adjusted for the azimuth and apparent velocity of this phase arrival as given in the NORSAR detection list. One can see that in these experiments the AOGF SNR gain relative to the conventional beamforming gain was betwen 16.2 and 24.5 dB for the 0.2–5 Hz frequency band, between 12.3 and 24.2 dB for the 0.2–10 Hz frequency band and around 10–11 dB for the 0.2–20 Hz frequency band. Note that the highest AOGF SNR gain of more than 24 dB was achieved on the FINESA records. This is due to the presence in these records of strong, highly coherent, low frequency background noise possibly caused by stormy seashore waves. This noise has been suppressed by the AOGF procedure, but not by conventional beamforming.

Examples of GRFADAPT and GRFFILT output traces as the result of event wavetrain and preceding noise processing are given in Figs. 7.4.3–7.4.5. In some of these examples, the AOGF and whitened beam output wavetrains are similar. One may conclude that the adaptive whitening procedure after conventional beamforming can provide the same results as the AOGF procedure (while being less time consuming). But this inference is true only for body waves of local low magnitude events, which as a rule have high frequency contents. Power spectra of surface waves and teleseismic body waves are often overlapping with those of coherent seismic noise. In this case, the AOGF procedure has a strong advantage over other filtering procedures since it retains the signal undistorted.

ESTDET command

Adaptive detection of distinct phases in the wavetrain is accomplished by the EP command ESTDET. This procedure is based on the optimal statistical algorithm described in Pisarenko *et al* (1987). During the ESTDET command execution the time interval of the data being processed is divided into two parts. The data in the first interval are regarded as "pure" noise and its AR model is estimated ("noise AR model"). The data in the second interval are presumed to contain the seismic phases. The detection of these phases is carried out using a moving time window. The detection algorithm consists of calculation of the simplified Bayesian test statistic for the hypothesis: a) the AR model of time series inside the moving time window is the same as the noise AR model versus the hypothesis: b) these two models are different (Kushnir *et al*, 1983). The ESTDET program takes as input the wavetrain at the top of the EP system data stack and produces nine new traces which in turn are placed on the top of this data stack. Eight of these traces contain the values versus time of the detection statistics calculated using data in a moving time window. These statistics are derived from four slightly different versions of the simplified Bayesian test described above. The first four traces are the statistical values in logarithmic scale, the next four are the same values in linear scale. The ninth output trace is the auxiliary trace for noise AR modelling checking. The detection triggering of the seismic phases is now performed in an interactive mode by comparing the detection statistic value with the threshold chosen to provide the acceptable false alarm rate. But it would clearly be straightforward to develop a special EP command for automatic phase detection triggering.

The ESTDET command format is

```
estdet start [first point, sec.] end [last point, sec.]
w [window length, sec.] o [AR model order] noise
[noise interval length, sec.]
```

where "start" and "end" are the first and last points of the trace being processed (in sec. relative to the initial point of this trace); "w" is the width of the moving time window, "noise" is the length of the first part of the data time interval used for the noise AR model estimation.

Examples of ESTDET command output traces and input wavetrains are given in Figs. 7.4.6–7.4.8.

ESTON1 and ESTON3 commands

The moving window detection procedure points out those time intervals where seismic wave phases are present. The next stage of the signal processing is an estimation of phase parameters. Among the most important parameters needed for event source location are the wave phase onset times. For rough estimates of these times, the moments of detection triggering may be used. But for precise estimation of each phase onset time, special statistical procedures have been developed (Pisarenko *et al*, 1987). In the framework of the EP system, this procedure is realized as two commands: ESTON1 and ESTON3. The first command is intended for single component trace processing. This may be the beam or AOGF output trace or a "raw" array single channel wavetrain. The second command is intended for 3-component seismogram processing with the purpose of onset time estimation. Both procedures are based on maximum likelihood algorithms for estimation of the moment in time when the time series AR model parameter values abruptly change. The ESTON1 procedure takes into account changing of the time series variance and frequency contents at the moment in time when the seismic phase arrives. The ESTON3 procedure also takes into account changs in the 3-dimensional time series polarization features at this moment.

Both commands use the traces at the top of the EP system data stack as input: ESTON1 takes the upper trace, ESTON3 — the three upper traces. Both commands produce one output trace containing the onset time likelihood function calculated for data inside a given time interval. After command execution, this trace is placed on the top of the EP data stack.

The ESTON1 and ESTON3 command format is:

```
eston1(3) start [first point, sec.] end [last point, sec.]
w [min. window length] o [AR model order]
```

where "start" and "end" are the first and last points of the wavetrain being processed (in sec. relative to the initial point of the trace); "w" is the minimum width of the data window for the AR model estimation. The onset time likelihood function is calculated for the data inside the time interval (start + w, end - w) (in sec. relative to the trace initial point).

Examples of ESTON1 output traces for different types of seismic wave phases are given in Figs. 7.4.9–7.4.11. The onset time values given in these figures as the arguments of the likelihood function absolute maximums coincide very well with the results of visual interactive analysis using the EP system's graphic options.

A.F. Kushnir, Int. Inst. of Earthquake Predic. Theory, Moscow, USSR
J. Fyen
T. Kværna

References

Kushnir, A.F. and V.M. Lapshin (1984): Optimal processing of the signals received by a group of spatially distributed sensors, in *Computational Seismology*, Allerton Press, Inc., Vol. 17, 163–174.

Kushnir, A.F., I.V. Nikiforov and I.V. Savin (1983): Statistical adaptive algorithms for automatic detection of seismic signals, in *Computational Seismology*, Allerton Press, Inc., Vol. 15, 145–162.

Kushnir, A.F., V.M. Lapshin, V.I. Pinsky and J. Fyen (1990a): Statistically optimal event detection using small array data, *Bull. Seism. Soc. Am.*, Vol. 80, 1934–1950.

Kushnir, A.F., V.I. Pinsky and S.L. Tsvang (1990b): Optimal group filtering and noise attenuation for the NORESS and ARCESS arrays, in *Semiannual Tech. Summary, 1 April – 30 September 1990*, NORSAR Sci. Rep. 1-90/91, Kjeller, December 1990.

Pisarenko, V.F., A.F. Kushnir and I.V. Savin (1987): Statistical adaptive algorithms for estimations of onset moments of seismic signals, *Phys. Earth Planet. Int.*, 47, 4–10.

Frequency Band (Hz)	Order of Multidimensional AR Model 6	8	12
0.2 – 5	16.7 (20.3)	17.9 (21.5)	18.8 (22.4)
0.2 – 10	13.2 (16.8)	—	16.5 (20.2)
0.2 – 20	—		14.0 (17.5)

Frequency Band (Hz)	Regularizator Value 0	10^{-6}	10^{-5}	10^{-4}
0.2 – 5	18.9 (22.5)	18.8 (22.4)	18.7 (22.3)	—
0.2 – 10	—	16.5 (20.2)	—	—
0.2 – 20		14.0 (17.5)	—	14.2 (17.6)

Table 7.4.1. Adaptive optimal group filtering SNR gain relative to beamforming for different values of the GRFADAPT procedure main parameters. Gain values are given in dB, values in brackets are AOGF SNR gains relative to average single array channel. The results are based upon using 120 sec NORESS noise recordings shown in Fig. 7.4.2. The results of the upper table are obtained with a regularizator value of 10^{-6}, whereas an AR model order of 12 has been used for obtaining the results in the lower table.

Event Origin Time	Array, Distance (km)	Phase (AR Model Order)	Gain Relative to Beam (dB)	Gain Relative to Single Chan. (dB)	Frequency Band (Hz)
298:17.51.50	ARCESS 508.4	P (12)	16.2	18.8	0.2–5
282:12.04.13	FINESA 287.9	P (12)	21.7	23.3	0.2–5
		P (12)	19.3	21.0	0.2–10
		S (12)	19.6	21.6	0.2–5
		S (12)	17.2	19.3	0.2–10
		Lg (12)	17.3	19.4	0.2–10
294:09.13.00	FINESA 772.3	P (12)	23.6	25.7	0.2–5
		S (12)	21.0	23.7	0.2–5
		Lg (12)	20.3	23.1	0.2–5
	NORESS 1302.7	P (12)	18.8	22.9	0.2–5
		S (12)	16.6	21.1	0.2–5
		Lg (12)	16.5	21.3	0.2–5
28:09.38.09	NORESS 1219.0	P (6)	16.0	19.6	0.2–5
		P (6)	12.3	16.1	0.2–10
		P (6)	10.1	13.8	0.2–20
		P (8)	10.9	14.6	0.2–20
	FINESA 1771.0	P (12)	23.1	24.3	0.2–5

Table 7.4.2. SNR gains of adaptive optimal group filtering relative to beamforming based on processing of local event phases.

Event Origin Time	Array Distance (km)	Phase (AR Model Order)	Gain Relative to Beam (dB)	Gain Relative to Single Chan. (dB)	Frequency Band (Hz)
292:12.31.45	FINESA 164.4	P (6)	14.6	17.6	0.2–1
		P (12)	16.3	19.4	0.2–10
	ARCESS 390.4	P (12)	16.4	20.8	0.2–10
294:19.32.03	FINESA 259.0	P (12)	24.5	26.0	0.2–10
	NORESS 564.6	P (12)	17.9	21.8	0.2–5
		S (12)	16.0	19.8	0.2–5
		Lg (12)	15.7	20.0	0.2–5

Table 7.4.2. cont.

```
Output from GRFADAPT:                    (Pn - phase, 0.2-5. Hz)

Start time: 1990-282:12.02.50.0    Seconds:  120.00 (Data time interval)

Input rarmeters:

Filter type:-1        (low pass(lp)=-1,band pass(bp)=0,high pass(hp)=1)
FCH          : 5.25    (lp,hp-filters cut frequency, hz)
FLH          : 20.00   (up-filter low cut frequency, hz)
FHH          : 20.00   (up-filter-high cut frequency, hz)
IRL          : 15      (one-side length of the filter impulse response)
ALPHA        : 0.00010 (decay factor of the filter frequency response)
AZIMUTH      : 153.80  (azimuth of the seismic phase to be extracted)
VELOCITY     : 7.80    (apparent velocity of this seismic phase)
DARB         : 10      (order of a beam noise AR-model)
LCRC         : 6       (number of autocovariance matrises)
REG          : 0.000001(regularizator value)
DARGRF       : 6       (order of the data multidimensional AR-model)
DARARF       : 10      (auxiliary parameter)
DMARF        : 20      (auxiliary parameter)
K            : 4       (resampling factor)

Output parameters:

NP           :  1193   (number of the data samples being processed)

AVCHPOW      :  0.1380 (averaged dispersion of the channel traces)
BMEAN        :  0.0000 (mean value of the beam trace, m)
BPOW         :  0.0946 (dispersion of the beam trace, σ^2)
IERLBLD      :  0   }
IERMLD       :  0   } (computation errors, error=1, otherwise=0)
IERGLD       :  0   }
GRTUN (M/P):    0.0003   0.0006 (m and σ^2 of the AOGF output trace)
GRTW  (M/P):    0.0098   1.0128 (m and σ^2 of the whitened output trace)
GRAUN (M/P):    0.0000   0.0007 (m and σ^2 of the auxiliary output trace)
GRMUN (M/P):    0.0006   0.0006 (m and σ^2 of the auxiliary output trace)
Gain (avch):    214.33   23.311 (AOGF SNR gain relative averaged channel)
Gain (beam);    146.95   21.672 (AOGF SNR gain relative beam, times, db )
```

(Description of the array data being processed)

Channel	X(E-W)	X(N-S)	ELEV	TDEL	CHMEAN	CHPOW
FIN_A0_sz	-180.0	-85.0	138.0	0.211	-0.0070	0.1287
FIN_A1_sz	0.0	0.0	138.0	0.211	-0.0181	0.1421
FIN_A2_sz	-308.0	-353.0	162.0	0.262	-0.0085	0.1308
FIN_B1_sz	275.0	-37.0	165.0	0.252	-0.0074	0.1264
FIN_B2_sz	121.0	-599.0	159.0	0.371	-0.0053	0.1280
FIN_B3_sz	-474.0	-555.0	176.0	0.292	0.0071	0.1258
FIN_B4_sz	-764.0	-85.0	158.0	0.143	-0.0167	0.1171
FIN_B5_sz	-436.0	257.0	143.0	0.098	0.0206	0.0913
FIN_B6_sz	83.0	277.0	147.0	0.153	-0.0255	0.1501
FIN_C1_sz	-1064.0	-657.0	158.0	0.248	-0.0223	0.1398
FIN_C2_sz	-1110.0	226.0	138.0	0.027	-0.0460	0.1368
FIN_C3_sz	-162.0	788.0	138.0	0.000	-0.0100	0.1507
FIN_C4_sz	629.0	420.0	138.0	0.182	-0.0373	0.1256
FIN_C5_sz	653.0	-518.0	138.0	0.413	-0.0160	0.1374
FIN_C6_sz	-185.0	-1108.0	138.0	0.460	-0.0329	0.2375

Fig. 7.4.1. Example of a GRFREPORT.OUTPUT file.

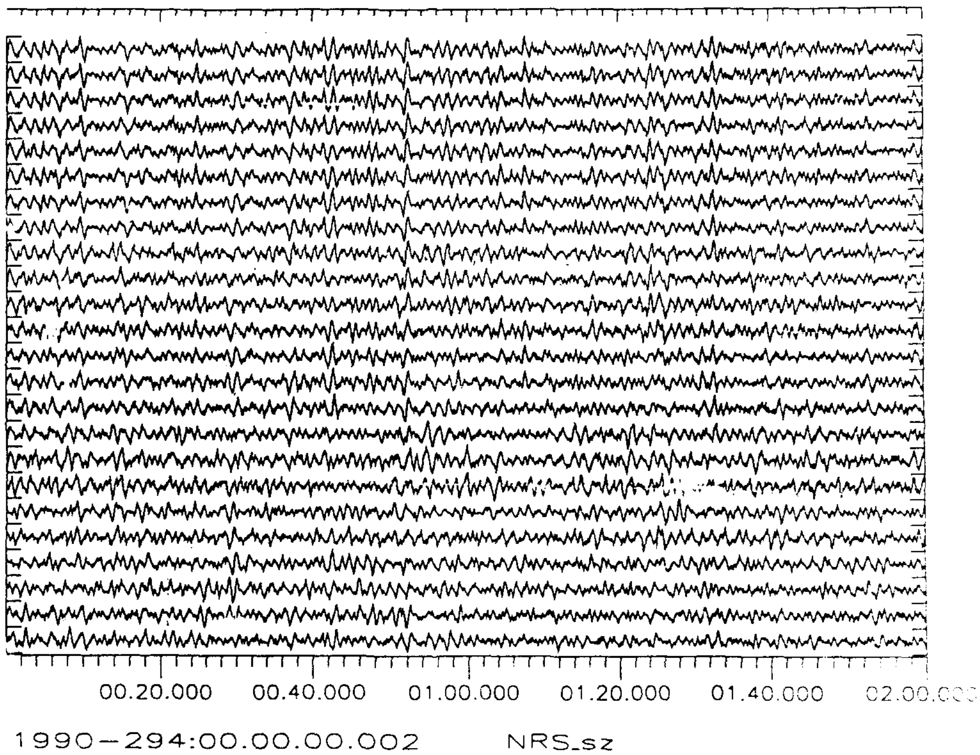

Fig. 7.4.2. NORESS noise recordings used for studying the influence of GR-FADAPT parameter values on SNR gain.

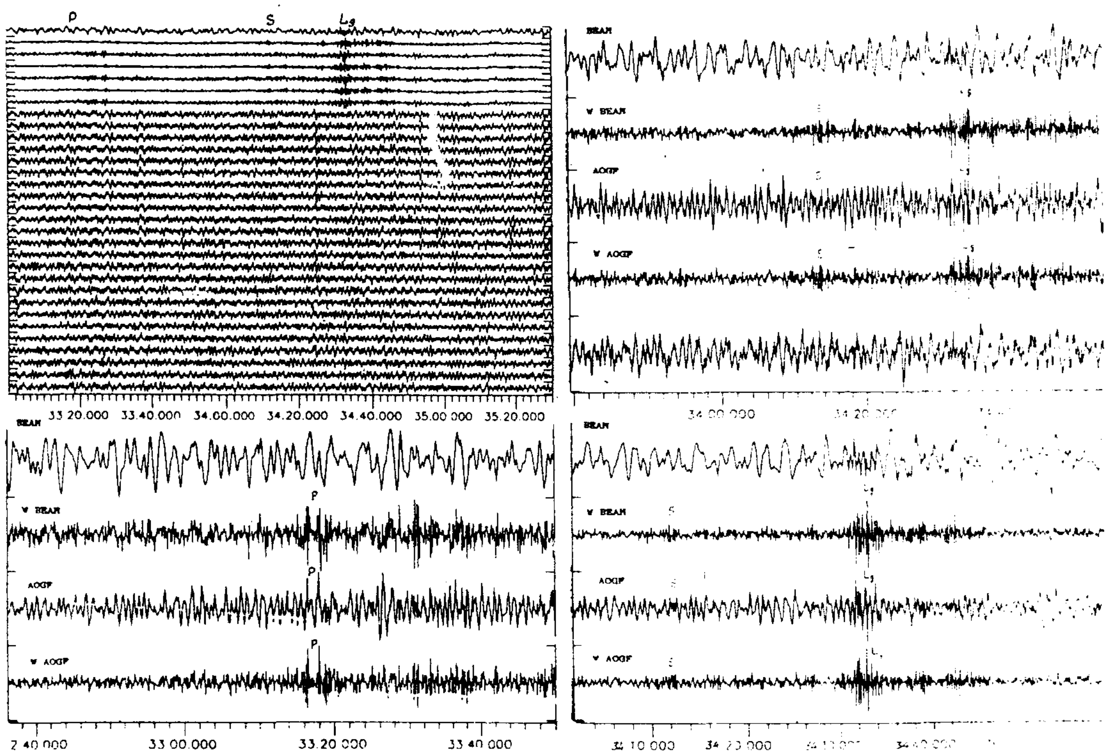

Fig. 7.4.3. Extraction of the main seismic phases from an event recorded at FINESA (1990:294:19.32.03, distance 259.0 km). (a) Input and main output traces of the GRFFILT procedure adjusted for Lg-phase extraction; (b), (c), (d) main output traces of the GRFFILT procedures adjusted for P, S and Lg-phase extraction. 0.2–5 Hz band processing.

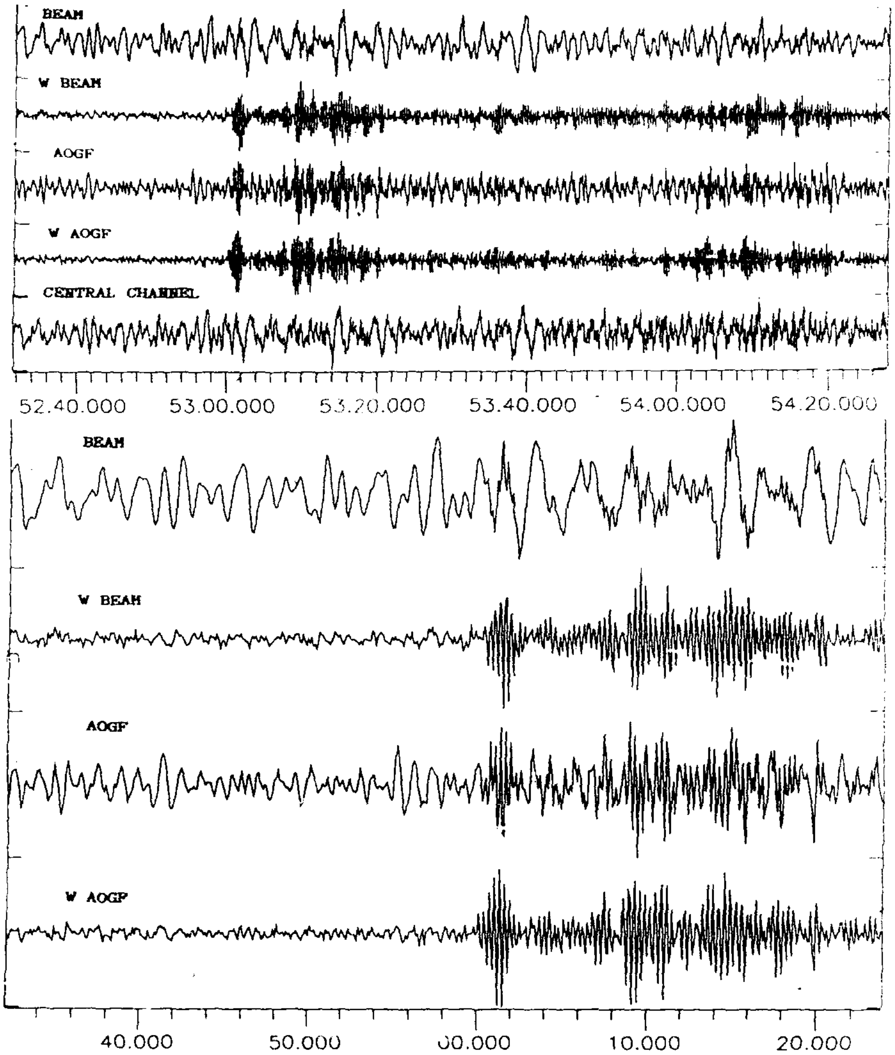

Fig. 7.4.4. Output traces of GRFFILT (0.2–5 Hz band) procedure adjusted for P-phase extraction from ARCESS recordings of a small regional event (1990:298:17.51.50, distance 508.4 km). Note the difference between P-phase waveforms of the AOGF, Whitened beam and Whitened AOGF output traces which implies a shift of onset time estimates.

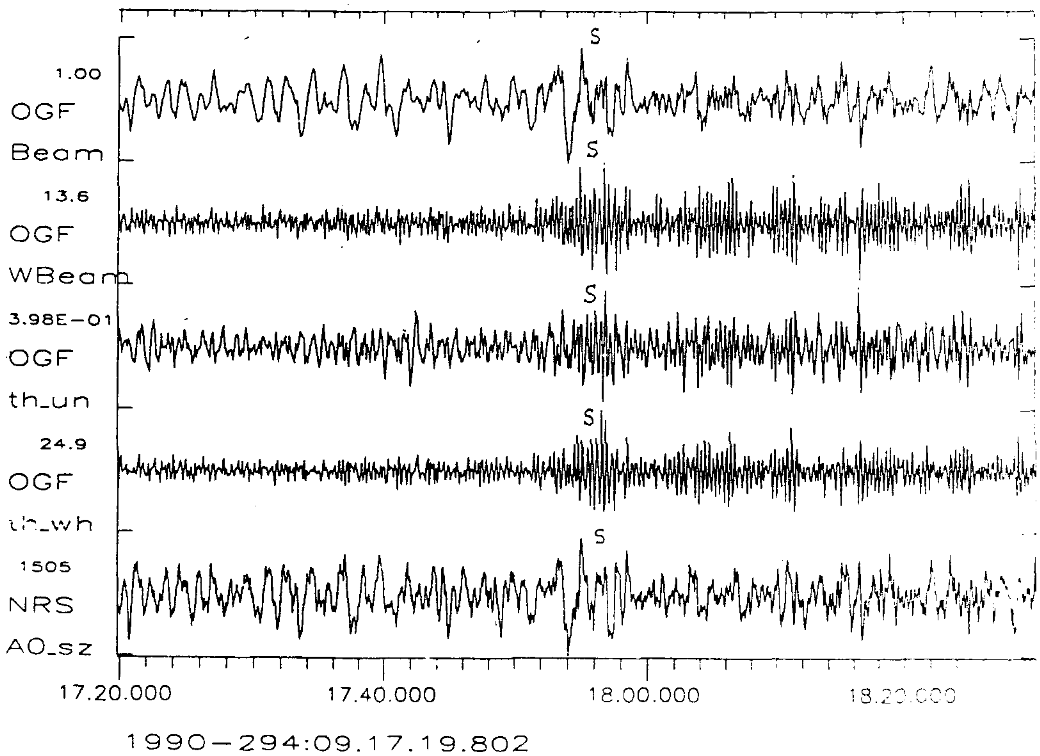

Fig. 7.4.5. Extraction of the S-phase from NORESS recordings of a regional event (1990:294:09.13.00, distance 1302.7 km); 0.2-5 Hz band processing.

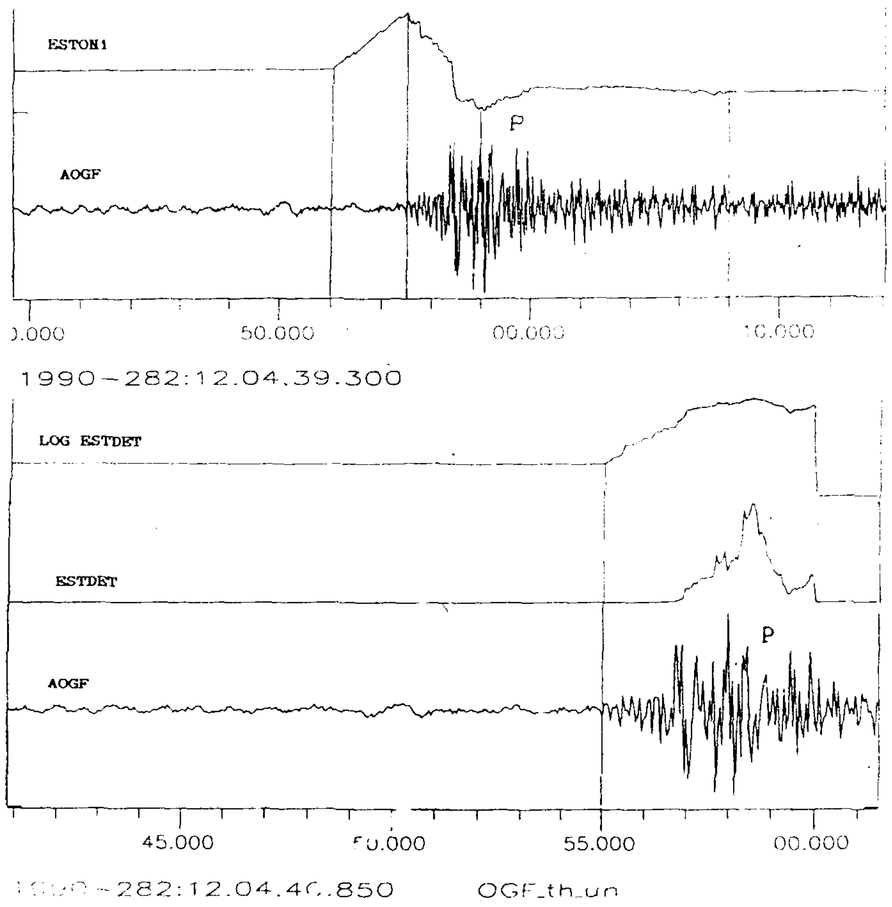

Fig. 7.4.6. P-phase detection and onset time estimation using the AOGF output trace of a FINESA local event recording (1990:282:12.04.13, distance 149.2 km).

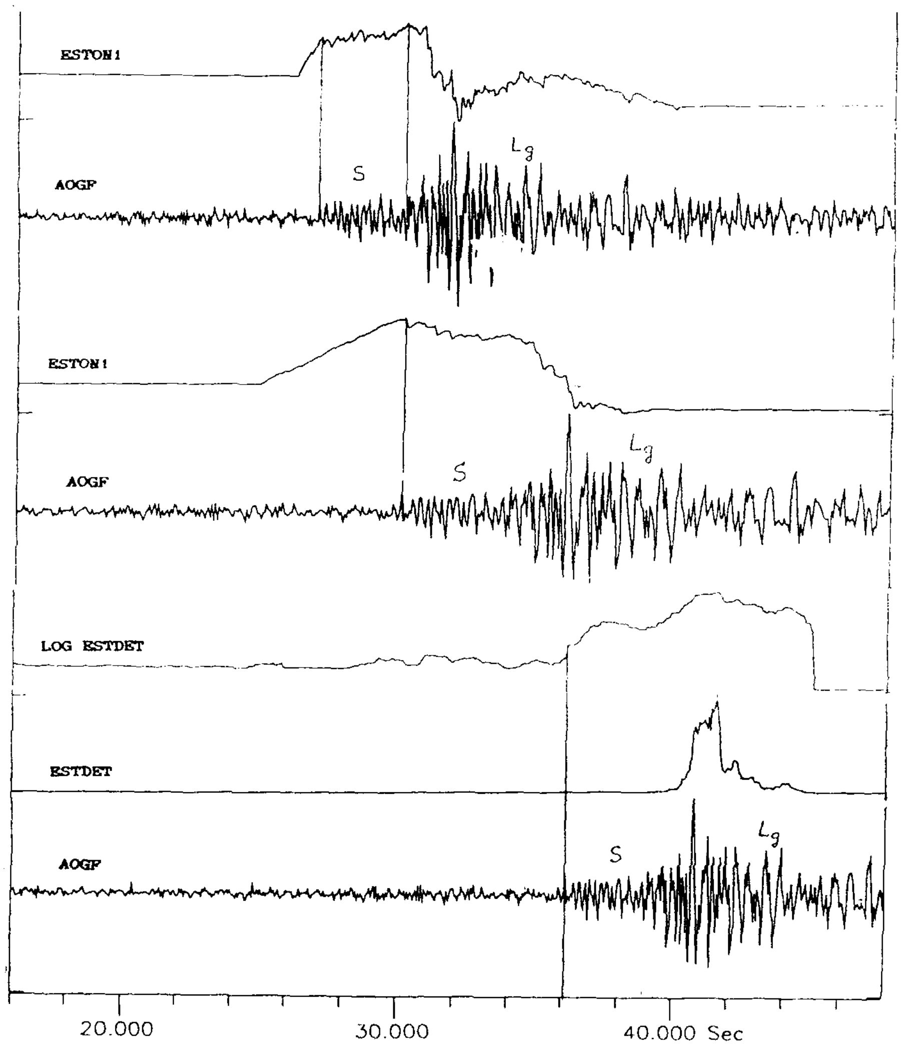

Fig. 7.4.7. S and Lg phase detection and onset time estimation using the AOGF output trace of the local event described in Fig. 7.4.6.

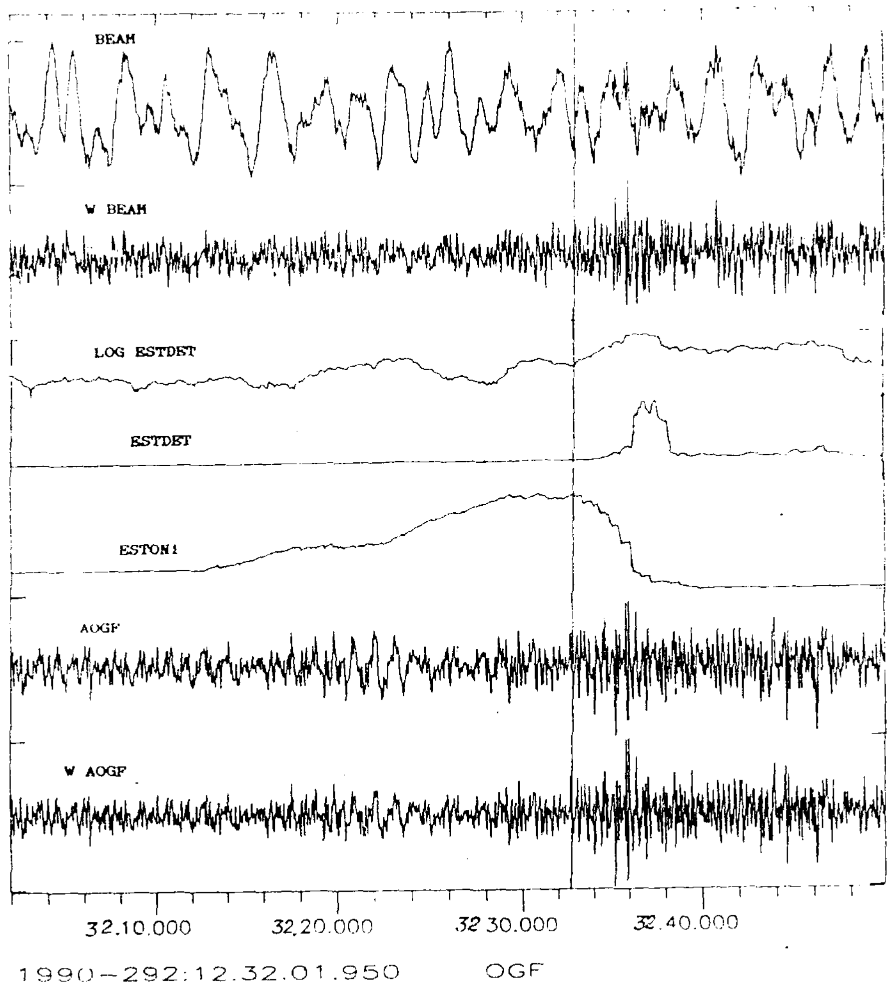

Fig. 7.4.8. P-phase detection and onset time estimation using the AOGF output trace from FINESA recordings of a small local event (1990:292:12.31.45.0, distance 166.4 km).

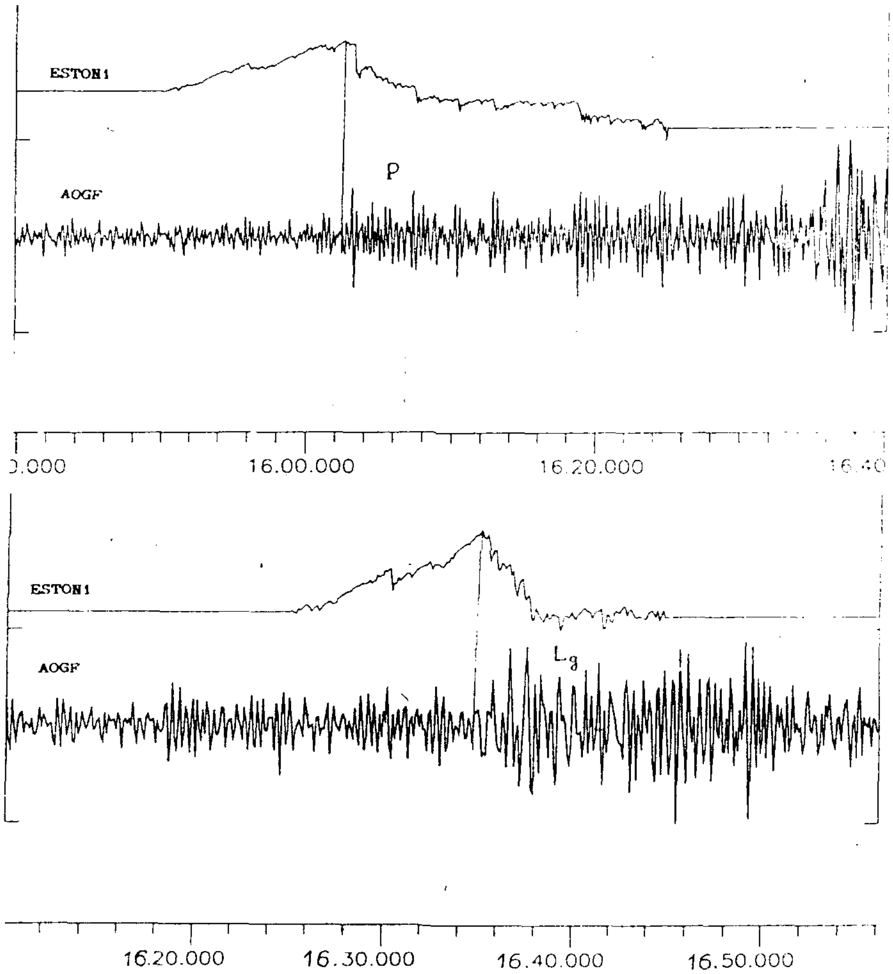

Fig. 7.4.9. P-phase and Lg-phase onset time estimation using the output of the AOGF procedure adjusted for Lg-phase extraction from FINESA recordings of a regional event (1990:294:09.13.00, distance 772.3 km).

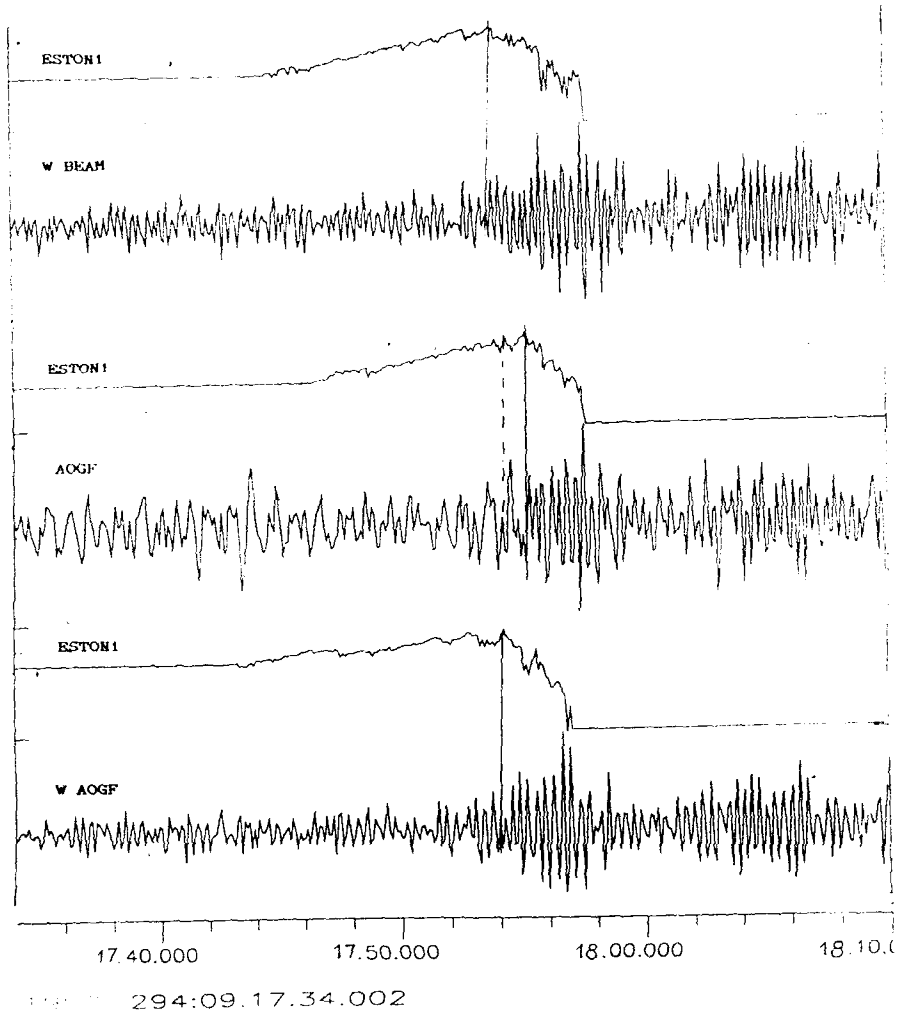

Fig. 7.4.10. S-phase onset time estimation for the event described in Fig. 7.4.5, using the Whitened Beam, the AOGF and the Whitened AOGF output traces. The time shifts of the estimates may be explained by the influence of the whitening filter impulse response.

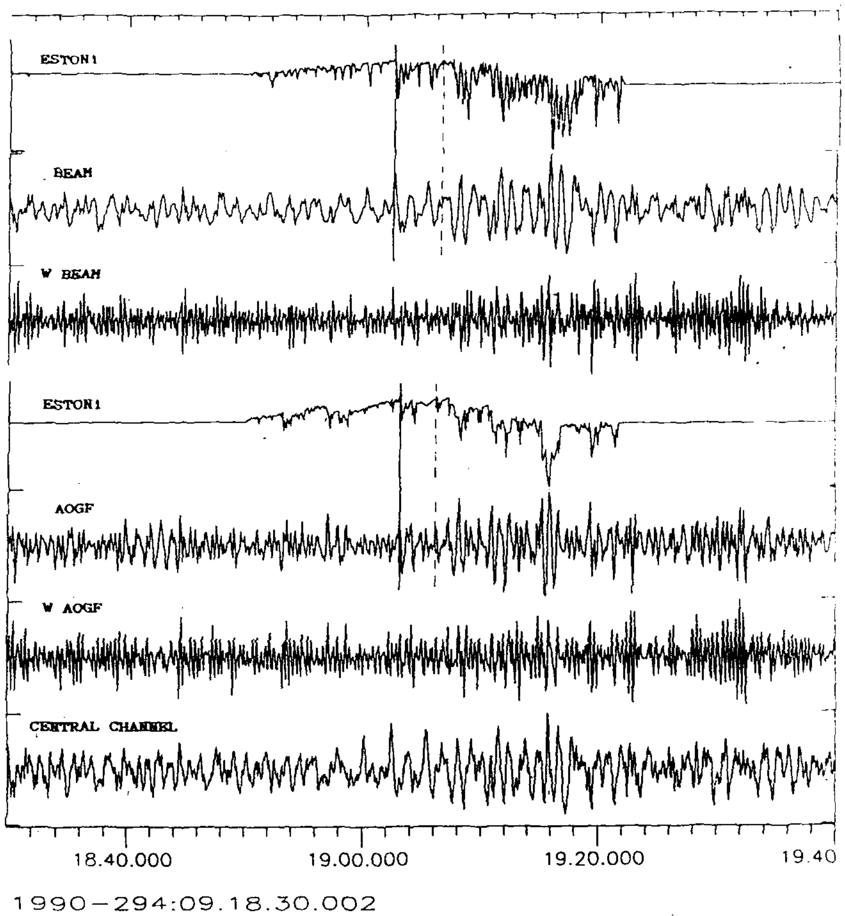

Fig. 7.4.11. Extraction of the Lg-phase from the recording described in Fig. 7.4.5 and onset time estimation of this phase using the beam and the AOGF output traces.

7.5 A 2-dimensional finite difference approach to modeling seismic wave propagation in the crust

Introduction

It is well known that the direct, discrete solution of the elastic wave equation constitutes an excellent platform for synthetic seismogram analysis as *all* propagation effects are included in the solution (e.g., see Mooney, 1983). A practical realization of this approach has been problematic until recently due to limitations imposed by currently available computers. This being said, we will report below on 2-dimensional (2D) finite difference seismogram synthetic experiments which have been achieved through cooperative efforts with scientists at IBM Bergen Scientific Centre (Bergen, Norway).

Elastic wave modeling formulation

The basic equations governing wave propagation in a continuous elastic medium are the momentum conservation and the stress-strain relation. Following Achenbach (1975), in the velocity-stress formulation, these are given by

$$\rho \frac{\partial}{\partial t} v_j = f_j + \frac{\partial}{\partial x_\ell} \sigma_{j\ell}, \qquad j, \ell = 1, \ldots, J \tag{1}$$

$$\frac{\partial}{\partial t} \sigma_{jj} = \lambda \frac{\partial}{\partial x_\ell} v_\ell + 2\mu \frac{\partial}{\partial x_j} v_j, \qquad j, \ell = 1, \ldots, J \tag{2}$$

$$\frac{\partial}{\partial t} \sigma_{j\ell} = \mu \left(\frac{\partial}{\partial x_j} v_\ell + \frac{\partial}{\partial x_\ell} v_j \right), \qquad j, \ell = 1, \ldots, J, \quad j \neq \ell \tag{3}$$

where Einstein's summation convention is used. J is the dimensionality of the problem, ρ is density, and λ and μ are Lamé's parameters. f_f are body forces and v_j and $\sigma_{j\ell}$ are velocities and stresses, respectively.

Numerical discretization

Spatial partial differentiation is achieved through cost-optimized, dispersion-bounded, high-order finite difference operators on a staggered grid. For time stepping a leap-frog technique is used. The discretization of the elastodynamic equations with two staggered numerical space differentiators, $\sigma^{\pm}$, applied as in Levander (1988) to stresses and particle velocities leads to:

$$\rho_j^+ \{V_j^+(t + \Delta t/2) - V_j^+(t - \Delta t/2)\} = \Delta t\{F_j^+(t) + \delta_j^+ S_{jj}(t) + \sum_{\substack{l=1 \\ l \neq j}}^{J} \delta_l^- S_{jl}^{++}(t)\}, j, l = 1, \ldots, J$$

$$S_{jj}(t + \Delta t) - S_{jj}(t) = \lambda \Delta t \sum_{r=1}^{J} \delta_r^- V_r^+(t + \Delta t/2) + 2\mu \Delta t \delta_j^- V_j^+(t + \Delta t/2), \quad j, l = 1, \ldots, J$$

$$S_{jl}^{++}(t + \Delta t) - S_{jl}^{++}(t) = \mu_{jl}^{++} \Delta t\{\delta_j^+ V_l^+(t) + \delta_l^+ V_j^+(t)\}, \quad j, l = 1, \ldots, J, \quad j \neq l$$

with

$$V_j^+(t) = v_j(\mathbf{x} + \mathbf{h}_j/2, t), \quad F_j^+(t) = f_j(\mathbf{x} + \mathbf{h}_j/2, t),$$

$$S_{jj}(t) = \sigma_{jj}(\mathbf{x}, t), \quad S_{jl}^{++}(t) = \sigma_{jl}(\mathbf{x} + \mathbf{h}_j/2 + \mathbf{h}_l/2, t),$$

$$\rho_j^+ = \rho(\mathbf{x} + \mathbf{h}_j/2), \quad \lambda = \lambda(\mathbf{x}), \quad \mu = \mu(\mathbf{x}) \quad \text{and} \quad \mu_{jl}^{++} = \mu(\mathbf{x} + \mathbf{h}_j/2 + \mathbf{h}_l/2).$$

$$\delta_j^+ q(\mathbf{x}) = \sum_{\ell=1}^{L^+/2} d_{2\ell-1}^+ \frac{q(\mathbf{x} + \ell\mathbf{h}_j) - q(\mathbf{x} - (\ell - 1)\mathbf{h}_j)}{\Delta x_j} \cong \frac{\partial q}{\partial x_j}(\mathbf{x} + \mathbf{h}_j/2),$$

$$\delta_j^- q(\mathbf{x}) = \sum_{\ell=1}^{L^-/2} d_{2\ell-1}^- \frac{q(\mathbf{x} + (\ell - 1)\mathbf{h}_j) - q(\mathbf{x} - \ell\mathbf{h}_j)}{\Delta x_j} \cong \frac{\partial q}{\partial x_j}(\mathbf{x} - \mathbf{h}_j/2).$$

Here $\mathbf{h}(j)$ is the unit vector in the jth direction. λ, μ and S_{jj} are defined at the nodes of the Cartesian mesh, ρ_j^+, V_j^+ and F_j^+ and defined at the links connecting the nodes and $S_{j\ell}^{++}$ and $\mu_{j\ell}^{++}$ are defined at the centers of the "plaquettes". $\sigma^{\pm}$ are numerical differentiators of coefficients $d_{2\ell-1}^{\pm}$. q is here velocity or stress and $L^{\pm}$ is the length of the operator. For the numerical dispersion relations, the stability limit and bandwidth introduced By the discretization, the reader is referred to Sguazzero *et al* (1990).

Absorbing and free surface boundary conditions

By necessity, the numerical modeling limits the medium, and to reduce artificial reflections from the numerical boundaries, the velocities and stresses are multiplied by exponentially decreasing terms near the edges. For this procedure to be efficient, relatively large models are required, that is, relatively large spatial distances to the wedges and this in 3D modeling would be computationally very demanding. In the latter case we have experimented with boundary operators recently introduced by Higdon (1990,1991), which at $x = 0$ read like

$$\prod_{j=1}^{m} \left(\cos\alpha_j \frac{\partial}{\partial t} - c_j \frac{\partial}{\partial x} \right)$$

which will absorb perfectly a plane wave travelling towards the boundary at angle

α_j and speed c_j. m is the order of the operator. Similar operators are used on the other boundaries. The condition for this method to be useful is that the number of time steps is small enough not to exceed a certain limit, after which the method will appear unstable.

On the top free surface, we use the vanishing stress conditions for a free boundary

$$\vec{n} \cdot \boldsymbol{T} = 0 \tag{4}$$

Here $\vec{n}$ is the outward normal unit vector on the surface and $\boldsymbol{T}$ is the stress tensor. To get computationally tractable conditions, we assume the free top surface to be locally plane. Then $\vec{n} = \vec{k}$, where $\vec{k}$ is the unit vector in the vertical z-direction. x and y are horizontal coordinates. (4) then leads to

$$\sigma_{zx} = \sigma_{zy} = \sigma_{zz} = 0 \tag{5}$$

To increase the generality, one may assume a topographic relief as the free surface. By relaxing the requirement of the surface being locally plane, one assumes a given slope locally in each spatial direction. The resulting conditions on the stresses become more complex, though tractable, as demonstrated by Jih *et al* (1988).

At present we have not incorporated the "topography" free surface in our software.

Crustal wave propagation — 2D finite difference synthetics

The task of "adapting" the 2D FD software for handling of seismological problems has been rather time consuming. Hence, only recently have we been able to produce seismic synthetics for crustal wave propagation. We can also handle 3D cases, but their seismological relevance at present is limited. Anyway, in the following we will present some examples of synthetic seismograms.

Model description and data analysis

Basically we use a homogeneous crust of thickness 30 km and $\mathrm{P}_{vel} = 6.5$ km/sec, which besides serves as a reference model. The options for perturbing this model comprise multilayering, piecewise linear velocity gradients, large-scale discontinuities like Moho bump(s), but so far no randomized scatter inclusions. A schematic model illustration is shown in Fig. 7.5.1. Although the source (point or line source) could be at any depth, the sensors are always on the free surface. Any sensor configuration could be used, although our performance is for a 10-element line array with 0.4 km sensor interspacing, which is convenient for velocity decomposition of the synthetics. Occasionally we use a sensor spacing of 5 km in order to visualize the distance variability in the records.

An objection against 2D solutions of the elastic wave equation is that all propagation effects are included and hence it would be difficult to isolate the response of a specific body within the synthetic wavetrain. To overcome this kind of problems, we would process the synthetic records in a manner similar to that used for real recordings. Principal techniques used are frequency wavenumber (f-k), semblance and 3-component polarization analysis (e.g., see Husebye and Ruud, 1989). Occasionally we would make comparisons with "ray tracing" synthetics for which more specific contribution effects are specified *a priori*.

Results

Examples of crustal synthetics using the procedure outlined above are shown in Figs. 7.5.2, 7.5.3 and 7.5.4. The following comments apply.

Figs. 7.5.2 and 7.5.3: Bump on Moho — ranges 160 km and 210 km

In Figs. 7.5.2b and 7.5.3b the homogeneous cases are shown, while the bump cases are shown in Figs. 7.5.2a and 7.5.3a, respectively. A comparison here gives that the Moho bump does not strongly change the records, which is also rather obvious from a corresponding comparison of the semblance plots in Figs. 7.5.2c,d and Fig. 7.5.3c,d, respectively. The dominant features in the synthetics appear to be crustal reverberations (PmP), which are particularly abundant since the signal source was put at a depth of 10 km.

Fig. 7.5.4: Bump on Moho — ranges 100–200 km

In this case, we used a linear velocity gradient in the crust and besides used a sensor spacing of 5 km in order to visualize distance-dependent changes in the records. As observed, the Pg-phase dominates the first part of the records, then comes the corresponding S-phases and finally multimode Rayleigh-type of waves. With the much larger sensor spacing the semblance resolution is very high, as illustrated in Fig. 7.5.4c,d. We have also tested the signal polarity, which further adds weight to the realism of the 2D FD synthetics displayed.

Discussion and future work

The synthetics generated seemingly include *all* major phases, while in comparison to real records the body wave coda is weak to nonexistent. As demonstrated, long wavelength heterogeneities like a bump on Moho do not contribute much in this respect. This in turn implies that the cumulative propagation effect of randomly distributed scatterers are likely to be of importance.

A specific advantage with our technique for 2D synthetic seismogram calculations is flexibility in choosing model parameters. In our future work, some sort of a reference crustal model would be established. Then we would systematically change the velocity structure both above and below Moho. Scatterers would be introduced at various parts of the travel path, and their effect would be visualized partly but taking the difference between "homogeneous" and "inhomogeneous" synthetics. Finally, we would naturally compute synthetics on the basis of crustal results presented in Section 7.6.

S. Hestholm, IBM Bergen Sci. Centre
B. Rosland, IBM Bergen Sci. Centre
B.O. Ruud, Geol. Inst., Univ. of Oslo
E.S. Husebye

References

Achenbach, J.D. (1975): *Wave Propagation in Elastic Solids*, North Holland Publ. Co., The Netherlands.

Higdon, R.L. (1990): Radiation boundary conditions for elastic wave propagation, *SIAM J. Num. Anal.*, April.

Higdon, R.L. (1991): Absorbing boundary conditions for elastic waves, *Geophysics*, to appear.

Husebye, E.S. and B.O. Ruud (1989): Array seismology — Past, present and future developments, in *Observatory Seismology*, J.J. Litehiser, Ed., Berkeley Univ. Press, Berkeley, California, 123–153.

Jih, R.-S., K.L. McLaughlin and Z.A. Der (1988): Free boundary conditions of arbitrary polygonal topography in a two-dimensional explicit elastic finite difference scheme, *Geophysics*, 53, 1045–1055.

Levander, A.R. (1988): Fourth-order finite-difference P-SV seismograms, *Geophysics*, 53, 1425–1436.

Mooney, H.M. (1983): Synthetic seismograms for body waves: An overview, *First Break*, dec, 9–20.

Sguazzero, P., M. Kindelan and A. Kamel (1990): Dispersion-bounded numerical integration of the Elastodynamic equations, *Comp. Meth. Appl. Mech. Eng.*, 18.

2D ELASTIC MODELLING - OSLO RIFT

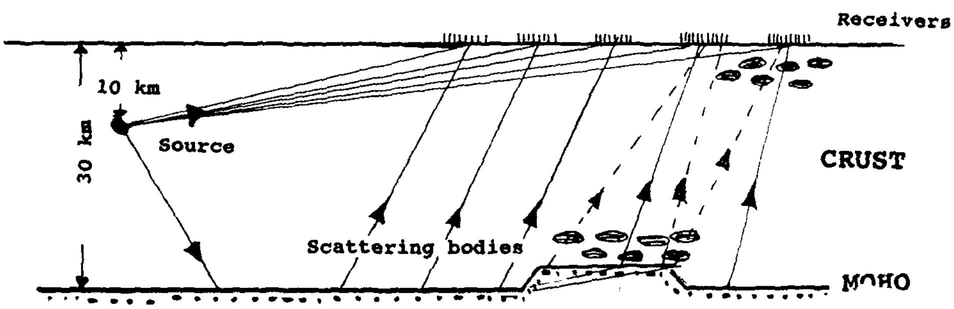

PROCESSING: F-K; SEMBLANCE AND 3C ANALYSIS

OBSERVATION: NORESS ARRAY RECORDINGS

Fig. 7.5.1. Simple one-layered crustal model used initially for computing synthetic seismograms based on finite difference solutions in 2-dimensional (2D) of the elastic wave equations. The point source is located at a depth of 10 km: crustal and sub-Moho velocities are 6.5 km/sec and 8.2 km/sec, respectively. Corresponding density values are 2.85 kg/m^3 and 3.34 kg/m^3. The Moho bump is 50 ? wide and 2 or 4 km high. Horizontal distance from source to nearest edge of Moho bump is 1.0 km. So far scatter inclusions with contrasts in velocity and density of the order of 2-5 per cent have not been included.

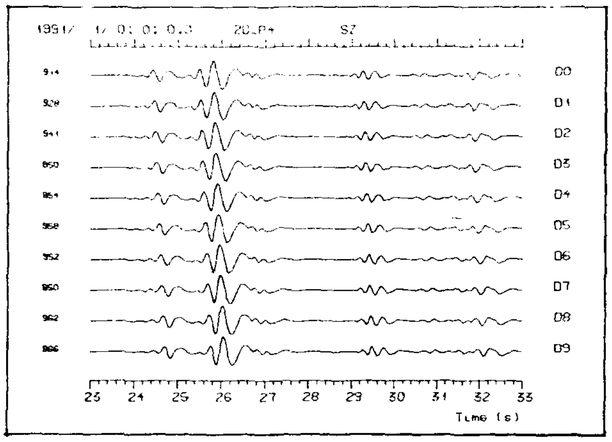

a)

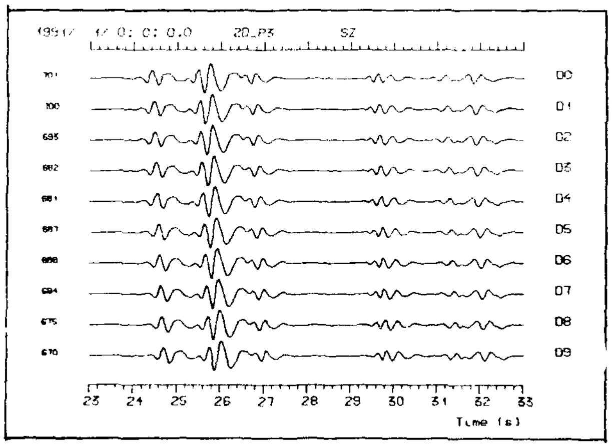

b)

Fig. 7.5.2a and b. 2D FD synthetics for the model shown in Fig. 7.5.1. In figure b, the Moho bump of 2 km has been removed. The horizontal distance from source to the nearest sensor is 160 km while sensor interspacing is 200 m.

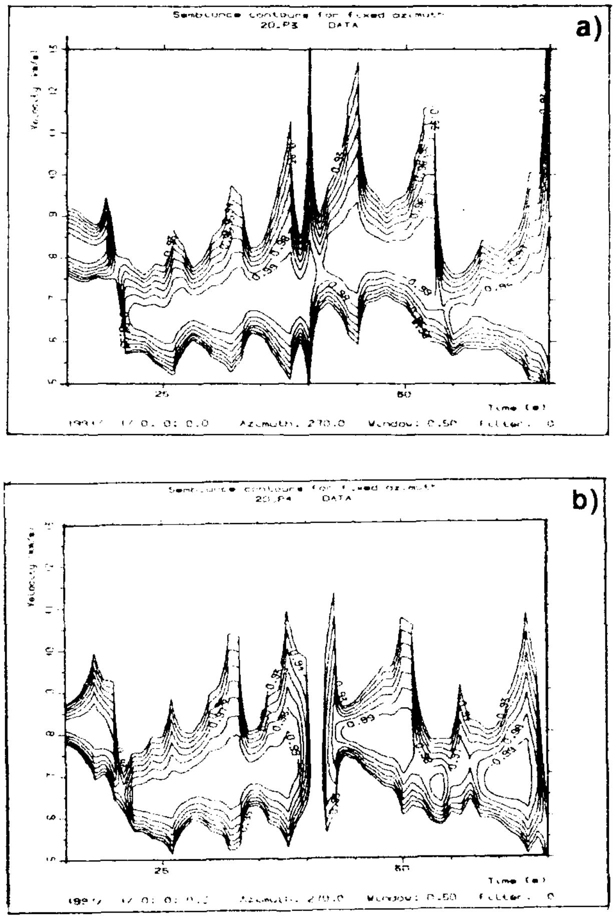

Fig. 7.5.3a and b. Semblance velocity (VESPAGRAM) analysis of the synthetics displayed in Fig. 7.5.2a and b, respectively. Seemingly the effect of a bumpy Moho is marginal. Also, "ray paths" within the crust and sub Moho are easily identified from this velocity plot.

a)

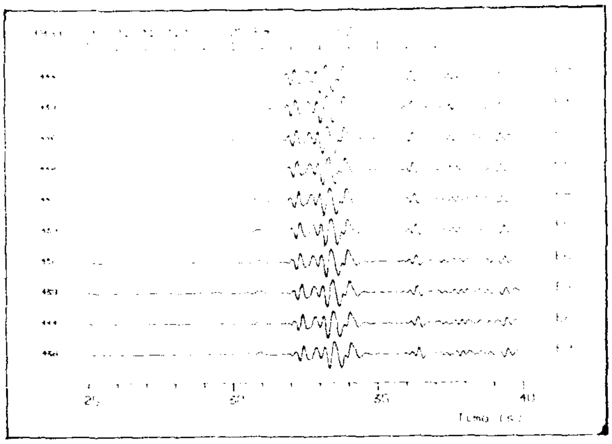

b)

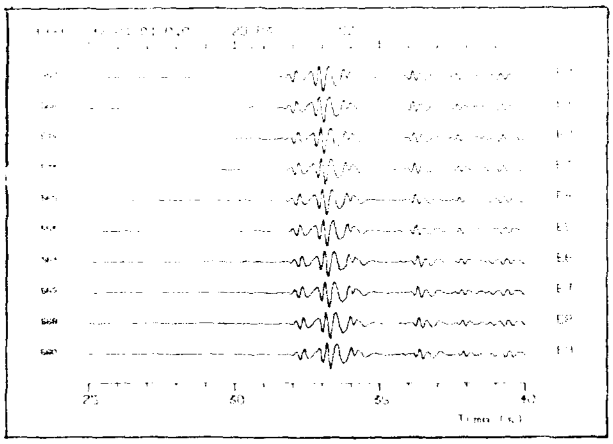

Fig. 7.5.4a and b. Same as for Fig. 7.5.2, but now the horizontal distance to the nearest sensor is 210 km.

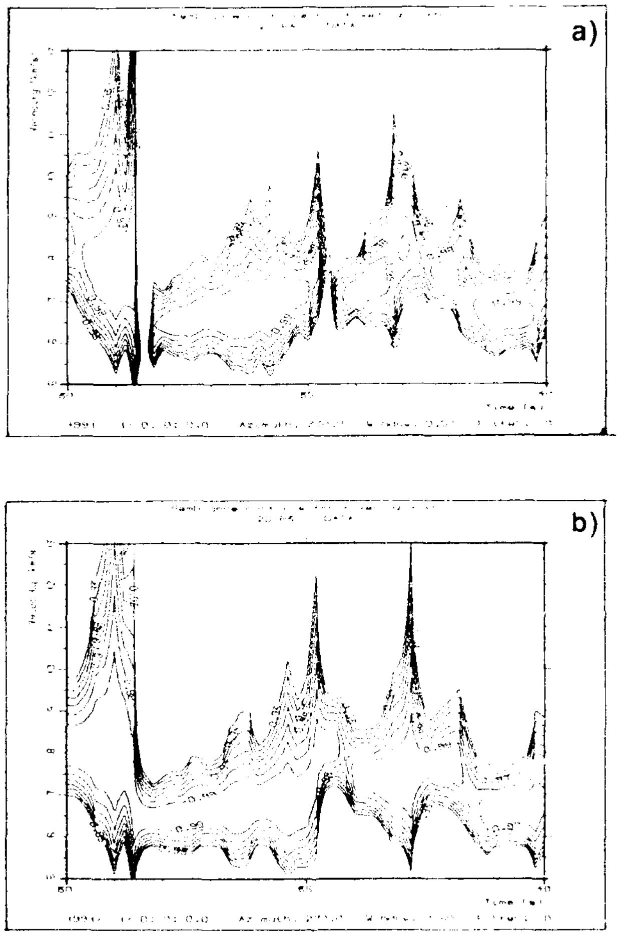

Fig. 7.5.5a and b. Semblance velocity (VESPAGRAM) analysis for the synthetics shown in Fig. 7.5.4.

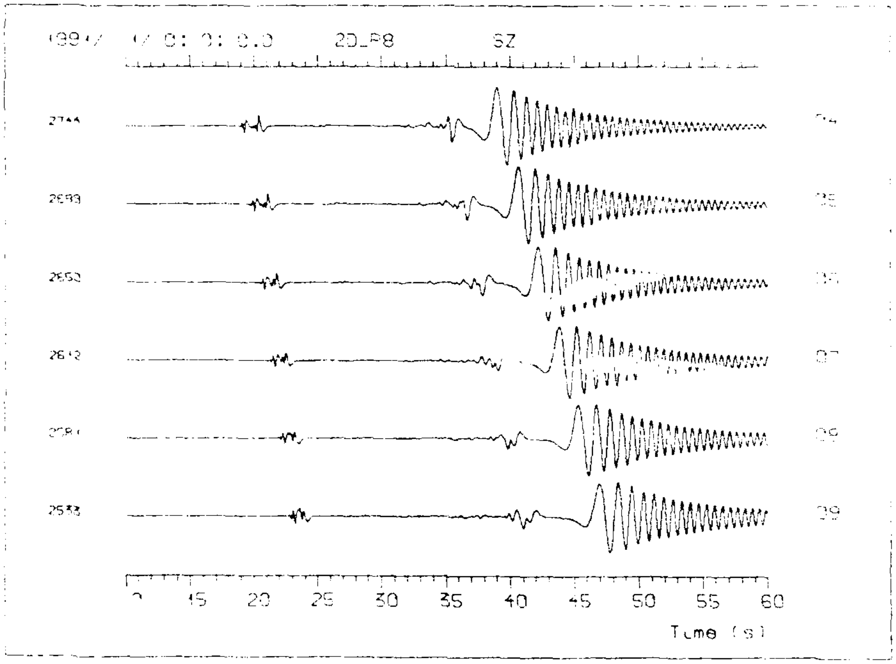

Fig. 7.5.6a. Crustal 2D FD synthetics of 60 sec duration. In this case the point source is just below the surface and the P velocity increases linearly from 6.2 to 7.0 km/sec at the bottom of the crust. Below Moho the P velocity increases linearly from 8.2 to 8.4 km/sec from 30 to 40 km. Below 40 km the velocity is fixed at 8.4 km/sec. Distance range is 115–140 km with a 5 km interspacing of sensors.

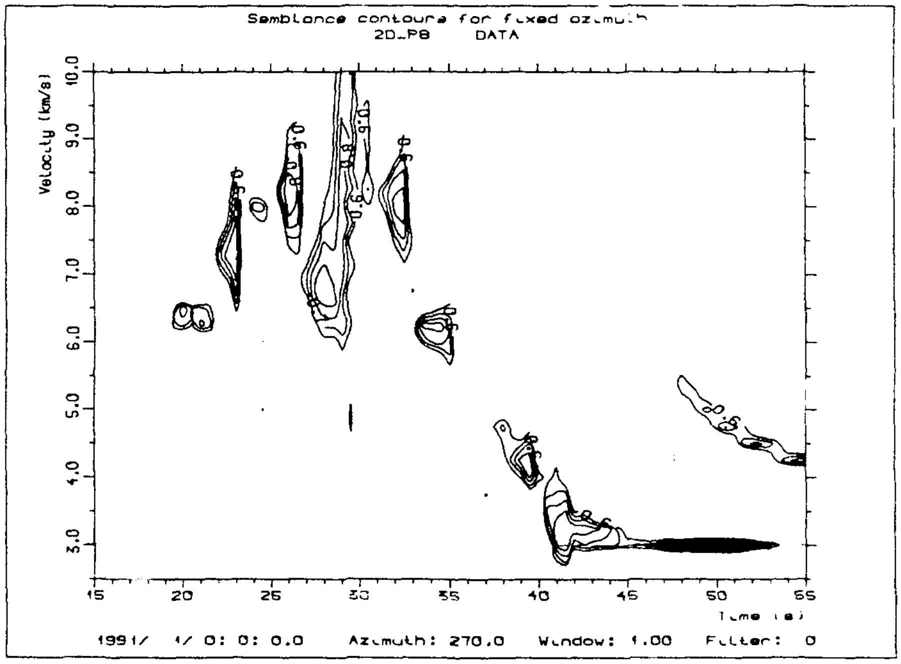

Fig. 7.5.6b. Semblance velocity (VESPAGRAM) analysis of the synthetics displayed in Fig. 7.5.6a. The first part of the synthetics is dominated by crustal reverberations (phase velocities above 8.0 km/sec hardly seen). The Pg-phase around 35 sec preceding the S-wave at around 39 sec is a commonly observed feature. Dispersive Rayleigh waves are also synthesized. Time reference is tied to sensor 06.

7.6 Crustal thicknesses in Fennoscandia — An overview

Background

Crustal studies became popular among seismologists in the Fennoscandinavian countries some three decades ago, and still remain so. The numerous seismic surveys conducted within this region are aimed at mapping crustal structures in ever-increasing detail. We have reviewed the knowledge accumulated from these studies and made a new crustal thickness map with contour intervals of 2 km for Fennoscandinavia. In some areas the sediment thicknesses exceed 10 km, so it is important to differentiate between Moho depths and the crust crystalline thicknesses. Hence for the southern parts of Fennoscandinavia, notably Denmark and adjacent seas, an additional map of crystalline crustal thicknesses was made. Below, we will present the major results from this crustal study, while for details we refer to a forthcoming paper by Kinck *et al* (1991).

Geological Framework

Geographically, the Fennoscandinavian part of the Baltic Shield comprises the Kola Peninsula (including the White Sea), Finland, the Scandinavian Peninsula, Denmark and adjacent seas (Skagerrak, Kattegat, the Baltic Sea and parts of the Barents Sea)In geological terms, this area (Fig. 7.6.1) exhibits a variety of different tectonic provinces, ranging in age from Archean to Permian. The more recent opening of the North Atlantic, commencing some 56 Ma ago, affected only peripheral parts of the shield, that is, the coastal areas of western and northern Norway.

Crustal profiling — Moho depth mapping

The principal aims of crustal profiling surveys are crustal thicknesses and velocity-depth distributions above and below Moho. The former parameter seems well constrained in view of small differences of the order of 2–3 km either between intersecting profiling lines or between reflection and refraction lines. Regarding velocity depth distributions the reflection profiling data have poor resolution. The refraction profiling data have relatively good resolution although the inversion schemes in general use do not give unique results. It suffices here to mention that different groups of researchers using the same set of observational data seldom produce the same velocity-depth distribution. The inherent problem here is that the identification and picking of secondary phase arrivals often are difficult and hence the final solution is not well constrained. Kinematic ray tracing is not too helpful in this respect since amplitude information and scattering contributions are mostly ignored. Also, there appears to be a significant improvement in the published profiling results from the mid-seventies and onwards, reflecting better recording instrumentation (digital), denser sampling and the use of more sophisticated analysis and interpretational methods. These brief comments on the reliability of seismic reflection and refraction profiling results should be kept in mind when judging the major outcomes of our study (Kinck *et al.* 1991), namely, a Moho depth map for Fennoscandinavia, thicknesses of the crystalline crust in the southern parts of the region (Denmark and adjacent sea) plus a tabulation of P-velocity depth distributions for selected profiles.

Fennoscandinavian seismic profiling surveys

We have carefully screened the available literature for profiling surveys within Fennoscandinavia, and the outcome of these efforts is tabulated in Table 7.6.1 and displayed in Fig. 7.6.2. Note that data from some of the profiling lines have been reanalyzed and reinterpreted and with few exceptions we only refer to the latest publication in tis regard. A final remark here is that indeed much effort has been invested in the crustal mapping of Fennoscandinavia.

Results: Moho depth and crystalline crustal thickness maps for Fennoscandinavia

In Fig. 7.6.3 the Moho depth map is shown and in Fig. 7.6.4 the crystalline crustal thickness map (limited to Denmark and adjacent seas) are shown. A map similar to that in Fig. 7.6.4 was attempted constructed for the Kola Peninsula area, the White Sea and the western Barents Sea, but at present there are not enough data available for such a task. Anyway, the Moho map in Fig. 7.6.3 is rather detailed, in particular in the areas offshore Norway, as we have been able to incorporate recent results from marine seismic reflection surveys. The crustal thickening is in general perpendicular to the coastal areas of southern and western Norway, and the Kola Peninsula, but less so for the interplate Baltic Sea. In general, the oldest parts of the Baltic Shield (the major parts of the Fennoscandinavian region) exhibit the greatest crustal thicknesses. This may be expressed in the following form:

$$H = 17.3 log(T) - 10.2 \qquad (1)$$

where H in km is Moho depth and T is *time in* Ma.

The sediment thicknesses in the basin areas offshore Norway are often formidable with corresponding thicknesses of the crystalline crust of the order of 15–20 km. There is no obvious correlation with age between the crustal P-velocity depth distribution, although whether we have piecewise negative, zero or positive velocity gradients is likely to affect profoundly seismic wave propagation in the crust. Regarding lateral Pn and Sn velocity variations within Fennoscandinavia, this problem has been studied by tomographic techniques using local seismological bulletin data (e.g., see Bannister *et al.* 1991). Their major findings are that pronounced low velocity areas are associated with the Caledonide mountains of western Norway and the rift and basin areas offshore Norway. The central parts of the shield are rather homogeneous in this respect. A corresponding tomographic study of crustal velocity variations (Pg and Sg phases) was not attempted since the Pg/Sg ray paths cannot uniquely be determined.

Discussion

Compared to many other continental regions, the results displayed in Fig. 7.6.3 and 7.6.4 are indeed very detailed. On the other hand, structural details are very poorly resolved, which in turn reflects the data at hand; mainly, refraction profiling results. Although these results are not adequate for restraining hypotheses on the tectonic evolution of Fennoscandinavia, we do think that these results may be instrumental in providing a better understanding of seismic records at local and regional distances through synthetic seismogram analysis. In this respect we consider the 2D finited difference technique presented in Section 7.5 to be most suitable since we could incorporate a tilting Moho together with any kind of velocity gradient above and/or below Moho.

A final remark is that the Moho depth variation appears to have a counterpart in the spatial distribution of earthquakes within this region. As is well known, the seismicity is by far largest in the coastal areas of Norway, where the crust is *exceptionally thin*. Furthermore, all the largest earthquakes, including the historical ones, have taken place in areas where the crust is thin. In other words, stress accumulations within Fennoscandinavia appear to be insufficient for cracking or causing major earthquakes in areas with thick crust ($H > 40$ km), which naturally is stronger than the thin crust in the coastal areas. Naturally, there are many areas, including Denmark, with thin crust but seismically quiescent.

E.S. Husebye
J.J. Kinck, Dept. of Geology, Univ. of Oslo
F.R. Larsson, Dept. of Geology, Univ. of Oslo

References

Avedik, F., Berendsen, D., Fucke, H., Goldflam, S., Hirschleber, H., Meissner, R., Sellevoll, M.A. and Weinrebe, W., 1984. Seismic investigation along the Scandinavian "Blue Norma" profile. Annales Geophysicae, 2, 5: 571-578.

Bannister, S.C., Ruud, B.O. and Husebye, E.S., 1991. Tomographic estimates of sub-Moho seismic velocities in Fennoscandia and structural implications. Tectonophysics, 189, 37-54.

Barton, P.J. and Wood, R., 1984. Tectonic Evolution of the North Sea Basin: Crustal Stretching and Subsidence. Geophys. J. R. astr. Soc., 79: 987-1022.

Bertcussen, K.-A., 1977. Moho Depth Determinations based on Spectral-Ratio Analysis of NORSAR Long Period P-waves. Physics of the Earth and Planetary Interiors, 15: 13-27.

Bungum, H., Pirhonen, S.E. and Husebye, E.S., 1980. Crustal thickness in Fennoscandia. Geophys. J. R. astr. Soc., 63: 759-774.

Båth, M., 1984. A Seismic Refraction Profile in Swedish Lappland. Report no. 2-84. Seismological Department, University of Uppsala, Uppsala, pp. 1-32.

Cassell, B.R., Mykkeltveit, S., Kanestrøm, R. and Husebye, E.S., 1983. A North Sea southern Norway seismic crustal profile. Geophys. J. R. astr. Soc., 72: 733-753.

Davydova, N.I., Pavlenkova, N.I., Tulina, Yu.V., and Zverev, S.M. (1985): Crustal structure of the Barents Sea from seismic data. Tectonophysics, 114: 213-231.

Drivenes, G., M.A. Sellevoll, V. Renard, F. Avedik and J. Pajchel, 1984. The continental margin/crustal structure off the Lofoten Islands, Northern Norway. Petroleum Geology of the North European Margin, Norwegian Petroleum Society, Graham & Trotman, 1984, pp. 211-216.

Egilson, T. and Husebye, E.S., 1991. An Oslo Graben Experiment - shooting at sea and recording on land. Tectonophysics, 189, 183-192.

EUGENO-S Working Group, 1988. Crustal structure and tectonic evolution of the transition between the Baltic Shield and the North German Caledonides (the EUGENO-S Project). Tectonophysics, 150: 253-348.

Faleide, J.I., Gudlaugsson, S.T., Eldholm, O., Myhre, A.M. and Jackson, H.R., 1991. Deep seismic transects across the western Barents Sea continental margin. Tectonophysics, 189, 91-108.

Fichler, C. and Hospers, J., 1990. Deep crustal structure of the Northern North Sea Viking Graben: results from deep reflection seismic and gravity data. *Tectonophysics, (in press).*

Gaál, G. and Gorbatschev, R., 1987. An outline of the Precambrian evolution of the Baltic Shield. Precambrian Res., 35, 15-52.

Galson, D.A. and Mueller St., 1986. An introduction to the European Geotraverse project: First results and present plans. Tectonophysics, 126: 1-30

Glaznev, V.N., Raevsky, A.B. and Sharov, N.V., 1989. A model of the deep structure of the northeastern part of the Baltic Shield based on joint interpretation of seismic, gravity, magnetic and heat flow data. Tectonophysics, 162: 151-163.

Grad, M., Guterch, A. and Lund, C.-E., 1991. Seismic models of the lower lithosphere beneath the southern Baltic Sea, between Sweden and Poland. Tectonophysics, 189, 219-228.

Grad, M. and Luosto, U., 1987. Seismic models of the crust of the Baltic shield along the SVEKA profile in Finland. Annales Geophysicae, 5B: 639-650.

Gregersen, S., 1991. Crustal structure acorss the Tornquist Zone (southwestern edge of the Baltic Shield): A review of the Eugeno-S geophysical results. Tectonophysics, 189, 165-182.

Hospers, J. and Ediriweera, K.K., 1988. Mapping the top of the crystalline continental crust in the Viking Graben area, North Sea. Nor. Geol. Unders., Special Publ. 3, pp. 21-28.

Kanestrom, R., 1971. Seismic Investigations of the Crust and Upper Mantle in Norway. In: A. Vogel (Editor). Deep seismic sounding in northern Europe. Swedish Natural Science Research Council, Stockholm, pp. 17-27.

Kinck, J.J., Husebye, E.S., and Larsson, F.R. (1991): The Moho depth distribution in Fennoscandia and the regional tectonic evolution from Archean to Permian times., submitted for publication *Lithos*

Korhonen, H., Kosminskaya, I.P., Azbel, I., Sharov, N., Zagorodny, V., and Luosto, U., 1990. Comparison of crustal structure along DSS profiles in SE Fennoscandia, Geophys. J. Int., 103: 157-162.

Kornfält, K. A. and Larsson, K., 1987. Geological maps and cross sections of Southern Sweden. Swedish Nuclear Fuel and Waste Management Co., Technical Report 1987-24, Stockholm, 44 pp.

Kværna, T., 1984. Reinterpretation of seismic refraction profiles in the framework of Fennoscandian tectonic evolution. Cand. Scient. Thesis, University of Oslo, Oslo (unpublished).

Lubimova, E.A., 1980. Heat flow, Epeirogeny and Seismicity for the east European plate. In: N. A. Mörner (Editor). Earth Rheology, Isostacy and Eustacy. Wiley, New York, pp. 91-109.

Lund, C. E., 1987. Crustal structure along the northern 'Fennolora' profile. Precambrian Res., 35, 195-206.

Lund, C. E., Roberts, R.G. and Juhlin, C., 1987. The reflectivity of the lower crust in southwestern Sweden. Annales Geophysicae, 5B: 375-380.

Lund, C. E., Roberts, R.G., Dahl Jensen, T. and Lindgren, J., 1988. Deep Crustal Structures in the Vicinity of the Siljan Ring. In: A. Boden and K.G. Eriksson (Editors). *Deep Drilling in Crystalline Bedrock, Volume 1: The Deep Gas Drilling in the Siljan Impact Structure, Sweden and Astroblemes.* Springer Verlag, pp. 355-361.

Luosto, U., Flueh, E.R., Lund, C.-E. and Working Group., 1989. The crustal structure along the Polar Profile from seismic refraction investigations. *Tectonophysics*, 162: 51-85.

Luosto, U., Tiira, T., Korhonen, H., Azbel, I., Burmin, V., Buyanov, A., Kosminskaya, I.P., Ionkis, V., and Sharov, N., 1990. Crust and upper mantle structure along the DSS Baltic profile in SE Finland. Geophys. J. Int., 101, 89-110.

Mykkeltveit, S., 1980. A Seismic Profile in Southern Norway. Pure and Applied Geophysics, 118: 1310-1325.

Olafsson, I., 1988. Deep crustal structure of the More margin from analysis of two ship multichannel seismic data. Dr. Scient. Thesis, University of Bergen, Bergen, 154 pp.

Planke, S., Skogseid, J. and Eldholm, O., 1991. Crustal Structure off Norway, 62° to 70° North. Tectonophysics, 189, 91-108.

Sellevoll, M.A., 1983. A Study of the Earth's Crust in the Island Area of Lofoten Vesteralen, Northern Norway. Nor. Geol. Unders., 380: 235-243.

Sellevoll, M.A. and Warrick, R.E., 1971. A Refraction Study of the Crustal Structure in Southern Norway. *Seismol. Soc. Amer.*, Bull., 61: 457-471.

Tryti, J. and Sellevoll, M.A., 1977. Seismic Crustal Study of the Oslo Rift. Pure and Applied Geophysics, 115: 1061-1085.

Vogel, A. and Lund, C. E., 1971. Profile section 2-3. In: A. Vogel (Editor), Deep seismic sounding in northern Europe. Swedish Natural Science Research Council, Stockholm, pp. 62-75.

[illegible]	Name Location	References	Type
A	Central Graben	[illegible]	Refrac
B	[illegible], West coast of Norway	[illegible] pers. comm., 1989	[illegible]/ Refrac
BALTIC	Baltic, Finland	Luosto et al., [illegible]	Refrac
C	Møre margin	Olafsson, [illegible]	ESP
D	Cannobe, South Norway	Cassell et al., 1983	Refrac
E1-E5	EUGENO-S, Denmark, Kattegat, SW Sweden	Eugeno-S Working Group, 1988; Lund et al., 1987	Refrac
F1-F3	Fennolora, Sweden	Clowes et al., 1987; Galson and Mueller, 1986	Refrac
G	Lappland, Sweden	Båth, 1984	Refrac
H	Trondheim-Sundsvall	Vogel and Lund, 1971	Refrac
I	Oslo-Trondheim	Kanestrøm, 1971	Refrac
J	Otta-Årsund	Mykkeltveit, 1980	Refrac
K	Flora-Åsnes	Sellevoll and Warrik, 1971	Refrac
L	Fedje-Grimstad	Sellevoll and Warrik, 1971	Refrac
LOF 1	Lofoten, Norway	Sellevoll, 1983	Refrac
LOF 2	Lofoten, Norway	Drivenes et al., 1984	Refrac
M-N	Oslo Rift	Tryti and Sellevoll, 1977	Refrac
LA-LY	Larvik-Lysekil	Egilson and Husebye, 1991	Refrac
P1-P4	NSDP84-01:04, Viking Graben-North Sea	Fichler and Hospers, 1989 Hospers and Ediriweera, 1988	Reflec
POLAR	Polar, N.Sweden-Norw.	Luosto et al., 1989	Refrac

Table 7.6.1. Page of 2.

Mapret	Name - Location	References	Type
B	Blue Norma	Avedik et al., 1984	Refrac
S	Barents Sea	Davydova et al., 1984	Refrac
SVEKA	Sveka, Finland	Grad and Luosto, 1987	Refrac
LADOGA	Ladoga, Finland/USSR	Korhonen et al., 199[illegible]	Refrac
T1-T3	Western Barents Sea	Faleide et al., 1991	ESP WRe
U1-U2	Baltic Sea-Poland	Grad et al., 1991	Refrac
Y1-Y2	Eastern Norwegian Sea	Planke et al., 1991	ESP WRe
Z1-Z6	Kola, USSR	Glaznev et al., 1989	Refrac
NAO	Norsar, Norway	Berteussen, 1977	Spec.r
COP HFS KEV KIR KJF KON KRK NUR SOD UME UPP	Copenhagen, *Denmark* Hagfors, Sweden Kevo, Finland Kiruna, Sweden Kajaani, Finland Kongsberg, Norway Kirkenes, Norway Nurmijärvi, Finland Sodankylä, Finland Umeå, Sweden Uppsala, Sweden	*Bungum et al.*, 1980	Spec.r
-	Balticum, USSR	Lubimova, 1980	Refrac
-	Siljan, Sweden	Lund et al., 1988	Reflec
-	Kattegat and S. Sweden	Kornfält and Larsson, 1987	Reflec

Table 7.6.1. Seismic profiling crustal mapping studies within Fennoscandinavia. (Refrac = refraction profiling; W.Re = wide angle reflection profiling; Spec.r. = long period seismic spectral ratio technique; ESP = expanding spread profile). (Page 2 of 2)

Profile 5		Profile 23		Profile F3(G)		Profile F3(F)	
H (km)	P-Vel (km/sec)	H (km)	P-Vel (km/sec)	H (km)	P-Vel (km/sec)	H (km)	P-Vel (km/sec)
0	2.0	0	6.2	0	6.1	0	6.0
1.5	4.5	20	6.5	24	6.5	5	6.0
5.2	5.6	32	6.8	24	6.6	5	6.2
15	6.2	32	7.2	35	6.9	20	6.5
27	6.3	45	7.2	35	7.1	20	6.6
27	6.7	45	6.8	45	7.4	41	6.9
34	7.0	50	7.4	45	8.1	41	8.1
34	8.1	50	8.0	--		--	
(1)		(2)		(3)		(4)	

Profile LOF2		Profile Sveka		Profile Baltic		Profile Ladoga	
H (km)	P-Vel (km/sec)	H (km)	P (km/sec)	H (km)	P-Vel (km/sec)	H (km)	P-Vel (km/sec)
0	6.1	0	6.0	0	6.0	0	6.0
12	6.1	30	6.5	18	6.7	12	6.0
12	6.5	30	6.8	30	6.7	12	6.2
19	6.5	40	6.8	30	7.1	30	6.5
19	7	40	7.3	42	7.2	40	6.8
23	7.1	52	7.3	42	8.1	40	8.3
23	8.4	52	6.8	50	8.2	--	
--		55	6.8	50	8.4		
--		55	7.9	-		--	
(5)		(6)		(7)		(8)	

Profile I		Profile L		Profile D		Profile LA-LY	
H (km)	P Vel (km/sec)	H (km)	P-Vel (km/sec)	H (km)	P-Vel (km/sec)	H (km)	P-Vel (km/sec)
0	6.0	0	6.3	0	5.5	0	5.6
14	6.3	17	6.3	6	6.2	5	5.6
14	6.7	17	6.4	6	6.5	5	6.3
36	6.8	33	6.8	26	6.8	13	6.3
39	7.3	33	8.1	28	7.5	13	6.8
39	8.0	--		28	8.1	31	6.8
--		--		--		31	8.1
(9)		(10)		(11)		(12)	

Table 7.6.2. Page 1 of 2.

Profile E3		Profile F2(L)		Profile F2(C)		Profile F2(B)	
H (km)	P-Vel (km/sec)	H (km)	P-Vel (km/sec)	H (km)	P-Vel (km/sec)	H (km)	P-Vel (km/sec)
0	6.1	0	5.8	0	6.1	0	6.1
16	6.4	6	6.0	20	6.2	20	6.2
24	6.5	16	6.3	20	6.7	20	6.7
30	6.7	18	6.5	35	6.7	27	6.3
33	6.9	34	7.0	3.5	8.0	33	7.0
39	7.1	43	7.4			33	8.0
39	8.1	48	7.9	--		--	
--		48	8.3	--		--	
(13)		(14)		(15)		(16)	

Profile U1		*Profile F1*		Profile E1		Profile E2	
H (km)	P-Vel (km/sec)	H (km)	P-Vel (km/sec)	H (km)	P-Vel (km/sec)	H (km)	P-Vel (km/sec)
0	2.2	0	5.2	0	4.1	0	4.0
1.5	2.5	4	5.2	10	5.9	4	5.5
2.5	5.2	4	6.0	21	6.5	8	6.0
2.5	6.0	12	6.0	21	6.7	13	6.3
19	6.[illegible]	12	6.7	31	6.8	18	6.7
31	6.9	32	6.7	31	8.0	30	6.9
42	7.2	32	8.0	--		30	8.0
42	8.2	--		--		--	
(17)		(18)		(19)		(20)	

Table 7.6.2. Tabulation of P velocity distributions presumed representative for Fennoscandinavia. The profile notation of Table 7.6.1 is retained and the corresponding part of the respective profiles for which the velocity distributions are valid are *marked* by dots in Fig. 7.6.2. The sources are not necessarily coinciding with the listings of the original profiling references in Table 7.6.1, and are as follows: Profile S: Davydova *et al* (1985); Profile Z3, F3(G), F3(F), SVEKA, BALTIC adn LADOGA: Korhonen *et al* (1990); *Profile* LOF2: *Drivenes et al* (1984); Profile F2(L): Lund (1987); Profile F1, F2(B), F2(C): Clowes *et al* (1987); Profile U1: Grad *et al* (1990); Profile E1, F2, E3: Gregersen (19[illegible]); Profile LAIY: Egilson and Husebye (1991); Profile D: Cassell *et al* (1983); Profile L, E: Kværna (1984). Note that for the two segments of the Fennolora profile F2 and F3, the letter indexing above is *from* south to north, i.e., F2(B), F2(C), F2(F), F3(F) and F3(G) — in Fig. 7.6.2 no such indexing. (Page 2 of 2)

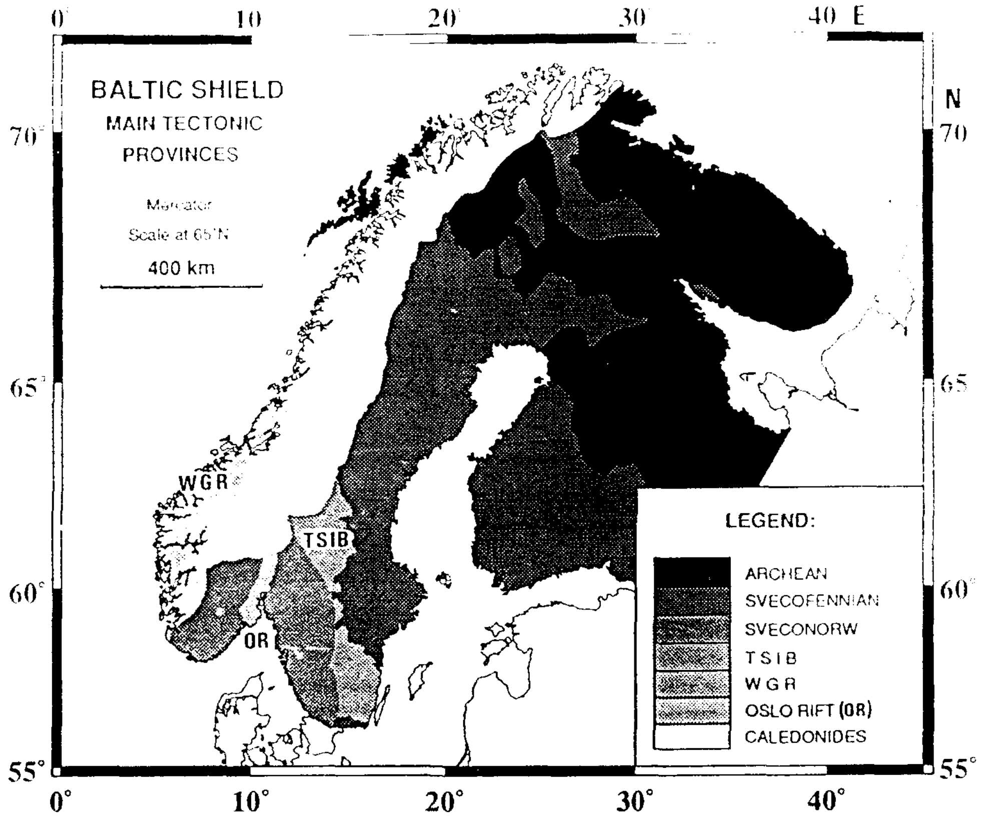

Fig. 7.6.1. Tectonic map of the Baltic Shield showing main age provinces. T.S.I.B.: Trans Scandinavian Igneous Belt. W.G.R.: Western Gneiss Region. Based on Gáal and Gorbatschev (1987).

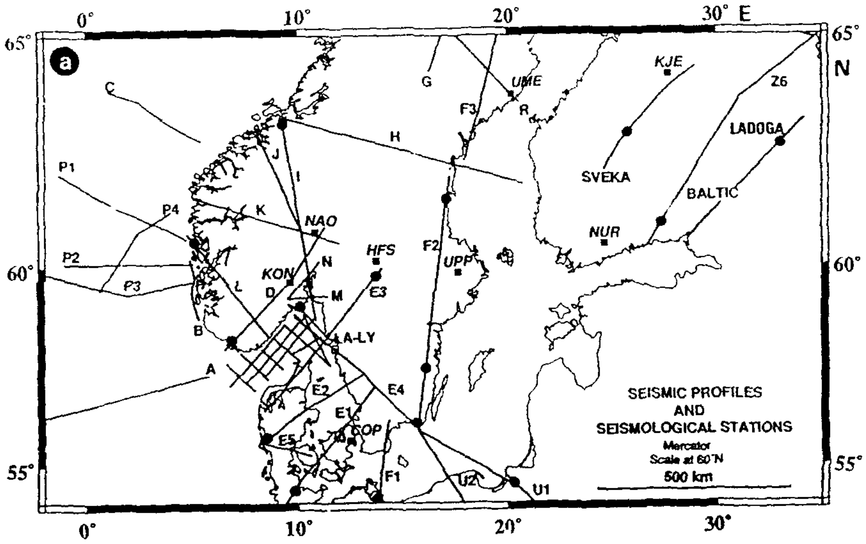

Fig. 7.6.2a. Seismic profiles and seismological stations (squares) in southern Fennoscandinavia. For references, see Table 7.6.1. The black dots mark small profiling areas for which P-velocity - crustal depth distributions are given in Table 7.6.2.

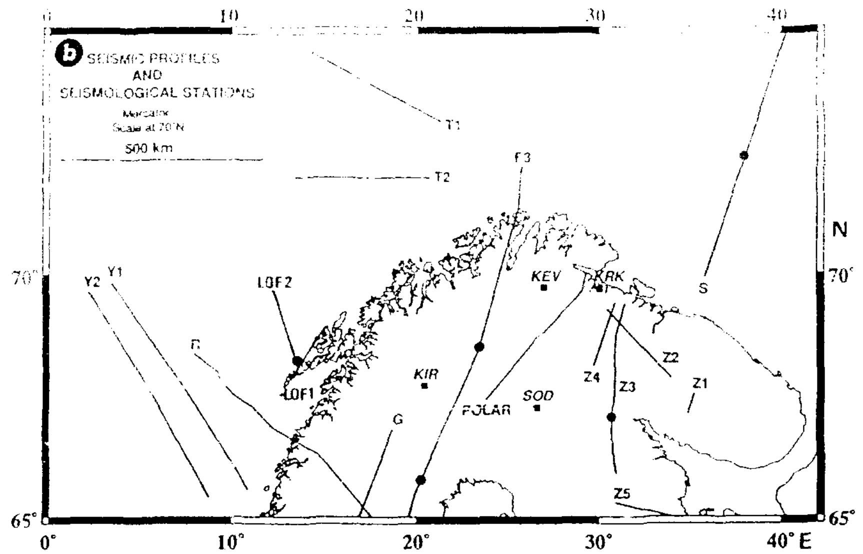

Fig. 7.6.2b. Seismic profiles and seismological stations (squares) in northern Fennoscandinavia. For references, see Table 7.6.1. The black dots mark small profiling areas for which P-velocity – crustal depth distributions are given in Table 7.6.2

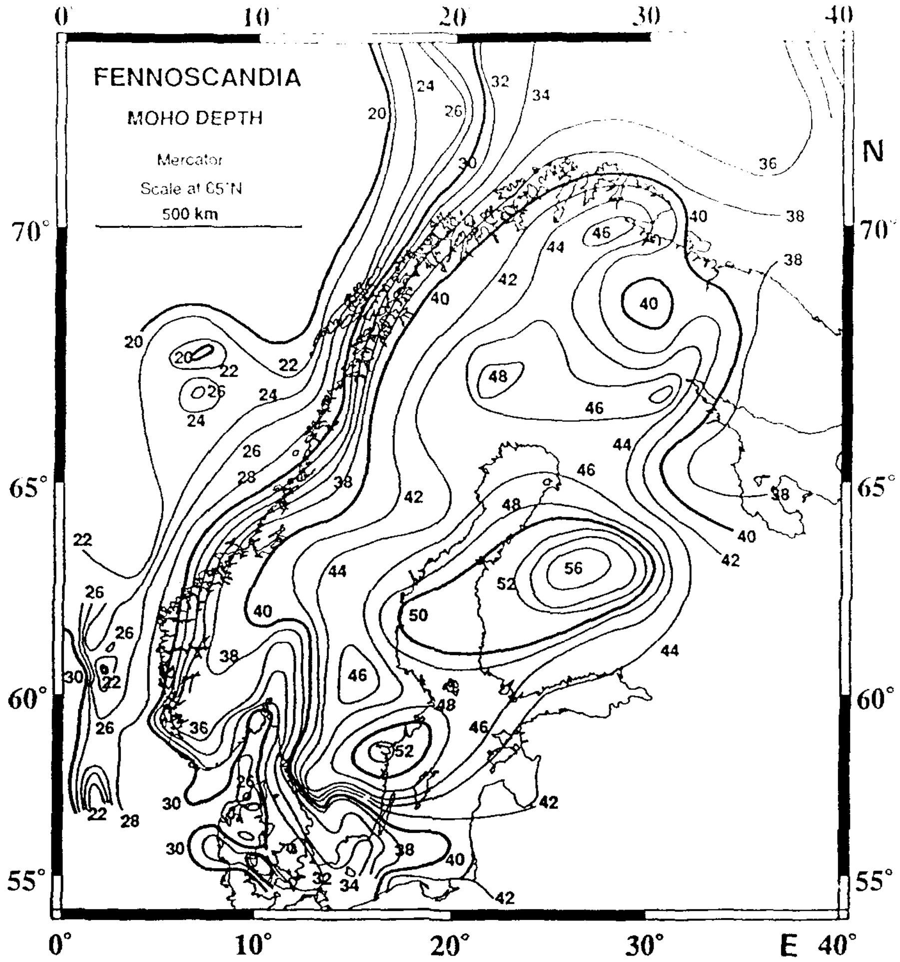

Fig. 7.6.3. Moho depth in Fennoscandinavia below sea level. A 2 km contour interval is used.

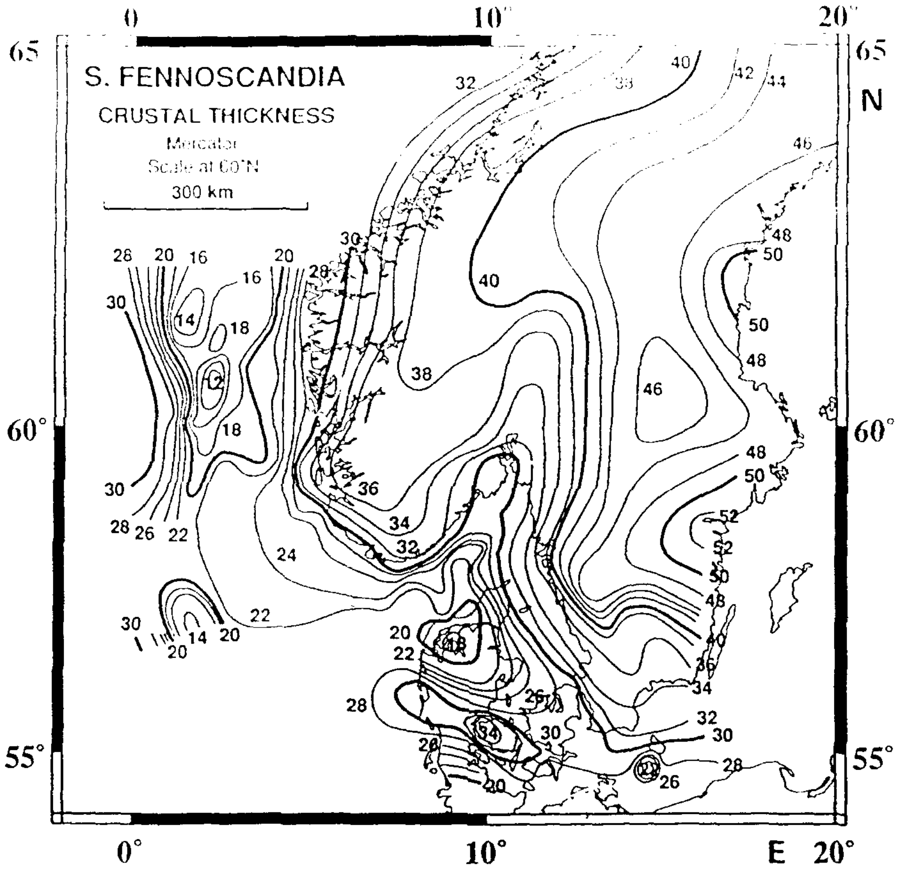

Fig. 7.6.4. Thickness of the crystalline crust in southwestern Fennoscandinavia where comprehensive sediment thickness data were available. A 2 km contour interval is used.

7.7 Initial development of generic relations for regional threshold monitoring

Introduction

In earlier reports (Kværna and Ringdal, 1990a, Kværna and Ringdal, 1990b) we have demonstrated applications of the threshold monitoring (TM) technique to regions of limited areal extent like mines and nuclear test sites. This method has proven to provide a simple and very effective tool in day-to-day monitoring of areas of particular interest. One of the basic underlying assumptions has been that each target region should be defined such that all events within the region show similar propagation characteristics. This has enabled us to get the necessary magnitude calibration factors from processing previous events with "known" magnitude, using the relation

$$\hat{b}_{i,j} = \hat{m}_j - \log(\hat{S}_{i,j}) \qquad (i = 1, \cdots, K;\ j = 1, \cdots, L) \tag{1}$$

where $\hat{b}_{i,j}$ is our estimate of the magnitude correction factor for phase i and event j, $\hat{m}_j$ is the estimate of the magnitude for event j (based on independent networks or knowledge about the explosive charge) and $\hat{S}_{i,j}$ is our estimate of the signal level at the predicted arrival time of phase i for event j. K is the number of phases considered (*there might be several stations and several phases per station*), and L is the number of events.

The magnitude correction factor to be used for phase i is then given by

$$b_i = E < \hat{b}_{i,j} > \tag{2}$$

where E denotes statistical expectation. Parameters like window lengths for signal level estimation, travel-times of the different phases, frequency filters and steering delays for array beamforming are taken from processing of the calibration events.

Extension of the TM method to regions where no calibration events are available, requires that we have generic formulas for all variables describing the processing. Such relations will make it possible to monitor new and larger geographical regions, and will in addition enable us to get a more thorough understanding on how events originating in one region influence the threshold in other regions. Applying such generic relations will of course involve a tradeoff where a wider geographical coverage is achieved at some expense with regard to optimized monitoring of limited target area. Thus it should be seen as a supplement, and not a replacement of, the target-specific threshold monitoring.

In the following we present results from a preliminary study on methods for obtaining such generic relations, with special application to the regional Fennoscandian array network.

Phases to consider and their travel-times

A standard method of estimating the magnitude of local and regional events is based on a measurement of the amplitude of the maximum peak in the S-wavetrain (Richter, 1935; Båth, 1981; Alsaker *et al.* 1990). The NORSAR recordings of Fig. 7.6.1 show that the position of the *maximum* peak vary strongly from one region *to another*. Events originating within the Fennoscandian Shield (event 1 and event 5) will usually have the maximum energy associated with the L_g phase (group velocity 3.5 km/s). On the other hand, events with propagation paths crossing the North Sea graben structures (event 4) or events originating in oceanic regions (event 6) will have the their *maximum energy* associated with the S_n arrival (group velocity about 4.5 km/s). In addition, Kværna and Mykkeltveit (1985) have shown that the regions in which the L_g arrival is the dominant phase are dependent on the frequencies considered. I.e., the S_n phase becomes more dominant as the frequencies increase.

The TM method require that the travel-times of the considered phases are given á priori for all target areas. For optimum performance, one phase should be associated with the energy maximum of the wavetrain. From the complexities described above, it is obvious that we cannot obtain generic formulas for the travel-time of this amplitude peak without extensive data analysis and regional mapping. For NORESS recordings, we have from the study of Kværna and Mykkeltveit (1985) an idea of the geographical regions for which S_n or L_g is the dominant phase, but similar information is currently not available for other seismic arrays and single stations.

From several years of experience with seismic data from local and regional events, we know that the energy associated with the P-phase often exhibits its amplitude maximum several seconds after the initial P onset. This feature is partly illustrated in Fig. 7.6.1. For optimum TM computations, it is also beneficial to make use of the phases for which the travel-time difference is as large as possible. We will therefore in the following proceed with the first arriving P-phase (P_n or P_g) and the L_g phase in the TM analysis, using the standard Fennoscandian travel-time tables as the generic formulas. To compensate for the uncertainties in the positioning of the maximum amplitudes of the wavetrain, we will introduce so-called time tolerances. This concept will be outlined in one of the following sections.

Frequency bands

To ensure optimum performance of the TM method, we introduce bandpass filtering of the data in the band where the considered phase is expected to have the largest SNR. These bands are however difficult to predict as large variations occur regarding attenuation properties of the different propagation paths, source spectra and noise conditions.

In the context of monitoring regions within local and regional distances, the work of Sereno (1991) gives an excellent picture of the average properties of regional phase attenuation, source spectral scaling and backgound noise conditions. From an assumption on the event magnitude M_L and the epicentral distance, we could use his results to predict the best SNR frequency band of a phase.

We will, however, in this preliminary study base our selection of filter bands on statistics from the detection processing of the regional arrays NORESS and ARCESS. The IAS/IMS system (Bache *et al*, 1990) is used for routine analysis of data from these arrays, and all information concerning the detected seismic phases are stored in a large data base. The statistics on the dominant frequency, i.e., the frequency with the largest SNR, give us an idea on how the optimum frequency band varies as a function of epicentral distance. The statistics cover both NORESS and ARCESS data from the time interval 1990/01/23 to 1991/04/29.

The P_n (P_g) results are given in Table 7.6.1, and show large variability, especially at distances below 500 km. At larger distances the frequency band 3 to 5 Hz cover the vast majority of the occurrences. To retain simplicity in this preliminary study, we have chosen to use the 3 to 5 Hz frequency band for the first arriving P-phase at all distances. For larger distances this is also in general agreement with predictions based on the results of Sereno (1991).

The L_g results given in Table 7.6.2 also show large variability at distances below 500 km. It should be noted that the dominant frequencies for L_g are relative to the preceding S_n coda, and not relative to backgound noise conditions, as was the situation for P_n. We want optimum performance relative to backgound noise conditions, so the L_g statistics should be interpreted with some caution. On the other hand, numerous studies of L_g propagation characteristics (a.o., Baumgardt, 1990; Sereno, 1991; Kværna and Mykkeltveit, 1986) confirm the "low-frequency" nature of L_g at distances above 500 km. Also in this case we will make a compromise and use the 1.5 to 3.5 Hz frequency band for L_g at all distances. This will give close to optimum performance for L_g at longer distances, which is considered the most important for the overall threshold monitoring capability.

Grid defintions and time tolerances

Threshold monitoring of a larger geographical region implies that each target point have to represent a finite surrounding area. If we divide the region to be monitored into a grid, as shown in Fig. 7.6.2, the area surrounding the target point is given by a rectangle as indicated on the same figure.

The travel-time of the considered phase is given by T_Δ, where Δ denote the distance from the station A to the target point M. Let T_{Δ_1} be the minimum travel-time from any point within the rectangle, e.g., $M1$, and let T_{Δ_2} be the maximum travel-time from any point within the rectangle, e.g., $M2$.

If the density of the grid is such that the magnitude calibration factors do *not* vary significantly within the rectangle surrounding each grid point (see Fig. 7.6.2), we use the following procedure for monitoring:

Let $S(t)$ denote the signal level observed at time t. Instead of measuring the signal level at time T_Δ as predicted from the position of the target point, we introduce time tolerances such that

$$S(T_\Delta) = \max(S(t)) \tag{3}$$

where $t \in [T_{\Delta_1}, T_{\Delta_2}]$. Thereby the estimated signal level can be said to represent an upper limit for any sources within the rectangle. The time tolerances can also be used to compensate for uncertainties in the position of the maximum amplitude of the wavetrain, but we note that the resolution of the TM method will be deteriorated if the time tolerances becomes too large.

STA lengths

In determining the optimum STA window length, we need to take three factors into account:

- Average STA during noise conditions.
- Variability of STA during noise conditions.
- Maximum STA value when the signal occurs.

In practice, it is desirable to have a signal-to-noise ratio as large as possible, measured relative to multiples of the noise standard deviation. Our approach toward solving this problem is outlined in the following.

In this initial study, we have chosen to sample the data by 1 second short-term-averages (STA) sampled at 1 second intervals. This decision is based on a compromise between data resolution and managable data volumes.

Intuitively, an instantaneous phase with short duration (e.g., P_n) should be represented by an STA averaged of a short time window, whereas the amplitude level of an emergent phase with long duration (e.g., L_g) should be represented by a longer time window. The initial data sampling (1 sec. STA values), allows us to use any integer multiple of 1 second as window lengths for the considered phases.

Let $\bar{A}(\Delta t)$ denote the average of the $\log(STA)$ under noise conditions, and let $\sigma(\Delta t)$ be the associated standard deviation. Δt refers to a particular STA

window length. Let $y(\Delta t)$ be what we consider the "worst case" noise situation given by

$$y(\Delta t) = \overline{A}(\Delta t) + x \cdot \sigma(\Delta t) \qquad (4)$$

Let $S(\Delta t)$ be the maximum of $\log(STA)$ for the signal. We introduce the term "noise damping", $z(\Delta t)$ by the formula:

$$z(\Delta t) = S(\Delta t) - y(\Delta t) \qquad (5)$$

The "noise damping" is then a measure of the "effective" signal-to-noise ratio, i.e., how much the signal exceeds the "worst case" noise situation. The optimum STA window length, Δt, is the argument for which the noise damping $z(\Delta t)$ attains its maximum.

To assess the optimum STA window lengths for P_n and L_g and to reveal any distance dependency, we computed maximum signal STA values with different window lengths for events at various epicentral distances.

Using the z-component of the center instrument of NORESS, ARCESS or FINESA, the P_n data were filtered in the 3-5 Hz passband. The starting point of the STA windows were at the predicted arrival time of the P-phase, and to accomodate for uncertainties in the positioning of the amplitude maximum of the P-wavetrain, we introduced a time tolerance of ± 5 seconds. Information on the P_n data are given in Table 3. The interpolated curves of Fig. 7.6.3 give $S(\Delta t)$ for several events for a set of different window lenghts. For this study, the absolute scale of $S(\Delta t)$ is without any significance, so for display purposes, an offset was added to each of the curves. As expected, the shortest window length (1 second) gave the largest $S(\Delta t)$, but there is a distinct difference in the slopes for events above and below 300 km epicentral distance. We will therefore in the following proceed with two average signal curves, one for all events within 300 km of the stations, and another for for the rest.

The noise characteristics for the 3-5 Hz frequency band was obtained from analysis of six 30 minute noise intervals. Information on the noise intervals are given in Table 7.6.4. For consistency with the P_n analysis, a time tolerance of 5 seconds was used. Values of $\overline{A}(\Delta t)$ for all noise samples are given in Fig. 7.6.4, together with the average over all six samples. Similar curves for $\sigma(\Delta t)$ are given in Fig. 7.6.5.

Now turning to the noise damping of the P_n phase for events within 300 km of the station. Fig. 7.6.6 give the noise damping $z(\Delta t)$ for a set of confidence levels $x \cdot \sigma(\Delta t)$ ($x = 1, 2, \ldots, 5$), and show that for any choice of confidence level, a 1 second window length will do the best. For events more distant than 300 km from the station, we get the same conclusion as inferred from the results of Fig. 7.6.7. It is clearly possible that a shorter time window than 1 second might further improve the P_n phase, but we have not so far investigated this possibility.

The definition of the "worst case" situation is somewhat arbitrary, but seen in conjuction with the total number of samples per day (86400), the 3σ level is a resonable practical compromise. This means that 99.9% of the data will be below this limit. We also see that for all confidence levels up to 5σ, the conclusion on the best window length for P_n will remain the same.

Similar analysis was conducted for the L_g phase. The data were bandpass filtered between 1.5 and 3.5 Hz, and the center point of the signal analysis window was set at the expected amplitude maximum of the L_g phase (i.e., at a group velocity of 3.5 km/s). To accomodate for uncertainties in the positioning of the amplitude maximum, we used a time tolerance of ± 5 seconds. Details on the L_g phases are given in Table 7.6.3, and the values of $S(\Delta t)$ for events at various distances are shown in Fig. 7.6.8. Also in this case events above and below 300 km show different slopes, and we will in the following proceed with the averages for these two populations.

The data intervals of Table 7.6.4 were also used to assess the noise characteristics of the 1.5-3.5 Hz frequency band. The estimated curves for $\overline{A}(\Delta t)$ are given in Fig. 7.6.9, and the corresponding σ-values are given in Fig. 7.6.10.

The noise damping, computed from "an average" L_g signal within 300 km epicentral distance and from "average" noise conditions, is given in Fig. 7.6.11. When considering the levels 3σ and higher, all window lengths of 5 seconds or less seem to do almost equally well. The corresponding curves for events exceeding 300 km epicentral distance are shown in Fig. 7.6.12. They indicate that an STA window length of 10 seconds will be close to optimum for all confidence levels up to 5σ.

Our preliminary assessment is that a 5 second window length should be used for L_g phases originating from events within 300 km epicentral distance, whereas a 10 second window should be used for events exceeding 300 km.

An increase in the time tolerances will increase the values of $\overline{A}(\Delta t)$, whereas $\sigma(\Delta t)$ will decrease. Fig. 7.6.13 illustrates this for a noise sample in the 1.5-3.5 Hz frequency band using a 10 second STA window length. We see that the value of $\overline{A}(\Delta t) + 3 \cdot \sigma(\Delta t)$ remain almost constant for any time tolerance, implying that the results we obtained with a time tolerance of $\pm$ 5 seconds, also seem to be valid for other choices of time tolerances.

Steering delays and effects of mis-steering

One of the main features of seismic arrays is the ability to improve the signal-to-noise ratio (SNR) by beamforming. Instead of computing the STA's from bandpass filtered single component sensors, we steer beams towards each target point, filter them in the appropriate frequency bands, and finally compute the

STA values. In this way, we significantly reduce the noise levels (for uncorrelated noise, by a factor of $\sqrt{N}$, where N is the number of sensors). Kværna (1989) have estimated the SNR gain, the noise suppression and the signal loss for P-phases, using data from the NORESS array. In the 3-5 Hz frequency band, appropriate for P_n, it was found that an SNR gain of 12 dB could be achieved with optimum plane-wave steering delays. It was also found that even though the array was steered with optimum steering parameters, the signal amplitudes were reduced by the beamforming, due to lack of coherency.

As shown in Fig. 7.6.14, the steering delays (apparent velocity and azimuth) appropriate for the target point, will not be optimum for the rest of the points within the surrounding rectangle. We will in the following consider the "worst case" situation, and account for the maximum signal loss for any points within the rectangle. If we assume that the expected slownesses of all points within the rectangle is identical, which is resonable for P_n and L_g, the mis-steering will primarily be caused by deviating azimuths, as shown in Fig. 7.6.14.

Fig. 7.6.15 illustrate the loss of the maximum STA as a function of mis-steering, for NORESS and ARCESS P-beams filtered between 3.0 and 5.0 Hz. Information on the events are given in Table 7.6.5. The apparent velocity of each phase is taken from broad-band f-k analysis, the STA length is one second, and the time tolerance is ± 5 seconds. The mis-steering is introduced as azimuth deviations normalized relative to an apparent velocity of 8.0 km/s. Let θ_n denote the azimuth deviation relative to an apparent velocity of 8.0 km/s and let v_p denote the apparent velocity of the incoming wave. If θ_{obs} is the azimuth deviation relative to v_p, we get the following relation:

$$\theta_{obs} = 2 \arcsin\left(\frac{v_p}{8.0} \sin \frac{\theta_n}{2} \right) \tag{6}$$

Fig. 7.6.15 shows that the signal loss is about 4 dB for a normalized azimuth mis-steering of 20 degrees. I.e., if our grid is constructed in such a way that the maximum allowed azimuth deviation is within 20 degrees (see Fig. 7.6.14), the P_n signal loss at NORESS and ARCESS will be within 4 dB. For arrays with smaller radius (e.g., FINESA), the signal loss will be less.

We have not so far investigated the signal loss due to azimuth mis-steering of the L_g phases. The apparent velocity is lower than for P_n, which indicate higher signal loss, but the lower frequency filter used for L_g (1.5-3.5 Hz versus 3.0-5.0 Hz) works in the opposite direction.

Due to the large regional variations in propagation characteristics, it is usually difficult to predict the apparent velocities, given the coordinates of the target point. Table 7.6.6 gives the estimated apparent velocity of the first arriving P-phase (P_g or P_n) as a function of epicentral distance. These statistics are taken from the IAS data base, and contain both NORESS and ARCESS observations.

Similar statistics on the L_g phase are given in Table 7.6.7. Both tables show a large scatter, illustrating the difficulty in predicting the apparent velocity given the epicentral distance. Another complicating factor is the dispersion of the L_g wave train, implying that the estimates of apparent velocity will be a function of both the frequency band and the positioning of the analysis window.

We have initially not attempted to do any systematic regionalization of the apparent velocity observations. In the mean time, we use an apparent velocity of 8.0 km/s when forming P_n beams steered towards target points more distant than 250 km. At closer distances, we use 6.5 km/s. For L_g beams, an apparent velocity of 4.3 km/s is assumed for target points at all distances. These parameters are currently used for all arrays (NORESS, ARCESS and FINESA).

The signal loss will also be dependent on the array geometry, but this has so far not been studied in connection with mis-steering of the beams. A natural next step will be to evaluate all the effects of beamforming, array geometries and mis-steering in the context of *threshold monitoring*. But in this preliminary study, the signal loss is accounted for by adding a constant term of 0.2 (4 dB) to the observed log(STA) values for P_n (P_g), and 0.3 (6 dB) to the log(STA) values for L_g.

Magnitude correction factors and variance

We are now in the position to compute the generic relations for the magnitude correction factors, as the other TM variables have been preliminary assessed. Alsaker *et al* (1990), collected a large event data base when estimating formulas for a M_L scale in Norway, and they subsequently computed network averaged M_L estimates for all events. We will in the following use their data base and magnitudes as a basis for computing the generic relations for the magnitude correction factors.

The data base contains observations from 21 different stations (see Fig. 7.6.16), most of which with different instrument response functions. In order to compare the STA values at the respective stations, we need to find a common basis for comparison. As the individual amplitude response functions show only small variations within the relatively narrow passbands considered for P_n and L_g, we can in an approximate way transfer the STA values into units of nm or nm/s simply by multiplying by the displacement or velocity response at the center frequency of the passband, such that

$$STA_{nm} \approx STA_{qu} \cdot |A_d(\omega_c)| \tag{7}$$

where STA_{qu} is the observed STA in quantum units, $|A_d|$ is the displacement amplitude response, and the center frequency $\omega_c = \sqrt{\omega_1 \omega_2}$ where ω_1 and ω_2 are the low and high cutoffs of the passband. A similar type of equation can be used if we instead convert the STA values to ground velocity.

In accordance with earlier regression analysis of magnitude relations (Alsaker et al., 1990), we choose the following parameterizition:

$$M_i = \log STA_i + C1 + C2 \cdot \log \Delta_i + C3 \cdot \Delta_i \qquad (i = 1, \cdots, N) \qquad (8)$$

where N is the number of observations, M_i is the network magnitude of the event, STA_i is the instrument corrected STA_{num} and Δ_i is the epicentral distance.

The data base of Alsaker *et al* (1990) contains 741 observations distributed among 195 events (see Fig. 7.6.17). To ensure good SNR in the P_n and L_g frequency bands, all data were visually inspected. After rejecting data with insufficient SNR or with other data quality problems, 453 observations remained for P_n analysis and 528 for L_g. The STA values were computed using the recipes outlined in the preceding sections, and the results from the regression analyses are given in Table 7.6.8. Estimates of the standard deviation are also given, and show a σ value of 0.19 for L_g. The P_n data show a much larger scatter, and we obtained a σ value of 0.36. Compared to site specific monitoring, these σ estimates are significantly higher, as the typical σ values for site specifc monitoring are less than 0.2 for P_n, and less than 0.1 for L_g. If different filters, travel-time models or other parameters were to be used in the TM analysis, new magnitude correction factors would have to be obtained from reanalysis of the calibration events, using the new recipies.

As the TM method computes upper magnitude limits from a cumulative distribution with a given mean and standard deviation, we have the option of balancing the term $C1$ against the standard deviation σ. This implies that we can reduce σ if $C1$ is increased. Our philosophy behind the TM computations has been to make conservative estimates of the upper magnitude limits, in order not to overestimate the capabilities. In this way, we can add a constant term to $C1$ or increase σ if some of the attenuation relations or other underlying parameter estimates of the TM method are considered particularly uncertain.

Discussion

The results presented in this study give us a means of testing the concept of threshold monitoring applied to large geographical regions. It enables us to extend the original "site-specific" threshold monitoring to what we might call "regional threshold monitoring". Using these initial generic relations, Ringdal and Kværna (1991, this issue) have already shown how colour computer displays can be applied to interpret the results from TM analysis. They also indicate new applications of the regional threshold monitoring concept which should be investigated in parallel with improvements of the generic relations.

The data base used for obtaining the magnitude calibration factors consists of events from Fennoscandia and adjacent areas, making the results representative for this kind of geological environment. If we want to extend the TM analysis to other types of geological regions, exhibiting different wave propagations characteristics, new generic relations have to be found. Another uncertain factor, concerning the current magnitude calibration factors, is the effect of using this particular data base for regression, as the same data base was used for obtaining the M_L scale for Norway (Alsaker *et al*, 1990).

The effect of signal loss due to mis-steering of the arrays should be more thoroughly investigated. The signal loss is a function of several variables, among others: phase type, signal coherency, frequency, degree of mis-steering and array geometry. This also implies that when new arrays, with different array geometries, are introduced in the TM computations, new models for signal loss have to be assessed.

We are also investigating the possibility of using several filter bands when representing the amplitude level of a phase. The current model of a fixed frequency band for P_n and L_g is clearly not optimal. But in order to make such improvements, new generic relations have to be obtained for a set of different filter bands.

Regionalization of the travel-time models for the maximum amplitude peaks in the wavetrain will optimize the TM computations. The data base of Alsaker *et al* (1990) contains several recordings at NORESS and ARCESS which can be used to regionalize the travel-time models at these two stations. But for the other stations currently providing digital data to NORSAR (FINESA, GERESS, Ksiaz and Stary Folwark), a new event data base will have to be collected. If independent network averaged magnitudes can be provided for these events, the generic relations for magnitude calibration can also be improved.

In conclusion, the key for further improvements of the generic relations for regional theshold monitoring is easy access to a large event data base including recordings at all relevant stations. Network locations and network averaged magnitudes should be avaliable for all events. With this at hand, we have the possibility to investigate regional behaviour and the effect of different parameter settings, in order to further improve the performance of regional threshold monitoring.

Tormod Kværna

References

Alsaker, A., L.B. Kvamme, R.A. Hansen, A. Dahle and H. Bungum (1991): The M_L scale in Norway. *Bull. Seism. Soc. Am.* Vol. 81, No. 2, In press.

Bache, T., S.R. Bratt, J. Wang, R.M. Fung, C. Kobryn and J.W. Given (1990). The Intelligent Monitoring System, *Bull. Seism. Soc. Am.* 80, Part B, 1833-1851.

Baumgardt, D.R., (1990). Investigation of Teleseismic L_g Blockage and Scattering Using Regional Arrays, *Bull. Seism. Soc. Am.* 80, Part B, 2261-2281.

Båth, M. (1981): Local magnitude — recent research and current trends, *Earth-Science Rev.* 17, 315-398.

Kværna, T. and S. Mykkeltveit (1985): Propagation characteristics of regional phases recorded at NORSAR, *Semiannual Tech. Summary, 1 Apr - 30 Sep 1985*, NORSAR Sci. Rep. 1-85/86, NORSAR, Kjeller, Norway.

Kværna, T. and F. Ringdal (1990a): Application of the threshold monitoring method. *Semiannual Tech. Summary, 1 Oct 1989 - 31 Mar 1990*, NORSAR Sci. Rep. 2-89/90, NORSAR, Kjeller, Norway.

Kværna, T. and F. Ringdal (1990b): Continuous threshold monitoring of the Novaya Zemlya test site, *Semiannual Tech. Summary 1 Apr - 30 Sep 1990*, NORSAR Sci. Rep. 1-90/91, NORSAR, Kjeller, Norway.

Richter, C.F. (1935): An instrumental earthquake magnitude scale, *Bull. Seism. Soc. Am.* 25, 1-32.

Ringdal, F. and T. Kværna (1989): A multi channel processing approach to real-time network detection, phase association, and threshold monitoring. *Bull. Seism. Soc. Am.* 79, 1927-1940.

Ringdal, F. and T. Kværna (1991): Continuous threshold monitoring using "regional thresholds displays", This volume.

Sereno, T.J., (1991): Simulation of the detection and location capability of regional seismic networks in the Soviet Union, *Final Report, 1 Jan 1989 - 31 Dec 1990, SAIC-91/1061* Sci. Appl. Int. Corp., San Diego, Calif., USA.

	0-250	250-500	500-750	750-1000	1000-1250	1250-1500	1500-1750	1750-2000	Total
1.0-2.0Hz	2	5	0	18	4	5	1	1	36
2.0-3.0Hz	153	264	24	88	94	59	10	4	696
3.0-4.0Hz	245	922	77	224	97	131	21	7	1724
4.0-5.0Hz	562	1991	160	243	245	100	13	3	3317
5.0-6.0Hz	351	670	61	85	93	13	1	1	1275
6.0-7.0Hz	513	523	74	98	62	5	1	1	1277
7.0-8.0Hz	183	121	27	21	7	0	0	0	359
8.0-9.0Hz	367	180	45	29	16	2	0	0	639
9.0-10.0Hz	284	179	36	31	9	1	1	0	541
Total	2660	4855	504	837	627	316	48	17	9864

Table 7.7.1. This table gives an overview of the frequencies with the highest SNR for the first arriving P-phase (P_n or P_g). Each element of this table gives the number of observations of the dominant frequency for a given frequency and distance range. The data are taken from routine detection processing of the IAS system, and the statistics cover both NORESS and ARCESS data from the time interval 1990/01/23 to 1991/01/29. All events were below M_L 3.0. The frequency band 3-5 Hz found suitable for TM analysis of P_n or P_g data is outlined by two horizontal lines.

	0-250	250-500	500-750	750-1000	1000-1250	1250-1500	1500-1750	1750-2000	Total
0.5-1.5Hz	34	22	9	91	26	34	0	0	216
1.5-2.5Hz	105	516	122	340	148	24	2	0	1257
2.5-3.5Hz	327	1595	162	166	31	8	1	0	2290
3.5-4.5Hz	671	1426	32	13	11	3	0	0	2156
4.5-5.5Hz	733	738	11	4	6	2	0	0	1494
5.5-6.5Hz	154	116	0	0	2	0	0	0	272
6.5-7.5Hz	324	150	4	0	3	0	0	0	481
7.5-8.5Hz	106	25	0	1	0	0	0	0	132
8.5-9.5Hz	148	21	3	0	0	0	0	0	172
9.5-10.5Hz	50	20	1	0	0	0	0	0	71
Total	2652	4629	344	615	227	71	3	0	8541

Table 7.7.2. Same as Table 7.7.1, but for the L_g phase. The frequency band 1.5-3.5Hz found suitable for TM analysis of L_g data is outlined by two horizontal lines.

Origin time	Lat.	Long.	Distance	M_L	Station	P_n data	L_g data
1990-101:11.51.55.4	62.8	27.6	170.8	-	FINESA	yes	yes
1990-101:13.46.07.0	60.9	29.3	183.8	-	FINESA	yes	yes
1989-167:11.23.26.0	69.4	30.6	200.0	3.0	ARCESS	yes	yes
1989-076:11.48.53.0	69.4	30.6	200.0	2.9	ARCESS	yes	yes
1990-101:10.21.21.0	59.5	25.0	224.8	-	FINESA	yes	yes
1989-033:18.28.55.0	67.1	20.6	338.5	2.5	ARCESS	yes	yes
1989-059:18.36.45.0	67.1	20.6	338.5	2.5	ARCESS	yes	yes
1989-105:08.50.53.0	68.1	33.2	348.9	2.7	ARCESS	yes	yes
1989-133:08:18.49.0	68.1	33.2	348.9	2.7	ARCESS	yes	yes
1988-258:08.59.58.0	64.7	30.7	584.0	2.9	ARCESS	yes	yes
1988-141:09.54.24.0	59.5	25.0	760.0	2.7	NORESS	no	yes
1989-051:13.19.57.0	59.5	25.0	760.0	2.5	NORESS	no	yes
1989-108:13.41.15.0	59.5	26.5	841.0	2.8	NORESS	no	yes
1988-075:11.52.22.0	61.9	30.6	882.2	2.8	ARCESS	yes	yes
1990-103:10.18.55.0	59.2	28.1	937.0	3.1	NORESS	yes	no
1989-005:10.09.07.0	61.9	30.6	1024.3	2.5	NORESS	no	yes
1988-258:08.59.58.0	64.7	30.7	1069.4	2.9	NORESS	no	yes
1990-103:10.28.41.0	64.6	31.2	1093.7	3.0	NORESS	yes	no
1989-090:12.16.17.0	59.5	26.5	1119.8	3.0	ARCESS	no	yes
1990-103:08.37.08.0	67.6	33.5	1302.7	2.8	NORESS	yes	no
1989-167:11.23.26.0	69.4	30.6	1307.3	3.0	NORESS	no	yes
1989-168:08.59.23.0	68.1	33.2	1314.3	2.9	NORESS	no	yes

Table 7.7.3. Information on the events used for computation of maximum signal amplitudes, denoted $S(\Delta t)$.

Start time	Station
1990-096:22.50.00	NORESS
1990-096:23.00.00	ARCESS
1990-097:14.30.00	NORESS
1990-097:14.30.00	ARCESS
1990-099:09.00.00	NORESS
1990-099:09.00.00	ARCESS

Table 7.7.4. Start times of noise intervals used for assessing average noise characteristics. The length of all intervals were 30 minutes

Origin time	Lat.	Long.	Station	Arrival time	Azimuth	App. vel.	SNR
1991-119:11.25.26.0	56.2	11.5	NORESS	1991-119:11.26.35.9	185.2	8.8	58.8
1991-120:03.40.34.0	51.4	16.2	NORESS	1991-120:03.42.53.4	156.9	8.6	33.0
1991-120:09.19.37.0	67.9	34.3	ARCESS	1991-120:09.20.35.1	120.4	7.8	128.4
1991-120:11.59.23.0	64.6	32.0	ARCESS	1991-120:12.00.45.3	154.3	8.7	54.1
1991 120:12.34.46.0	69.4	31.0	ARCESS	1991-120:12.35.19.7	94.4	7.7	283.4

Table 7.7.5. List events used for the preliminary assessment of signal loss due to mis-steering of the P-beams. The event locations are the automatic network solutions from the generalized beamforming method, see Ringdal and Kværna (1989).

	0-250	250-500	500-750	750-1000	1000-1250	1250-1500	1500-1750	1750-2000	Total
6.0-6.5km/s	194	56	2	2	1	2	0	0	257
6.5-7.0km/s	808	485	8	3	2	2	0	0	1308
7.0-7.5km/s	599	1487	28	27	7	13	0	0	2161
7.5-8.0km/s	482	1479	61	77	62	33	11	1	2206
8.0-8.5km/s	372	664	107	86	171	69	14	4	1487
8.5-9.0km/s	140	380	111	122	158	79	10	1	1001
9.0-9.5km/s	32	181	71	107	78	61	4	1	535
9.5-10.0km/s	13	76	54	99	56	27	4	4	333
10.0-10.0km/s	6	17	24	108	24	12	1	2	194
10.5-11.0km/s	6	10	16	95	32	7	2	0	168
11.0-11.0km/s	3	6	18	47	13	2	1	0	90
11.5-12.0km/s	2	6	7	23	8	1	0	2	49
Total	2657	4847	507	796	612	308	47	15	9789

Table 7.7.6. This table give an overview of the estimated apparent velocity of the first arriving P-phase (P_n or P_g). Each element of this table, give the number of observations of the apparent velocity for a given apparent velocity and distance range. The data are taken from routine detection processing of the IAS system, and the statistics cover both NORESS and ARCESS data from the time interval 1990/01/23 to 1991/04/29. All events were below M_L 3.0.

	0-250	250-500	500-750	750-1000	1000-1250	1250-1500	1500-1750	1750-2000	Total
2.5-2.8km/s	0	6	0	0	1	1	0	0	8
2.8-3.1km/s	52	108	18	21	31	5	1	0	236
3.1-3.4km/s	41	446	34	39	59	5	0	0	624
3.4-3.7km/s	154	358	45	66	35	4	0	0	662
3.7-4.0km/s	616	832	83	168	40	20	1	0	1760
4.0-4.3km/s	913	1335	80	211	25	20	0	0	2584
4.3-4.7km/s	480	883	45	85	20	9	1	0	1523
4.7-5.0km/s	208	434	16	20	8	4	0	0	690
5.0-5.3km/s	112	165	10	4	4	2	0	0	297
5.3-5.5km/s	58	36	5	0	2	0	0	0	101
Total	2634	4603	336	614	225	70	3	0	8485

Table 7.7.7. Same as Table 7.7.6, but for the L_g phase.

Phase	$C1$	$C2$	$C3$	σ	nobs
P_n, P_g	-1.5737	1.4236	0.6819E-03	0.355	453
L_g	-0.9537	0.8292	1.3188E-03	0.192	528

Table 7.7.8. Results from regression analysis of the data used by Alsaker *et al* (1990). The regression coefficients and the σ values for P_n (P_g) and L_g were obtained from processing the data with the TM recipies outlined in the preceding sections.

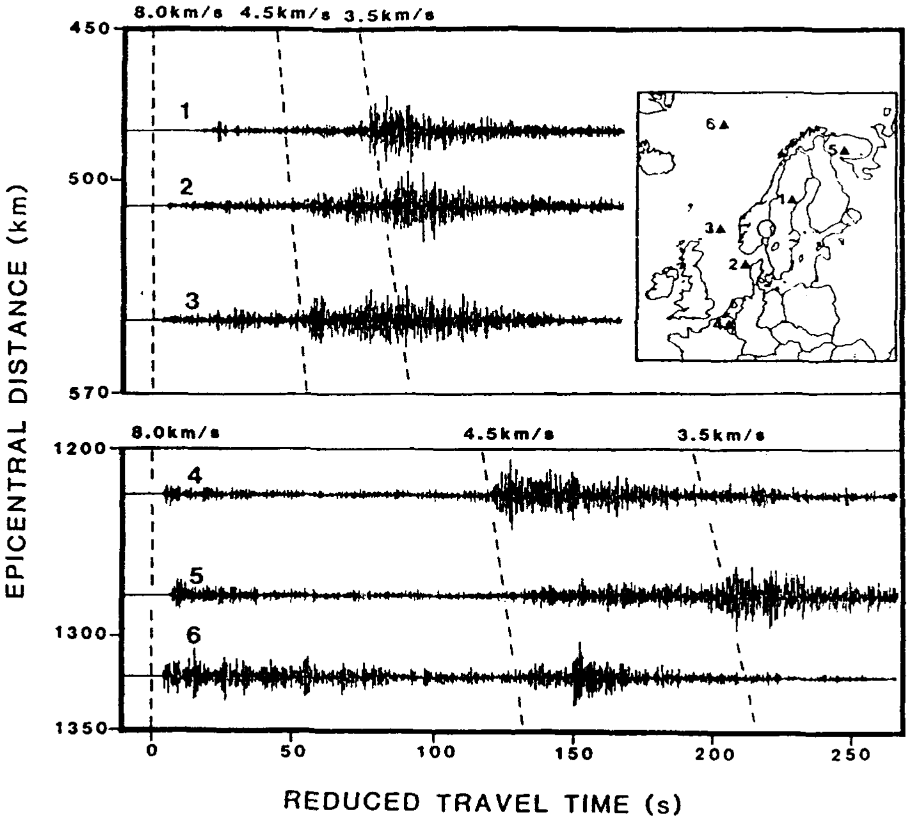

Fig. 7.7.1. Illustration of variation of relative importance of the phases S_n and L_g. The standard group velocities of 4.5 and 3.5 km/s, commonly assigned to S_n and L_g, respectively, are marked by dashed lines. The upper three traces cover the distance interval 480-550 km, while the three lower traces correspond to epicentral distances in the range 1225-1320 km. The location of the NORSAR array is denoted by a ring on the map, and the traces are from the NORSAR seismometer 02B01. The data are bandpass filtered 1 to 5 Hz. The reduction velocity is 8.0 km/sec.

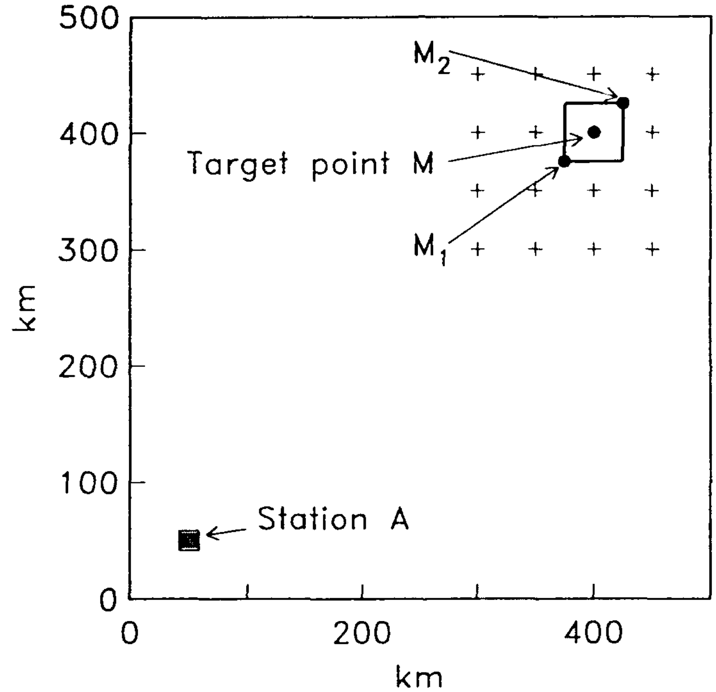

Fig. 7.7.2. This figure illustrates the necessity of using time tolerances. The plus signs indicate target points, and a rectangle surrounding one of the target points (M) is also given. The point within the rectangle with the minimum travel-time is denoted M_1, whereas the point with the maximum travel-time is denoted M_2.

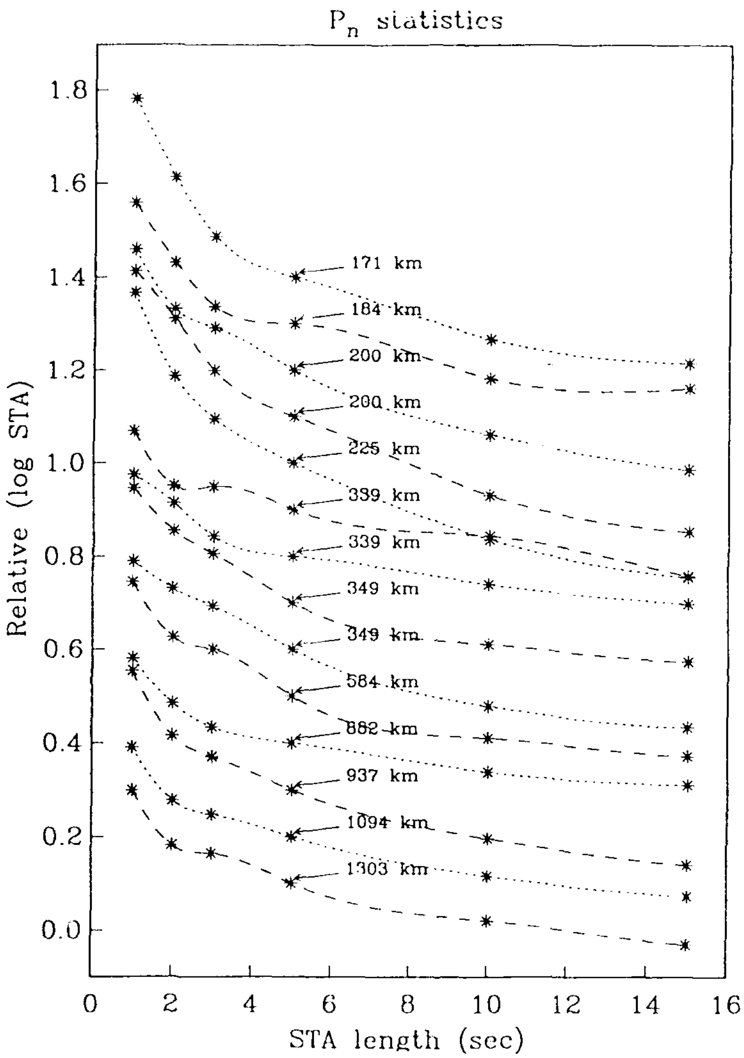

Fig. 7.7.3. The asterisks of this figure show observations of maximum log(STA) (denoted $S(\Delta t)$) for P_n for a set of STA lengths. The observations corresponding to the same phase are interpolated by dashed or dotted lines, and the epicentral distance of each event is indicated. Information on the events are given in Table 7.7.3. For display purposes an offset was added to each of the curves, as the absolute scale is without any significance. Note the difference in the slopes for events above and below 300 km epicentral distance.

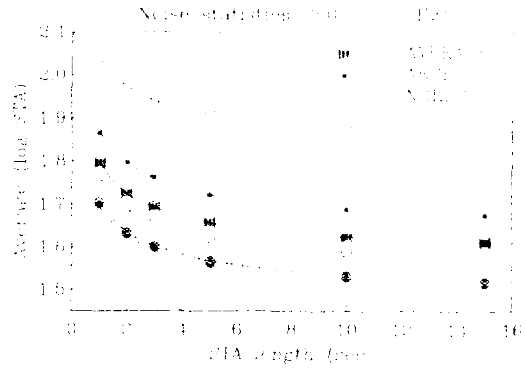

Fig. 7.7.4. Using data from the center instrument A0 of both the NORESS and the ARCESS array, this figure shows the average of log(STA) under noise conditions (denoted $\overline{A}(\Delta t)$) for a set of STA lengths. The data were filtered in the passband 3-5 Hz and a time tolerance of ±5 seconds was used. Information on the data intervals is given in Table 7.7.4. The average of the six noise observations, used for subsequent analysis of noise damping, is indicated by filled squares and a solid line.

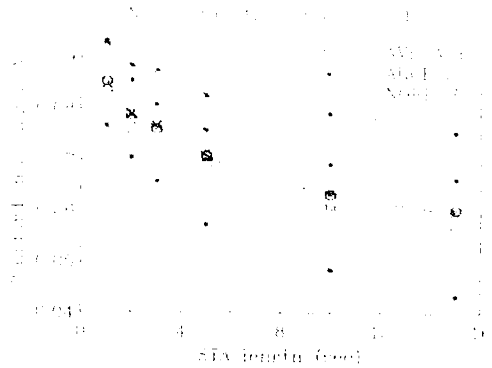

Fig. 7.7.5. This figure gives the standard deviation of the noise observations analyzed in Fig. 7.7.4. The average of the standard deviation curves, used for subsequent analysis of noise damping, is indicated by filled squares and a solid line.

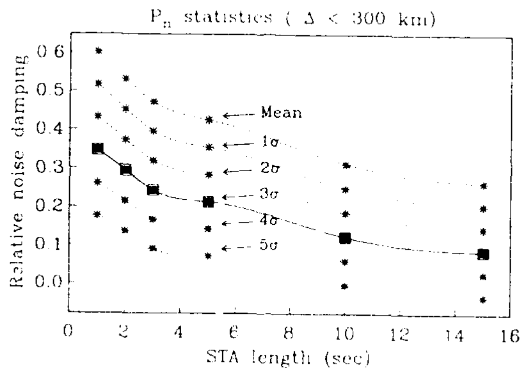

Fig. 7.7.6. The relative noise damping given in this figure is computed from average P_n signal behavior for events within 300 km epicentral distance (taken from Fig. 7.7.3), average noise conditions (taken from Fig. 7.7.4) and average values of noise standard deviation (taken from Fig. 7.7.5). The relative noise damping for a set of confidence levels is shown and the 3σ level used to characterize a "worst case" situation is given by filled squares and a solid line.

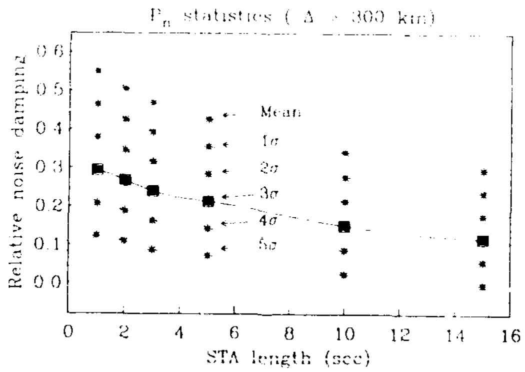

Fig. 7.7.7. Same a Fig. 7.7.6, but representing events with epicentral distances exceeding 300 km.

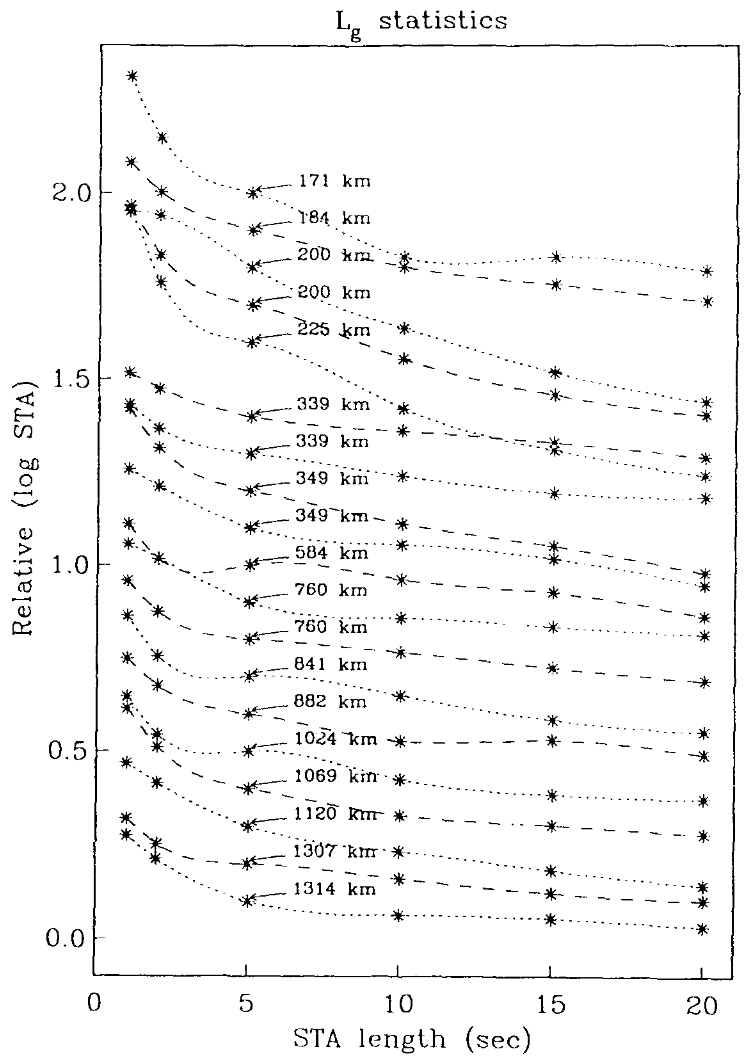

Fig. 7.7.8.. The asterisks of this figure show observations of maximum log(STA) (denoted $S(\Delta t)$) for L_g for a set of STA lengths. The observations corresponding to the same phase are interpolated by dashed or dotted lines, and the epicentral distance of each event are indicated. Information on the events is given in Table 7.7.3. For display purposes an offset was added to each of the curves, as the absolute scale is without any significance. Note the difference in the slopes for events above and below 300 km epicentral distance.

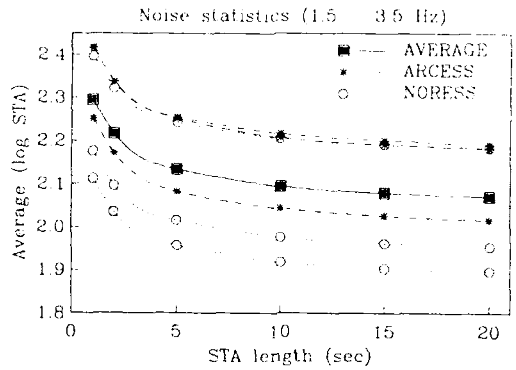

Fig. 7.7.9. Same a Fig. 7.7.4, but the noise intervals were analyzed in the 1.5-3.5 Hz filter band.

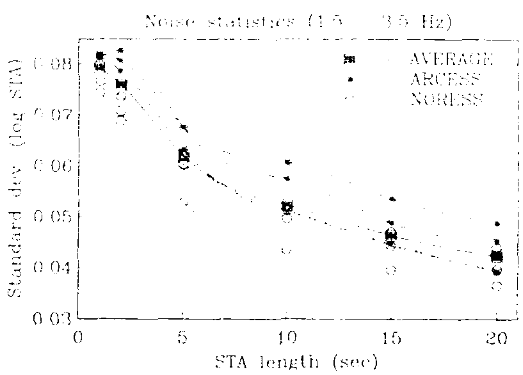

Fig. 7.7.10. This figure gives the standard deviation of the noise observations analyzed in Fig. 7.7.9. The average of the standard deviation curves, used for subsequent analysis of noise damping is indicated by filled squares and a solid line.

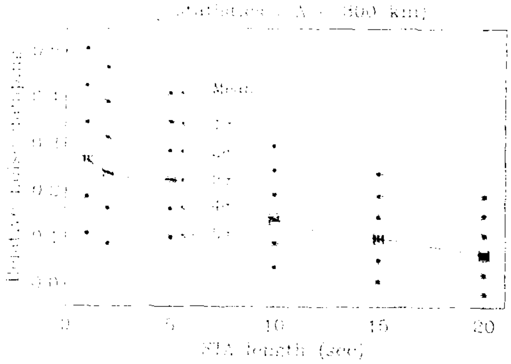

Fig. 7.7.11. The relative noise damping given in this figure is computed from average L_g signal behaviour for events within 300 km epicentral distance (taken from Fig. 7.7.8), average noise conditions (taken from Fig. 7.7.9) and average values of noise standard deviation (taken from Fig. 7.7.10). The relative noise damping for a set of confidence levels is shown and the 3σ level used to characterize a "worst case" situation is given by filled squares and a solid line.

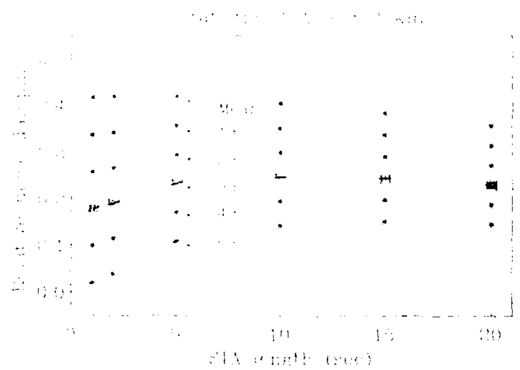

Fig. 7.7.12. *Same a Fig. 7.7.11, but representing* events with epicentral distances exceeding 300 km

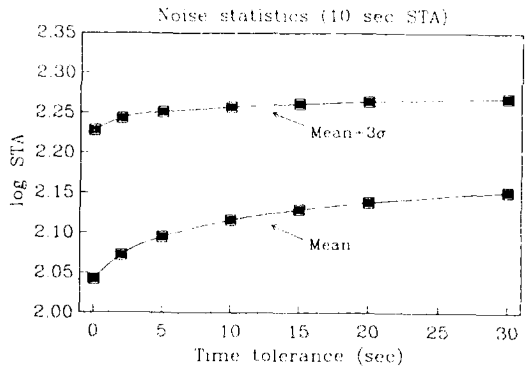

Fig. 7.7.13. This figure gives the mean of log(STA) together with the mean+3σ level for a set of time tolerances. The first noise segment of Table 7.7.4 was bandpass filtered between 1.5 and 3.5 Hz, and the estimates were obtained using an STA length of 10 seconds.

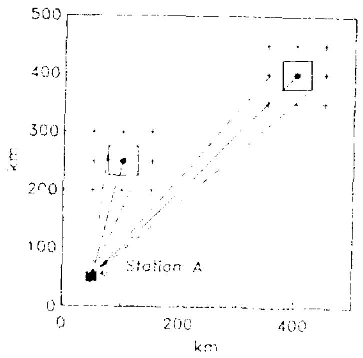

Fig. 7.7.14. In order to monitor a finite area surrounding each of the target points, a mis-steering in azimuth is introduced when the beams are steered towards the target points. This figure illustrates this for two target points at different distances. The azimuth deviations are indicated by dashed lines. Also note that for a fixed grid spacing, the mis-steering is a function of distance to the target points.

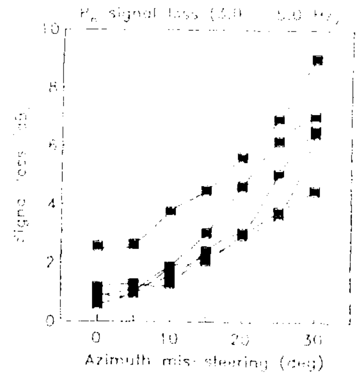

Fig. 7.7.15. The filled squares of this figure give the estimated signal loss for P_n as a function of azimuth mis steering. Observations corresponding to the same phase are interpolated by dashed lines and information on the P-phases are given in Table 7.7.5. For a circular array, it is common to map the signal loss as a function of deviations in horizontal slowness. We have therefore computed signal losses as a function of azimuth, where the azimuth deviations are normalized to provide equal deviations in horizontal slowness. The x axis of this plot is given as normalized azimuth deviations relative to an apparent velocity of 8.0 km/s.

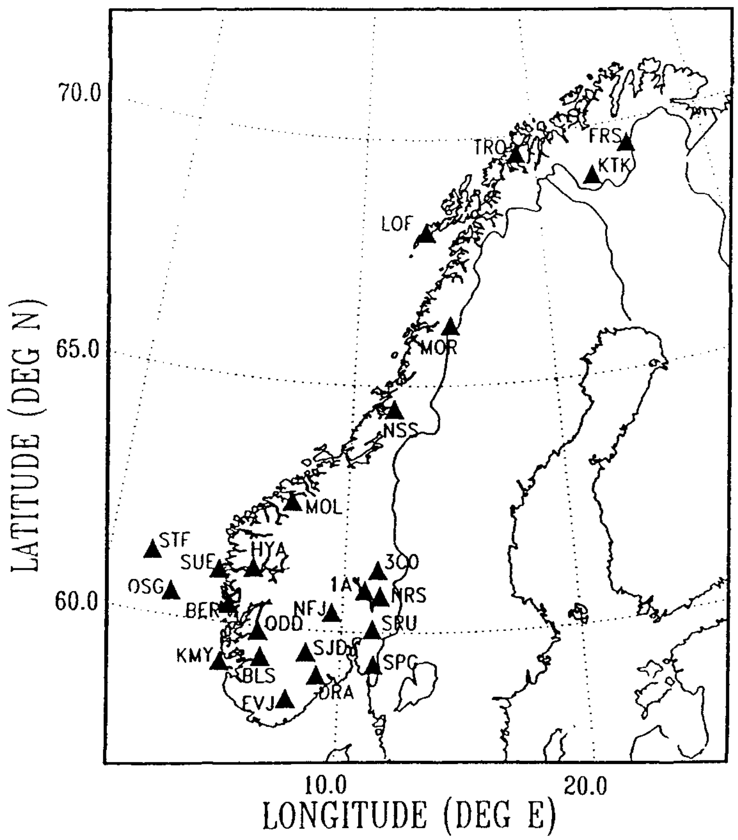

Fig. 7.7.16. Recording stations providing data for regression analysis. Adapted from Alsaker *et al* (1990).

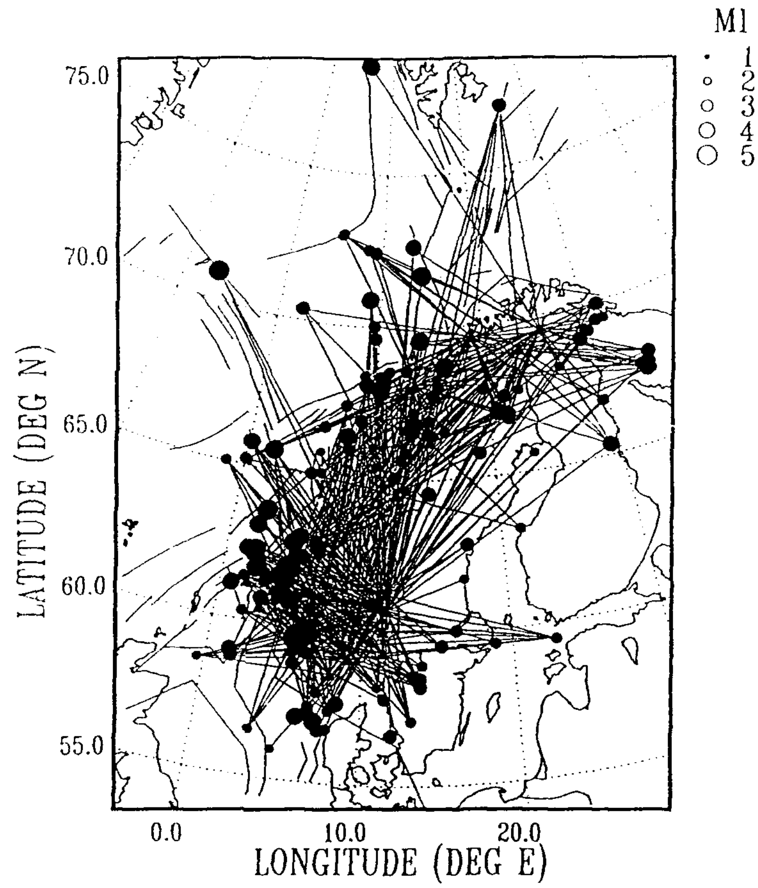

Fig. 7.7.17. Recordings selected by Alsaker *et al* (1990) for estimation of an M_L scale for Norway. Applying regression analysis, a subset of these recordings was used for obtaining generic relations for the magnitude *correction factors*. Adapted from Alsaker *et al.* 1990.

7.8 Continuous threshold monitoring using "regional threshold displays"

Introduction

Continuous threshold monitoring (Ringdal and Kværna, 1989) is a method of monitoring seismic amplitude levels for the purpose of assessing the largest size of events in a given target region that might go undetected by a monitoring network. The method has recently been implemented within the Intelligent Monitoring System (IMS) (Bache *et al*, 1990). In previous Semiannual Technical Summaries, as well as in the present issue, several examples of application have been presented. In particular, Kværna and Ringdal (1990) conducted a one-week monitoring experiment of the Novaya Zemlya test site using the Fennoscandian regional array network, and concluded that continuous threshold monitoring down to event size as low as $m_b = 2.5$ appeared feasible for this site.

Regional threshold monitoring

In the current IMS implementation of the TM technique, a limited number of specific target sites are monitored. These sites include several mines in Scandinavia and Western Russia, along with the Novaya Zemlya and Semipalatinsk nuclear test sites. For each of these sites, a number of calibration events are available, and thus it has been possible to fine tune the parameters in order to obtain close to optimum monitoring performance.

"Regional threshold monitoring" is defined as an extension of the original "site-specific" threshold monitoring concept. It entails using the same basic principles to obtain wide geographical coverage, including coverage of regions for which no calibration events are available. The key to achieving this is to develop "generic" relations for attenuation and magnitude corrections of seismic phases of interest, and to deploy a sufficient number of beams to ensure adequate geographical coverage.

Kværna (1991, this issue) has developed initial such generic relations for the Pn and Lg phases of NORESS, ARCESS and FINESA. His relations are applicable to Northern Europe and adjacent regions, and are based on a systematic analysis of several hundred phase observations of regional events in various geographical areas. Kværna's results form the basis for the study presented in this paper.

Threshold maps

The regional threshold monitoring approach lends itself naturally to displays in the form of contoured geographical maps. By using a spatial grid covering the area of interest, interpolation can be applied to get a visual representation of threshold variations over an extended geographical region, and examples will be given later.

These contour maps are in many ways similar to the standard network capability maps traditionally used in seismic monitoring studies (Networth, Snap/D, etc.). However, there are some fundamental differences:

- Standard capability maps use as a basis statistical models of signal and noise characteristics; in particular a signal variance and a noise variance is assumed to compensate for statistical fluctuations. In contrast, the regional TM maps give "snapshots" of the capability as actually observed at a given point in time.

- With standard maps, no allowance is made for unusual conditions, such as, e.g., the occurrence of a large earthquake or an aftershock sequence which may cause the network capability to deteriorate for hours. With the TM approach, the actual variation in detection capablity is immediately apparent.

- Standard capability maps require assumptions, e.g., with regard to "SNR threshold required for detection" and "minimum number of stations required to locate". The TM maps require no such assumptions since they are not tied to "detecting and locating" seismic events, but rather describe directly the observed "seismic field" at any point in time.

We will briefly comment further on the last item mentioned above: The requirement of multistation detection with the standard method will sometimes result in unrealistically high thresholds, e.g., in areas near a station of the monitoring network. The multistation requirement also implies that the method is not able to adequately represent the possibility of particularly favorable source station paths. A case in point is the outstanding capability of the NORESS array in detecting explosions at Shagan River. Thus, if NORESS has no detection, it is highly unlikely that any explosion at that site of $m_b > 3$ has occurred, whereas a capability map based on 4-station detection requirement may well show a threshold an order of magnitude higher.

The threshold monitoring approach will avoid these inconsistencies. Thus, under normal noise conditions, the thresholds will be very low within a few hundred km of each network station. Furthermore, since the TM thresholds are dominated by the "best" station of the network, particularly favorable source/receiver paths may be accommodated, although this would require a combination of regional and site-specific monitoring.

Display examples

Using the generic relations developed by Kværna (1991), we computed a threshold monitoring grid of 20 x 20 geographical aiming points for a 40 minute time interval. Data from the three arrays NORESS, ARCESS and FINESA were used. Contouring maps were developed by interpolation in this grid, and displayed in the form of color maps where the color scale is tied to the actual threshold.

Figs. 7.8.1 and 7.8.2 show two representative examples of output from this procedure.

Fig. 7.8.1 shows the "absolute" TM threshold levels (with m_b units indicated on the color template) at a specific time during a typically "quiet" period (i.e., no seismic event occurring). We note that the areas immediately surrounding each array (deep or light blue) show the lowest thresholds (below $m_b = 0.5$), whereas most of the remaining area at regional distances has a green color, indicating thresholds in the range $m_b = 0.5$–1.5. The yellow color seen further away from the network stations indicates thresholds of 1.5 to 2.5.

Fig. 7.8.2 shows a typical map at a time corresponding to a mining explosion (magnitude 2.2) at the Apatity mine in the Kola Peninsula. In contrast to Fig. 7.8.1, we have here chosen to display *relative* thresholds (i.e., thresholds relative to the average thresholds during noise conditions at each geographical point). This is done to emphasize more clearly the effects of the seismic event in causing threshold increases outside the source area. We note that, naturally, the area surrounding the mining site has the highest relative threshold (red), whereas the "side lobe" effect causes significant threshold increase also in other regions, some of which quite far apart from the mine.

The computer displays shown in Figs. 7.8.1 and 7.8.2 also include fields for displaying threshold traces and selecting various plotting options. At the present time, however, these features have not been operationally implemented.

Perspectives

We consider that the regional approach to threshold monitoring would imply a significant enhancement of practical monitoring of underground nuclear explosions. In particular, a graphics display system could be developed to provide the analyst with very useful interactive tools. Among features that might be desirable are:

- "Snapshots" of regional threshold maps taken at times when a peak occurs on a threshold monitoring trace. For example, if a peak is observed on the threshold trace used to monitor Novaya Zemlya, such a snapshot could immediately reveal that this peak might, e.g., be a side lobe effect from a remote earthquake.
- Threshold displays taken during the coda of very large earthquakes, indicating the resulting effects on detectability in various regions.
- "Cumulative" displays showing the largest possible events that might have occurred during a given time period (e.g., 24 hours).

- Combinations of threshold displays and conventional epicenter maps of detected events.

An extremely interesting application would be a real time "video" display of how the threshold situation fluctuates with time. When a seismic event occurs, a real time display of this type would illustrate how the threshold first increases at "side lobe" locations, with subsequent focusing upon the actual epicentral area. Such a video option could of course just as easily be implemented for off-line (retroactive) display of time periods of interest.

In order to make effective use of the regional threshold monitoring approach and the associated display options, a workstation with powerful computational and graphical capabilities will be required, and we are currently evaluating possibilities in this regard. We are also continuing our research aimed at integrating the "regional" and "site-specific" threshold monitoring methods, which we consider to have a combined potential of becoming a basic tool in practical monitoring applications.

F. Ringdal
T. Kværna

Acknowledgement: The prototype interactive regional threshold monitoring display which forms the basis for the illustrations in this paper has been developed by Rolf M. Aasen of NORSAR, using the "NOGRA" graphics software system.

References

Bache, T.C., S.R. Bratt, J. Wang, R.M. Fung, C. Kobryn and J.W. Given (1990): The Intelligent Monitoring System, *Bull. Seism. Soc. Am.*, Vol. 80, Special Issue, 1833-1851.

Kværna, T. and F. Ringdal (1990): Continuous threshold monitoring of the Novaya Zemlya test site, *Semiannual Tech. Summary, 1 Apr - 30 Sep 1990*, NORSAR Sci. Rep. 1-90/91, NORSAR, Kjeller, Norway.

Kværna, T. (1991): ;;;;; *Semiannual Tech. Summary, 1 Oct 90 - 31 Mar 91*, NORSAR Sci. Rep. 2-90/91, NORSAR, Kjeller, Norway.

Ringdal, F. and T. Kværna (1989): A multichannel monitoring approach to real time network detection, phase association and threshold monitoring. *Bull. Seism. Soc. Am.*, Vol. 79, 1927-1940.

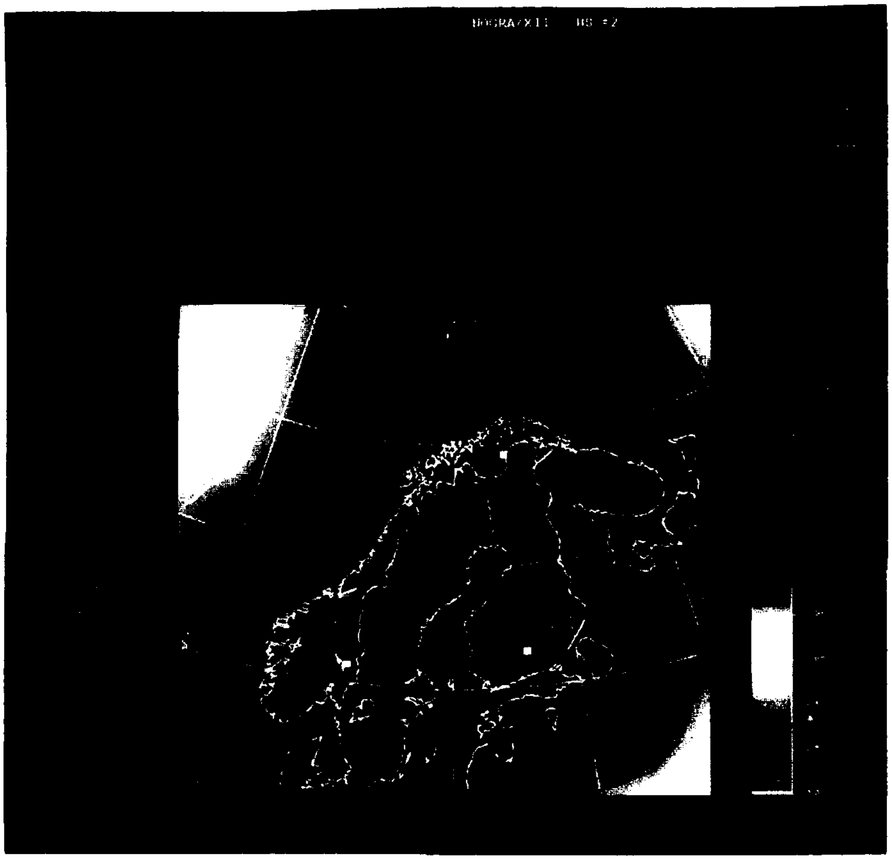

Fig. 7.8.1. Example of regional threshold display of "absolute" threshold levels, at a typical "quiet" period. See text for detailed explanation.

Fig. 7.8.2. Example of regional threshold display of "relative" threshold levels at a time when a mining explosion occurred in the Kola Peninsula. See text for detailed information.